Characterisation of the Mechanism of B-Cell Receptor Triggering

Martin James Wilcock

Corpus Christi College, University of Oxford

Supervisors: Simon J. Davis, Richard J. Cornall

Thesis submitted for the degree of Doctor of Philosophy

Trinity Term, 2018

Abstract

B cells are key mediators of humoral immunity and rely on signals initiated by the B cell receptor (BCR). The structure of the BCR and mechanism of ligand binding are well characterised, but what remains to be understood is how ligand binding triggers intracellular signalling. A number of opposing models have been proposed. In this thesis, these models have been tested experimentally using a toolkit of reagents based on the HyHEL10 BCR and its natural ligand Hen-Egg Lysozyme (HEL). Whilst a receptor crosslinking-based model accounts for multivalent ligand presented in solution, the inability of monovalent ligands to trigger robust B cell signalling, except when they are surface-associated, implicates a second triggering mechanism. To narrow down potential theories of BCR triggering, the stoichiometry of the BCR in the resting state was established using multicolour fluorescence microscopy and shown to be predominantly monomeric. Using fluorescence imaging, it was found that BCR triggering by surface associated monovalent ligands correlated with the exclusion of the large phosphatases, CD45 and CD148, from regions of BCR/ligand engagement. In addition, BCR triggering was shown to be dependent on both the size of the BCR/ligand complex and the size of the extracellular domain of CD148. These findings suggest that the size-dependent exclusion of CD45/CD148 functions as a second mechanism of BCR triggering for surface bound ligand, and complements the ability of BCR to be directly triggered by cross-linking multivalent ligands. These observations have important implications in terms of differential signalling, and the positive and negative selection of B cells. The mature B cell immune response to foreign antigen is thought to be predominantly focused on membrane bound antigen, displayed via complement or immunogloblin Fc receptors, whilst soluble antigens may be tolerogenic or lead to T-independent activation, at high avidity. It is also to be expected that differential expression of CD45/CD148 on B cell subsets will tune their response to membrane bound antigens.

Acknowledgments

Firstly, I would like to thank my supervisors, Simon Davis and Richard Cornall. Thank you for introduced me to the mesmerising field of immunology, guiding me gently along the way, but at the same time giving me the freedom to follow my scientific curiosity and make my own mistakes. To Simon, thank you for welcoming me into your laboratory, your commitment and dedication is unquestionable and has instilled in me the principle of conducting science to the highest possible standards. To Richard, whose passion and enthusiasm initially brought me to Oxford and inspired me to undertake this DPhil, thank you for supporting me along the way and always having my back.

I acknowledge the financial support provided by the Medical Research Council through a Clinical Research Training Fellowship that has enabled me to undertake this 3 year DPhil project.

The work undertaken within this thesis would not have been possible without the support and day-to-day assistance of all members of the Davis group: Mai, Jemma, Heather, Jan, James, Mafalda, Oliver, Debbie, DongDong, Chris, Elizabeth, Meike, Carmelita, Rita, Ed and Caitlin. Special thanks go to: Mai for introducing me to the laboratory and being patient with me as I learned; Jiandong Huo for teaching me the intricacies of the BIAcore; and Mafalda for day-to-day supervision and discussions which have been invaluable to the progress of this project. More widely within the WIMM I would like to thank Craig Waugh from the Flow Cytometry Facility for help with sorting cell lines, Christoffer Lagerholm from the Wolfson Imaging Facility for assistance with microscopy and Erdinc Sezgin for teaching me how to produce supported lipid bilayers.

The work undertaken in Chapters 5 and 6 of this thesis would not have been possible without the support of our excellent collaborators from the Klenerman group, Department of Chemistry, University of Cambridge. They are world leading experts in the field of single molecule fluorescence microscopy and their contribution to the work presented in this thesis has made it immeasurable stronger. Thank you to David Klenerman for allowing me to undertake experiments in his laboratory and for helpful discussions. To James McColl for all his support undertaking the imaging work presented in Chapters 5 and 6. To Anna Lippert for assistance undertaking the close contact work presented in Chapter 6 and for help tackling the analysis. To Jane Humphrey for help with production of supported lipid bilayers and the imaging experiments undertaken in Chapter 6. More widely, thank you to all for the fun and friendship during my frequent trips to Cambridge.

The journey I have undertaken during this thesis would not have been possible without the unwavering support of my friends and family. To my parents, for their enduring love and support, and their resolute belief in me that has allowed me to follow my dreams knowing that all I ever needed to do was my best. Specifically, to mum, whose enthusiasm for academia has never failed to astound me, and I'm sure in another time would have beaten me to the finishing of this thesis- this one is for both of us. Finally, thank you to my beloved Emma. Thank you for accompanying me along this journey with all the ups and downs it has entailed. It has been quite a journey not just academically, but also personally, and I am proud to call you my wife and excited to welcome our baby to the world. Here's to the next part of our journey.

Contents

List of Figures

Abbreviations

AID	Activation-Induced Cytidine Deaminase
APC	Antigen Presenting Cell
BCR	B Cell Receptor
BiFC	Bifluorescent Complimentary Assays
BLNK	B Cell Linker Protein
BN-PAGE	Blue Native Polyacrylamide Gel Electrophoresis
BSA	Bovine Serum Albumin
C	Constant
CARD11	Caspase Recruitment Domain-Containing Protein 11
CD	Cluster of Differentiation
CDR	Complementary Determining Regions
CHO	Chinese Hamster Ovary
CLP	Common Lymphoid Progenitor
CMP	Common Myeloid Progenitor
CMV	Cytomegalovirus
CRISPR	Clustered Regularly Interspaced Short Palindromic Repeats
cSMAD	Central Supramolecular Activation Cluster
CSR	Class Switch Recombination
D	Diversity
DAG	DAG
DDT	Dichlorodiphenyltrichloroethane
DMEM	Dulbecco's Modified Eagle's Medium
DMSO	Dimethyl Sulphoxise
DsRed	Discosoma Species Red Fluorescent Protein
dSTORM	Direct Stochastical Optical Reconstruction Microscopy
EDTA	Ethylenediaminetetraacetic Acid
EGFR	Epidermal Growth Factor Receptor
Fab	Fragment Antigen Binding
FACS	Fluorescence-Activated Cell Sorting
Fc	Fragment Crystallisable
FCS	Foetal Calf Serum
FcεR1	High affinity receptor for IgE
FPLC	Fast Protein Liquid Chromatography
FRAP	Fluorescence Recovery After Photobleaching
FRET	Förster Resonance Energy Transfer
GFP	Green Fluorescent Protein
HBS	Hepes Buffered Saline
HEK	Human Embryonic Kidneys
HEL	Hen-Egg Lysozyme
Ig	Immunoglobulin
IL	Interleukin
IP_3	Inositol Trisphosphate
IRES	Internal Ribosome Entry Site
IRF	Interferon Regulatory Factor

IS	Immunological Synapse
ITAM	Immunoreceptor Tyrosine-based Activation Motif
ITIM	Immunoreceptor Tyrosine-based Inhibitory Motif
J	Joining
KS	Kinetic Segregation
LPS	Lipopolysaccharide
MAPK	Mitogen-Activated Protein Kinase
MHC	Major Histocompatibility Complex
mIg	Membrane Bound Immunoglobulin
MPP	Multipotent Haematopoietic Progenitor
MSX	Methionine Sulfoximine
NFAT	Nuclear Factor of Activated T-cells
NFκB	Nuclear Factor κB
NK	Natural Killer
PAMP	Pathogen Associated Molecular Patterns
PBS	Phosphate Buffered Saline
PCR	Polymerase Chain Reaction
PCR	Polymerase Chain Reaction
pHSC	Pluripotent Haematopoietic Stem Cell
PI3K	Phosphoinositide-3-Kinase (PI3K)
PLL	Poly-L-lysine
PKC	Protein Kinase C
PLA	Proximity Ligation Assay
PRR	Pattern Recognition Receptor
pSMAC	Peripheral Supramolecular Activation Cluster
RAG	Recombination-Activating-Gene
RPMI	Roswell Park Memorial Institute Medium
RPTP	Receptor-Type Protein Tyrosine Phosphatase
S1P	Sphingosine-1-Phosphate
SDS-PAGE	Sodium Dodecyl Sulphate Polyacrylamide Gel Electrophoresis
SFFV	Spleen Focus Forming Virus
SHM	Somatic Hypermutation
SLB	Supported lipid bilayers
TCR	T Cell Receptor
TD	T Cell Dependent
TdT	Terminal Deoxynucleotidyl Transferase
T_{FH}	T follicular helper
TI	T Cell Independent
TIRF	Total Internal Reflection Fluorescence
Treg	Regulatory T Cell
UV	Ultraviolet
V	Variable
WPRE	Woodchuck Hepatitis Virus Posttranscriptional Regulatory Element

Chapter 1

General Introduction

1.1 Overview of the immune system

The world is a hazardous place replete with pathogens, toxins and allergens which threaten the existence of other organisms in broad and evolving ways. To counteract this, vertebrates have developed complex mechanisms of host defence to protect themselves. These defences are collectively known as the immune system. The immune system consists of multiple layers of protection of progressively increasing complexity and is classically divided into two distinct but overlapping arms: the innate immune system and the adaptive immune system [1].

1.1.1 The innate immune system

The innate immune system is the first line of host defence against pathogens. It is evolutionarily conserved and present in all species from primitive multicellular organisms to vertebrates. The innate immune system acts quickly in a stereotyped and non-specific manner to prevent microbial invasion. The innate immune system is comprised of multiple components including anatomical barriers, cellular components and secretory molecules [2].

Simple physical barriers including skin, respiratory epithelium and gastrointestinal epithelium provide a first barrier of defence, preventing access of harmful agents into the body. If these barriers are breached, other defences are poised to act. Neutrophils, macrophages and monocytes phagocytose bacteria and destroy them, while Natural Killer (NK) cells are specialised to target virus or tumour infected cells. Dendritic cells are also

able to phagocytose cells but serve to act as the principal antigen-presenting cell (APC) rather than directly killing pathogens. These cellular elements of the innate immune system produce cytokines and chemokines which lead to the accumulation and activation of leukocytes and other immune cells. The other major humoral component of the innate immune system is complement. Complement can be activated by the classical, alternative or mannose binding pathway, and effects its activity either by opsonisation, recruiting inflammatory cells or direct membrane attack [3].

The innate immune system recognises microbes through various pattern recognition receptors (PRRs). These are invariant receptors that are germline encoded. They utilise one of several immune surveillance strategies including recognising microbial non-self, missing self or induced/altered self [4]. PRRs include secreted and circulating proteins (anti-microbial peptides, collectins and pentaxins), and transmembrane and intracellular signal transducing receptors (Toll-like receptors, C-type lectin receptors, NOD-receptors, RIG-I-like receptors). These receptors activate conserved common downstream signalling pathways leading to activation of transcription factors including nuclear factor κB (NF κB), interferon regulatory factor (IRF) and nuclear factor of activated T-cells (NFAT). These receptors target pathogen associated molecular patterns (PAMPs). PAMPs are highly conserved structures that are typically invariant within a class of microorganism. They often have an essential role in microbial physiology, such that a pathogen cannot mutate its PAMP to avoid an immune response and still survive. Importantly, PAMPs are the product of pathways unique to microorganisms thus allowing the innate immune system to discriminate self from non-self [5, 6].

Activation of the innate immune system leads to the release of inflammatory cytokines, type I interferon, nitric oxide production and induction of phagocytosis. The ultimate outcome of the innate immune response is to prevent, control or eliminate a pathogen. However, inappropriate responses can lead to inflammation and auto-immune diseases [7]. In the event that a pathogen overcomes these defences the adaptive immune system must act. There is considerable two-way crosstalk between both arms of the immune system such that if a pathogen does evade the innate defences the adaptive immune system is already primed for action [8].

1.1.2 The adaptive immune system

1.1.2.1 Overview

The adaptive immune system is the second line of host defence against pathogens [1]. It evolved later than the innate immune system and is found in jawed fish and all higher vertebrates [9]. The responses of the adaptive immune system are slower but more specific. Specificity arises due to the formation of highly diverse receptors on lymphocytes generated by somatic diversification. The adaptive immune system provides memory such that a quicker and enhanced immune response occurs on re-challenge with the same antigen [1].

A typical adaptive immune response commences with invasion and take up of pathogen in the periphery by APCs, such as dendritic cells and macrophages. APCs migrate to secondary lymphoid organs where peptide fragments of the antigen are presented to T cells bound to major histocompatibility complex (MHC) proteins. The peptide/MHC complex is recognised by immature T cells expressing the complementary T cell receptor

(TCR). Recognition of antigen by a T cell leads to activation and stimulates the T cell to mature and differentiate into an effector T cell. Various subtypes of effector T cells exist with different functions. Cluster of Differentiation (CD) 4+ T helper cells provide help to B cells, CD8+ T cells kill virus infected cells, and regulatory T cells (Tregs) modulate immune cell activity. The help provided by CD4+ T cells to B cells enables them to differentiate into antibody producing plasma cells or memory B cells. The ultimate outcome of an adaptive immune response is to eliminate the pathogen, and in the process generate memory B and T cells to provide protection from re-challenge with the same antigen [1].

1.1.2.2 Antigen recognition

Antigen recognition by the adaptive immune system is undertaken by highly variable receptors expressed on the surface of B and T cells. Antigen recognition by B cells is mediated by the B cell receptor (BCR). B cells differentiate into plasma cells which produce a secreted form of the BCR known as antibody. The BCR and antibodies both recognise antigen in their native form. Antigen recognition by T cells is undertaken by the TCR which is only expressed in a membrane bound form. The TCR typically binds antigen only in the context of MHC molecules. B cells help to defend against extracellular pathogens and their toxins while T cells kill intracellular pathogens which are inaccessible to antibodies [1].

The BCR consists of a membrane bound immunoglobulin (consisting of a heterodimer of two heavy and two light chains) linked to an Ig (Immunoglobulin)-αβ (CD79 α/β) heterodimer. The structure of the TCR consists of a heterodimer of either αβ (95% T

cells) or γδ chains (5 % T cells) linked to the CD3 complex (one CD3δε heterodimer, a CD3γε heterodimer and a CD3ζζ homodimer) [10, 11]. In both cases, the antigen binding region is formed by membrane distal immunoglobulin variable domains. Binding is centred on three highly variable complementary determining regions (CDRs). The diversity of the binding region is generated via a number of processes [1].

Both the BCR and TCR are encoded by multiple gene segments: variable (V), diversity (D), joining (J) and constant (C) regions. V(D)J segments encode the variable immunoglobulin domains and are randomly brought together in a process known as somatic recombination. Somatic recombination is under the control of the lymphocyte specific enzymes recombination-activating-gene (RAG)-1 and RAG-2. In B cells, the heavy chain of the BCR undergoes VDJ re-arrangement, and the light chain VJ rearrangement. In T cells, TCR-α is formed by VJ re-arrangement and TCR-β by VDJ re-arrangement. The process of somatic diversification is deliberately error prone [12]. Furthermore, short random nucleotide sequences are added by terminal deoxynucleotidyl transferase (TdT) [13]. An additional layer of combinatorial variability is added by the paring of two protein chains: heavy and light for the BCR, and α and β for the TCR. The result of these processes means that an almost limitless range of receptor can be generated allowing recognition of virtually any pathogen [12].

Additional post-rearrangement mechanisms occur in B cells: gene conversion, somatic hypermutation (SHM) and class switch recombination. These processes are controlled by activation-induced cytidine deaminase (AID), and diversify the antigen receptor repertoire further. SHM is the process by which point mutations are generated in variable genes

without a template while gene conversion does so with pseudo variable genes. These processes create a range of affinities of BCR. In sequential rounds of selection, progressively higher affinities of BCR are selected for a given antigen resulting in affinity maturation. This process occurs in a carefully regulated manner within the germinal centres of secondary lymphoid organs [14].

1.1.2.3 Antigen processing and presentation

In order to induce an immune response, antigens must be processed and presented to T-cells. Antigen presentation is mediated by MHC molecules. There are two MHC molecules, class I and class II. MHC molecules are highly variable allowing the presentation of virtually any antigen. The extensive polymorphic nature of the MHC ensures that a T cell can only recognise a peptide in association with a given MHC molecule, a process known as MHC restriction. Humans express six MHC class I and eight MHC class II alleles. MHC class I and class II molecules are similar but differ in terms of their structure, cell distribution, peptide source and subtype of T cell to which antigen is presented [15, 16].

1.1.2.4 B cell mediated immunity

B cells mediate immunity by secreting antibodies into the blood and at mucosal sites. B-cells bind antigen in their native form via the cell surface BCR. Antibody mediated humoral immunity can be produced in one of two ways: (1) T cell dependent (TD) or (2) T cell independent (TI). The vast majority of antigens activate B cells in a TD manner [17].

In TD responses, antigen recognised by the BCR is internalised, degraded and loaded onto MHC class II molecules and presented to previously activated T helper cells. T helper cells that recognise the specific peptide/MHC expressed on the surface of the B cell are able to

help activate B cells by secreting cytokines, such as interleukin (IL)-4, and upregulation of cell surface markers, for example, CD40L. This is the mechanism of activation of follicular B cells [18].

TI antigens activate B cells without the need for T cell help. Two types of TI antigens are recognised based on the mechanism by which they activate B cells and whether this process requires Bruton tyrosine kinase. TI antigens are important early in an immune response [17]. TI-1 antigens, such as of lipopolysaccharides (LPS), are able to activate B cells directly via ligation of Toll-like receptors. TI-2 antigens activate B cells by crosslinking the BCR as they have a highly repetitive structure, for example, bacterial cell walls. TI antigens lead to the production of relatively low affinity IgM antibodies by marginal zone and B1 cells [19].

Upon activation, B cells proliferate and differentiate into either plasma cells or memory B cells. Both cells produce antibody against a specific antigen. Different functional antibodies can be generated with the same specificity through AID mediated class switching [14]. Antibodies are able to eradicate pathogens by a number of mechanisms: (1) neutralization; (2) activation of the complement cascade via the classical pathway; or (3) opsonisation to allow recognition by Fc receptor bearing cells which kill by antibody dependent cell-mediated cytotoxicity or phagocytosis [20].

1.1.2.5 T-cell mediated immunity

T cells require two signals to become fully activated [21]. Signal 1 is antigen dependent and provided by the interaction between the TCR and peptide/MHC complex on the surface of the APC. Signal 2 is antigen independent and provided by co-receptors on the surface of the T cell. Co-receptors include CD28 which interacts with CD80/86, which are

upregulated on the surface of APCs in the context of infection. Ligation of the TCR in the absence of co-stimulation leads to T cell anergy. Co-stimulation is therefore an important mechanism by which T cells are only activated in the appropriate context thereby preventing inappropriate responses to self [22].

T cells can be broadly categorised into two types based on the expression of either CD4 or CD8. T cells are initially dual negative but during development become double positive and then single positive [23]. CD8+ T cells recognise MHC class I restricted antigens. They are cytotoxic and kill by either releasing cytotoxic granules into the immunological synapse or the expression of FAS-ligand [24]. CD4+ T cells recognise MHC class II restricted antigens. Upon activation local cytokines induce CD4+ T cells to differentiate into diverse subsets: Th1; Th2; Th17; T-follicular helper (T_{FH}) and Treg cells. Th1 cells produce IL-2 and interferon-γ and are important in cellular immune responses by macrophages to intracellular bacteria and protozoa. Th2 cells release IL-4 and stimulate recruitment of eosinophils, basophils, mast cells and macrophages to protect epithelial barriers. Th17 produce IL-17 and protect against extracellular bacteria and fungi. T_{FH} cells are derived from Th1 and Th2 cells and provide help to B cells to produce antibodies. Tregs express the transcription factor FoxP3 and are anti-inflammatory contributing to peripheral tolerance [25].

1.1.2.6 Immunological memory

Protective immunity against reinfection is a cardinal feature of the adaptive immune system [1]. It was first demonstrated in Jenner's seminal work of 1798 [26] in which he described the protective effect of coxpox against smallpox and has been utilised since for therapeutic

purposes in vaccines [27]. Immunological memory results in a response that is quicker and quantitatively better than the primary immune response. Memory results from a heterogeneous population of long-lived cells of both B and T cell origin and is dependent on the local tissue microenvironment and cytokine release [28].

1.1.3 Interface between the innate and adaptive immune systems

The innate and adaptive immune responses have been considered separately but it is important to emphasise the crosstalk between them. This ensures that that if the innate defences are breached the adaptive immune system is ready to act [8]. The priming of the adaptive immune system by the innate immune system occurs by upregulating co-receptors and release of cytokines that contribute to signal 2. Furthermore, cells of the innate immune system, such as dendritic cells and macrophages, act as professional APCs to initiate adaptive T cell responses

Two cell types exhibit features of both the innate and adaptive immune responses: NK cells and γδ T cells. NK cells kill virus and tumour infected cells and cells displaying the absence of self. This process is innate-like, occurring rapidly and controlled by multiple germline encoded activating and inhibiting receptors. However, NK cells also have the ability to form immunological memory bridging the divide into the adaptive immune system [29]. γδ T cells differ from conventional T cells in that the TCR expresses the γδ chains instead of the αβ chains. However, γδ T cells are not peptide/MHC restricted and can rapidly recognise pathogens in a PRR like manner that place them firmly at the initiation of immune responses [30].

1.2 B cells

1.2.1 History of the discovery and function of B cells

In 1890, Emil von Behring and Shibasaburo Kitasato discovered that circulating "anti-toxins" were important in providing immunity to diphtheria and tetanus [31]. The "anti-toxins" described would later be called antibodies and shown to be gamma globins [32]. Paul Ehrlich proposed that the origin of these "anti-toxins" were cells with pre-formed antibody receptors [33] and in so doing he anticipated the existence of cells that would later be called B cells [34].

The cellular source of antibodies was only identified in the 1940s when plasma cell development was noted to correlate with antibody responses following immunisation [35]. Circulating lymphocytes were subsequently shown to give rise to plasma cells [36, 37]. Prior to the 1960's the function of lymphocytes was largely unknown and there was no distinction between B and T cells. The first indication of a two-lymphocyte model arose out of a series of contemporaneous studies: adoptive transfer experiments in guinea pigs [38, 39], removal of the bursa of Fabricus in birds [40], and clinical evaluation of patients with immune deficiency syndromes [41, 42]. In 1965, Max Cooper and Robert Good defined the separate B and T cell lineages in experiments conducted on chickens. They selectively removed either the thymus or Bursa of Fabricus from newly hatched chicks followed by whole body irradiation to destroy any cells produced prior to organ removal. Removal of the thymus resulted in severely impaired cell mediated immunity but normal antibody production and germinal centres; while removal of the Bursa of Fabricus resulted in normal cell mediated immune responses but the loss of germinal centres, plasma cells and antibodies [43].

1.2.2 B cell development and lineage differentiation

1.2.2.1 Central B cell development

B cells differentiate from pluripotent haematopoietic stems cells (pHSC). pHSC differentiate into the multipotent haematopoietic progenitor (MPP) which give rise to the common myeloid progenitor (CMP) and common lymphoid progenitor (CLP). The CLP generates B cells, T cells, NK cells and lymphoid dendritic cells. In mice, the earliest possible site of pHSC is in the paraoartic splanchnopleura. pHSC from the paraortic splanchnopleura populate the fetal liver during pre-natal life, and it is here that an initial transient wave of B cell development occurs, dominated by B1 B cell production. After birth, continuous B cell development occurs in the bone marrow producing B2 cells [44, 45]. Commitment to the B cell lineage is dependent on the transcription factors E2A, EBF and Pax5 [45, 46]. B cell development is also critically dependent on the local microenvironment with stromal cells providing signals in the form of cytokines (IL7, CXCL12 or galectin-1) [45, 47, 48] and direct cell-cell contact (VCAM-1/VLA-1 interaction) [49].

Central B cell development occurs in a series of defined stages: stem cell, pro-B cell, pre-B cell and immature B cell [50]. These stages are characterised by: rearrangement of Ig heavy chain genes, rearrangement of Ig light chain genes, expression of a surface Ig, RAG and TdT expression (in bone marrow), and expression of adhesion molecules and cytokine receptors [45, 51]. B cell development begins by re-arrangement at the heavy chain locus. If successful, the heavy chain is expressed on the cell surface as the pre-BCR in combination with a surrogate light chain. The expression of the pre-BCR on the surface is

an important checkpoint. Successful production of a complete heavy chain stimulates 4-5 cycles of cell proliferation and signals for transition from pro-B cell to pre-B cell stage resulting in cessation of further heavy chain re-arrangement, enforcing allelic exclusion [52]. In the next stage, pre-B cells undergo light chain re-arrangement. This occurs first at the kappa locus. If successful, the complete BCR is expressed on the surface of the immature B cell. If unsuccessful, re-arrangement is attempted at the second kappa locus and then at the lambda locus. B cells therefore have several opportunities to correctly rearrange their antigen receptors [45, 51]. Critical to B cell development and progress through these central development checkpoints is the expression of a pre-BCR or BCR on the cell surface and induction of tonic signals. Tonic signalling is thought to suppress RAG genes and maintain progress through the developmental stages [53]. Tonic BCR signalling mediates differentiation of immature B cells into transitional and mature B cells via activation of the Ras-Mek-Erk pathway [54] and expression of the BAFF receptor, which then results in the receipt of BAFF-dependent pro-survival signals [55].

During the process of re-arrangement of the heavy and light chain loci, a vast array of specificities of BCR are generated. Each set of recombinations generates a B cell clone expressing a single specificity of BCR. This diversity ensures all potential antigens can be recognised. However, by chance this process will generate B cells expressing receptors against self-components. These must be removed in a process known as central tolerance to prevent autoimmunity [56]. High affinity interactions with membrane-bound or multivalent self leads to apoptosis and clonal deletion [57, 58]. Autoreactive cells can normally be rescued from clonal deletion in a process known as receptor editing, during which further gene re-arrangements occur in an attempt to produce a non-autoreactive BCR [59-61]. Binding of autoreactive B cells to soluble or low affinity membrane bound

self does not kill B cells but induces a state of B cell anergy [62-66]. Low avidity binding of autoreactive B cells can also lead to positive selection of B1 cells in early ontogeny, by mechanisms that are poorly understood but dependent on a fetal immature B cell phenotype (X Xu, personal communication), while B cells which fail to recognise autoantigens enter the periphery as conventional B2 cells. The consequence of these central checkpoints is that of the 10-20 million B cells produced each day, only 15% will enter the circulation as long lived cells where they survive for approximately 8 weeks [45].

1.2.2.2 Peripheral B cell development

The final stage of development from an immature to a mature naïve B cells occurs in the periphery. In the interim they are known as transitional B cells. The hallmark functional characteristic of immature, transitional B cells is the induction of apoptosis in response to BCR cross-linking, rather than activation as occurs in mature B cells [67, 68]. Transitional B cells must pass through a series of development checkpoints during which they acquire immune competence. Two thirds of transitional B cell development occurs in the spleen giving rise to follicular and marginal zone B cells, while the remaining transitional B cells develop in the bone marrow giving rise to follicular cells only [69].

Upon maturation, naïve B cells circulate between secondary lymphoid organs. This migration is not random but mediated by chemokine receptors and sphingosine-1-phosphate (S1P) receptors [70]. Mature B cells migrate to B cell follicles where they will survey antigen. After approximately 24 hours B cells that have not encountered antigen leave the follicle and recirculate to survey other lymphoid organs [70]. Mature B cells that do encounter antigen cease recirculating, localise to the T cell zone and, if they receive sufficient T cell help, enter the germinal centre. They cycle between the light zone and dark

zone of the germinal centre, undergoing iterative rounds of somatic hypermutation and clonal selection in a process known as affinity maturation [71]. B cells that have undergone affinity maturation have one of three fates: they differentiate into a plasma cell, become a memory B cell or undergo further rounds of affinity maturation [45]. Mature B cells that have responded to antigen can switch immunoglobulin class to IgA, IgG or IgE by alternative splicing and class switch recombination [72].

1.2.3 B cell subsets.

While B cells share many fundamental similarities, they are a heterogeneous population of cells differing in their cell surface phenotype, function, ability to migrate and the likelihood that they will be activated in a TD or a TI manner [73]. The different maturation stages and B cell subsets have been most clearly defined in mice.

1.2.3.1 B1 cells

B1 cells are produced during fetal/neonatal B cell development but not adult B cell development. They reside within the pleural and peritoneal cavities, though they recirculate, and are self-renewing [74]. B1 cells express high levels of sIgM and low levels of sIgD and CD45 (B220). They can be further subdivided into B1a and B1b cells on the basis of their expression of CD5 [75]. Their existence was defined in mice but it remains controversial whether a B1 cell equivalent exists in humans [76-79]. The origin and development of B1 cells has also been controversial. Evidence now points towards a multi-lineage model of B cell development rather than a single lineage model with antigen driven selection [80]. B1 cells have a restricted BCR repertoire and produce natural antibodies

against self-antigens and antigens with repetitive epitopes e.g. LPS and carbohydrates. B1 cells can therefore be considered to reside partially within the innate immune system [74].

1.2.3.2 B2 cells

B2 cells are produced during adult B cell development and include a predominant population of follicular B cells and a minor population of marginal zone B cells.

Follicular B cells

Follicular B cells are mature B cells that continuously re-circulate through B cell follicles in secondary lymphoid organs. In this follicular niche, B cells present antigen to T cells and undertake their principal role in TD immune responses. Follicular B cells also contribute to a lesser extent to TI responses in the "perisinusoidal niche" of the bone marrow [73]. Follicular B cells express high levels of sIgM, sIgD, CD45 (B220) and low levels of CD148 [75].

Marginal zone B cells

Marginal zone B cells reside in the marginal sinus of the spleen, between the red and white pulp [81, 82]. They are non-circulating and express high levels of sIgM and CD148 but low levels of sIgD [75] . Together with B1 cells, marginal zone B cells are involved in the early phase on an immune response and play a predominant role in delivering rapid TI responses to encapsulated blood borne pathogens. Their location, low activation threshold, high expression of complement receptors and constant exposure to large volumes of blood make them ideally suited to this role [81, 82]. Marginal Zone B cells also

contribute to a lesser extent to TD immune responses, shuttling antigen from the marginal zone into splenic follicles [83].

1.2.3.3 Anergic B cells

Anergic B cells are refractory to stimulation in the context of cognate antigen [84]. They were first described in experiments in which B cell precursors cultured in low doses of antibody gave rise to normal B cell numbers but functionally they were refractory to activation [85]. It was subsequently shown that anergy could be induced in animal models in the context of excess soluble antigen [86]. The induction of anergy is a useful mechanism to silence autoreactive B cells stimulated early in development when only autoantigens are present. However, given sufficient stimulation anergic B cells can be activated with the potential to cause autoimmunity [63, 84]. Anergic B cells are characterised by low sIgM expression, reduced lifespan, altered migration and anatomical localization, attenuated upregulation of CD80 and CD86 and an inability to interact productively with helper T cells [87, 88].

1.2.3.4 Regulatory B-cells

Regulatory B cells differ from conventional B cells in that they are reported to suppress immune responses contributing to the maintenance of tolerance [89]. Their discovery arose out of experiments in which B cells were targeted as a potential therapy for autoimmune diseases. Despite B cell depletion there was no recovery from autoimmunity leading to the concept that certain B cell lineages must be negatively regulating the immune response [90-96]. The key feature of regulatory B cells is the secretion of IL-10 which occurs independently of antibody production [89]. Multiple regulatory B cell subsets have been described in mice and humans but their exact lineage remains to be elucidated [97].

1.2.3.5 Memory B cells

Long-term B cell immunity is derived from two sources. Firstly, long-lived plasma cells which secrete immunoglobulin at local sites for prolonged periods after antigen clearance; and secondly, from memory B cells which rapidly proliferate and differentiate into plasma cells following re-exposure to antigen. Memory B cell responses differ from primary responses in that they are faster and of greater magnitude, and produce isotype switched antibody of higher affinity [98]. Memory cells are characterised by increased size relative to naïve cells, a cell surface phenotype that is $CD23^{-}CD80^{+}CD86^{+}CD95^{+}$, SHM of re-arranged immunoglobulin genes and a class switched BCR [98]. The majority of memory B cells arise from germinal centre dependent pathways, however, there is evidence of a distinct germinal-centre independent mechanism. Different subpopulations of memory cells are defined based on antigen exposure, expression of CD27, and the heavy chain isotype of their BCRs [99].

1.2.3.6 Plasma cells

Plasma cells are terminally differentiated B cells that secrete antibody. They can be subdivided into short-lived plasmablasts and long-lived plasma cells. Transition from a short-lived plasmablast to a long-lived plasma cell typically requires homing to the bone marrow niche. Differentiation of antibody-secreting cells from B cells is dependent on the transcription factors Blimp-1, IRF4 and Xbp-1. Plasma cells do not express traditional pan-B cell markers, but are characterised by the expression of CD138, CD78 and IL6R [100, 101].

1.3 The B cell receptor

1.3.1 Theories of B cell selection and antibody production

A defining feature of all B cells is the BCR. The concept of the BCR was first postulated by Paul Ehrlich in 1900 in his "side-chain theory of immunity"[33]. Ehrlich theorised that cells express "side-chains" (receptors) on their cell surface that were specific for an individual toxin. The binding of a toxin to a side-chain would activate a cell to produce more side-chains which would then bud-off from the cell into the bloodstream (in a manner analogous to antibody secretion) to neutralise the toxin [33]. While most of these remarkable insights hold true today, Ehrlich's theory was wrongly rejected at the time in favour of the "antigen-template theory" [102, 103] which predominated for the first half of the twentieth century [104-106].

In 1955 Niels Jerne proposed the "Natural Selection Theory" of antibody production. This theory returned to the principles expressed in Ehlrich's original theory, proposing that the specificity of all antibodies was encoded within the host [107]. This theory served as the inspiration for the "clonal selection theory". In 1957, David W Talmage [108] correctly proposed the cell as the basic unit of selection. Later in the same year Burnet published his definitive theory [109]. This theory proposed that each antibody producing cell expresses on its surface only a single specificity of receptor which is pre-determined by the host and when bound by its specific antigen secretes antibody of the same specificity. The theory explained the full range of immunological phenomena [110]. In 1958, Gustav Nossal and Joshua Lederberg generated the first definitive evidence for the theory when they showed that each B cell can produce only a single specificity of antibody [111]. This theory has served as a guiding principle of immunity to date [105, 106].

1.3.2 B cell receptor structure

The BCR, originally theorised over 100 years ago by Paul Ehrlich, has now been extensively studied. The BCR comprises a membrane spanning form of immunoglobulin (mIg) that does not possess any inherent enzymatic activity. It is, however, non-covalently linked to an Ig-αβ (CD79-αβ) heterodimer that contains immunoreceptor tyrosine-based activation motifs (ITAMs), which transduce downstream signalling when they are phosphorylated (Figure 1.1) [112].

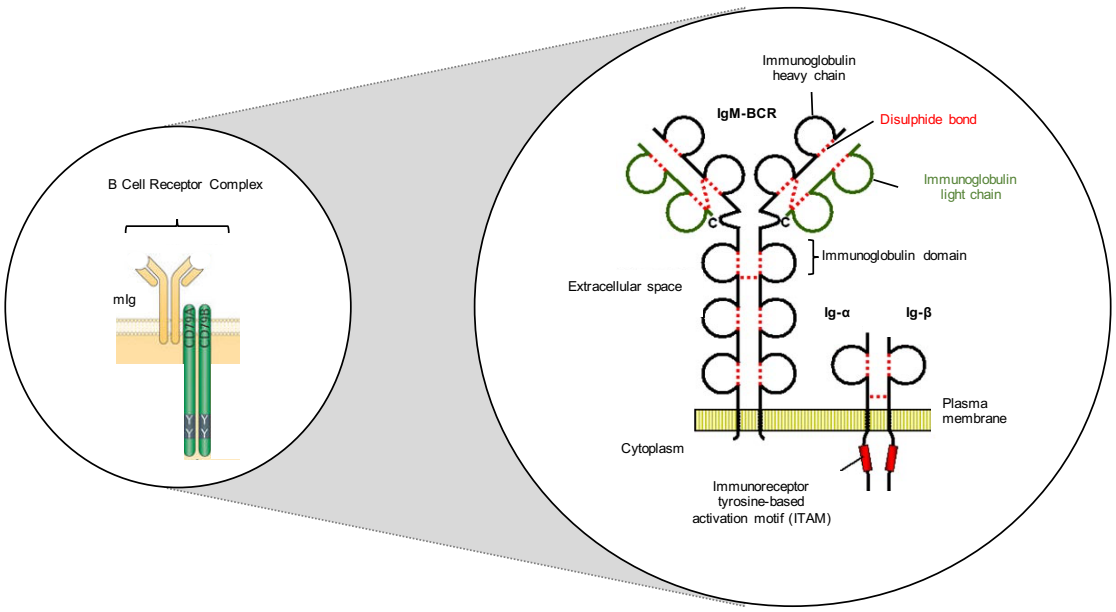

Figure 1.1 Structure of the B Cell Receptor Complex
Schematic (left) and detailed (right) structure of the IgM B Cell Receptor complex.

1.3.2.1 Membrane-bound immunoglobulin

Understanding of the structure of the membrane bound immunoglobulin has been based on landmark studies of the secreted immunoglobulin [113, 114]. Both proteins share similar structures and differ only in their C-terminal amino acid sequence [115].

An immunoglobulin consists of two heavy chains forming a covalently bound homodimer and two light chains each covalently bound to one of the heavy chains. There are five different classes of heavy chain: IgA, IgD, IgE, IgG and IgM. In humans, IgG is further sub classified into IgG1, IgG2, IgG3 and IgG4, and IgA into IgA1 and IgA2. There are two different classes of light chain: kappa and lambda. The heavy and light chains are each made up of variable and constant domains. The heavy chain is made up of one variable domain followed by different numbers of constant domains: 4 (IgM, IgE); 3 (IgG, IgA) and 2 (IgD). The light chain consists of one variable and one constant domain. All domains consist of between 70-120 amino acids and form immunoglobulin fold motifs which consist of two anti-parallel beta sheets between which a single disulphide bond forms [116].

Immunoglobulins have been studied by enzymatic digestion. Papain enzymatically digests the immunoglobulin into three fragments: two identical fragments responsible for antigen binding (Fab); and one fragment crystallisable (Fc) portion responsible for effector function. The Fab fragments mediate antigen binding using a pair of heavy and light chain variable domains. The most variable region of a Fab is formed from three CDRs, one of which corresponds to the VDJ junction. The Fc region is responsible for effector function and differs between antibody isotypes [116].

The different antibody isotypes differ in terms of their size, and their complement fixation and Fc receptor binding ability. IgM is expressed at high levels on naïve B cells and predominates during the early stages of an immune response. Natural IgM antibodies have low affinity but once secreted form a pentamer giving higher avidity. IgD is expressed at low levels on naïve cells and is co-expressed with IgM. It has a short half-life and its biological function remains unclear. IgG is the predominant class of immunoglobulin and

has a long half life. IgG can be sub-classified into multiple isotypes which differ in terms of their antibody flexibility, Fc receptor binding, ability to fix complement, disulphide bond structure and ability to cross the placenta. IgA is important in mucosal immunity and can exist as a monomer or dimer. IgE is important in responses to parasites, and allergy and hypersensitivity [116].

All BCR isotypes can exist as secreted or membrane bound forms. The membrane bound form is generated by alternative splicing of a primary transcript in which two exons (M3 and M4) are appended to the C4 exon and code for an extracellular spacer, transmembrane domain and cytoplasmic domain [115].

The transmembrane domain of the membrane bound immunoglobulin is the most conserved element of the molecule, both between immunoglobulin isotypes and across different species. It spans the membrane as an alpha helix. One side of the alpha helix is highly conserved and contains multiple hydrophobic residues which form the site of interaction between the mIg and Ig-αβ heterodimer. Expression of the polar motif (TTAST) present in the transmembrane region appears to signal intracellular retention of mIg unless associated with the Ig-αβ heterodimer, thereby ensuring only fully formed BCR complexes reach the cell surface [115].

The cytoplasmic domain of the mIg is short and varies between different isotypes: 3 amino acids (IgM, IgD), 14 amino acids (IgA) and 28 amino acids (IgG, IgE). They all start with KVK, apart from IgA. The sequence of the cytoplasmic domains is conserved for a given isotype across different species. IgM and IgD are expressed on naive cells whereas IgA, G and E are only expressed after class switching. This raises the possibility that the extended

cytoplasmic tail of IgA, IgG and IgE may be indicative of a specialised function in class switched activated B cells [115]. There is evidence that the cytoplasmic domain of IgG and IgA enhances high titre antibody memory responses. Deletion of the cytoplasmic domains of IgG1 or IgA, or exchange of the cytoplasmic domain of IgG1 for IgM failed to produce effective memory responses. [117, 118]. Furthermore, B cells expressing IgG show an enhanced response to antigen stimulation compared with those expressing IgM and/or IgD [119].

1.3.2.2 Immunoglobulin α/β heterodimer

The first evidence that the BCR was not just a mIg came from experiments undertaken in myeloma cell lines. Transfection of heavy chain constructs into the J558L myeloma cell line, which expresses only a light chain, resulted in assembly of BCRs within cells but not on the cell surface [120, 121]. This suggested other factors were required for cell surface expression. Subsequent biochemical analysis of a myeloma cell variant, J55Lμm3, which expresses BCR on the surface, found it to be associated with a disulphide linked heterodimer consisting of a 34 kDa and a 39 kDa glycoprotein [122, 123]. The genes encoding Ig-α and Ig-β were later identified from a B cell specific cDNA library produced by subtractive hybridisation against T cell RNA. This identified the Ig-α gene, mb-1[124, 125], and the Ig-β gene, B27 [126, 127], which are only expressed in B cells. All membrane bound immunoglobulin subclasses have subsequently been shown to associate with the same Ig-αβ heterodimer [115, 128].

Ig-α and Ig-β are both type-1 transmembrane proteins consisting of an extracellular Ig-like domain connected by a transmembrane domain to a cytoplasmic tail. Both proteins are

evolutionarily conserved and like the mIg the most highly conserved region is the transmembrane domain. The transmembrane domains is responsible for heterodimer formation, and, in the case of Ig-α, binding to the mIg [115]. Ig-α consists of a 109 amino acid extracellular domain, a transmembrane domain and a 61 amino acid cytoplasmic domain. The transmembrane domain contains polar amino acids on both sides of its α-helix for interaction with the transmembrane domain of the mIg on one side and Ig-β on the other. Ig-β consists of a 129 amino acid extracellular domain, a transmembrane domain and a 44 amino acid cytoplasmic domain. The transmembrane domain contains polar amino acids on one side only for interaction with Ig-α. Both Ig-α and Ig-β are heavily glycosylated [115].

The cytoplasmic domains of Ig-α and Ig-β each contain a single ITAM motif [129]. An ITAM motif is a conserved amino acid sequence corresponding to the sequence YxxI/Lx(6-12) YxxI/Lx. They exist in one or more copies in the cytoplasmic domain of immunoreceptors and immune cell adaptor molecules including the TCR, BCR and FcεRI receptor. They become transiently phosphorylated on triggering, creating docking sites for SH2 domain containing proteins, such as Syk, to transduce downstream signals [129, 130].

The stoichiometry of the BCR complex is one mIg to one Ig-α/β heterodimer. This model was originally proposed based on a combination of biochemical techniques including peptide tagging of Ig-α, blue native polyacrylamide gel electrophoresis (BN-PAGE) and biosynthetic labelling of B cells [131]. This has subsequently been confirmed by fluorescence microscopy in which the mIg and Ig-α were labelled with fluorescent probes and the ratio of fluorescence intensity analysed [132].

1.3.3 B cell receptor signalling

1.3.3.1 Signalling pathways

Antigen binding to the BCR initiates ITAM phosphorylation and activates a series of signalling pathways which lead to assembly of the signalosome, re-organisation of the cytoskeleton, internalisation of the BCR and presentation of antigen to T cells (Figure 1.2) [112].

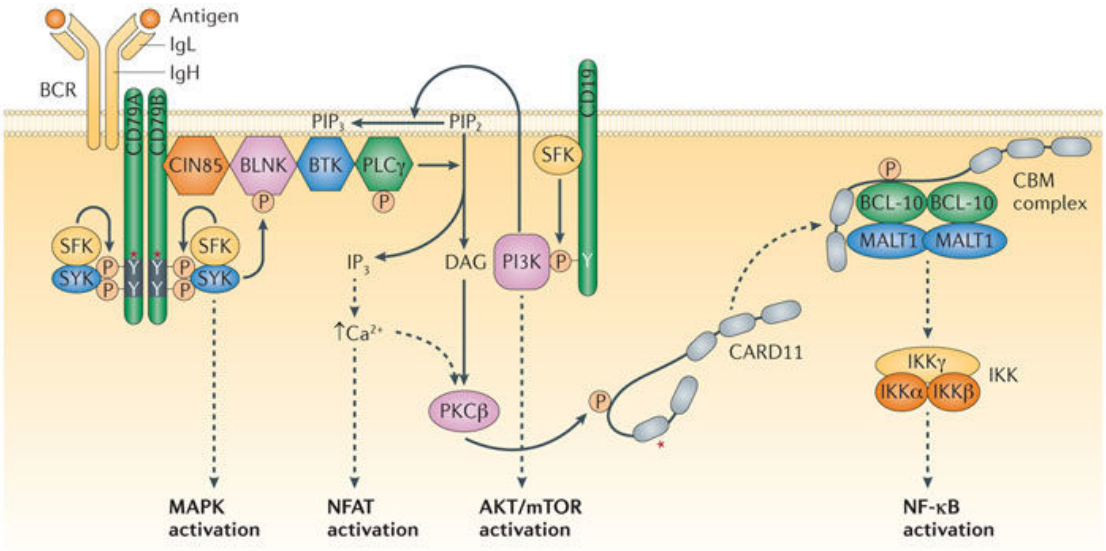

Figure 1.2 B Cell Receptor Signalling
Signalling pathways emanating from the B Cell Receptor (BCR) following activation. BLNK, B-cell linker protein; BTK, Bruton tyrosine kinase; CARD11, caspase recruitment domain-containing protein 11; CBM, CARD11–BCL-10–MALT1; CIN85, Cbl-interacting protein of 85 kDa; DAG, diacylglycerol; IKK, inhibitor of NF-κB kinase; IgH, immunoglobulin heavy chain; IgL, immunoglobulin light chain; IP3, inositol trisphosphate; MALT1, mucosa-associated lymphoid tissue lymphoma translocation protein 1; MAPK, mitogen-activated protein kinase; mTOR, mammalian target of rapamycin; NF-κB, nuclear factor-κB; NFAT, nuclear factor of activated T cells; PI3K, phosphoinositide 3-kinase; PIP2, phosphatidylinositol-4,5-bisphosphate; PIP3, phosphatidylinositol-3,4,5-trisphosphate; PKCβ, protein kinase Cβ; PLCγ, phospholipase Cγ; SFK, SRC family kinase. Adapted from [133].

The tyrosine residues within the ITAM motifs of Ig-α and Ig-β are phosphorylated by Src-family kinases, including Lyn [134]. Initial phosphorylation recruits more Lyn molecules via their SH2 domain leading to activation and additional phosphorylation [135]. Phosphorylation occurs asymmetrically with preferential phosphorylation of the membrane proximal tyrosine and only a fraction becoming doubly phosphorylated [136].

Phosphorylation of both ITAMs leads to recruitment of the cytosolic SH2 domain containing protein, Syk [137]. The binding of Syk to dually phosphorylated ITAMs and its phosphorylation by Lyn and/or its autophosphorylation leads to full activation [138]. Syk then phosphorylates neighbouring ITAMs generating a positive feedback loop in which there is more recruitment and activation of Syk. Thus, an initial signal generated by Lyn is amplified by Syk. Phosphorylated, activated Syk propagates signalling by phosphorylating downstream targets and acting as a docking site for other proteins (Figure 1.2) [138, 139].

Phosphorylated Syk interacts with the adaptor molecular, B cell linker protein (BLNK). BLNK acts as a molecular scaffold for the initiation of several different signalling pathways emanating from the BCR. Phospholipase Cγ2 (PLCγ2) binds to phosphorylated BLNK, localising it to the plasma membrane where it can access its substrate, phosphatidylinositol-4,5-bisphosphate ($PI(4,5)P_2$). $PI(4,5)P_2$ is hydrolysed by PLCγ2 generating the second messengers inositol trisphosphate (IP_3) and diacylglycerol (DAG), with an ensuing increase in intracellular calcium. DAG and increased intracellular calcium activate protein kinase C (PKC) which in turn activates the NFκB pathway via caspase recruitment domain-containing protein 11 (CARD11). DAG also regulates the mitogen-activated protein kinase (MAPK) pathway which can in addition be activated via Vav and Grb2/SOS association with phosphorylated BLNK. BCR triggering also activates the phosphoinositide-3-kinase (PI3K) pathway via Lyn mediated phosphorylation of CD19 which binds and recruits PI3K. The net outcome is that initial BCR-proximal events are converted into multiple signalling pathways (Figure 1.2) [133, 139].

1.3.3.2 Modulation of BCR signalling

Signals initiated by the BCR are not simple linear pathways but instead inputs are integrated from multiple receptor-associated accessory molecules and co-receptors [139]. Positive regulators of BCR signalling include CD19 [140, 141]. CD19 increases signalling by enhancing recruitment of Lyn, PI3K, Btk and Vav via either the CD21-CD81-C3d complex or direct association with the BCR [142]. Negative regulators of BCR signalling contain immunoreceptor tyrosine-based inhibitory motifs (ITIMs). These include CD22 and FcγRIIB. ITIM phosphorylation by Src family kinases such as Lyn allows the recruitment of SH2 domain containing protein tyrosine phosphatases, for example SHP1, facilitating downregulation of the B cell response. Lyn is therefore both a positive and negative regulator of B cell function [143]. CD45 is also a positive and negative regulator of BCR signalling, and is thought to be important for setting the threshold for triggering [144].

1.3.3.3 Propagation of B-Cell receptor signals

Following B cell receptor triggering the earliest observable event is the formation of microclusters. They consist of between 10-100 BCRs and are isotype specific. They were first identified by placing B cells onto antigen containing planar lipid bilayers and imaging using Total Internal Reflection Fluorescence (TIRF) microscopy and time lapse far field microscopy [142, 145]. The formation of microclusters is dependent on cytoskeletal re-arrangements [142]. Microclusters have been observed in Lyn deficient mice suggesting their formation occurs independent of BCR mediated signalling [146]. Fluorescence microscopy has shown the sequential recruitment of Lyn, Syk, Vav, BLNK and PLCγ2 to microclusters [146, 147].

A single microcluster is insufficient to trigger a B cell to full activation, but to reach the threshold for activation the signal must be amplified [146]. Early BCR microclusters trigger a re-organisation of the cytoskeleton which induces spreading of the B cell across the surface of the antigen containing surface generating a larger contact area for additional BCR/antigen interactions. The extent of spreading is dependent on the affinity, avidity and density of antigen and provides a means of selection. The cell then undergoes a more prolonged period of contraction, collecting all of the microclusters together in the central contact area. This process is dependent on CD19 [145].

The spreading and contraction of the B cell membrane results in the formation of the immunological synapse (IS). The IS was first described in T cells but was later observed in B cells [148, 149] and NK cells [150]. The structure consists of a bullseye arrangement of proteins. In the middle is the central supramolecular activation cluster (cSMAC) which contains the antigen bound receptors trafficked during the contraction phase. This is surrounded by the peripheral supramolecular activation cluster (pSMAC) which contains adhesion molecules and the phosphatases CD45 and CD148. The immunological synapse forms on a time scale greater than that needed for calcium signalling and therefore does not function as the signalling unit as initially assumed. The IS allows antigen internalisation and signalling termination [151]. The former is particularly important in B cells to allow antigen loading onto MHC class II molecules for presentation to T cells.

1.4 B Cell Receptor triggering: the key players

In order to consider BCR triggering in more detail, it is necessary to understand the key players in the process (Lyn, CD45, CD148), their distribution within the plasma membrane and the manner in which antigen is encountered in vivo. This will set the scene for a thorough analysis of current models of BCR triggering.

1.4.1 Balance of phosphorylation: Src kinases, CD45 and CD148

B cell activation is initiated following antigen binding to the BCR. This leads to an increase in the number and/or half-life of phosphorylated tyrosines within the ITAM motifs of the BCR complex. The key players in this process are the Src family kinases, including Lyn, and the protein tyrosine phosphatases, CD45 and CD148 [112]. A clear understanding of the structure, function and regulation of these proteins and the equilibrium that exists between them is essential to understanding the triggering problem.

1.4.1.1 Lyn

Src-family protein tyrosine kinases are a family of multidomain proteins. Each share a common domain structure: N-terminal SH4 domain, unique domain, SH3 domain, SH2 domain, linker, catalytic tyrosine kinase domain, and finally, a short C-terminal tail (Figure 1.3). Acylation of the SH4 domain localises Src-family kinases to the plasma membrane [152, 153]. Src-family kinases can exist in either an open/active or closed/inactive state. In the case of Lyn, transition between these states is controlled by phosphorylation of the inhibitory tyrosine, Y527 in the C-terminal tail, by Csk. Phosphorylated Y527 binds to the SH2 domain in an arrangement that is stabilised by binding of the SH3 domain to a PxxP motif in the linker sequence. This arrangement leads to displacement of a key glutamate

residue from the active site of the catalytic domain rendering it inactive. Conversion to the open/active state requires either dephosphorylation of the inhibitory tyrosine, Y527, a competing interaction for the SH2 domain by another phosphotyrosine, or phosphorylation of the activating tyrosine, Y416, in the catalytic domain. Y416 is required for full activation of Lyn (Figure 1.3) [153-155].

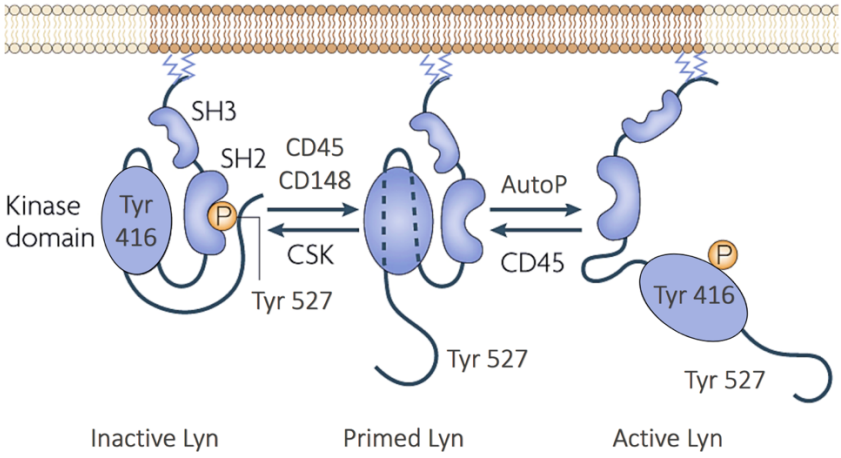

Figure 1.3 Structure and regulation of the Src-family kinase, Lyn
Lyn can exist in either an inactive (left), primed (middle) or active state (right). In the inactive state, the inhibitory tyrosine, Tyr 527, is phosphorylated and binds to the SH2 domain. This inhibitory arrangement is supported by binding of the SH3 domain to the linker region. Dephosphorylating of Tyr 527 (or completion for SH2 binding) releases Lyn from inhibition and primes it for activation. Full activation requires phosphorylation of the activation tyrosine, Y416. Adapted from [156].

1.4.1.2 CD45

CD45 is a receptor-type protein tyrosine phosphatase (RPTP). It is expressed on all nucleated haematopoietic cells at high levels (up to 10% of cell surface proteins). It is a type 1 glycoprotein consisting of a large extracellular domain, transmembrane domain and cytoplasmic domain containing tandem protein tyrosine phosphatase domains, one of which is inactive. The extracellular region contains variable domains generated by alternative splicing, a cysteine rich globular domain and three fibronectin type III domains. It is heavily glycosylated. Multiple isoforms exist resulting from alternative splicing. B cells express the highest molecular weight isoform, CD45 RABC [157].

CD45 deficiency leads to severe phenotypic and functional consequences in T cells, but in B cells the consequences are less severe [158-164]. CD45 deficient B cells develop normally up until the transitional 2 stage to mature follicular B cell step of maturation. This late developmental block leads to an accumulation of relatively immature $IgM^{high}IgD^{low}$ B cells, and accounts for the increased overall number of B cells seen in CD45 knock out mice [158-161]. This accumulation in IgM B cells may represent an impairment of constitutive signalling such that only B cells with sufficiently high BCR levels receive sufficient constitutive signals for survival [165]. This is supported by experiments in which the BCR repertoire is restricted by crossing CD45-/- mice with HEL specific mice. In this setting, soluble HEL does not induce anergy as would be expected in WT mice, but instead results in positive selection and accumulation of IgD^{high} cells indicated further maturation as a function of BCR signalling [166, 167]. In contrast, transgenic Ig^{HEL} CD45E613R mice, in which the CD45 is constitutively active has the opposing phenotype, with soluble ligand inducing deletion. These results support a model in which CD45 acts as a rheostat controlling the threshold for BCR signalling.

The regulatory effect of CD45 on Lyn has been examined in CD45 deficient mice. CD45 deficient mice are constitutively hyperphosphorylated at the C-terminal inhibitory tyrosine of Lyn. This is consistent with Y527 being the target for the phosphatase activity of CD45 [168-170]. However, in vitro kinase assays suggest Lyn is hyperactive in CD45 deficient cells. This finding can be reconciled with studies which show that the catalytic site tyrosine, Y416, is also hyperphorphorylated in CD45 deficient B cells [169]. CD45 is therefore proposed to be both a positive and negative regulator of Lyn by dephosphorylating both the inhibitory and activating tyrosine of CD45 with the latter effect being dominant. CD45

deficient mice do not phenocopy Lyn deficient mice, suggestion a role for another phosphatase, CD148.

1.4.1.3 CD148

CD148 is a second RPTP expressed by B cells. It consists of a large extracellular domain made up of 8-9 fibronectin domains and 34 potential N-glycosylation sites [171]. The intracellular domain contains a single protein tyrosine phosphatase domain whose function is critically dependent on a cysteine residue [172]. CD148 is expressed not just in cells of the haematopoietic system but also in epithelial cells and fibroblasts [173-175]. CD148 expression differs between humans and mice. In mice it is predominately expressed on platelets, B cells and myeloid lineage cells with limited expression on T cells. However, in humans CD148 is additionally expressed on thymocytes, T cells, macrophages, NK cells and certain DC populations [157].

Three attempts have been made to generate CD148 deficient mice. In an initial experiment deletion of the phosphatase domain led to embryonic lethality due to defects in vascular development [176]. Deletion of exons 3, 4 and 5 led to healthy viable mice but no further analysis of immune function was undertaken [177]. In a third experiment, the transmembrane domain was deleted generating a cell line that lacked CD148 phosphatase activity at the cell surface, but continued to express soluble truncated CD148. These mice were an almost complete phenocopy of CD45 deficient mice implying high functional redundancy between CD45 and CD148 [178]. CD45/CD148 doubly deficient mice have defects not seen in singly deficient mice: a severe B cell development block, impaired calcium flux, impaired protein tyrosine phosphorylation and diminished MAP kinase activation. Significantly, CD148 and CD45 were both required to optimally

dephosphorylate the inhibitory C-terminal tyrosine of Lyn, implicating both as positive regulators of Lyn [178].

The interplay between Lyn, CD45 and CD148 in BCR triggering serves to highlight the critical importance that the balance of phosphorylation plays in BCR triggering. It is noteworthy that the ratio of expression of CD45 and CD148 varies between different B cell subsets [179] implying potentially unique roles in given subsets. To this end, CD148-deficient mice have severely impaired TI antibody responses. This is compatible with the high levels of CD148 expressed on B1 cells and a unique role for CD148 in the control of BCR signalling by Lyn exclusively in these cells [180]

1.4.2 The nanoscale organization of the B cell membrane

Thus far, the structure and function of the BCR, Lyn, CD45 and CD148 have been considered in relative isolation. However, it is necessary to consider them within the correct biological context of the cell surface. It is important to realise that the location of any protein within the plasma membrane per se puts important constraints on its behaviour. Diffusion is limited to 2D/lateral diffusion meaning affinities need to be considered as 2D K_d rather than classical 3D K_d parameters. Diffusion within the plasma membrane is determined by protein density, lipid viscosity, extracellular protein size and intracellular interactions. This limits diffusion by 10-100 fold versus in solution. However, while proteins are able to diffuse their orientation is relatively well preserved, which likely enhances interactions. Proteins are restricted in tilt by 10° and move axially versus the plane of the membrane by 5Å [181].

The classic model of the plasma membrane is the "fluid mosaic model" proposed by Singer and Nicolson [182]. This model proposes that the membrane is a phospholipid bilayer incorporating various lipids and proteins which are able to freely diffuse. However, subsequent evidence has clouded this view of the plasma membrane by suggesting the membrane can be divided into ordered and disordered phases. This is embodied in the concept of distinct membrane sub-compartments which limit lateral heterogeneity at the sub-micrometre level [183], referred to as the lipid raft model [184]. Evidence for the lipid raft model comes mostly from model membranes. To date, direct evidence for their existence in vivo is inconclusive, and if lipid rafts do exist it is at a lower spatial resolution than nanometers and timescale of milliseconds [183]. A potential role for lipid rafts has nevertheless been proposed for B-cell receptor triggering. Lipid rafts are argued to concentrate Lyn and compartmentalise it from the BCR and other negative regulators. Upon crosslinking, the BCR is proposed to transiently associate with lipid rafts and Lyn leading to phosphorylation and signalling [185-187].

The diffusion of proteins within the plasma membrane is also proposed to be restricted by the underlying cytoskeleton [188]. Some transmembrane proteins have domains to connect them directly to the cytoskeleton [189] while the free movement of other proteins is indirectly restricted by the cytoskeleton[190]. Single molecule tracking experiments on fibroblasts showed that proteins were free to diffuse within a confined area of circa 30-700 nm. While long range diffusion was possible, it required molecules to skip between adjoining confinement zones. These experiments led to the "Picket-Fence" theory in which transmembrane proteins are limited in diffusion to a defined area but are able to pass between areas separated by pickets where diffusion is slowed [190-193].

The cytoskeleton has also been implicated in BCR triggering. BCR diffusion is reduced in areas of actin and disruption of the actin cytoskeleton appears to be sufficient to induce signalling [188]. Furthermore, the BCR has been shown to be confined by an ezrin-defined actin network which controls diffusion and signalling in the resting state and following antigen induced activation [194]. In support of a role for the cytoskeleton in BCR activation is the observation that mutations in cytoskeletal regulators are associated with antibody deficiency syndromes in humans [195].

1.4.3 Mechanism of antigen encounter

In considering the mechanism by which B cells are triggered by antigen it is important to understand the exact spatiotemporal context in which antigen encounter occurs. The great diversity of antigen and large repertoire of B cells means that the likelihood of an encounter by chance is extremely low. To facilitate this process interactions occur within secondary lymphoid organs (lymph nodes and the spleen). Secondary lymphoid organs are well supplied with the two key elements: B cells and antigen [196, 197]. Antigen can be detected in secondary lymphoid organs within minutes of subcutaneous injection [198]. There is not a single mechanism for antigen encounter but instead multiple mechanisms exist to facilitate this interaction dependent on the nature and size of the antigen and the cellular location [112].

Small soluble low-molecular-mass antigens of <70 kD may gain access to B cells in the follicle directly. This is proposed to occur by diffusion through pores in the subcapuslar sinus [199]. However, the evidence for these pores is controversial and even if they exist they only provide a mechanism for entry of small antigens. An alternative explanation

suggests that small antigens can enter via a conduit system [200]. The other means of presentation of antigen to B cells is by other cells. These include macrophages [201-205], dendritic cells [206, 207], follicular dendritic cells [208-210] and B cells themselves. Visualisation of the spatiotemporal dynamics of antigen presentation in vivo using multiphoton microscopy has shown that the predominant mechanism of presentation of antigen to B cells is cell mediated [142, 211, 212]. The threshold of antigen required to trigger B cells is higher for soluble antigen than membrane bound antigen, suggesting the latter is a more effective trigger for B cells [142, 148, 211, 213, 214]. Thus, any mechanism of triggering must reflect the ability of B cells to respond predominantly to membrane bound antigens.

1.5 B-cell receptor triggering: an unsolved problem

It is clear that much is known about the structure of the BCR and the signalling pathways activated by the receptor. However, what remains unresolved is how antigen binding by the BCR results in phosphorylation of the ITAMs of the Ig-αβ heterodimer, i.e. BCR triggering. A number of models of BCR triggering have been proposed to tackle this problem.

1.5.1 The cross-linking model

The cross-linking model is the original model of BCR triggering. It proposes that in the resting, non-antigen bound state the BCR is a bivalent complex (a single BCR with two antigen binding sites). Signalling occurs when two or more BCRs are brought into close proximity *i.e.* cross-linked by a multivalent ligand (Figure 1.4) [215].

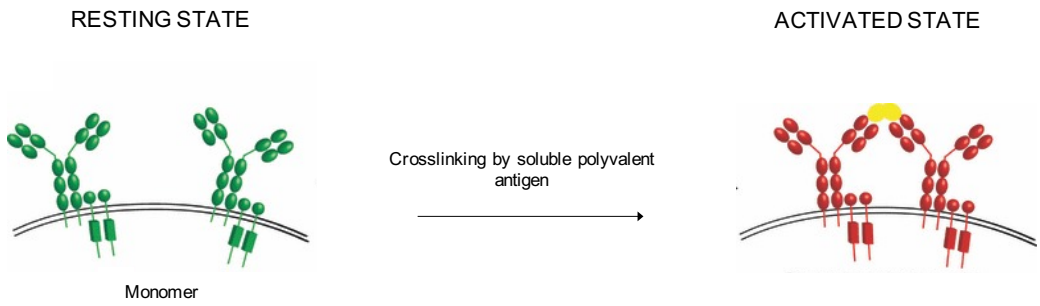

Figure 1.4 The Cross-Linking Model
Schematic diagram of the cross-linking model of B Cell Receptor (BCR) triggering. In the resting state, the BCR is monomeric and inactive (green BCR). Antigen binding by a multivalent ligand leads to receptor clustering and activation (red BCR). Adapted from [216].

The cross-linking model was based on early work demonstrating that bivalent anti-BCR antibodies or F(ab)′$_2$ fragments could activate B cells, whereas monovalent Fab fragments could not [217-221]. Further work supported this viewpoint by demonstrating that soluble multivalent antigens but not soluble monomeric antigen were able to activate B cells [222-224].

While crosslinking can undoubtedly activate B cells it remains unclear if this is the quintessential triggering model. The BCR must be capable of responding to a vast array of antigens. This presents a challenge to the cross-linking model, as not all antigens would be expected to crosslink the BCR in precisely the same way [225]. Furthermore, B cells predominantly encounter antigen that is not soluble, but membrane bound, and in this scenario monovalent antigen is able to activate B cells [203, 204, 226-228]. Thus, if monovalent antigen is able to activate B cells then by definition it must do so by a method other than cross-linking. This has led to the development of alternative models.

1.5.2 Conformation-induced oligomerisation model

The conformation-induced oligomerisation model proposes that in the resting, non-antigen bound state the BCR is a bivalent complex. Antigen binding to the BCR induces a conformational change, exposing a previously hidden Cμ4 clustering domain. This clustering interface promotes receptor oligomerisation and opening of the cytoplasmic domains for initiation of downstream signalling (Figure 1.5) [229].

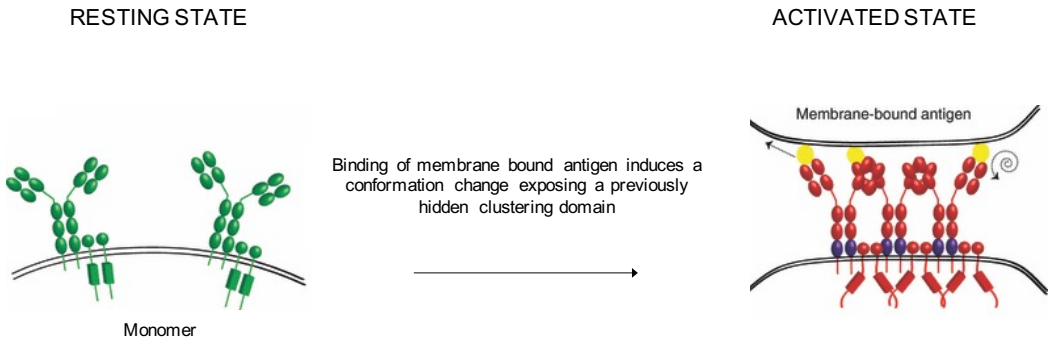

Figure 1.5 The Conformation-Induced Oligomerisation Model
Schematic diagram of the conformation induced oligomerisation model of B Cell Receptor (BCR) triggering. In the resting state, the BCR is monomeric and inactive (green BCR). Antigen binding induces a pulling or twisting force (arrows) leading to a conformational change. This exposes a previously hidden Cμ4 clustering domain (purple) leading to oligomerisation and opening of the cytoplasmic domains for the initiation of downstream signalling (red BCR). Adapted from [216].

The conformation induced oligomerisation model is based on the results of Förster resonance energy transfer (FRET) studies [132], single particle tracking experiments [230], and mutational analysis [230].

B cell lines were engineered expressing BCRs in which a FRET donor or acceptor was attached to the cytoplasmic domain of Ig-α to report on interactions between BCRs. On resting B cells no inter-BCR FRET was detected implying it was a monomer. However, when cells were activated by membrane associated antigens there was an increase in inter-BCR FRET interpreted as oligomerisation. The FRET signal exhibited an initial rise on

cell activation followed by a decrease that was sustained above background. The interpretation of these results was that on clustering the extracellular domains of the BCR remain in close proximity but the cytoplasmic domains undergo initial clustering followed by a conformation change (akin to the opening of an umbrella) possibly to allow downstream signalling. The conformation change on antigen binding correlated with the initiation of signalling and did not occur in the presence of PP2, suggesting continued phosphorylation of the ITAMs was necessary to maintain the open conformation [132].

Further evidence for the conformation-induced oligomerisation model comes from single molecular tracking of BCRs using TIRF microscopy [230]. BCRs were labelled with fluorescently tagged Fab fragments and their diffusion monitored in the presence or absence of membrane associated antigen. In the absence of antigen, 82% of BCRs were mobile with their short-range movement consistent with free diffusion. In the presence of antigen, BCRs remained highly mobile outside antigen clusters but showed a high probability of stopping once they encounter an antigen cluster. Similar results were obtained with monovalent and polyvalent antigen excluding cross-linking as the mechanism of oligomerisation [230].

In order to identify the oligomerisation domain BCR mutants were produced in which various parts of the mIg were deleted. Deletion of the membrane proximal Cμ4 domain resulted in failure of oligomerisation and signalling, while Cμ4 domains alone clustered spontaneously and led to B cell activation. Thus, it was concluded that this Cμ4 domain was not only the clustering domain, but that it was normally hidden by neighbouring domains preventing oligomerisation in the resting state. This domain must be exposed on

antigen binding to allow oligomerisation, and this was proposed to be induced by a conformational change [230].

The main unresolved issues for the conformation-induced oligomerisation model is how the conformational change induced by antigen binding is transduced (a) from the antigen binding region to Cμ4, and (b) through the membrane to the intracellular domain. Any conformational change would especially need to be transmitted through the flexible hinge of the BCR. Crystal structures of antibody bound to antigen also show no evidence of an allosteric conformational change [231].

1.5.3 Dissociation activation model

The dissociation activation model is an alternative, mutually exclusive, theory of BCR triggering. This proposes that in the resting, non-antigen bound state the BCR is an oligomer, which is auto-inhibitory. Antigen binding promotes dissociation of BCR oligomers and exposure of the previously hidden intracellular ITAM to enable downstream signalling (Figure 1.6) [232].

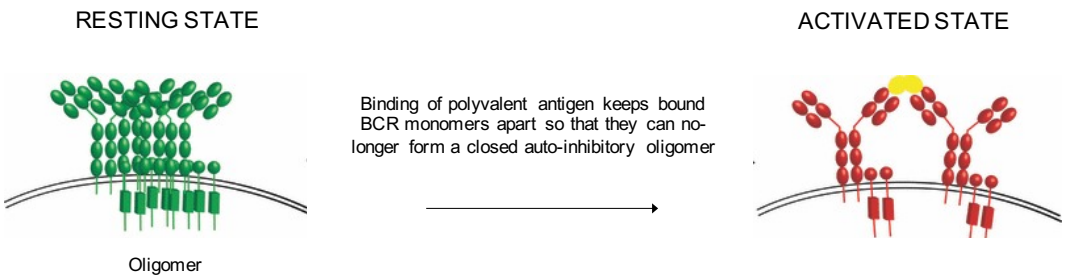

Figure 1.6 The Dissociation Activation Model
Schematic diagram of the dissociation activation model of B Cell Receptor (BCR) triggering. In the resting state, the BCR forms auto-inhibitory oligomers (green BCR). Antigen binding promotes dissociation of receptor oligomers and exposure of previously hidden intracellular ITAMs to enable downstream signalling (red BCR). Adapted from [216].

A key prediction of the dissociation activation model is that in the resting state the BCR is that of a preformed oligomer. Evidence for this comes from BN-PAGE. Under minimal detergent lysis conditions the BCR of both IgM and IgD isotype run as large macromolecules. These oligomers are class specific. [233]. These results were interpreted as implying the BCR exists as a pre-formed oligomer, however, such techniques leave open the possibility of artefacts arising from the lysis process, and the tendency of the hydrophobic parts of membrane proteins to mediate aggregation.

The dissociation activation model is, however, supported by evidence from quantitative biflouresecent complimentary assays (BiFCs). S2 *Drosophila* Schneider cells were used as a host to rebuild the BCR in which the cytoplasmic domains of the Ig-α chain contained either the N- or C-terminal half of a fluorescent protein. On resting cells, fluorescence was detected indicating the presence of clusters and interpreted as an intrinsic ability of BCRs to form oligomers in resting cells. The observed oligomers were concluded to be the resting, inactive state of the BCR as mutations that resulted in the failure of oligomerisation increased signalling and antigen internalisation [232]. Further evidence for this model was obtained using another biochemical assay, the high resolution proximity ligation assay (PLA). Plus and minus oligonucleotides for annealing were attached to Fab fragments directed against the constant region of the IgM BCR followed by rolling circle amplification and detection by fluorescence coupled oligonucleotides. This study showed a reduction in PLA signal on antigen encounter, once again suggesting B cell activation is accompanied by opening of tightly packed BCR oligomers as predicted by the dissociation activation model [234].

The dissociation activation model has the advantage that it can account for the vast array of antigens that activate B cells as it does not require that they be bound in a specific orientation but only that they are able to hold receptor monomers apart. However, the main evidence for this model comes from the biochemical assays, BiFC and PLA, which have the drawback of potentially stabilising random collisions rather than reporting only true associations.

1.5.4 Collision-coupling model

The collision-coupling model proposes that in the resting state the BCR forms nanoclusters which are confined by the actin cytoskeleton, relatively immobile and segregated from co-receptors and activating kinases. Conversion to the activated state involves alteration of the actin cytoskeleton such that the BCR is unconfined and more mobile, allowing it to encounter co-receptors and activating kinases (Figure 1.7)[235].

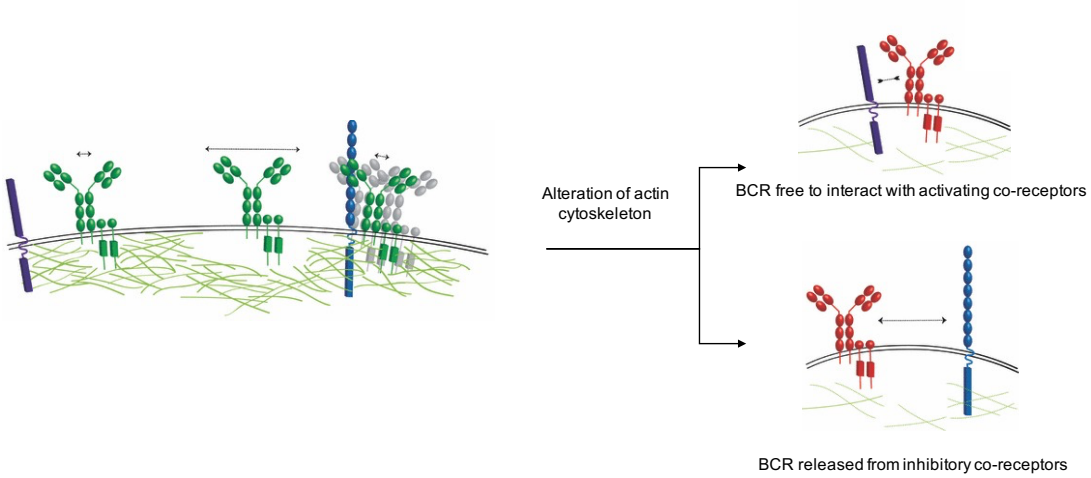

Figure 1.7 The Collision-Coupling Model
Schematic diagram of the collision-coupling model of B cell activation. In the resting state, the BCR is confined by the actin cytoskeleton (green BCR), clustering the BCR with negative co-receptors (blue) or segregating if from positive co-receptors (purple). Antigen binding leads to changes in the actin cytoskeleton and an increase in BCR diffusion (red BCR). This releases the BCR from inhibitory interactions (blue) and enables it to interact with activating co-receptors (purple). Adapted from [216].

The collision-coupling model is based on results obtained by advanced fluorescence microscopy. Direct stochastical optical reconstruction microscopy (dSTORM) revealed that resting B cells display nanoscale membrane organisation with the BCR arranged in preformed clusters. Upon stimulation, a convergence of receptors and co-receptors on a local level was observed [236]. These results are consistent with single particle tracking TIRF microscopy experiments in which restricted steady state diffusion of the BCR was detected in areas of the actin cytoskeleton. Disruption of the actin skeleton was sufficient to increase BCR diffusion and induce signalling that originated from the BCR itself. Signalling strongly correlated with changes in BCR diffusion, in particular with a reduction in the proportion of very slowly diffusing (or immobile) BCRs [188].

The collision-coupling model proposes that in the resting state the BCR exists in preformed nanoclusters, but the stoichiometry of the BCR within these clusters is not specified. The model provides a framework for understanding the potential mechanism of BCR signal propagation following triggering but does not explain how this triggering occurs. It cannot, therefore, be considered to be a triggering model.

The concept of a pre-clustered BCR identified by dSTORM would appear to ostensibly give evidence to the dissociation-activation model. However, the choice of surface for such experiments is critical. Experiments conducted on Poly-L-lysine (PLL) have suggested receptors and signalling proteins cluster by default on the surface of resting cells [237]. The results obtained in these experiments were analogous to those observed for B cells landing on anti-MHC class II coated cover slips. [236]. It is therefore possible that the results observed using dSTORM represent the activated, rather than resting state of the BCR.

This interpretation may explain why only a local convergence of receptors was seen upon B cell activation in these experiments without any dramatic global reorganisation, potentially because the cells had already been activated by the surface

1.5.5 Kinetic Segregation model

The kinetic segregation (KS) model is an alternative theory of receptor triggering. This model was originally proposed to account for TCR triggering. It proposes that in the resting, non-antigen bound state the receptor is free to diffuse through the membrane interacting with kinases and phosphatases but generating no net signal. Antigen binding traps the BCR within the close contact zone, from which bulky phosphatases are excluded but smaller kinases continue to diffuse freely. The balance is therefore switched in favour of phosphorylation in the close contact zones and signalling ensues. Ligand discrimination is based on the half-life of receptor/antigen interactions and the time spent by the receptor within the close contacts (Figure 1.8) [238, 239].

The KS model has yet to be studied in B cells but it has been studied extensively in T cells. Evidence for the KS model in T cells comes from a number of key experimental findings: (1) the extracellular domain of CD45 is rigid and extends beyond the distance spanned by TCR-ligand complexes allowing it to be sterically excluded upon TCR/ligand engagement [240]; (2) the exclusion of CD45 and CD148 has been visualised during contact formation in the IS [241, 242], microclusters [243], close-contacts [240] and a giant unilamellar vesicle systems [244]; (3) triggering is dependent on the dimensions of the peptide/MHC ligand [245, 246]; (4) truncating the extracellular domains of CD45 and CD148 quenches signalling by allowing these molecules to enter close contacts [240, 247, 248]; (5) increasing

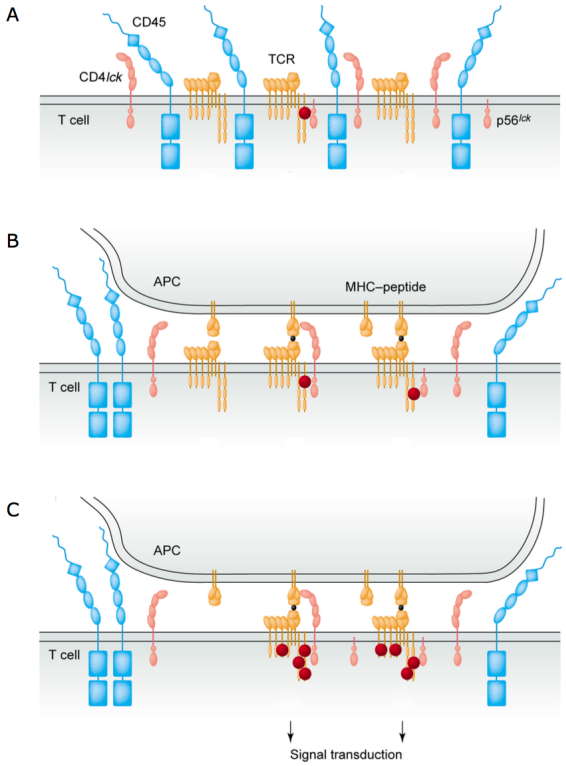

Figure 1.8 The Kinetic Segregation Model
Schematic diagram of the kinetic-segregation (KS) model of T cell receptor (TCR) triggering. (A) In the resting state, the TCR (orange) is free to diffuse through the membrane interacting with Lck (red) and CD45 (blue) but generating no net signal. (B) MHC:peptide(orange) binding to the TCR creates close contact zones from which CD45 is excluded. Lck is free to diffuse within the close contact zone and phosphorylate the TCR. (C) Ligand discrimination is based on the half-life of receptor:antigen interactions and the time spent within close contacts to allow recruitment of co-receptors and downstream signalling proteins. Adapted from [239].

the extracellular size of proteins, for example, fusing the extracellular domain of CD45 to Lck, is sufficient to affect distribution in close-contacts [240]; (6) surface bound TCR ligands are more effective in inducing triggering than soluble ligands [249-251]; (7) TCR triggering driven by engineered TCRs occurs most potently when they engage a membrane proximal epitope on the target cell [252, 253]; and (8) T cells can be triggered in a ligand independent manner by inducing artificial close-contacts, an important result because all other theories of signalling require the ligand to alter the state of the receptor, e.g. through conformational changes or oligomerization [240].

The BCR presents a challenge to the KS model since it is a much larger molecule than the TCR and can bind antigen with a much higher affinity. On the other hand, the balance of phosphorylation is known to be critical to B cell activation [254]. In contrast to T cells, B cells co-express the phosphatases CD45 and CD148. These phosphatases are developmentally regulated and have been shown to be important in BCR signalling [178]. Furthermore, B cells express larger quantities of the very large phosphatase CD148 and express the largest isoform of CD45ABC, which would theoretically allow passive exclusion from close contact zones despite the extra size of the receptor, assuming that antigens are presented in the form of relatively small complexes [247].

The evidence presented highlights the uncertainty that remains regarding the exact mechanism of BCR triggering. A thorough understanding of these early events in B cell activation is necessary for a comprehensive understanding of the B cell immune response and what constitutes immunogenic and tolerogenic antigens. Understanding BCR triggering has significant potential clinical implications. Abnormal B cell activation can result in autoimmune diseases, hypersensitivity and lymphoid cancer. The ability to manipulate the triggering mechanism therefore also has implications for possible drug design. Furthermore, full utilisation of the B cell response could be harnessed to optimise immunity induced by vaccination.

1.6 Aims of this thesis

The overarching aim of this thesis is to gain a more detailed understanding of the actual triggering mechanism of the BCR. The initial focus will be on generating a set of reagents (Chapter 3) which will then be used to:

1. Test the cross-linking model by assessing the ability of monomeric and multivalent ligand to trigger the BCR in solution and at a surface (Chapter 4).
2. Test the conformation-induced oligomerisation model against the dissociation-activation model by establishing the stoichiometry of the BCR in the resting state (Chapter 5).
3. Test the KS model by establishing if calcium triggering and close contacts formation is dependent on the size of the extracellular region of the phosphatase and the dimensions of the BCR/antigen complex. The latter will also test the conformation-induced oligomerisation model since this should be unaffected by BCR/antigen complex size (Chapter 6).

Chapter 2

General Materials and Methods

2.1 Molecular cloning methods

2.1.1 General cloning overview

Standard molecular biological techniques were utilised for the experiments outlined in this thesis [255]. To generate proteins of interest within a target cell line expression vectors were generated containing the relevant gene. Genes were first amplified from plasmid or cDNA using appropriately designed 5' and 3' oligonucleotide primers incorporating restriction enzymes sites. Polymerase chain reaction (PCR) products and associated vectors were digested with the appropriate restriction enzymes, purified to obtain fragments of the correct size and ligated to form a continuous vector. The ligation product was then used to transform chemically competent bacteria. Bacteria incorporating the vector were selected by antibiotic resistance and screened for incorporation and orientation by colony PCR. Positive colonies were used to prepare larger quantities of DNA. The nucleotide sequence was confirmed by DNA sequencing.

2.1.2 Vectors used in this thesis

pHR

The pHR-SIN-CSGW (pHR) vector is a lentiviral vector derived from the human immunodeficiency virus genome. The gene of interest is expressed under the control of the spleen focus forming virus (SFFV) promotor and includes an additional woodchuck hepatitis virus posttranscriptional regulatory element (WPRE) enhancer at the 3' end. The vector confers resistance to ampicillin in bacterial cells.

pHRI

The pHRI vector is identical to the pHR vector but the promotor is changed to the ecdysone inducible promoter, E/GRE. This promotor requires the activity of the nuclear factors RXR and FB-ERV (together with ponasterone) for optimal protein expression. These are not present in any of the target cells used in this study and hence this vector gives low expression levels.

pHR-U6-CMV-DsRed

This is a variant of the pHR vector. It allows expression of short hairpin RNA (shRNA) under the control of a U6 promoter. Discosoma species red fluorescent protein (DsRed) is expressed under the control of a CMV promoter to allow selection.

LentiCRISPRv2

This is a lentiviral vector used for CRISPR/Cas9 mediated gene editing. It contains the Streptococcus pyogenes Cas9 nuclease together with restriction sites that allow insertion of a single guide RNA. The vector confers resistance to ampicillin in bacterial cells and puromycin in mammalian cell culture [256].

pOPINEE12G

This expression vector is used for stable transfection of the Chinese hamster ovary (CHO)-K1 cell line. The gene of interest is cloned upstream of an internal ribosome entry site (IRES) and green fluorescence protein (GFP) reporter, both of which are under the control of the human cytomegalovirus (hCMV) promoter. The vector confers resistance to penicillin in in bacterial cells. The SV40 promoter-driven glutamine synthetase allows selection via glutamine metabolism [257].

2.1.3 Molecular Biological Methods

RNA extraction

RNA was extracted from cells of interest using the TRIzol (Invitrogen) RNA extraction method. Cells were spun down and re-suspended in residual media and 1 ml of TRIzol added per 5-10 x 10^6 cells followed by repetitive pipetting to induce cell lysis. The homogenised sample was then incubated at room temperature for 5 minutes. 0.3 mls of chloroform was then added per 1 ml of TRIzol originally used. Samples were shaken vigorously by hand for 15 seconds, incubated at room temperature for 2-3 minutes and then centrifuged at 4000 revolutions per minute (rpm) for 30 minutes at 4 °C. The RNA in the top (colourless) aqueous phases was removed and transferred to a fresh Eppendorf tube while the phenol waste was disposed of according to local guidelines. 0.5 ml isopropyl alcohol was then added to the aqueous phase per 1ml TRIzol originally used, mixed and incubated for 10 minutes at room temperature, followed by centrifugation at 4000 rpm for 30 minutes at 4 °C. The supernatant was then discarded, the pellet washed with 1 ml 75% ethanol per 1 ml of TRIzol originally added and vortexed. The samples were then centrifuged at 4000 rpm for 15 minutes at 4 °C, the ethanol removed and then centrifuged again for 5 minutes before removing any residual ethanol. The RNA pellet was finally re-suspended in an appropriate volume of MilliQ and the purity checked spectrophotometrically. All RNA preparation steps were conducted using RNase-free equipment.

cDNA preparation

Prior to cDNA preparation any contaminating genomic DNA was removed by treating total RNA with DNase and incubating with ethylenediaminetetraacetic acid (EDTA) for

10 minutes at 65 °C. cDNA was then prepared using random priming. The reaction mixture was prepared as outlined below and incubated at 25 °C for 10 minutes, 43 °C for 50 minutes and 70 °C for 15 minutes. The integrity of cDNA was checked by PCR for actin. All cDNA preparation steps were conducted using RNase-free equipment.

	Volume (µl)	Concentration	Company
Total RNA	10	500 ng/ µl	
Random hexamers	1	50 µM	Invitrogen
dNTP	1	10 mM	Bioline
Reverse Transcriptase buffer	2	x10	Invitrogen
Superscript II™ Reverse Transcriptase	0.25	200 U/µl	Invitrogen
Mg^{2+}	2	50 mM	Invitrogen
Dichlorodiphenyltrichloroethane (DDT)	2	0.1 mM	

Polymerase chain reaction

Genes were amplified from plasmid or cDNA templates using PCR. Oligonucleotide primers were designed with appropriate restriction enzyme sites at the 5' and 3' ends to allow subsequent cloning into the appropriate vector. For most PCR reactions, the following mixture was used.

	Volume (µl)	Concentration	Company
HF DNA polymerase buffer	4	x 5	NEB
dNTP	1	10 mM	Bioline
Template DNA	1	100 ng/µl	
5' primer	1	10 µM	Sigma-Aldrich
3' primer	1	10 µM	Sigma-Aldrich
Fusion	0.25	5 U/µl	NEB
MilliQ	11.75		

Reactions were carried out in a Bio-Rad T100 Thermal Cycler using the following settings.

		Temperature (°C)	Time
1	Enzyme activation	98	1 minute
2	DNA denaturation	98	10 seconds
3	Primer annealing	55	30 seconds
4	Extension	72	1minute/kb
5	Repeat stages 2-4		x 19
6	Final extension	72	5 minutes
7	Cooling	10	Infinity

To create chimeric proteins a two-step protocol was used. Each fragment of DNA was first amplified separately with complementary overlapping ends (of approximately 15-20 base pairs). The two overlapping products were then joined together by chimera PCR according to the protocol outlined above except that the number of repeat cycles was reduced to 15. For PCR reactions in which amplification of the desired product was problematic the annealing temperature was varied between 45-65 °C and/or dimethyl sulphoxise (DMSO) was added to the reaction mixture to a final concentration of 1-5%. Desired PCR products were separated by agarose gel electrophoresis.

Agarose gel electrophoresis

Agarose gel electrophoresis was used to separate DNA on the basis of size for visualisation and purification. Molecular grade agarose was mixed with TBE (Tris/Borate/EDTA buffer, Sigma-Aldrich) to achieve the desired concentration. The mixed was then heated in a microwave for 90 seconds per 75 ml until dissolved. The mixture was then cooled and ethidium bromide (Sigma-Aldrich) added to a final concentration of 0.5 μg/ml. Agarose gels were cast into Flowgen Bioscience gel tanks with combs of the appropriate size and allowed to set. Samples were mixed with x 10 agarose gel loading buffer (40% w/v sucrose, 0.25 % bromophenol blue) and added to the wells. A Bio-Rad powerpack was used to

electrophorese the samples at 70 mA for 45-60 minutes. Post electrophoresis DNA was visualised with ultraviolet (UV) light using a Gel Doc XR+ (Bio-Rad) and analysed with Image Lab (Bio-Rad). If extraction of DNA was required DNA was excised using a clean scalpel under low-UV irradiation. DNA was subsequently extracted using a Gel Extraction Kit (Qiagen) following the manufacturer's instructions.

Restriction enzyme digest

Enzymatic cleavage of PCR products or vectors at defined restriction sites was undertaking by incubating DNA with the appropriate restriction enzyme. Up to 1 µg DNA was digested according to the following reaction mixture.

	Volume (µl)	**Concentration**	**Company**
DNA		Up to 1 µg total DNA	
Restriction enzyme	2	5 U/ µl	NEB
Restriction enzyme buffer	5	x 10	NEB
MilliQ	To 50		

In the case of a double digest 2 µl of each enzyme was added and the amount of MilliQ reduced accordingly. The choice of restriction enzyme buffer for double digests was determined by the highest enzymatic activity for both enzymes within a given buffer. Samples were digested for 60 minutes (or 15 minutes in the case of High Fidelity enzymes) at the temperature recommended by the manufacturer. Post restriction enzyme digest, samples were purified by either agarose gel electrophoresis or using a PCR purification kit (Qiagen).

Dephosphorylation of 5'-ends of DNA

Dephophosporylation of 5' ends of vector DNA with antarctic phosphatase was undertaken to prevent re-ligation and hence decrease vector background during cloning. Up to 1 pmol of DNA ends was dephosphorylated using the following reaction mixture.

	Volume (µl)	**Concentration**	**Company**
DNA	1-5	Variable	
10x antarctic phosphatase buffer	2	x 10	NEB
Antarctic phosphatase	1	5 U/µl	NEB
MilliQ	To 20		

The reaction mixture was incubated at 37 °C for 15 minutes in a Bio-Rad T100 Thermal Cycler. To stop the reaction the mixture was heat inactivated at 80 °C for 2 minutes.

Ligation

Digested DNA was ligated into the desired cut plasmid using the following reaction mixture.

	Volume (µl)	**Concentration**	**Company**
Insert DNA	Variable ratio of insert DNA to vector DNA		
Digested vector	Approximately 100 ng total of vector DNA		
DNA ligase buffer	2	x 10	NEB
T4 DNA ligase	1	400 U/µl	NEB
ddH20	To 20		

The optimum ligation reaction mixture was based on 100 ng of digested vector and a vector:insert molar ratio of cut free ends of 1:5. In addition to this optimum ratio, a variable ratio of digested vector to insert DNA was used for each reaction to maximise ligation success. The amount of digested vector was kept contact and the amount of insert DNA added was either the optimum amount or reduced by $1/5^{th}$ or $1/25^{th}$. Control reactions were undertaken using no insert and no insert/no ligase to control for vector re-ligation and incomplete vector digestion. All ligation reactions were undertaken by incubating at 16 °C for 2 hour in a Bio-Rad T100 Thermal Cycler.

Transformation into chemically competent bacteria

Transformation of ligation products was undertaken by heat shock transformation of chemically competent bacteria. TOP10 E. coli competent bacterial cells were thawed on ice and then 10 µl added to 10 µl of ligation mix. Samples were then incubated on ice for 30 minutes. Heat shock transformation was undertaken by incubating the samples at 42 °C for 45 seconds in a Bio-Rad T100 Thermal Cycler before returning to ice for a further 2 minutes. To each transformation mix 150 µl of SOC outgrowth media was added followed by incubation with agitation for 1 hour at 37 °C. Transformed bacteria were then plated out onto LB agar containing the appropriate antibiotic and incubated at 37 °C overnight.

PCR Screen

Bacterial colonies were screened for insert incorporation and orientation by colony PCR. The number of colonies screened was dependent on the number of colonies within experimental samples versus the background colony number in control experiments.

Individual colonies were picked with a sterile plastic tip, streaked onto a reference LB agar plate containing the appropriate antibiotic and then added to the reaction mixture as outlined below.

	Volume (µl)	**Concentration**	**Company**
HF DNA polymerase buffer	4	x 5	NEB
dNTP	0.5	10 mM	Bioline
Template DNA	Colony		
5' primer	0.5	10 µM	Sigma-Aldrich
3' primer	0.5	10 µM	Sigma-Aldrich
Fusion	0.25	5 U/µl	NEB
MilliQ	14.25		

Reactions were carried out in a Bio-Rad T100 Thermal Cycler using the following settings including an extended stage 1 to ensure bacterial cell lysis prior to amplification.

		Temperature (°C)	**Time**
1	Lyse Bacteria	98	5 minute
2	DNA denaturation	98	10 seconds
3	Primer annealing	55	30 seconds
4	Extension	72	1minute/kb
5	Repeat stages 2-4		x 24
6	Final extension	72	5 minutes
7	Cooling	10	Infinity

PCR products were separated by agarose gel electrophoresis and the presence of a correctly sized insert visualised using UV light with a Gel Doc XR+ (Bio-Rad) and analysed with Image Lab (Bio-Rad). The reference LB agar plate was incubated at 37 °C for 8 hours.

Vector extraction

Streaks from the PCR screen reference plate corresponding to colonies incorporating the correctly sized PCR product were used to prepare larger quantities of vector DNA. Positive colonies were used to inoculate LB media containing selective antibiotic and incubated at 37°C overnight with agitation. Plasmid DNA was then extracted and purified from the overnight culture using PureLink™ Quick Plasmid Miniprep Kit (Invitrogen) as per the manufacturers instruction. DNA concentration was determined spectrophotometrically using a Nanodrop II (Thermo Fisher Scientific). Purity was determined by measuring the 260nm/280nm ratio with a value > 1.8 indicating DNA purity.

DNA sequencing and analysis

DNA sequencing was undertaken by the Weatherall Institute of Molecular Medicine (University of Oxford) sequencing facility. DNA alignment against reference sequences was undertaken using SnapGene software (GSL Biotech; available at snapgene.com). Sequence identity and integrity was confirmed by analysis using the Basic Local Alignment Search Tool (BLAST; available at https://blast.ncbi.nlm.nih.gov/Blast.cgi) and cross referenced against known protein sequences within the UniProt database (available at http://www.uniprot.org).

CRISPR

CRISPR mediated gene editing was undertaken to knockout genes of interest within target cell lines [258]. Guide sequences were identified by submitting genes of interest to the CRISPR design tool available at http://crispr.mit.edu. Guide selection was based on proximity to the Kozak (and hence low probability of producing a truncated protein) and CRISPR score (a surrogate score taking account of on-target activity minus a weighted sum of off target hit scores). Selected guides were ordered from NEB as follows.

Forward	5'	CACCGNNNNNNNNNNNNNNNNNN	3
Reverse	3'	CNNNNNNNNNNNNNNNNNNNCAAA	5

Oligonucleotides were annealed using the following reaction mixture

	Volume (µl)	**Concentration**	**Company**
Forward oligonucleotide	1	100 µM	NEB
Reverse oligonucleotide	1	100 µM	NEB
x 10 T4 DNA Ligase buffer	1	x 10	NEB
MilliQ	18		

The annealing reaction was carried out in a Bio-Rad T100 Thermal Cycler as follows.

Step	**Temperature (°C)**	**Time (min)**
1	37	30
2	98	5
3	Reduce by 5°C/min until 25°C	

Annealed oligonucleotides were ligated into the lentiviral CRISPRv2 vector via the BsmBI restriction site and transformed into chemically competent bacteria. Plasmid DNA was

extracted from colonies using PureLink™ Quick Plasmid Miniprep Kit (Invitrogen) and correctly incorporation guides confirmed by DNA sequencing. Guides were transfected into target cell lines using the small-scale lentiviral transfection method. Cells incorporating the guides were selected by puromycin. Knockdown of target proteins was confirmed by flow cytometry. Cell sorting was undertaken to obtain a pure population of cells negative for the protein of interest.

2.2 Cell culture

2.2.1 General Cell culture

Cell culture work was undertaken in a sterile manner within a level 2 tissue culture facility. All work using mammalian cell lines was undertaken within HEPA filtered cell culture cabinets using disposable plastic pipettes. All cells lines were grown at 37 °C and 5 % CO_2 in an IncuSafe CO_2 Incubator (Panasonic). Cell viability and density were monitored regularly by light microscopy and counting using a haemocytometer. Cell lines were split regularly to maintain viability. Early cell passages were frozen down to maintain cell stocks.

2.2.2 Cell lines used in this thesis

A20 B cells

The A20 cell line is a BALB/c B cell lymphoma line derived from a spontaneous reticulum cell sarcoma [259]. It is a suspension cell line. The A20 B cell line was grown in Roswell Park Memorial Institute Medium (RPMI; Sigma-Aldrich) supplemented with 10 % foetal calf serum (FCS, Sigma-Aldrich), 200 mM L-glutamine (Sigma-Aldrich), 10 mM Hepes (Sigma-Aldrich), 1 % Penicillin/Streptomycin/Neomycin (Sigma-Aldrich) and 50 μM β-mercaptoethanol (Gibco). Cultures were maintained between 2 x 10^5 and 1 x 10^6 cells/ml.

293T cells.

The 293T cell line is an epithelial cell line isolated from human embryonic kidneys (HEK) transformed with large T antigen. T293 cells are an adherent cell line. Cells were grown in in Dulbecco's Modified Eagle's Medium (DMEM; Sigma-Aldrich), supplemented with 10 % FCS (Sigma-Aldrich), 200 mM L-glutamine (Sigma-Aldrich), and 1 % Penicillin/Streptomycin/Neomycin (Sigma-Aldrich).

CHO-K1 cells.

The CHO-K1 cell line is an epithelial cell line isolated from the ovary of an adult Chinese Hamster. They are an adherent cell line. Cells were grown in DMEM (Gibco, Invitrogen) supplemented with 10 % FCS (Sigma Aldrich), 1 % L-glutamine (Sigma Aldrich), 1 % sodium pyruvate (Invitrogen), 1 % Penicillin/Streptomycin/Neomycin (Sigma-Aldrich) and an amino acid supplement.

DO-11.10 cells

The DO.11.10 cell line is a murine T cell lymphoma cell line. It is a suspension cell line. Cells were grown in RPMI (Sigma-Aldrich) supplemented with 10 % FCS (Sigma Aldrich), 1 % L-glutamine (Sigma Aldrich) and 1 % Penicillin/Streptomycin/Neomycin (Sigma-Aldrich).

2.2.3 Cell culture methods

Storage and retrievable of cells lines

Cells were stored for short periods at -80 °C. The long-term storage of cells was undertaken by cryopreservation in liquid nitrogen. To cryopreserve cells, 5 x 10^6 cells were spun down

and resuspended in 1 ml of freezing media (10 % FCS (Sigma-Aldrich) with 10 % (w/v) DMSO) and transferred to a cryovial. Cryovials were put into a Nalgene freezing chamber (Thermo Scientific) and placed at -80 °C. This method ensures cell viability by allowing water to move out of cells before freezing occurs. Cells were subsequently transferred to liquid nitrogen for long-term storage.

The thawing of cells was undertaken by rapid warming. Cryovials were incubated in a waterbath at 37 °C until the cells had just defrosted. Cells were then immediately added to 30 ml of complete media at 37 °C followed by centrifugation at 1200rpm for 2 minutes at room temperature. The supernatant was discarded and the cell pellet resuspended in an appropriate volume of complete media and incubated at 37 °C/5% CO_2. Cells were examined microscopically and counted at 24/48hrs to check viability.

Counting of cells

Cell viability and density were monitored regularly by light microscopy and counting using a haemocytometer. Counting was undertaken by mixing 30 µl of cells with 30 µl of trypsin blue. A hemocytometer was then used to count viable cells.

Sub-culturing

Sub-culturing of suspension cells was undertaken by counting cell numbers using a hemocytometer and then dilution in a suitable volume of complete media to maintain the appropriate cell density.

Sub-culturing of adherent cells was undertaken by firstly removing the growth media and washing cells with sterile phosphate buffered saline (PBS). Cells were then incubated with

an appropriate volume of EDTA trypsin (Sigma Aldrich) at 37 °C to induce dissociation. Following dissociation, the tryspin was neutralized by the additional of twice the volume of complete growth media. Cells were then pelleted at 1200 rpm for 2 minutes and re-suspended in an appropriate volume of complete media. Cells were counted using a hemocytometer and sub-cultured by dilution in a suitable volume of complete media.

2.3 Protein methods

2.3.1 General protein methods

SDS PAGE

Proteins were analysed on 12 % sodium dodecyl sulphate polyacrylamide gel electrophoresis (SDS PAGE) under reducing and non-reducing conditions. For direct visualisation, gels were stained with Coomassie Blue Solution (0.05 % Coomassie Brilliant Blue, 50 % methanol, 10 % acetic acid) followed by destaining (repeated washes with a solution of 10 % acetic, 12 % methanol) to visualise protein. Precision markers (Bio-Rad) were run in parallel with experimental samples.

Size exclusion chromatography

Size exclusion chromatography was undertaken to purify or analyse antibody and protein mixtures using Fast Protein Liquid Chromatography (FPLC). FPLC was undertaken using an AKTA pure FPLC system. The column required was selected based on the optimum separation range and quantity of protein to be purified. Prior to use, the column and pumps were washed with 0.5 M sodium hydroxide followed by filtered MilliQ water. The system was then calibrated with 1.5 column volumes of the appropriate buffer (either filtered PBS or HBS, with or without sodium azide). The injection loop was also flushed with filtered

buffer. The protein to be purified was concentrated to an appropriate volume (500-1000 µl) and centrifuged at 13000 rpm for 5 minute at 4 ˚C to pellet any aggregate. A maximum of 10 mg of protein was used per injection. The protein was eluted with the appropriate buffer into 500 µl fractions. The concentration of each fraction was measured by spectrophotometry at 280 nm. Selected fractions were then run on reducing and non-reducing SDS-PAGE to check purity. Protein were either used immediately for downstream applications or aliquoted and frozen at -80 ˚C.

Spectrophotometry.

Protein concentrations were assessed by spectrophotometry using a Nanodrop One (ThermoFisher Scientific). Absorption was measured at 280 nm. Protein concentration were then calculated by dividing the absorption at 280 nm by the extinction co-efficient.

Western Blot

Proteins were separated by SDS PAGE and transferred to Hybond-C nitrocellulose membranes (Amersham Biosciences, UK) using an XCell II Blot module (Invitrogen, UK). Nitrocellulose blots were blocked by overnight incubation at 4 °C in 1% (w/v) bovine serum albumin (BSA) dissolved in PBS. Primary antibody was diluted in PBS containing 1% w/v BSA and incubated at 45 minutes at 4 °C. Secondary antibody conjugated to HRP was diluted in PBS containing 1% w/v BSA and incubated at 30 minutes at 4°C. Blots were washed for three periods of 5 minutes following each incubation using TBS-T (TBS-T; 137 mM NaCl, 20mM Tris-HCl, pH 7.6, 0.1% v/v Tween 20). Blots were immunodetected using Amersham's enhanced chemiluminescence western blotting technique, followed by exposure to Fuji X-ray film. Anti-His immunoblots were

performed using anti-pentaHis (1 in 1000; Qiagen). Anti-HEL immunoblots were performed using HyHEL10 antibody (1 in 1000). The secondary antibody was goat anti-mouse IgG (Fc-specific) horseradish peroxidase (HRP; 1:2000; Sigma).

2.3.2 Expression of membrane bound proteins

Small-scale lentiviral transfection

To express cell membrane proteins within target cell lines a small-scale lentirival transfection method was utilised. On day 1, T293 T cells were plated out in a 6 well plate at 3 x 10^5 cells/ml (2ml per well) so they would be 90 % confluent the following day ready for transfection. On day 2, the T293 media was exchanged for 2.5 ml fresh complete media of the target cell to be infected. For each well within the six well plate the following transfection mixture was used.

	Reaction mixture per well	**Company**
DNA	0.5 μg	
PMDG	0.5 μg	
P8.91	0.5 μg	
Genejuice	4 μl	MilliQ
DMEM	100 μl	Lonza

The reaction mixture was prepared and incubated at room temperature for 30 minutes. The mixture was then added dropwise to a single well of T293 cells. The virus containing media was harvested after 48 hours, the T293 cells refed with complete media, and harvested again after a further 24 hours. Virus was pooled and filtered through a 0.2 micron filter. To infect cells of interest 5 ml of filtered virus was added to 1 ml of cells at a density

of 1 x 10^6 cells/ml. The day following infection a further 5mls of completed media was added. The cells were then grown up according to standard methods.

2.3.3 Expression of soluble His-tagged proteins

Soluble His-tagged proteins were produced by either stable or transient transfection of cell lines with a gene of interest. Stable transfection was undertaken using a glutamine synthetase selection step following either a conventional or streamlined approach. Transient transfection was undertaken using large scale lentiviral transfection.

Stable transfection using the glutamine synthetase-based protein expression system

Conventional method

On day 1, CHO-K1 cells were plated out in 20 ml complete media in a T75 flask at a density of 4 x 10^6 cells/ml. For each construct to be transfected a separate flask was seeded. An additional flask was set up as a control transfection. On day 2, prior to transfection the media was changed to DMEM (Gibco, Invitrogen) supplemented with 10 % FCS dialysed against PBS (First Link Ltd., Wolverhampton), 1 % sodium pyruvate (Invitrogen), 1 % Penicillin/Streptomycin/Neomycin and an amino acid supplement. The transfection mixture was prepared as outlined below.

	Volume (µl)	**Company**
DNA		Total 10 µg
Genejuice	30	MilliQ
DMEM (no supplements)	500	Gibco

The transfection mixture was incubated at room temperature for 20 minutes and added to the appropriate flask. On day 3, the supernatant was removed and the cells washed with PBS. Cells were then tryspinised prior to addition of twice the volume of complete DMEM media. The cells were then spun down at 1300rpm for 2 minutes at room temperature. Cells were then resuspended in 10 ml complete media. 100 µl of cells were then added to each well of a 96 well plate and incubated overnight at 37 °C, 5% CO_2. On day 4, L-methionine sulfoximine (MSX, Sigma Aldrich) was added at a range of concentrations (30 µM to 40 µM). To achieve this, a x2 stock solution was prepared for each MSX concentration and 100 µl added to each well of the 96 well plate thereby achieved the desired final MSX concentration. Every 7 days, 100 µl of media was removed and a fresh 100 µl complete media added containing x2 the desired concentration of MSX (thereby maintaining the appropriate concentration of MSX). Media was refreshed in this manner every 7 days until substantial number of clones developed (approximately 3-4 weeks). At this point all wells were examined by light microscopy to identify wells containing single colonies and colony sizes scored. A dot blot analysis was then undertaken to identify highly expressing clones. 4-8 of the most highly expressing single colonies were then expanded and when confluent in a 6 well plate supernatant assessed for protein expression by Western Blot. The clone expressing the correct sized protein product at the highest level was selected to be expanded further to collect supernatant for protein extraction. Stocks of highly expressing cells were frozen down for future use.

Stream-lined method

The stream lined implementation of the glutamine synthetase-based expression system involves a single fluorescence-activated cell sorting (FACS) selection step rather than

production of individual clones. This approach uses the same method on days 1 and 2 as the convectional approach. The protocol differed from day 3 when the MSX was added directly to the T75 flasks at the desired concentration. Cells were then refed with complete media containing the appropriate concentration of MSX after 5 days, and then again every 7 days until there was evidence of substantial clones. Upon the appearance of substantial clones, cells were removed with cell scrapers (Corning) and spun down at 1300 rpm for 2 minutes at room temperature. Cells were then resuspended in PBS and sorted by FACS for the highest 10% of GFP expressing cells. These cells were then returned to cell culture and grown in MSX-containing media. Supernatant was assessed for protein expression by Western Blot. Samples expressing the correct sized protein product at the highest level were expanded further to collect supernatant for protein extraction. Stocks of highly expressing cells were frozen down at this time for future use.

Transient transfection using the large scale lentiviral transfection method

On day 1, 293T cells were plated out in a T75 so that they would be 90% confluent on day 2 ready for transfection. For each T75 requiring transfection the following reaction mix was prepared.

	Reaction mixture	**Company**
DNA	6.5 µg	
PMDG	6.5 µg	
PEI	6.5 µg	
PEI	39 µl	
DMEM	2500 µl	Lonza

The mixture was incubated at room temperature for 10 minutes to allow PEI:DNA complexes to form. The mixture was then topped up to 8 ml with complete DMEM media. The existing T293 media was removed from the cells and replaced with the infection mixture. The virus containing media was harvested after 48 hours, the T293 cells refed with 10 ml complete media, and harvested again after a further 24 hours. Virus was pooled and filtered through a 0.2 micron filter and kept at 4˚C ready to infection.

CHO cells were plated out at 3 x 10^6 cells per T75 on the day prior to infection. On the day of infection, CHO media was decanted and 10 mls of infection mix added. A further 10 mls of complete media was added the day following infection. Cells were then left until confluent at which point a small sample of media was harvested to check protein expression levels via Western blot. For production of soluble protein, cells were expanded into 4 x T175's. Media was harvested and replaced every 2-4 days until sufficient supernatant had been harvested ready for protein purification.

2.3.4 Purification of histidine-tagged proteins

Tissue culture supernatant was mixed with 1-2 x volume of PBS/0.5 M NaCl, adjusted to pH 8.0 and sodium azide added to a final concentration of 0.05%. Ni-NTA beads were then added, stirred gently at 4 ˚C overnight and packed onto a column ready for elution. Pre-elution was undertaken with 10 mM imidazole in 1 ml fractions and continued until the optical density had fallen satisfactorily. Recombinant His-tagged proteins were then eluted from the column with 250 mM imidazole in 1 ml fractions. The absorption at 280 nm of each fraction was measured. Selected fractions were then run on reducing and non-

reducing SDS-PAGE to check purity. Selected fractions were further purified by size exclusion chromatography.

2.3.5 Purification of antibody using protein G

Tissue culture supernatant was mixed with 1x volume of PBS, adjusted to pH 8.0 and sodium azide added to a final concentration of 0.05%. 10 ml protein G beads were then added and stirred gently at 4 ˚C overnight and then packed onto a column ready for elution. Prior to elution beads were washed with PBS/0.5 M NaCl pH 7.4 (approximately 200 ml). Antibody was eluted in 5 ml 0.1 M glycine fractions into 2 M Tris. The volume of 2 M Tris required had been predetermined as that required to neutralise 5 mL of 0.1 M glycine pH 2.5. A total of 12 fractions were collected. The column was then immediately neutralize with PBS to prevent damage to the beads. The absorption at 280 nm of each fraction was measured. Selected fractions were then run on reducing and non-reducing SDS-PAGE to check purity. Pure antibody fractions were pooled and concentrated using a 10 kDa centrifugal filter device (Merck Millipore Ltd). The antibody was then purified using an AKTA FPLC and a superdex S200GL column. Antibody was eluted in filtered PBS/0.05 % sodium azide. The absorption at 280 nm of each fraction was measured. Selected fractions were then run on reducing and non-reducing SDS-PAGE to check purity. Pure antibody fractions were pooled and concentrated using a 10 kDa centrifugal filter device (Merck Millipore Ltd) to the desired concentration (usually 1-2 mg/ml). Antibody not used immediately was aliquoted and stored at -80 ˚C.

2.3.6 Fluorescent labelling of Halo®/Snap®-tag fusion proteins

Halo®-tag and Snap®-tag fusion proteins were labelled with the corresponding ligand using the following reaction mixture.

	Volume (µl)	Concentration	Company
Halo®-/Snap®-tag fusion protein	200	1 mg/ml	
Halo®/Snap® ligand	20	250 µM	Promega/NEB
DDT	10	50 mM	
PBS	270		

The reaction mixture was incubated at 4 °C overnight in the dark with gentle rotation. The mixture was then either used directly or subjected to FPLC to remove free dye.

2.3.7 Immunodepletion

Conjugation of antibody to tosylactivated beads

To undertake immunodepletion experiments, antibody was first conjugated to M450 tosylactivated Dynabeads (Thermo Fisher Scientific). 500 µl Dynabeads were washed and resuspended in 500 µl 0.1M sodium phosphate buffer, pH 7.4. 100 µg of HyHEL10 antibody was then added and incubated at room temperature with gentle tilting and rotation for 16-24 hours. The beads were then washed twice in in Ca^{2+} and Mg^{2+} free PBS (supplemented with 0.1 % BSA and 2mM EDTA, pH 7.4). Between each wash the mixture was incubated for 5 minutes at 4 °C with gentle tilting and rotation. Following the final wash step the beads were resuspended in 500 µl of 0.2 M Tris/0.1% BSA, pH 8.5 and incubated at 37 °C with gentle tilting and rotation to deactivate any remaining tosyl groups. The beads were then washed again in Ca^{2+} and Mg^{2+} free PBS (supplemented with 0.1 % BSA and 2 mM EDTA, pH 7.4) before being resuspended in 500 µl of this buffer.

Immunodepletion

To undertake immunodepletion, 50 µl of goat anti-mouse dynabeads conjugated to HyHEL10 were added to 30 µl of a 5mg/l solution of the protein to be immunodepleted and incubated for 2 hours at 4 °C with gentle rotation. The supernatant was then removed and subject to SDS PAGE and Western blot analysis.

2.4 Phenotypic analysis

2.4.1 Flow cytometry

Flow cytometry was used to assess the expression of proteins of interest in target cells. Cells were harvested from culture and resuspended in PBS containing 0.05 % sodium azide to a final concentration of 1 x 10^6 cells/ml. Cells expressing fluorescent reporters required no further labelling. If labelling was required cells were incubated with fluorescently conjugated primary antibody or fluorescently labelled ligand for 45 minutes at 4°C. If a directly conjugated antibody was unavailable cells were sequentially labelled with primary antibody and then a secondary conjugated antibody. Cells were washed with 3 ml of PBS/0.05 % sodium azide followed by centrifugation at 1000 rpm 4°C for 2 minutes pre and post each labelling step. After the final wash step the pellet was re-suspended in 400 µl 2 % formaldyde. Cells were analysed using a Cyan ADP (Beckman Coulter) or Attune™ NxT (Thermo Fisher Scientific) flow cytometer. Data was analysed using FlowJo. Estimates of surface receptor numbers were undertaken using BD QuantiBrite-PE beads. Cell sorting was undertaken by the WIMM FACS facility.

2.5 Cellular imaging

2.5.1 Calcium-based imaging

Calcium triggering experiments were undertaken on a spinning disc confocal microscope (Carl Zeiss). The microscope was fitted with a Yogokawa spinning disc unit and AxioCam camera. Zen software was used for controlling the microscope. A x10 air objective was used. The microscope was housed within an incubation box for controlling the temperature at 37 °C and 5% CO_2.

To prepare cells for calcium triggering experiments, 1 x 10^6 cells of the appropriate cell line were harvested and spun down at 2000 rpm for 90 seconds at room temperature. The supernatant was discarded and the cells washed with 500 µl HBS. Each wash step consisted of resuspending the cell pellet in 500 µl of HBS and then spinning at 2000 rpm for 90 seconds at room temperature. The washed cell pellet was then resuspended in a mixture of 200 µl RPMI (no supplements; Sigma-Aldrich), 200 µl HBS/ 2.5 µM probenecid and 1 µl of flouro-4. The cell-labelling mixture was incubated at 37 °C/5 % CO_2 for 20mins in the dark. After incubation, the cells were spun down at 2000 rpm for 90 seconds at room temperature following by two rounds of washing as above with HBS/2.5 µM probenecid. The final cell pellet was resuspended in 200 µl HBS/2.5 µM probenecid ready for imaging.

Imaging was undertaken on a range of surfaces including glass, Ni-NTA and Ni-containing bilayers with or without the addition of proteins of interest. Prior to use surfaces were washed three times with HBS/2.5mM probenecid and then a final volume of HBS/2.5 µM probenecid added. To focus the microscope to the correct confocal plane 1

µl of fluro-4 labelled cells were added to the surface. When the correct focal plane had been achieved iomage acquisition was commcned and 20 µl of fluro-4 labelled cells added. Images were collected every 0.5 seconds for a total of 10 minutes. Images were collected in the 488 nm channel at 50 % laser power.

Ionomycin or a crosslinking antibody were used as a positive control to check calcium flux and receptor triggering. Ionomycin was prepared as a stock solution at 10 µM in HBS-probenecid and added in the last minute of image acquisition at a final concentration of 1µM. If a BCR crosslinking antibody was used it was at a final concentration of 10 mg/l.

2.5.2 Supported lipid bilayers

Supported lipid bilayers (SLBs) were used as a model surface for microscopy based experiments. Two different approaches were used to prepare SLBs

Spin coating

Glass slides were cleaned in piranha solution (2/3^{rds} sulphuric acid, 1/3rd hydrogen peroxide) for 1 hour and then washed in MilliQ. Slides were air dried and then placed on a spin coating machine. 25 µl of the appropriate lipid mix were then added and the slide immediately spun at 3000 rpm for 30 seconds. The glass slide was immediately transferred to an Attoflour Cell Chamber (Life Technologies Ltd) and 500 µl of HBS/2.5 mM probenecid added. If required protein was added at this stage and incubated for 1 hour at room temperature. The protein buffer was then diluted out by the addition of 500 µl of

HBS/2.5 mM probenecid followed by removal of 500 µl of buffer. This was repeated a total of 10 times ensuring that the SLB was never left dry.

Small unilamellar vesicles

To prepare small unilamellar vesicles (SUVs) a total of 1 mg lipids were mixed in the required ratio in a glass vial. The vial was rotated under nitrogen until the chloroform had evaporated and then a vacuum pump applied for 1 hour. The lipid film was then hydrated with 200 µl of PBS, covered with nitrogen and incubated for 1 hour at room temp. The sample was then vortexed until cloudy and sonicated until clear. 10 µL PBS followed by 20 µL SUVs were then added to coverslips which had been cleaned with both Piranha solution and plasma. The SUVs were incubated at room temperature for 30 minutes and then washed 3 times with PBS. If required protein was added at this stage, incubated for 1 hour at room temperature followed by 3 washes with PBS.

Chapter 3

A Toolkit For Studying B Cell Receptor Triggering

3.1 Introduction

The overarching aim of this thesis is to gain a more accurate understanding of the exact mechanism of BCR triggering. To achieve this, key principles of existing theories of BCR triggering will be tested in a model system. Multiple model systems have been utilised to study B cell immunity including BCRs directed against: the class I MHC molecules H-2K^k and H-2K^b [260]; CD8.2 [261]; double stranded DNA [262] and red blood cells [263]. In this thesis, the most extensively studied model system in B cell biology will be employed, the Hen-Egg Lysozyme (HEL) system. HEL is well suited to this role as it is inexpensive, easy to produce, stable, strongly immunogenic and comprises a wide range of natural variants. HEL has served as a model system for studying: protein structure [264-266]; enzyme mechanisms [266, 267]; protein-folding [268]; protein-protein interactions [269]; B-cell immunity; self-fate decisions; tolerance and autoimmunity [270] in a range of in vitro and in vivo systems.

HEL is a glycoside hydrolase. The enzyme hydrolyses the 1,4-beta-linkages between N-acetylglucosamine and N-acetylmuramic acid within the peptidoglycan of bacterial cell walls. It also catalyses the hydrolysis of chitin, a primary component of cell walls in fungi and the exoskeleton of arthropods [266]. In humans, lysozyme is found in tissues and bodily fluids including liver; articular cartilage; plasma; saliva; tears and milk. It functions as part of the innate immune system degrading the cell walls of microorganisms [271].

HEL was the third protein and the first enzyme to have its three-dimensional structure determined by X-ray crystallography [264-266]. HEL is a 129 amino acid protein with a molecular mass of 14.6 kDa. It is formed from a single polypeptide chain with 4 intra-chain disulphide bonds. The structure consists of five alpha helices and two beta sheets arranged in two domains: one that is predominantly alpha helices, and a second that is predominantly beta sheets [266]. The active site is centred around a cleft containing the residues Glutamine-35 and Aspartate-52. [266, 267].

Complexes of antibody bound to HEL have served to understand the general principles that govern molecular recognition in protein-protein complexes. Multiple structures of HEL bound to antibodies, Fabs or Fv have been determined, identifying three principle epitopes [272-284]. The different HEL-specific antibodies vary in their affinity for HEL, and mutational analysis has enabled further dissection of the critical residues in these interactions [285-289]. The highest affinity interaction is between HEL and the HEL-specific antibody, HyHEL10, with a K_a 4.5 x 10^{10} M^{-1}[289], which is among the highest measured for a natural antibody. This interaction has served as the basis for the MD4 mouse model.

The MD4 mouse strain carries a transgene for the heavy and light chain encoding the HyHEL10 antibody enabling immune responses to HEL to be studied in vivo [62]. Transgenic mice have also been generated with HEL expressed as either a systemic membrane bound antigen, soluble antigen [270] or intracellular antigen [290]; and crossed with MD4 mice to create doubly transgenic mice. These mice have proven a powerful tool

to study tolerance, demonstrating that it is dependent on both the affinity of the BCR for its antigen together with the form and abundance of self-antigen presented [270].

In summary, the HEL/HyHEL10 interaction is a well-established and highly characterised model for studying a range of biological phenomena both in vitro and in vivo. This makes it an ideal choice for studying BCR triggering This chapter will describe the extension of the HEL/HyHEL10 model system, involving the generation of a set of complementary reagents for studying BCR triggering by advanced fluorescence microscopy. The toolkit generated will include:

- A range of HEL-fusion proteins for use in fluorescence imaging.
- A HyHEL10-specific B cell line.
- The production of surrogate HyHEL10 BCRs for use in surface based experiments.

3.2 Materials and Methods

3.2.1 Construct design and cell line preparation

HEL-Snap and HEL-Snap-Halo constructs were produced using a multi-step PCR protocol. HEL, Snap AND Halo genes were amplified separately from plasmid templates with complementary overlapping ends of approximately 15-20 base pairs. HEL and Snap genes were amplified in a single PCR reaction, while Halo was amplified in a two-stage PCR protocol to remove an endogenous MluI site. Chimera PCR was then undertaken to sequentially join HEL to Snap; and in the case of HEL-Snap-Halo, HEL-Snap to Halo. The terminal His-tag of all constructs was added by extension PCR. Final PCR products were cloned into either the pOPINEE12G vector, (via AgeI and EcoRI, for stable

transfection using a glutamine synthetase-based selection step), or the pHR vector (via MluI and NotI, for large scale lentiviral transfection). Constructs were verified by DNA sequencing.

3.2.2 Protein expression, extraction and purification

HEL-Snap constructs were expressed in CHO cells using both a standard and streamlined version of the glutamine synthetase-based expression model. Cells were seeding into 2 HYPERflasks (Corning) and incubated at 37 °C/5 % CO_2 for 3 weeks prior to harvesting of supernantant. HEL-Snap-Halo constructs were expressed in CHO cells using the large scale lentiviral protocol with supernatant harvested every 2-4 days until 1 litre had been collected. Protein purification was undertaken by Ni extraction regardless of the initial method of protein expression.

3.2.3 Surface Plasma Resonance

Surface plasma resonance as implemented in the Biacore™ T200 (GE Healthcare) was used for kinetic characterisation of the interaction between HyHEL5/10 antibodies and Halo-Snap-HEL (N-terminal-His-tag; N-HSH)/lysozyme (Sigma). Experiments were performed at 37 °C in HBS-P buffer (25 mM HEPES pH 7.4, 150 mM NaCl, 0.05% sodium azide, 0.005% v/v Surfactant P20) or TBS-P buffer (25 mM Tris pH 7.4, 150 mM NaCl, 0.05% sodium azide, 0.005% v/v Surfactant P20).

The matrix surface of the sensor chip was firstly activated through amine coupling using EDC/NHS reagents supplied by the manufacturer (GE Healthcare) with an activation time of 6 minutes. The anti-mouse IgG antibody from the Mouse Antibody Capture Kit

(GE Healthcare) was then injected at 10 μg/ml in 10 mM sodium acetate, pH 5.0, and directly immobilised onto the matrix surface, resulting in immobilization levels of ~ 3000 RU. The matrix surface of the sensor chip was then inactivated by an injection of 1.0 M ethanolamine-HCl pH 8.5 for 5 minutes.

To indirectly immobilise antibody onto the dextran matrix, HyHEL5/10 were injected at 0.0025 mg/ml at the second and fourth flow cells (Fc_2 and Fc_4), resulting in immobilisation levels of ~ 200-500 RU; Fc_1 and Fc_3 were used as the negative control for binding events at Fc_2 and Fc_4, respectively. Soluble, monomeric N-HSH or lysozyme were then injected into the flow-cells using 2-fold dilutions. Subsequent injections of five different concentrations were performed automatically: each injection was of 60 seconds duration at a buffer flow-rate of 30 μl/min, followed by a dissociation period of 70 seconds before the next injection was performed, and a final dissociation period of 30 minutes. Injections of buffer were performed exactly as those of the samples for secondary blank subtraction. The binding data was then fitted with the single-cycle kinetics model using Biacore T200 evaluation software (GE Healthcare) in order to directly derive kinetic parameters.

3.2.4 Characterisation of the surface of A20 cells

1 x 10^6 A20 cells were washed in PBS containing 0.05 % sodium azide and stained with either: anti-IgA-FITC (Lifespan Biosciences); anti-IgD-FITC (eBioscience); anti-IgE-FITC (eBioscience); anti-IgG1-PE (Southern Biotech); anti-IgG2a-PE (Southern Biotech); anti-IgG2b-PE (Southern Biotech); anti-IgG3-PE (Southern Biotech); anti-IgM-FITC (eBioscience); anti-kappa-APC/Cy7 (Biolegend); anti-lambda-APC (Biolegend); isotype-

FITC (Biolegend); isotype-PE (Biolegend); isotype-APC (Biolegend) or isotype-APC/Cy7 (Biolegend). Stained cells were then examined by flow cytometry using a Cyan 2 FACS machine and data analysed using FlowJo software.

3.2.5 RACE PCR

RACE PCR was undertaken as per the manufactures instructions (Firstchoice RLM-RACE-PCR kit). 5' RACE of kappa light chain and IgG2a heavy chain was undertaken using the following pairs of custom primers

5' RACE kappa light chain

- External primer CTCATTCCTGTTGAAGCTCTTGACGACGGG
- Inner primer GGTGCATGCGGATACAGTTGGTGCAGCATC

5' RACE IgG2a heavy chain

- External primer (1) AGGACAGGGCTTGATTGTGGG
  (2) TCGTCCTTGGTCAACGTGAG
- Internal primer (1) GCACACCACTGGACAGGGATCCAGAGTTCC
  (2) GCTCACTGGATGGTGGGAAG

Analysis of final products was undertaken by agarose gel electrophoresis and bands visualised by UV transillumination. Correctly sized bands were cut out, gel purified and analysed by DNA sequencing.

3.2.6 CRISPR

DNA sequences corresponding to the 5' regions (including the Kozak) of murine IgG2a, kappa light chain, Ig-α and Ig-β were submitted to http://crispr.mit.edu. Four guides were

chosen for each construct. Selected guides were ordered from NEB, ligated into the lentiviral CRISPRv2 vector via the BsmB1 restriction site and transformed into chemically competent bacteria. Plasmid DNA was extracted from colonies using PureLink™ Quick Plasmid Miniprep Kit (Invitrogen) and correct incorporation of guides confirmed by DNA sequencing. Guides were transfected into A20 cells using the small-scale lentiviral transfection method. Cells incorporating the guides were selected by puromycin (Cayman Chemicals) at a concentration of 0.5 μg/ml. Knockdown of target proteins was confirmed by flow cytometry for total BCR expression (IgG2a or IgMa). A pure population of cells negative for BCR expression was selected by FACS.

3.2.7 Cloning and expression of HyHEL10

Total RNA was extracted from MD4 mouse fetal liver using Qiagen RNA extraction kit and used to prepare cDNA. The IgM heavy chain and kappa light chain were cloned from cDNA using primers incorporating a 5' Mlul site and 3' NotI restriction site and ligated into the pHR and pHRI vectors. Ig-α and Ig-β genes were cloned from cDNA and joined by chimera PCR to Snap/Halo tags amplified from vector templates. CRISPR resistant constructs were produced by non-code changes to the nucleotide sequence at the site of CRISPR guides using customer oligonucleotide primers ordered from NEB. External primers incorporating a 5' Mlul site and 3' NotI site were utilised to allow subsequent ligation into pHR and pHRI vectors. Sequences were confirmed by DNA sequencing. Vectors were transfected into A20 cells using the small-scale lentiviral transfection method and expression confirmed by flow cytometry for total BCR expression (IgMa).

3.2.8 Cloning and expression of shRNA constructs

The DNA sequence of mouse IghM gene (ID 16019) was submitted to Whitehead Institute of Biomedical Research. Guide selection was based on the algorithm N2(GC)N[A]N6[VT]N2[ATUC]N5[A]N2. Four guides were chosen based on: (1) presence in 1st/2nd constant immunoglobulin domain of IgM; (2) highest predicted score; and (3) presence in clusters of higher than 70% expression. shRNA guides were designed as follows:

5' BamH1-Sense-Loop(TTCAAGAGA)-Antisense-5T-Mlul-EcoR1 3'

Complementary oligonucleotides were ordered, annealed and ligated into the pHR-U6-R-CMV-DsRed vector via BamHI and EcoRI and transformed into chemically competent bacteria. Plasmid DNA was extracted from colonies using PureLink™ Quick Plasmid Miniprep Kit (Invitrogen) and correct incorporation of guides confirmed by DNA sequencing. DsRed fluorescent protein was removed from the vector by MluI digestion and re-ligation thereby avoiding any interference with flow cytometry or fluorescence imaging. Vectors containing shRNA were transfected into A20 HyHEL10 cells using the small-scale lentiviral transfection method. Levels of BCR were monitored by flow cytometry for total BCR (IgMa) expression.

3.2.9 Protein G purification of HyHEL10 antibody

A20 HyHEL10 hybridoma was a gift from Facundo Batista (Cancer Research UK London Research Institute, Lincoln's Inn Fields Laboratories). Cells were thawed and grown up in complete A20 media. Western blot analysis of supernatant with goat anti-mouse (Fc specific)-HRP (Sigma) confirmed good antibody expression levels. Cells were bulked up

and seeded into 2 HYPERflasks (Corning) with low IgG FCS (HyClone) and incubated at 37 °C/5 % CO_2 for 3 weeks. Supernatant was harvested and antibody extracted by protein G purification.

3.2.10 HyHEL10 Fab production by whole antibody papain digest

5 mg of HyHEL10 antibody was buffer exchanged with 20 mM sodium phosphate 10 mM EDTA, pH 7.0, followed by concentration to 500 µl in a 10 kDa centrifugal filter device (Merck Millipore Ltd). 500 µl papain slurry was washed twice with digest buffer (20 mM cysteine HCL) and spun at 3000 rpm for 1 minute. The papain slurry was re-suspended in 1 ml digest buffer and added to the antibody mixture. The mixture was incubated at 37 °C overnight with rotation at 10 rpm. The following morning the mixture was spun out at 3000 rpm for 5 minutes followed by two washes with 0.5 ml PBS. The supernatant after every spin was kept, pooled together, washed twice with 10 ml PBS, followed by concentration to ~1 ml in a 10 kDa centrifugal filter device (Merck Millipore Ltd). 2 ml of Protein-A coupled Sepharose beads were loaded onto a column. The beads were then pre-eluted with 10 ml 0.1 M citric acid, pH 3.0, followed by neutralisation with 15 ml PBS. The supernatant was then applied to the column and washed with 1 ml PBS. This process was repeated 10 times, retaining the flow through each time. The column was then eluted with 1 ml 0.1 M citric acid, pH 3.0, into 100 µl 2.75M TRIS, pH 8.5, to immediately neutralise. This was repeated 10 times, retaining the flow through each time. After all samples were collected the column was immediately neutralised with 15 ml PBS. The absorption at 280 nm of each fraction was measured. Selected fractions were then run on reducing and non-reducing SDS-PAGE to check purity. Fractions containing only Fab (and no Fc) were

pooled and purified by AKTA FPLC using a Superdex S200GL column. The absorption at 280 nm of each fraction was measured. Selected fractions were then run on reducing and non-reducing SDS-PAGE to check purity. Pure fab fractions were pooled and concentrated using a 10 kDa centrifugal filter device (Merck Millipore Ltd) to the desired concentration (usually 1-2 mg/ml). Fab not used immediately was aliquoted and stored at -80 ˚C.

3.3 Results

3.3.1 Construction and characterisation of HEL-fusion proteins

To probe the triggering mechanism of the HyHEL10 BCR using advanced fluorescence microscopy a HEL protein was required that could be fluorescently labelled. Direct labelling of HEL with organic fluorophores (via cysteine or amine groups) is a convenient option but labelling is dependent on the amino acid sequence of the protein and results in a variable number of attached fluorophores per molecule. This approach is useful for bulk imaging, but does not lend itself easily to stoichiometric analysis which requires a 1:1 (or constant known ratio) of protein to fluorophore. To circumvent this problem, HEL was produced as a Snap®-tag and/or Halo®-tag fusion protein. These protein tags are self-labelling enzymes that can be covalently linked to fluorescently labelled substrates [291]. The fixed ratio of HEL to protein tags potentially allows 1:1 labelling of HEL, assuming 100% enzymatic labelling efficiency, making it ideal for both stoichiometric analysis as well as bulk imaging.

3.3.1.1 HEL can be expressed as a fusion protein

A range of HEL-fusion proteins have been generated for fluorescence-based imaging (Figure 3.1). Each protein contains a His-tag for purification and a Snap®-tag and/or Halo®-tag to allow specific labelling with synthetic probes, such as fluorophores.

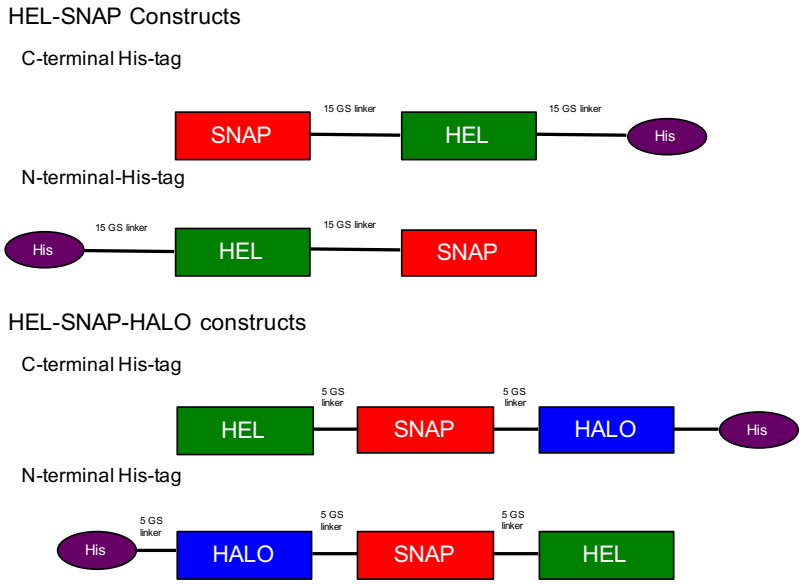

Figure 3.1 HEL-fusion proteins
Schematic representation of HEL-fusion proteins. HEL (green), Snap-tag® (red) and Halo-tag® (blue) domains are separated by flexible linkers composed of a variable number of glycine (G) and serine (S) residues. Each protein contains a double hexa histidine-tag (purple).

Constructs were cloned using a multi-step PCR-based protocol and soluble protein expressed by either stable or transient transfection of CHO cells. Stable transfection is time consuming and labour intensive but has the advantage that, once cells that have integrated the gene into their genome have been selected, a stable cell line is generated that maintains gene expression and can be stored for prolonged periods. Transient transfection is quicker but the foreign gene is not integrated into the host genome so the new gene will not be replicated and hence expression is lost. [292]. Stable transfection is often undertaken using a glutamine synthetase-based selection step that can be implemented using both a conventional and streamlined approach. The streamlined method involves a single FACS-

based selection step (rather than production of individual clones) and has been shown to reduce the number of handling steps, handling time and time to achieve protein-expressing cultures [257]. Transient transfection has been undertaken using large scale lentiviral transfection. In both cases, soluble proteins have been produced in CHO cells as this produces large protein yields and as a mammalian cell line ensures correct protein folding and glycosylation.

HEL-Snap constructs were initially expressed using both the standard and streamlined version of the glutamine synthetase-based expression method [257]. Proteins were His-tag extracted and purified using size exclusion chromatography. Both HEL-Snap constructs were expressed using the streamlined method, however, only the C-terminal His-tag construct was expressed using the standard method. SDS-PAGE analysis of extracted protein indicated that during production there appeared to be cleavage of the protein, most probably at the linker region. The two forms could be partially separated by gel filtration (Figure 3.2).

To optimise protein production the constructs were re-designed. The linkers were shortened and the HEL left free at one end to aid its folding. Both a Snap and Halo tag were incorporated to add flexibility to any subsequent fluorescent labelling strategy. Large-scale lentiviral infection was used for protein production followed by His-tag purification and separation by gel filtration (Figure 3.3 and Figure 3.4). Expression of the new constructs was no-longer compromised by protein cleavage. Halo-Snap-HEL (N-terminal His-tag; N-HSH) produced the highest yield of clean monomeric protein and was therefore taken forward for future experiments as described in this chapter.

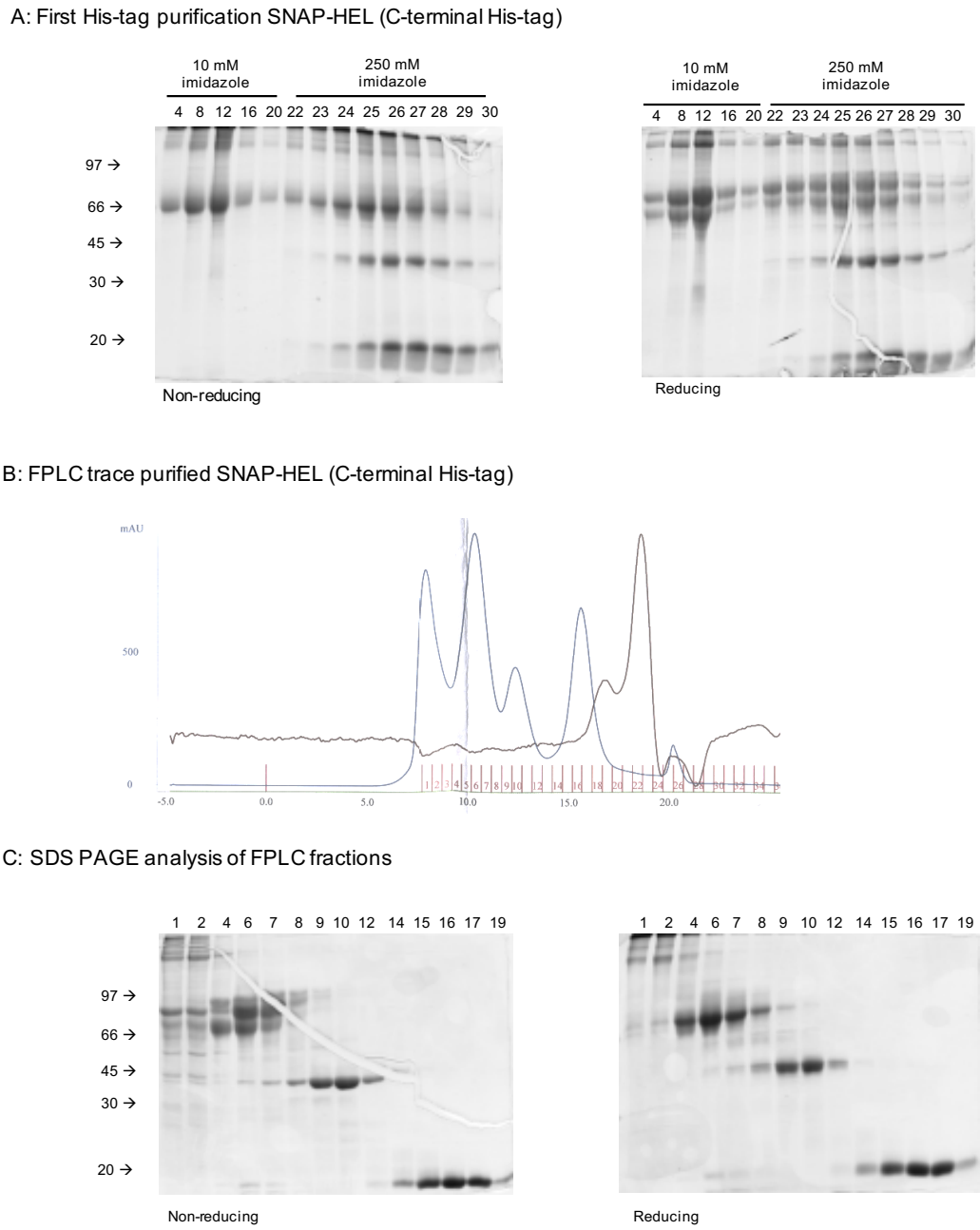

Figure 3.2 Purification of Snap-HEL (C-terminal His tag)
(A) Non-reducing and reducing 12 % SDS PAGE gels of Snap-HEL (C-terminal His-tag) fractions eluted from a Ni-NTA column. The numbers above the lanes correspond to the fractions eluted from the Ni-NTA column. (B) Separation of His-tag purified Snap-HEL (C-terminal His-tag) by size exclusion chromatography using a Superdex S200 column. (C) Eluted FPLC fractions were analysed on 12 % SDS PAGE gels under non-reducing and reducing conditions. The numbers above the lanes correspond to the fractions eluted from the FPLC.

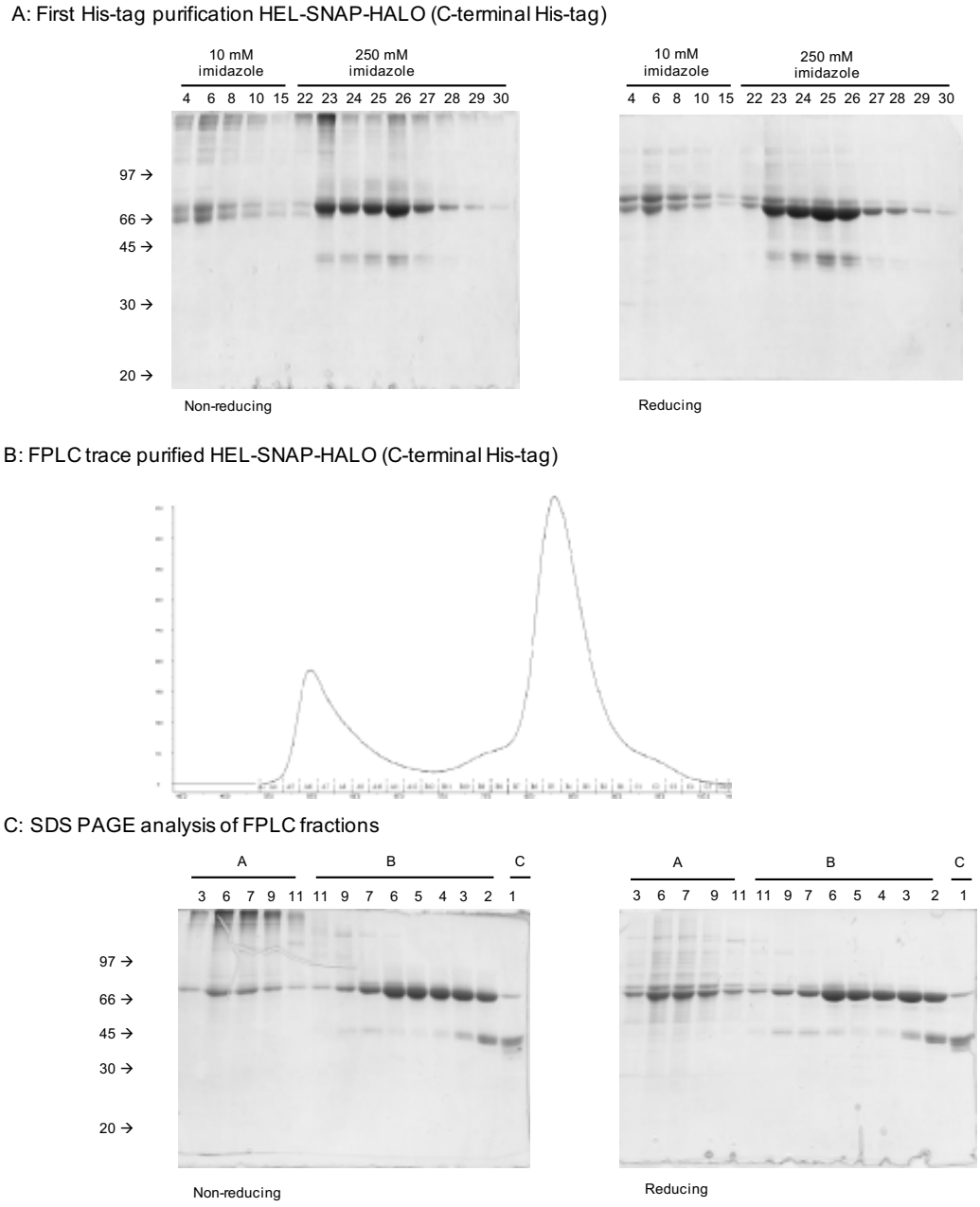

Figure 3.3 Purification of HEL-Snap-Halo (C-terminal His-tag)
(A) Non-reducing and reducing 12 % SDS PAGE gels of HEL-Snap-Halo (C-terminal His tag) fractions eluted from a Ni-NTA column. The numbers above the lanes correspond to the fractions eluted from the Ni-NTA column. (B) Separation of His-tag purified HEL-Snap-Halo (C-terminal His-tag)) by size exclusion chromatography using a Superdex S200 column. (C) Eluted FPLC fractions were analysed on 12 % SDS PAGE gels under non-reducing and reducing conditions. The numbers above the lanes correspond to the fractions eluted from the FPLC.

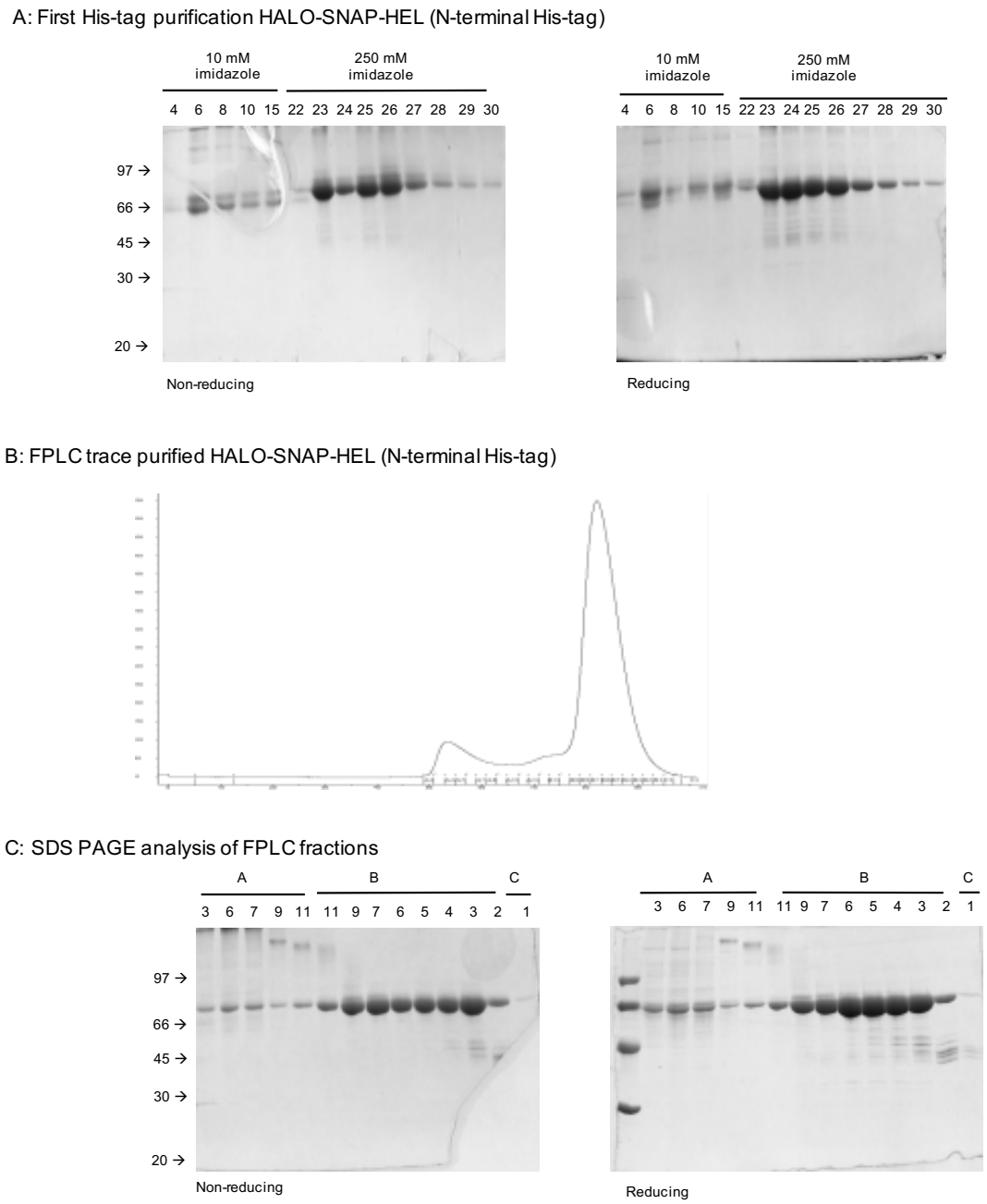

Figure 3.4 Purification of Halo-Snap-HEL (N-terminal His-tag)
(A) Non-reducing and reducing 12 % SDS PAGE gels of Halo-Snap-HEL (N-terminal His tag) fractions eluted from a Ni-NTA column. The numbers above the lanes correspond to the fractions eluted from the Ni-NTA column. Representative example of two extractions. (B) Separation of His-tag purified Halo-Snap-HEL (N-terminal His tag) by size exclusion chromatography using a Superdex S200 column. (C) Eluted FPLC fractions were analysed on 12 % SDS PAGE gels under non-reducing and reducing conditions. The numbers above the lanes correspond to the fractions eluted from the FPLC.

3.3.1.2 Characterisation of HEL fusion proteins

The monomeric HEL-fusion proteins produced were subsequently analysed to check protein folding, binding kinetics to HEL-specific antibodies and binding to HEL-specific B cells.

HEL-fusion proteins are appropriately folded

To establish that the HEL-fusion proteins were correctly folded, immunodepletion of a solution of each protein was undertaken with the HEL-specific antibody HyHEL10 (Figure 3.5). All of the HEL-fusion proteins were completely depleted by the conformation sensitive HyHEL10 antibody thereby implying correct folding.

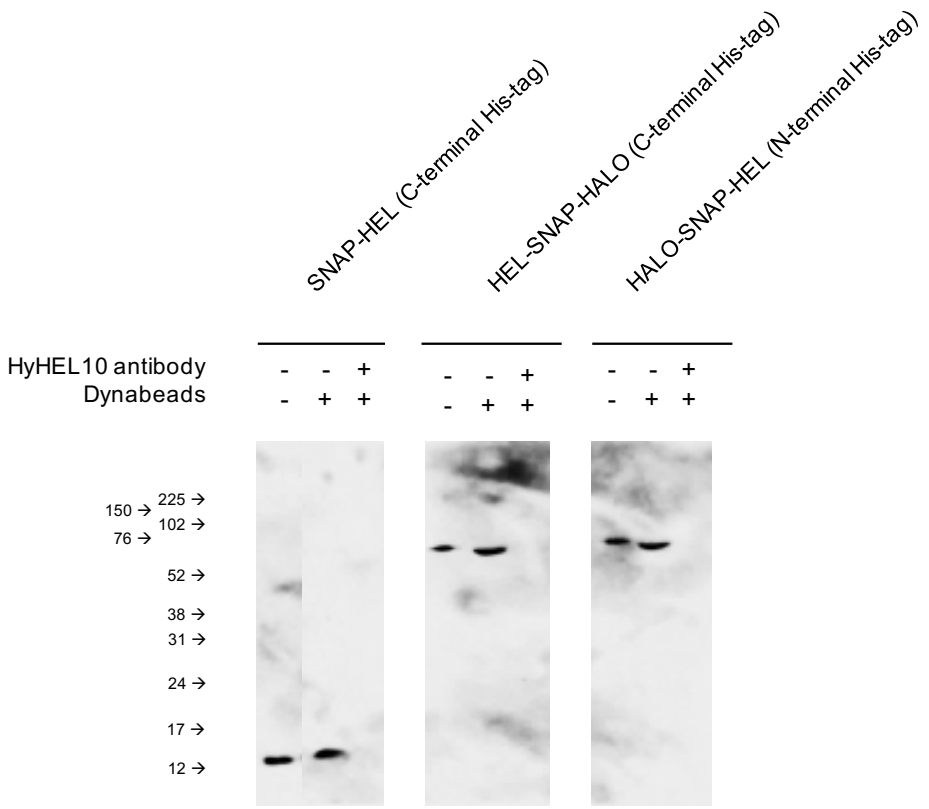

Figure 3.5 Immunodepletion of HEL-fusion proteins by HyHEL10
A 5mg/l solution of Snap-HEL (C-terminal His tag), HEL-Snap-Halo (C-terminal His tag) or Halo-Snap-HEL (N-terminal His tag) was incubated alone, with Dynabeads or HyHEL10 bound to Dynabeads. The supernatant was then removed and subject to SDS PAGE and anti-penta-His Western blot analysis.

HEL-fusion proteins bind with high affinity to HEL-specific antibodies

To establish that the HEL-fusion proteins produced bind to HEL-specific antibodies with comparable kinetics to wildtype lysozyme, surface plasmon resonance-based analysis, as implemented by BIAcore was undertaken. The conformationally sensitive anti-HEL antibodies, HyHEL5 and HyHEL10, were indirectly immobilised onto a BIAcore sensor chip. N-HSH and wildtype lysozyme (Sigma) were then passed through the flow cell to assess binding. Sensorograms and dissociation constants for the interaction are shown in Figure 3.4. N-HSH and lysozyme showed comparable binding to HyHEL10, however, the binding of HyHEL5 to HEL was an order of magnitude less than to wildtype lysozyme.

A

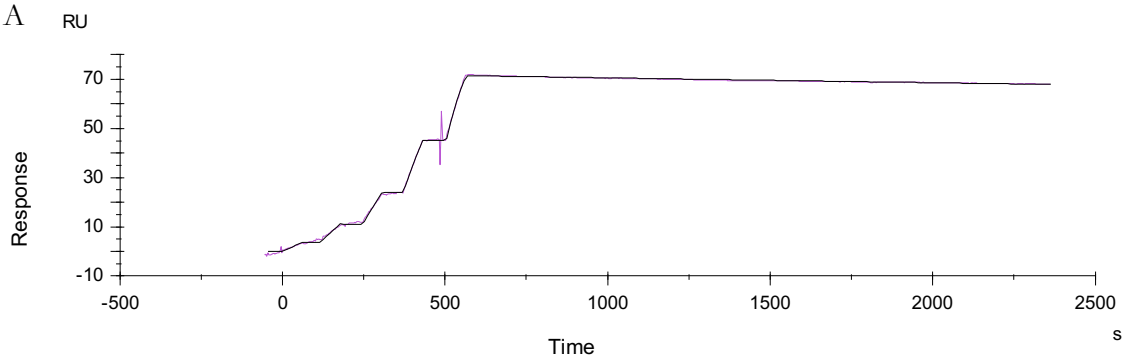

B

Immobilised ligand	Soluble ligand	K_{on} (1/Ms)	K_{off} (1/s)	K_d (pM)	Repeats
HyHEL10	HALO-SNAP-HEL	$4.6 \pm 3.0 \times 10^{6}$	$3.3 \pm 1.0 \times 10^{-5}$	8.9 ± 3.5	4
HyHEL10	Lysozyme	$1.3 \pm 0.8 \times 10^{6}$	$7.3 \pm 1.4 \times 10^{-5}$	8.0 ± 6.5	2
HyHEL5	HALO-SNAP-HEL	$6.2 \pm 2.6 \times 10^{6}$	$8.2 \pm 3.6 \times 10^{-4}$	131 ± 18	4
HyHEL5	Lysozyme	$1.1 \pm 0.7 \times 10^{8}$	$9.0 \pm 9 \times 10^{-4}$	8.1 ± 4.2	3

Figure 3.6 Binding kinetics of HEL-fusion proteins
Surface plasma resonance analysis of the binding of Halo-Snap-HEL (N-terminal His-tag) and lysozyme to the immobilised HEL-specific antibodies, HyHEL5 and HyHEL10. (A) Representative sensorogram of single cycle kinetics for Halo-Snap-HEL (N-terminal His tag) binding to HyHEL10 by surface plasma resonance. (B) Summary of kinetics.

HEL-fusion protein binds to HEL-specific B cells

To establish that the HEL-fusion proteins produced bind to HEL-specific B cells, binding of N-HSH to the D1.3 cell line was assessed by flow cytometry. The D1.3 cell line was a gift from Facundo Batista (Cancer Research UK London Research Institute, Lincoln's Inn Fields Laboratories). This cell line expresses the lower affinity HEL-specific BCR, D1.3. N-HSH was fluorescently labelled with Alexa-488 or -647 via either the Halo®-tag or Snap®-tag, respectively, and incubated with the D1.3 cells followed by flow cytometry analysis (Figure 3.7). Fluorescently labelled N-HSH bound to D1.3 cells with a saturating dose response curve. This binding was specific as there was no binding of fluorescently labelled N-HSH to A20 cells lacking a HEL specific BCR. Both the Snap®-tag and Halo®-tag could be fluorescently labelled and gave similar results indicating correct folding of these parts of the construct.

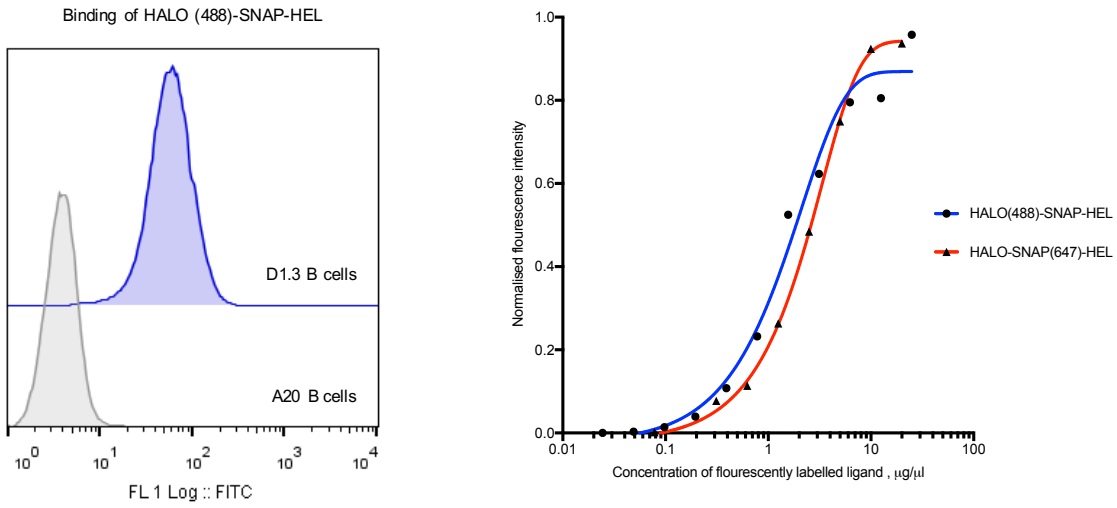

Figure 3.7 Binding of HEL-fusion protein to D1.3 cells
(A)Binding of Halo-Snap-HEL (N-terminal His-tag) fluorescently labelled with Halo-Alexa-488 to D1.3 cells (blue) and A20 cells (black) as determined by flow cytometry. (2) Dose response curves of the binding of HEL-Snap-Halo to D1.3 cells in which the protein is labelled with either Halo-Alexa-488 (blue) or Snap-Alexa-647(red).

3.3.2 Establishment of a HEL specific B cell line

The HEL-fusion proteins produced and characterised were to be used to label HEL-specific B cells in fluorescence-based microscopy experiments. HEL-specific B cells are widely available from mouse models. However, primary cells have a limited lifespan. Cell lines have the advantage of being immortal and the ability to be genetically modified. This section describes the production and characterisation of a HEL-specific B cell model based on the A20 cell line and expressing the highest affinity anti-HEL BCR, HyHEL10.

3.3.2.1 The A20 B cell expresses an IgG2a/kappa BCR

In initial experiments, the surface phenotype of A20 B cells was established. Flow cytometry demonstrated that A20 B cells express an endogenous BCR with isotype IgG2a with a kappa light chain (Figure 3.8).

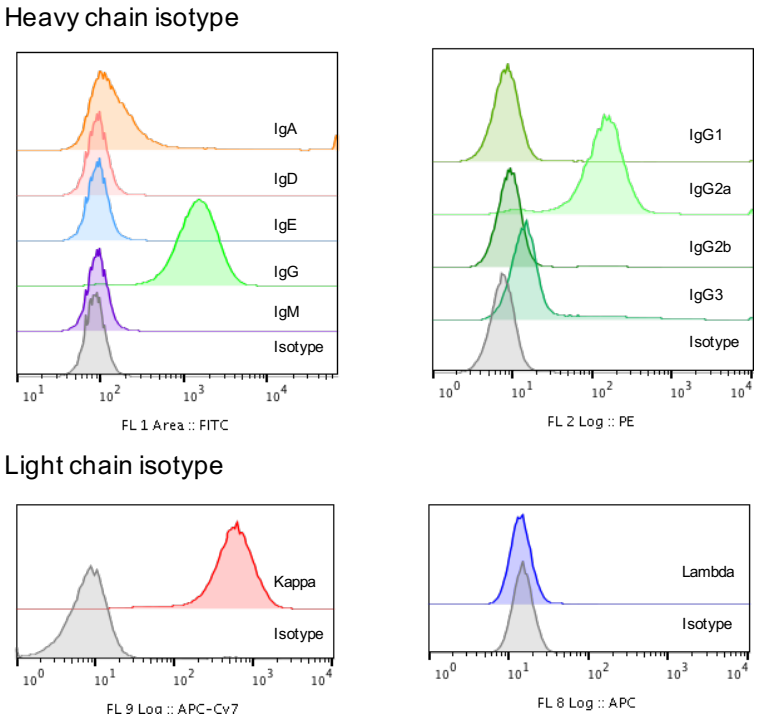

Figure 3.8 Surface phenotype of A20 B cells
A20 B cells were stained with directly conjugated antibodies against the specified targets and analysed by flow cytometry. (A) Surface phenotype of BCR heavy chain. (B) Surface phenotype of BCR light chain.

3.3.2.2 Generating a HEL-specific B cell line expressing a single BCR specificity

The presence of the IgG2a surface immunoglobulin presented a problem since it meant that if the HyHEL10 BCR was expressed in A20 B cells there would be two specificities of BCR on the cell surface. Theoretically, the surface immunoglobulin should not be problematic as it does not bind HEL. Furthermore, previous studies have shown that different isotypes of BCR within the same cell behave in distinct manners, for example clustering in an isotype dependent fashion [131, 236]. However, to avoid any confounding factors endogenous BCR expression was deleted using CRISPR-mediated gene editing to produce a B cell line expressing only the HyHEL10 BCR. The heavy- and light chain-encoding genes were targeted and knockdown assessed by flow cytometry for total BCR expression. Knocking out either the heavy or light chain genes of the endogenous BCR would immediately lead to loss of surface BCR expression making attempts to knock out the remaining chain problematic. To overcome this, CRISPR targeting of both chains was undertaken in a sequential manner alongside expression of the new chains, as outlined in Figure 3.9. This approach was critically dependent on efficient transfection and knowledge of the sequence of the endogenous heavy and light chain.

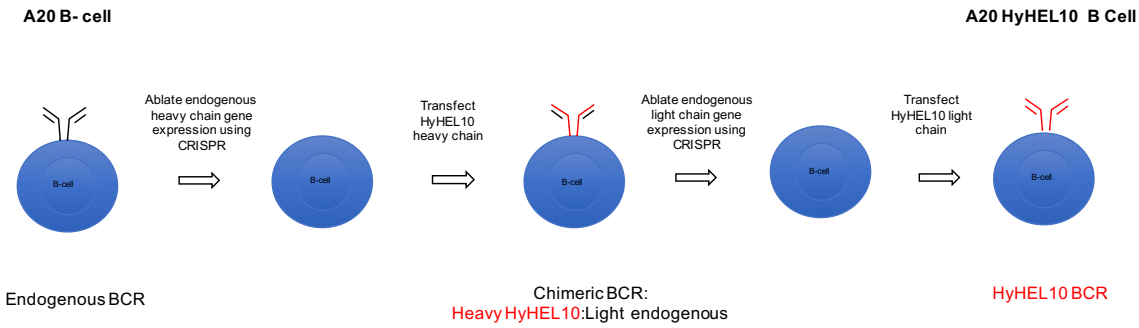

Figure 3.9 Experimental approach for generating an A20 HyHEL10 B Cell Line
Schematic representation of the experimental approach to generate an A20 B cell line expressing a HyHEL10 BCR (red) in which the endogenous BCR (black) has been removed by CRISPR.

3.3.2.3 Optimisation of transfection protocol for A20 B cells

Generating the A20 (HyHEL10) B cell line as outlined in Figure 3.9 requires an effective mechanism of transfection for both CRISPR guides and new heavy and light chain constructs. Multiple biological, physical and chemical methods of transfection exist [292]. In this study, the widely employed lentiviral transfection method has been used in which transfection of a packaging cell line is used to generate virus to infect the cell line of interest. Expressing the BCR represents a challenge as it is a multi-chain receptor. A number of methods exist to achieve multiple gene expression using this system: (1) simultaneous transfection and infection of multiple single plasmids; (2) mixing virus for infection produced from single plasmids transfected separately; (3) mixing virus for infection produced from multiple plasmids transfected simultaneously; (4) sequential transfection and infection, and (5) expression of multiple genes simultaneously from a multi-cistronic plasmid. Methods (1) to (4) were chosen to express the IgM HyHEL10 BCR using genes cloned from MD4 mouse cDNA. Transfection efficiency was assessed by surface expression of the BCR by flow cytometry for IgMa.

Initial experiments using lentiviral transfection to express the BCR highlighted inherent difficulties in achieving high levels of expression in A20 cells. The rules of transfection for the BCR were therefore first established in the easy-to-transfect murine suspension cell line, DO.11.10. In DO.11.10 cells (Figure 3.10A), expression of IgM HyHEL10 BCR was only detected as expected when all four chains of the BCR complex were present. The pooling of individual viruses produced better results than virus produced from the simultaneous transfection of multiple plasmids. The combination of both approaches produced comparable results as shown by mixing virus produced from the simultaneous

transfection of heavy/light chain and Ig-α/β. There were mixed results from adjusting the ratio of virus from an equal to an equimolar ratio based on construct molecular weight. The best result was achieved by sequential transfection. No significant improvement in levels was seen with re-infection.

Expression of the IgM HyHEL10 BCR was then tested in A20 B cells (Figure 3.10B). The A20 cell line differs from the D0.11.10 in that it already expresses an endogenous BCR and therefore has endogenous expression of Ig-α and Ig-β. As expected expression of HyHEL10 heavy and light chain together was sufficient for IgM HyHEL10 BCR expression. Heavy chain expression alone led to detection of IgM HyHEL10 BCR, presumably because of pairing with the endogenous light chain. HyHEL10 light chain expression should theoretically pair with the endogenous heavy chain but this was not detected because the endogenous heavy chain is IgG2a isotype and was therefore not detected by the anti-IgMa antibodies. No additional expression was obtained by transfecting Ig-α and Ig-β into A20 cells, implying that the levels of these proteins is not limiting BCR expression. Across all experiments the transfection efficiency was lower in A20 cells than D0.11.10 cells for comparable conditions. As seen in DO.11.10 cells, pooling of individual viruses produced higher expression levels than virus produced from the simultaneous transfection of multiple plasmids. The combination of both approaches produced similar results with marginally better results when virus was mixed in an equimolar ratio The highest expression level was obtained by transfecting heavy chain alone. The common element of optimal conditions was maximising the amount of HyHEL10 heavy and light chain DNA used.

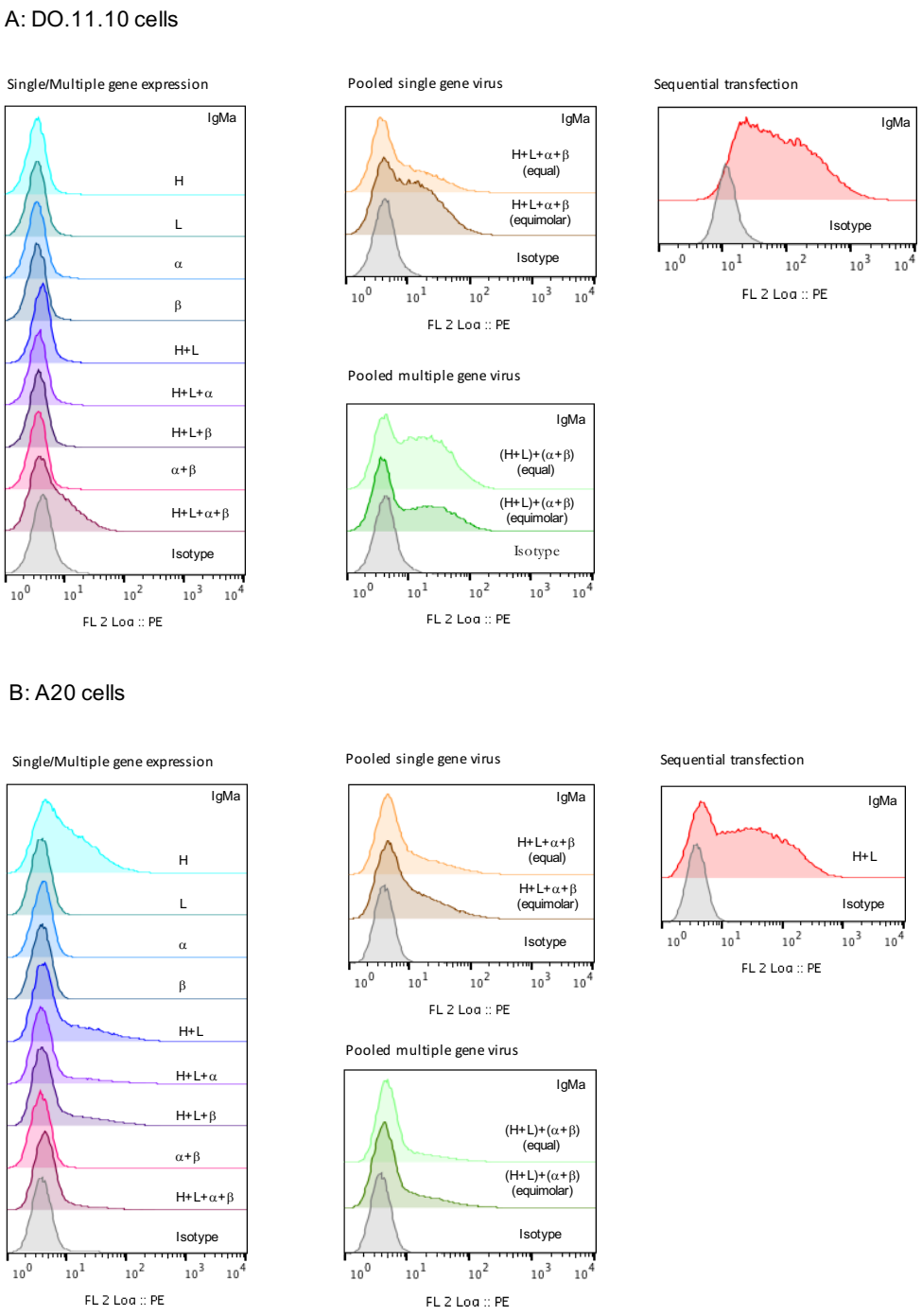

Figure 3.10 Optimising lentiviral transfection of the B cell receptor
(A) DO.11.10 cells or (B) A20 cells were lentivirally infected with HyHEL10^{IgMa} heavy chain (H), HyHEL10^{kappa} light chain (L), Ig-α chain (α) and/or Ig-β chain (β) followed by flow cytometry analysis for IgMa expression. Different variations of the lentiviral transfection method were trialled: simultaneous transfection of single/multiple plasmids and then co-infection; pooling virus for infection produced from single plasmids transfected separately; pooling virus for infection produced from multiple plasmids transfected simultaneously; and sequential transfection and infection of single plasmids. Isotype controls (grey) are shown for comparison.

3.3.2.4 RACE PCR establishes the sequence of the endogenous A20 BCR

To knockout the endogenous A20 BCR, it was first necessary to establish the nucleotide sequence of the endogenous A20 heavy and light chains. This was undertaken using 5' RACE PCR. A single sequence was obtained for the heavy chain consistent with the previously published sequence (Figure 3.11A)[293]; while two sequences were obtained for the light chain, only one of which mapped to the kappa locus (Figure 3.11B).

A A20 B cell Heavy Chain (IgG2a)

```
atggtcttcttgacaacaacagctccagttgtccactccccggtccaattgcaacagtcc
M  V  F  L  T  T  T  A  P  V  V  H  S  P  V  Q  L  Q  Q  S
gggcctgaccttgtgaaacctgggatgtccgtgaaactgtcctgtaagactttgggttac
G  P  D  L  V  K  P  G  M  S  V  K  L  S  C  K  T  L  G  Y
aatttctccgacaagtggattcactggattaaacagaagcctggccgaggccttgaatgg
N  F  S  D  K  W  I  H  W  I  K  Q  K  P  G  R  G  L  E  W
gttggaaggattgatccttctaacggtgatactgactataatacggacttcaagaccccg
V  G  R  I  D  P  S  N  G  D  T  D  Y  N  T  D  F  K  T  P
gccacactaactgttgacagaccctccaacacagcctacttagaactcagcaacctgaca
A  T  L  T  V  D  R  P  S  N  T  A  Y  L  E  L  S  N  L  T
tctggggactctgcggtctattattgttcaatatcgggtgattattccgcctgcgactat
S  G  D  S  A  V  Y  Y  C  S  I  S  G  D  Y  S  A  C  D  Y
tggggccaaggcaccgaactcacagtctcctcagccaaaacaacagccccatcggtctat
W  G  Q  G  T  E  L  T  V  S  S  A  K  T  T  A  P  S  V  Y
ccactggccccctgtgtgtggagatacaactggctcctcggtgactctaggatgcctggtc
P  L  A  P  V  C  G  D  T  T  G  S  S  V  T  L  G  C  L  V
```

B A20 B cell Light Chain (Kappa)

```
atgaagttgcctgttaggctgttggtgctgatgttctggcttcctgtttccagtagtgat
 M  K  L  P  V  R  L  L  V  L  M  F  W  L  P  V  S  S  S  D
gttgtgatgacccagactccactctccctggccgtcagtcttggagatcacgtgaaaatg
 V  V  M  T  Q  T  P  L  S  L  A  V  S  L  G  D  H  V  K  M
tcttgtagatgtaatcagagccttgtaaacagtcatggagactccttttacactggttt
 S  C  R  C  N  Q  S  L  V  N  S  H  G  D  S  F  L  H  W  F
ctgcagaagccaggccagtctccaaagctcctgatctacaaggtttccagccgatttttt
 L  Q  K  P  G  Q  S  P  K  L  L  I  Y  K  V  S  S  R  F  F
ggggtcccagagaggttcagtggcagtggttcagggacagatttcacactcgagatcagt
 G  V  P  E  R  F  S  G  S  G  S  G  T  D  F  T  L  E  I  S
cgagtggaggctgaggatctgggagtttatttctgttctcaaggtgcacatgttccgtgg
 R  V  E  A  E  D  L  G  V  Y  F  C  S  Q  G  A  H  V  P  W
acgttcggtggaggcaccaagctg
 T  F  G  G  G  T  K  L
```

Figure 3.11 Sequence of the endogenous A20 BCR
(A) Heavy chain and (B) Light chain DNA sequences of the A20 BCR as established by RACE PCR. Leader sequence (green), variable region (yellow) and constant region (blue).

3.3.2.5 Design of CRISPR guides

To knockout the endogenous A20 BCR the CRISPR-Cas9 gene editing system was used. Consensus sequences obtained by RACE PCR were used to design guides targeting the variable domain of the A20 heavy and light chains. The variable domain was chosen for guide selection to ensure any subsequently transfected HyHEL10 chain would not be targeted by the same guides. Guides were chosen based on proximity to the start codon and low off-target activity. Guides were cloned into the lentiCRISPRv2 vector, virus produced in HEK 293T cells and used to infect A20 cells. Cells were selected using puromycin and knockdown confirmed via flow cytometry for total BCR expression.

3.3.2.6 Sequential establishment of a HEL-specific B-cell line

The IgG2a endogenous heavy chain was firstly targeted by CRISPR mediated gene editing. This was successfully knocked down in a small population of cells as seen by loss of cell surface expression of IgG2a by flow cytometry. Cells negative for IgG2a BCR were sorted by FACS. The IgM HyHEL10 heavy chain, cloned from MD4 mouse cDNA into pHR, was then transfected into the cell line with reconstitution of surface expression of a BCR. A pure population of positive highly-expressing cells were selected by FACS. The kappa light chain was then targeted. Using CRISPR mediated gene editing the kappa chain was successfully knocked down in a small population of cells as seen by loss of cell surface expression of IgM via flow cytometry. Cells were again sorted by FACS. The HyHEL10 light chain, cloned from MD4 mouse cDNA into pHR, was then transfected into the cell line with reconstitution of surface expression of BCR as identified via FACS (Figure 3.12).

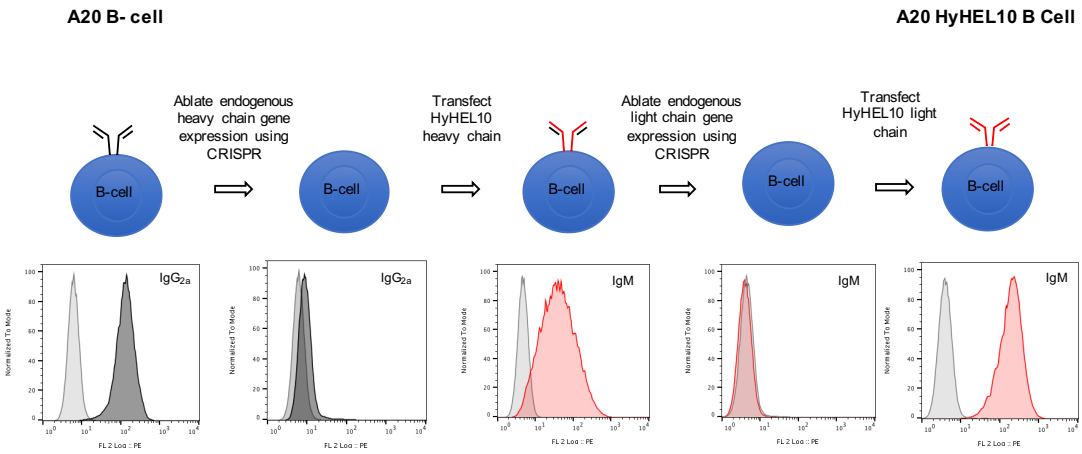

Figure 3.12 Sequential generation of the A20 HyHEL10 B Cell Line
Experimental approach resulting in the generation of an A20 B cell line expressing an IgM HyHEL10 BCR (red) in which the endogenous IgG2a BCR (black) has been removed by CRISPR. Histogram plots display the expression of IgG2a BCR (black) or IgMa BCR (red) at the different stages. Isotype control shown in grey.

3.3.2.7 HyHEL10 BCR can be expressed at a range of levels in A20 cells

The HEL-specific B cell line generated was to be used for a range of downstream applications including fluorescence-based microscopy experiments. These experiments would require variable HyHEL10 expression levels dependent on whether single molecule or bulk imaging was conducted.

To generate an A20 (HyHEL10) B cell line with a range of HyHEL10 BCR expression levels, a number of different approaches were trialled (Figure 3.13). It had previously been observed during optimising the transfection protocol, that the total amount of DNA transfected (and subsequently infected) was critical to HyHEL10 BCR expression levels. In view of this, the total amount of DNA transfected or the volume of virus used per infection was adjusted. Increasing the amount of DNA transfected or the volume of virus infected led to increased expression levels, however, this was at the expense of a larger co-efficient of variance. Therefore, rather than producing a single population a larger spread

of expression levels was seen. Similar results were seen with the use of shRNA directed against IgM. To achieve more uniform levels, cell sorting was undertaken to attempt to capture high and low levels of expression. However, while cell sorting was successful in achieving short term control of expression levels, ultimately levels quickly returned back to pre-sort levels.

To achieve control of expression levels an alternative approach was conceived using the different vectors, pHR and pHRI. The pHR vector expresses the gene of interest under the control of the highly efficient SFFV viral promotor. The pHRI vector is identical to the pHR vector aside from it has a different promotor. The pHRI vector expresses proteins under the control of the E/GRE which requires the activity of the nuclear factors RXR and FB-ERV (together with ponasterone) for optimal protein expression. These are not present in A20 cells leading to inefficient protein expression. Two distinct populations of cells were obtained using these two vectors: the pHR vector gave high levels of approximately 25000 receptors/cell whereas the pHRI vector gave low levels of approximately 1000 receptors/cell (Figure 3.13)

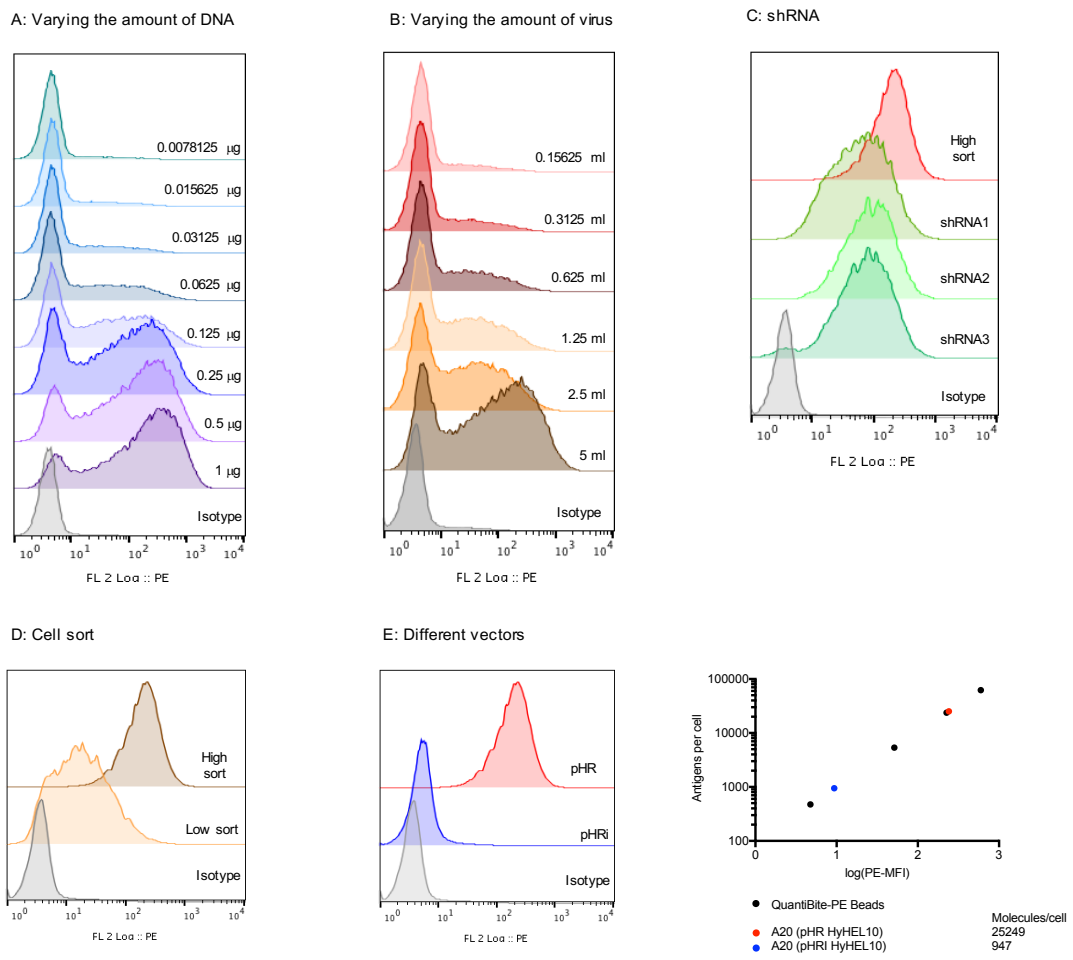

Figure 3.13 The HyHEL10 BCR can be expressed at a range of levels in A20 cells
The expression levels of IgM HyHEL10 BCR were determined by flow cytometry following a range of interventions. (A) Varying the total amount of DNA (IgM HyHEL10 heavy chain (H) plus HyHEL10 kappa light chain(L)) used to transfect packaging cell line. (B) Varying the total volume of virus used to infect A20 cells. (C) Lentivirally transfecting three different shRNA guides (1-3) into A20 HyHEL B cells to down regulate BCR expression. (D) Sorting a population of A20 HyHEL10 B cells into two distinct populations. (E) Expression of the IgM HyHEL10 BCR using either the pHR or pHRI vector followed by quantification of expression levels using QuantiBrite-PE beads.

3.3.2.8 HyHEL10 BCR can be labelled in a 1:1 ratio via the Ig-alpha chain

To extend the BCR toolkit further an intrinsically labelled HyHEL10 BCR was generated to allow fluorescent labelling of the BCR in microscopy-based experiments. Attaching a tag to the immunoglobulin heavy or light chain is a potential option but results in labelling that is always bivalent. To overcome this, an approach was devised in which a Halo®-tag

or Snap®-tag was connected to the intracellular domain of the Ig-α thereby allowing 1:1 labelling of each BCR. (Figure 3.14) The endogenous Ig-α was firstly knocked out by CRISPR-mediated gene editing. A CRISPR resistant form of Ig-α connected by a short linker to a Halo®-tag or Snap®-tag was then transfected into the cell line, reconstituting BCR surface expression. Importantly, transfection of wildtype Ig-α failed to reconstitute BCR expression due to ongoing activity of integrated CRISPR guides thereby confirming appropriate targeting and knockdown. Transfection with CRISPR resistant forms of Ig-α-Snap/Halo from either the pHR or pHRI vectors again provided a means of controlling cell surface expression levels for downstream applications.

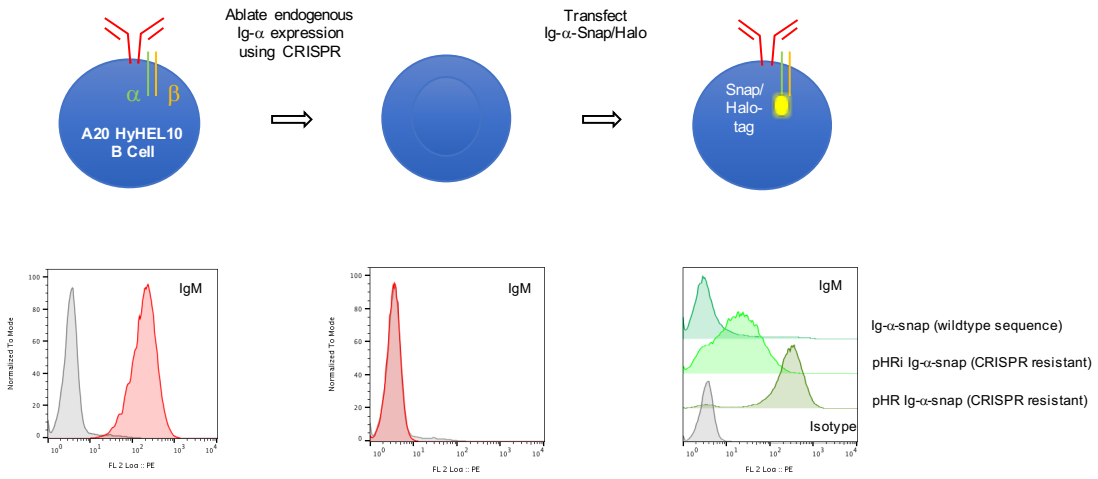

Figure 3.14 Generating a tagged form of the A20 B Cell Line
Experimental approach resulting in the generation of an A20 (HyHEL10) B cell line expressing a Snap-tag® on the Ig-α chain (green). Histogram plots display the expression of IgMa BCR (red) pre-CRISPR, post-CRISPR and following re-infection of a wildtype Ig-α-Snap, a CRISPR-resistant Ig-α-Snap construct from the pHRI vector or a CRISPR-resistant Ig-α-Snap construct from the pHR vector. Similar results were obtained for Halo®-tag constructs

3.3.2.8 A20 HyHEL10 could be generated in a range of isotypes

This chapter describes the production of an A20 B cell line expressing the IgM HyHEL10 BCR. However, the BCR is not a single entity but can be expressed in 5 different isotypes which have varying functions. To allow future investigation of any differences in triggering between BCR isotypes, HyHEL10 heavy chain has been cloned as IgA, IgD, IgE, IgG1, IgG2a, IgG2b and IgG3 isotypes ready for future expression in A20 cells.

3.3.3 Production of surrogate BCRs for surface bound experiments

The BCR is essentially a membrane bound immunoglobulin. It is therefore possible to use anti-HEL antibodies as surrogate BCRs for in vitro experiments with soluble reagents. HyHEL10 was expressed and purified for this purpose. The binding of HEL to HyHEL10 is always dimeric, therefore, to allow studies of the binding of single HEL molecules at a surface fab fragments were also produced.

3.3.3.1 Expression and purification of HyHEL10 antibody

A HyHEL10 expressing hybridoma was grown and 1000ml of supernatant harvested. HyHEL10 was then extracted from the supernatant by protein G purification. Eluted fractions were characterised by SDS-PAGE. Fractions containing clean whole antibody were pooled and subjected to size exclusion chromatography. A single peak corresponding to HyHEL10 antibody was obtained. Eluted FPLC fractions were analysed by 12 % SDS PAGE gels under non-reducing and reducing conditions. SDS PAGE confirmed pure antibody production with appropriate reduction of whole antibody to light and heavy chains under reducing conditions (Figure 3.15)

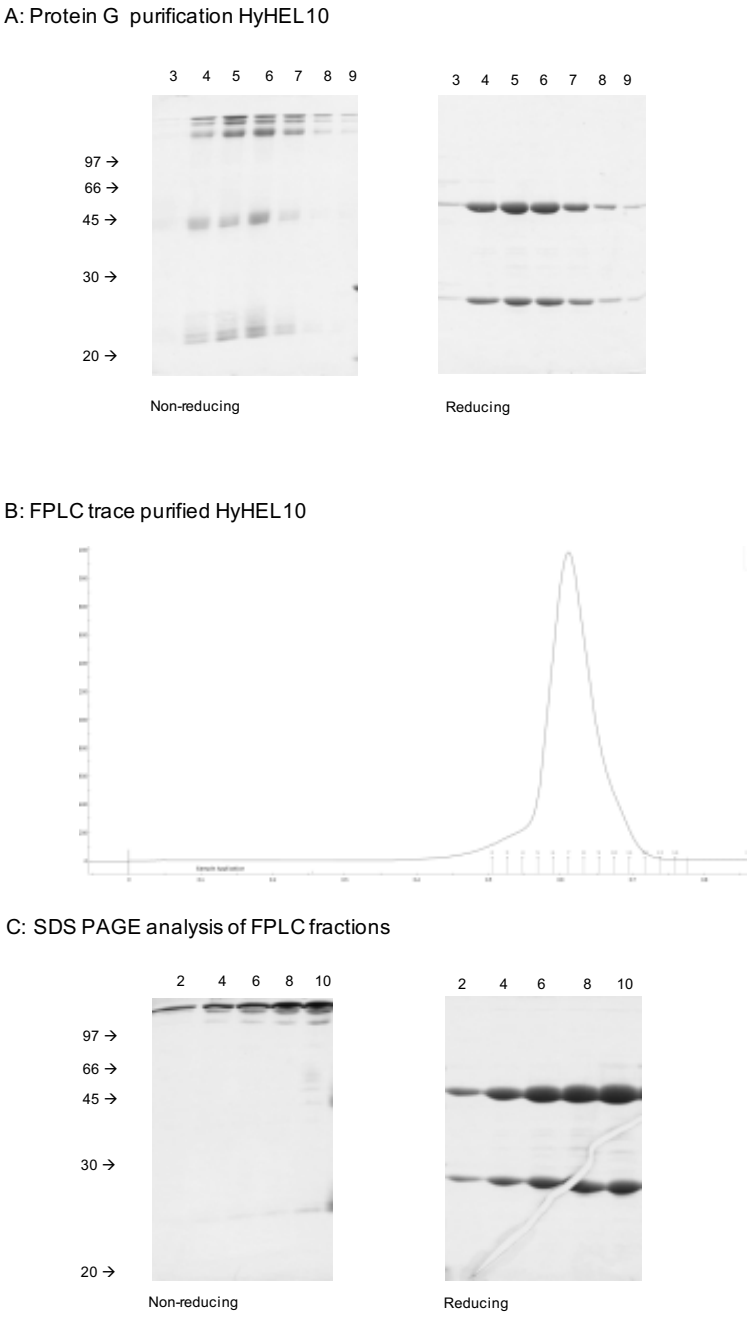

Figure 3.15 Purification of HyHEL10 antibody
(A) Non-reducing and reducing 12 % SDS PAGE gels of HyHEL10 antibody eluted from protein G beads. The numbers above the lanes correspond to the fractions eluted from the protein G column. (B) Separation of HyHEL10 antibody by size exclusion chromatography using a Superdex S200 column. (C) Eluted FPLC fractions were analysed on 12 % SDS PAGE gels under non-reducing and reducing conditions. The numbers above the lanes correspond to the fractions eluted from the FPLC.

3.3.3.2 HyHEL10 Fab production by whole antibody papain digest

HyHEL10 fab fragments were generated by digesting whole HyHEL10 antibody with papain. The Fab and Fc generated were then separated using protein A. Pure Fab was pooled and separated by size exclusion chromatography. The final SDS PAGE demonstrated relatively pure HyHEL10 Fab, but with some residual Fc contamination.

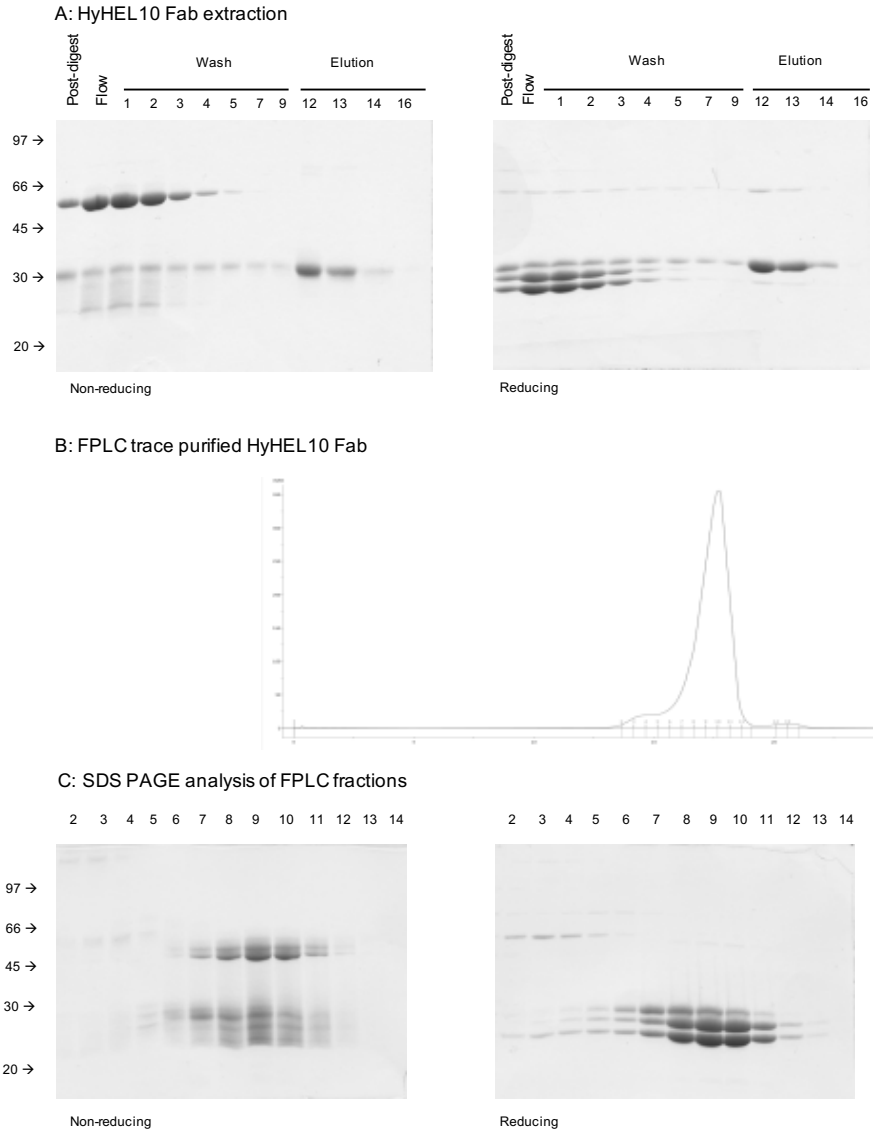

Figurre3.16 Papain digest of HyHEL10
(A) Non-reducing and reducing 12 % SDS PAGE gels of HyHEL10 whole antibody following papain digestion. Samples include: post digest; first Protein A flow through; numbered fractions following each wash set; and numbered fractions eluted from Protein A column (B) Flow through and wash fractions 1-5 were pooled and purified by size exclusion chromatography using a Superdex S200 column. (C) Eluted FPLC fractions were analysed on 12 % SDS PAGE gels under non-reducing and reducing conditions. The numbers above the lanes correspond to the fractions eluted from the FPLC.

3.4 Discussion

The results presented in this chapter describe the production of a toolkit of reagents that will be used to probe the mechanism of triggering of the BCR. These reagents are complementary to, and supplement the well-established HEL model system.

3.4.1 HEL-can be expressed as a fusion protein to allow fluorescent labelling

A main focus of the early part of this thesis has been on producing a high quality HEL-fusion protein that can be used for fluorescence based microscopy experiments. Proof of principle has been shown that HEL can be produced as a fusion protein. N-HSH produced the highest yield of protein. Importantly, this protein was clean and monomeric. It has subsequently been shown using immunodepletion experiments with conformationally sensitive antibodies that HEL folds correctly within these fusion proteins. Furthermore, the HEL-fusion proteins generated bind both to HEL-specific B cell and HEL-specific antibodies. Plasma surface resonance experiments have shown that HEL binds to HEL-specific antibodies with a very low equilibrium dissociation constant making them excellent for receptor labelling. There was no difference in the binding kinetics of N-HSH to HyHEL10 compared to wildtype lysozyme. However, there was a difference in the binding kinetics of N-HSH to HyHEL5 compared to wildtype lysozyme. The difference was exclusively accounted for by a reduction in the association constant. This suggests that the engineered N-HSH may be folded in such a way that it impedes access of HyHEL5, but not HyHEL10, to its epitope, thereby reducing the association constant but not affecting the dissociation constant. In view of this, future work will focus on the HyHEL10 antibody and BCR.

3.4.2 The A20 HyHEL10 B cell line provides two options for BCR labelling

In this chapter, the generation of a HEL-specific B cell line has been described. Following optimisation of the transfection protocol both the endogenous heavy and light chain of the A20 B cell have been knocked out and replaced with HyHEL10 heavy and light chains. The HyHEL10 BCR has been further modified by the additional of an intracellular Snap® or Halo®-tag to the Ig-α chain. This provides two options for receptor labelling: internal BCR labelling via Snap®-tag or Halo®-tag or external BCR labelling using fluorescently labelled HEL. The former method allows 1:1 labelling of the BCR but is limited to use in cell lines in which the genetic modifications to insert Ig-α-Snap/h=Halo be undertaken. The external labelling strategy is more complex in that each BCR will be labelled twice, however, it provides an option for labelling primary cells. This is important as ultimately the work presented in this thesis will be expanded to examine primary cells from the MD4 mouse to allow both correlation of results and examination of B cell subsets.

In generating a HEL specific B cell line two distinct populations of HyHEL10 expressing B cells have been produced. The pHRI vector has been used to generate an A20 (HyHEL10) cell line expressing low BCR expression levels of approximately 1000 molecules per cell. This cell line is ideally suited for single molecule imaging experiments. The pHR has been used to generate an A20 (HyHEL10) B cell line expressing high BCR expression levels of approximately 25,000 per cell. This cell line is ideally suited for bulk fluorescence imaging. However, it is important to note that the expression levels generated by the pHR vector are still significantly lower than the 100,000 receptors expressed on an

individual primary B cell. It will therefore be necessary to conduct future experiments on MD4 primary cells to ensure results obtained using cell lines are truly generalisable. This emphasises further the importance of the external labelling strategy developed that is transferable to a system of primary cells.

3.4.3 HyHEL10 antibody and fab can be used as surrogate BCRs

In the third part of this chapter, HyHEL10 whole antibody has been produced. This has been generated to allow it to be used as a surrogate BCR in surface bound experiments. In addition, HyHEL10 fab has been produced to allow single HEL binding as a monomer control in such surface bound experiments. These reagents therefore allow the development of an in vitro surface bound system to replicate the B cell surface for experimental analysis.

The toolkit of reagents generated and characterised in this Chapter will now be used to assess the mechanism of triggering of the BCR. These experiments form the basis of the next three Chapters.

Chapter 4

The Cross-Linking Model and B Cell Receptor Triggering

4.1 Introduction

In Chapter 3, the generation of a toolkit of reagents, for probing the triggering mechanism of the BCR using advanced fluorescence microscopy, was described. These reagents were used to test key predictions of existing models of BCR triggering. The first model examined was the cross-linking model. The cross-linking model is the original model of BCR triggering. It proposes that in the resting, non-antigen bound state the BCR is a bivalent complex (a single BCR with two antigen binding sites). Signalling occurs when two or more BCRs are brought into close proximity *i.e.* 'cross-linked' by a multivalent ligand [215].

Aggregation driven signalling is a widely-accepted model of transmembrane receptor triggering. The classic example is signalling via the epidermal growth factor receptor (EGFR). Binding of ligand to the extracellular domain of the EGFR leads to an increase in the fraction of dimeric forms of the receptor and activation via trans-autophosphorylation of the cytoplasmic domains of the receptor, which have intrinsic kinase activity [294]. In contrast to the EGFR, the BCR does not possess any inherent enzymatic activity, however, the Src-family kinase Lyn associates with the BCR. It is easy to conceive how aggregation of BCRs could lead to triggering via the accumulation of weakly bound Lyn, favouring the phosphorylation of the ITAMs of neighbouring receptors leading to the recruitment and activation of additional Lyn [295]. BCR

crosslinking and aggregation could therefore induce rapid and large-magnitude triggering and downstream signalling.

The cross-linking model is based on early work, demonstrating that bivalent anti-BCR antibodies or $F(ab)'_2$ fragments can activate B cells, whereas monovalent Fab fragments do not [217-221]. Further work has supported this viewpoint by demonstrating that soluble multivalent antigens but not soluble monomeric antigen are able to activate B cells [222-224]. While artificial crosslinking of BCRs in solution is undoubtedly sufficient to activate B cells, it remains unclear if this is the quintessential, or only triggering mechanism operating in vivo.

Any plausible model of BCR triggering needs to explain how the BCR is capable of responding to the vast array of antigens it is likely to encounter in vivo. This presents a challenge to the cross-linking model, as not all antigens would be expected to crosslink the BCR to the extent needed for activation. Furthermore, any triggering mechanism needs to explain triggering within the correct biological context. The crosslinking model is based on evidence from experiments in which antigen was presented in solution. However, it is now clear that B cells predominantly encounter antigen that is not soluble, but membrane associated, [202, 203, 226-228] presented by macrophages [201-205], dendritic cells [206, 207], follicular dendritic cells [208-210] and B cells themselves.

In experiments described in this chapter, the principles of the cross-linking model were tested by assessing the ability of monomeric and multivalent ligand to activate B cells not only in solution, but also at a surface. This allowed, firstly, verification of the utility of the

BCR toolkit described in Chapter 3, versus published data on BCR triggering in solution. Secondly, it allowed assessment of whether the crosslinking model is capable of explaining all phenomena related to BCR triggering including in the physiological setting of surface associated antigen.

4.2 Materials and Methods

4.2.1 Construct design and cell line preparation

HEL-Snap-Halo-BirA-His-tag constructs were amplified from existing HEL-Snap-Halo-His-tag plasmids using custom oligonucleotides, which added a BirA-His-tag to the appropriate terminus by extension PCR. The final PCR products were cloned into the pHR vector using the MluI and NotI restriction sites and the sequence verified by DNA sequencing.

4.2.2 Protein expression, extraction and purification

HEL-Snap-Halo-BirA-His-tag constructs were expressed in CHO cells using the large scale lentiviral protocol with supernatant harvested every 2-4 days until 1.6 litres had been collected. Protein purification was undertaken by Ni extraction.

4.2.3 Biotinylation

N-Halo-Snap-HEL-BirA-His-tag (N-HSH-BirA-Histag) were buffer exchanged with 10ml 10 mM Tris/HCL pH 8.0 using a 10 kDa cut off spin concentrator followed by concentration to approximately 2 mg/ml. A sample of unbiotinylated protein was saved for subsequent analysis. The biotinylation mix was made up as follows:

	Volume (μl)	Concentration	Company
Protein	700	2 mg/ml	
Biomix A	100	10x	Avidity
Biomix B	100	10x	Avidity
d-Biotin	100	10x	Avidity
BirA enzyme-biotin ligase	10	1 mg/ml	Avidity

The reaction mix was incubated for 2 hours overnight at room temperate with gentle rocking. The following day the protein mix was concentrated using a 10 kDa cut off spin concentrator and run over an AKTA pure FPLC system using an S200 10/30 GL column (GE Healthcare). Factions corresponding to biotinylated protein were pooled and concentrated using a 10 kDa cut off spin concentrator and either used immediately for downstream applications or aliquoted and frozen at -80 °C.

4.2.4 Assessment of biotinylation efficiency

Biotinylation efficiency was assessed using a gel shift assay. 5 μg of unbiotinylated protein and 5 μg biotinylated protein were incubated for 30 mins at room temperature, both with and without 5 μg streptavidin. Samples were then run directly on a non-reducing gel (without a prior denaturing step) and directly visualised by staining with Coomassie Blue Solution

4.2.5 Tetramer production

Tetramers of HEL-Snap-Halo-BirA-His-tag were generated by mixing biotinylated protein with streptavidin in a 4:1 molar ratio (42.3 µl, 1 mg/ml biotinylated HEL-Snap-Halo-BirA-His-tag; 7.7 µl, 1 mg/ml Streptavidin, NEB) and incubating at 4 °C for 1 hour.

4.2.6 Surface preparation

Antibody/PLL coated glass. Glass cell culture dishes (FD3510-100 FluoroDish, 35 mm) were coated with 200 µl of PLL (150-300 kDa; Sigma-Aldrich), 10 µg/l anti-IgG (Sigma), 10 µg/l anti-IghM (Jackson ImmunoResearch), or 10 µg/l isotype antibody (POPC, Sigma Aldrich) and incubated overnight at 4°C. The following day the dishes were washed twice with HBS. Finally, 200 µl of HBS/2.5 mM probenecid was added to the plates.

FCS/glass. Glass cell culture dishes (FD3510-100 FluoroDish, 35 mm) were blocked by overnight incubation with 200 µl of complete A20 media. The following day the dishes were washed twice with HBS followed by addition of a final 200 µl of HBS/2.5 mM probenecid.

SLBs for triggering "in solution". Pure POPC SLBs for triggering in solutions were generated by spin coating and hydrated in 500 µl of HBS/2.5 mM probenecid in an Attoflour Cell Chamber (Life Technologies Ltd).

Ni-TA HisSorb plates. Ni-TA HisSorb plates (Qiagen) were prepared by coating wells with 100 µl of protein at the desired concentration followed by incubation overnight at 4°C. The following day the dishes were washed twice with HBS followed by addition of a final 100 µl of HBS/2.5mM probenecid.

SLBs for "surface bound experiments". 96% POPC/4% DGS-NTA(Ni) SLBs were prepared by spin coating and hydrated with 500 μl of protein at the desired concentration in HBS/2.5 mM probenecid in an Attoflour Cell Chamber (Life Technologies Ltd). The protein was allowed to bind to the NiNTA for 1 hour at room temperature. The protein buffer was then diluted out by addition of 500 μl HBS/2.5mM probenecid, followed by removal of 500 μl of buffer. This process was repeated 10 times ensuring the SLB was never left dry.

4.2.7 Binding of HEL-fusion proteins to Ni-NTA plates

The binding of N-HSH to Ni-NTA plates was determined by producing a dose response curve. 100 μl N-HSH labelled with 647-SiR via the Halo-tag was added at a range of concentrations to each well of a Ni-NTA plate and incubated overnight at 4˚C. The plates were then washed with HBS before the fluorescence at 647 nm was detected with a Clariostar fluorescence microplate reader. Nonlinear regression analysis with a 1:1 Langmuir binding model was then used to derive B_{max} and K_d values.

4.2.8 Calcium triggering experiments

Prepared surfaces were transferred to the stage of a spinning disc confocal microscope (Carl Zeiss) fitted with an AxioCam camera and housed within an incubation box kept at 37 ˚C/5% CO_2. For "in solution" experiments", Flou-4 labelled cells were added to the surface, allowed to settle for 2 minutes, and then time-lapse imaging commenced with an image taken every 500 milliseconds for 10 minutes in the 488 nm channel. During the first 30 seconds of each video, soluble ligand was added in a volume <10 μl to achieve the final

desired concentration in HBS/2.5mM probenecid. For "surface-bound experiments", a small volume of Flou-4 labelled cells were added to the surface to focus the microscope to the correct plane. Time-lapse imaging was then commenced every 500 milliseconds for 10 minutes in the 488 nm channel. During the first 30 seconds of each video, approximately 20 μl of Flou-4 cells were added to the buffer to achieve approximately 100-400 cells within the field of view.

4.2.9 Fluorescence Correlation Spectroscopy

Ni-NTA supported lipid bilayers were formed with 0.001% KK-DPPE and labelled with N-HSH (which had been labelled with Halo-647SiR) followed by Fluorescence Correlation Spectroscopy (FCS) with confocal illumination using a Zeiss780 LSM microscope fitted with a x 40 oil objective (NA1.2). The microscope was focused on a diffraction limited spot on the bilayer and three measurements taken. This process was repeated multiple times at different points on each SLB. Data was fitted with the 2D + triplet model using FoCuS point correlator software [296]

4.2.10 Fluorescence recovery after photobleaching

Ni-NTA supported lipid bilayers were formed and labelled with N-HSH (which had been labelled with Halo-SiR). Bilayers were then imaged with TIRF using a custom built microscope fitted with a 641 nm laser (100 mW, CUBE 640-100C, Coherent) and 1.4 NA TIRF objective (100x oil objective, UPLSAPO100XO/1.4, Universal Plan Super Apochromat). Pre-bleach images were acquired, followed by illumination of a region of interest with 100% laser power, followed by post-bleach image acquisition.

4.3 Results

4.3.1 Production of monomeric and tetrameric HEL

A key prediction of the cross-linking model is that multivalent, but not monovalent ligands are able to trigger the BCR. To test this hypothesis, directly comparable monovalent and multivalent ligands were required. Chapter 3 described the production of monomeric HEL-fusion proteins, however, experiments in this chapter required the additional production of a multivalent form of HEL.

Initial attempts to make a multivalent protein were undertaken by expressing linked copies of HEL under the control of a single promoter. Constructs that had generated high yields of monomeric HEL were chosen and an additional HEL added via a short linker producing HEL-Snap-HEL and HEL-Snap-Halo-HEL. However, while cloning of the construct was successful, protein expression using the large scale lentiviral method resulted in minimal quantities of poor quality protein.

An alternative strategy was conceived of producing the HEL-Snap-Halo constructs descripted in Chapter 3 as BirA-His-tag fusion proteins. The BirA-His-tag attaches both a His-tag and a single biotinylation site to proteins. HEL tetramers can then be produced by conjugating biotinylated protein to streptavidin. This strategy utilised construct designs already established in experiments described in Chapter 3 to express high quality protein. Furthermore, the method utilised the same protein either directly as a monomer or as a tetramer bound to streptavidin, meaning the reagents were biologically comparable aside from their valency.

4.3.1.2 HEL can be expression as a BirA-His-tag fusion protein

HEL-Snap-Halo (C-terminal BirA-His-tag; C-HSH-BirA-His) and Halo-Snap-HEL (N-terminal BirA-His-tag; N-HSH-BirA-His) constructs were generated using a multi-step PCR-based protocol and soluble protein expressed using the large-scale lentiviral infection method. Protein was polyhistidine affinity tag extracted and purified by size exclusion chromatography (Figures 4.1 and 4.2). Purification of the C-HSH-BirA-His protein resulted in two bands, with the additional band potentially representing a protein cleavage product due to breakage at one of the linker regions. These products could be partially separated by gel filtration. Comparable results were obtained for the C-terminal double His-tag construct described in Chapter 3, suggesting this was intrinsic to the construct design. The N-HSH-BirA-His protein was much cleaner with only a single band apparent under denaturing conditions, as previously seen for the double his-tag construct described in Chapter 3. The N-HSH-BirA-His protein was therefore chosen for studying the cross-linking dependence of signalling by the BCR.

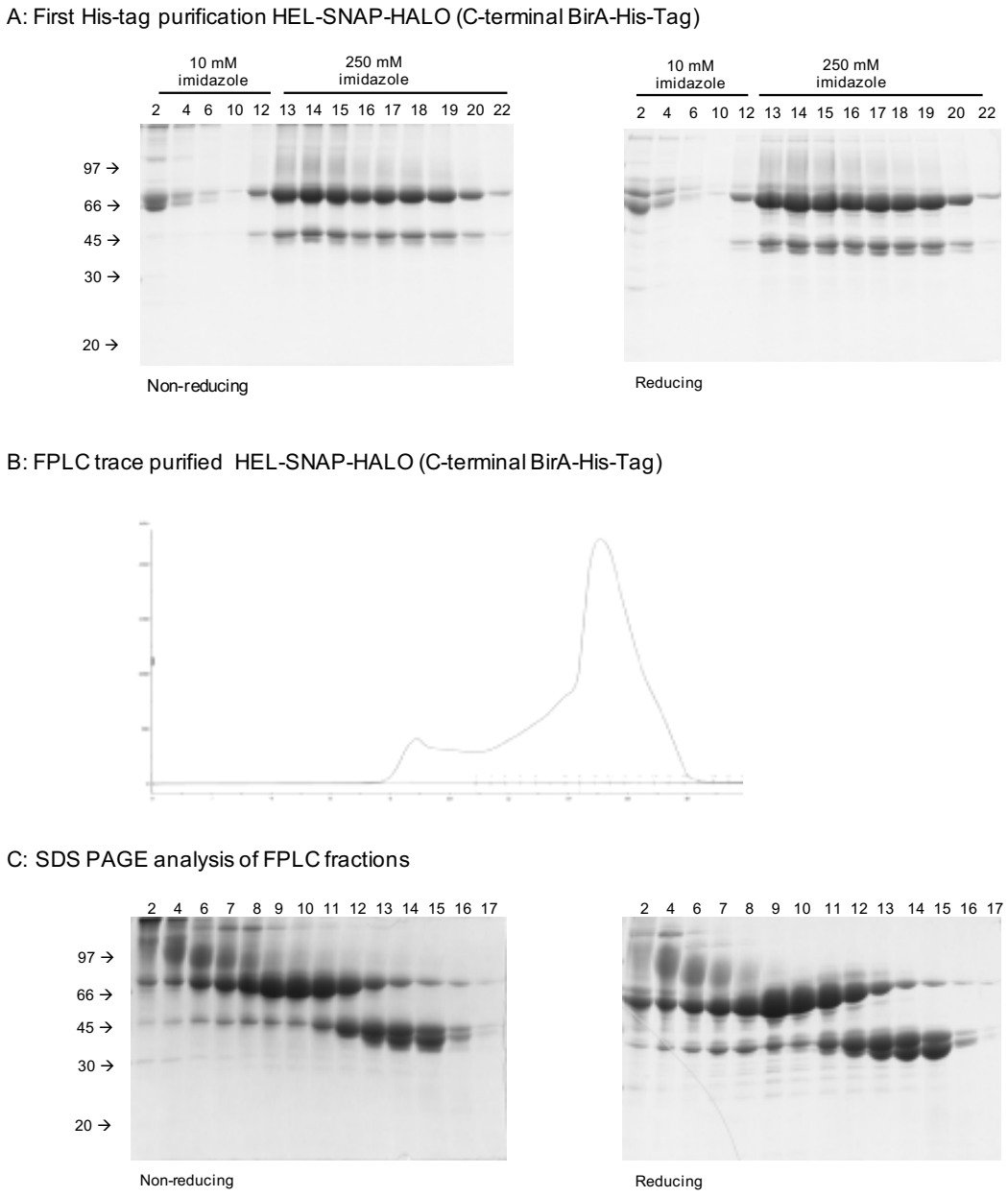

Figure 4.1 Purification of HEL-Snap-Halo (C-terminal BirA-His tag)
(A) Non-reducing and reducing 12 % SDS PAGE gels of HEL-Snap-Halo (C-terminal BirA-His tag) fractions eluted from a Ni-NTA column. The numbers above the lanes correspond to the fractions eluted from the Ni-NTA column. Representative example of two extractions. (B) Separation of His-tag purified HEL-Snap-Halo (C-terminal BirA-His-tag) by size exclusion chromatography using a Superdex S200 column. (C) Eluted FPLC fractions were analysed on 12 % SDS PAGE gels under non-reducing and reducing conditions. The numbers above the lanes correspond to the fractions eluted from the FPLC.

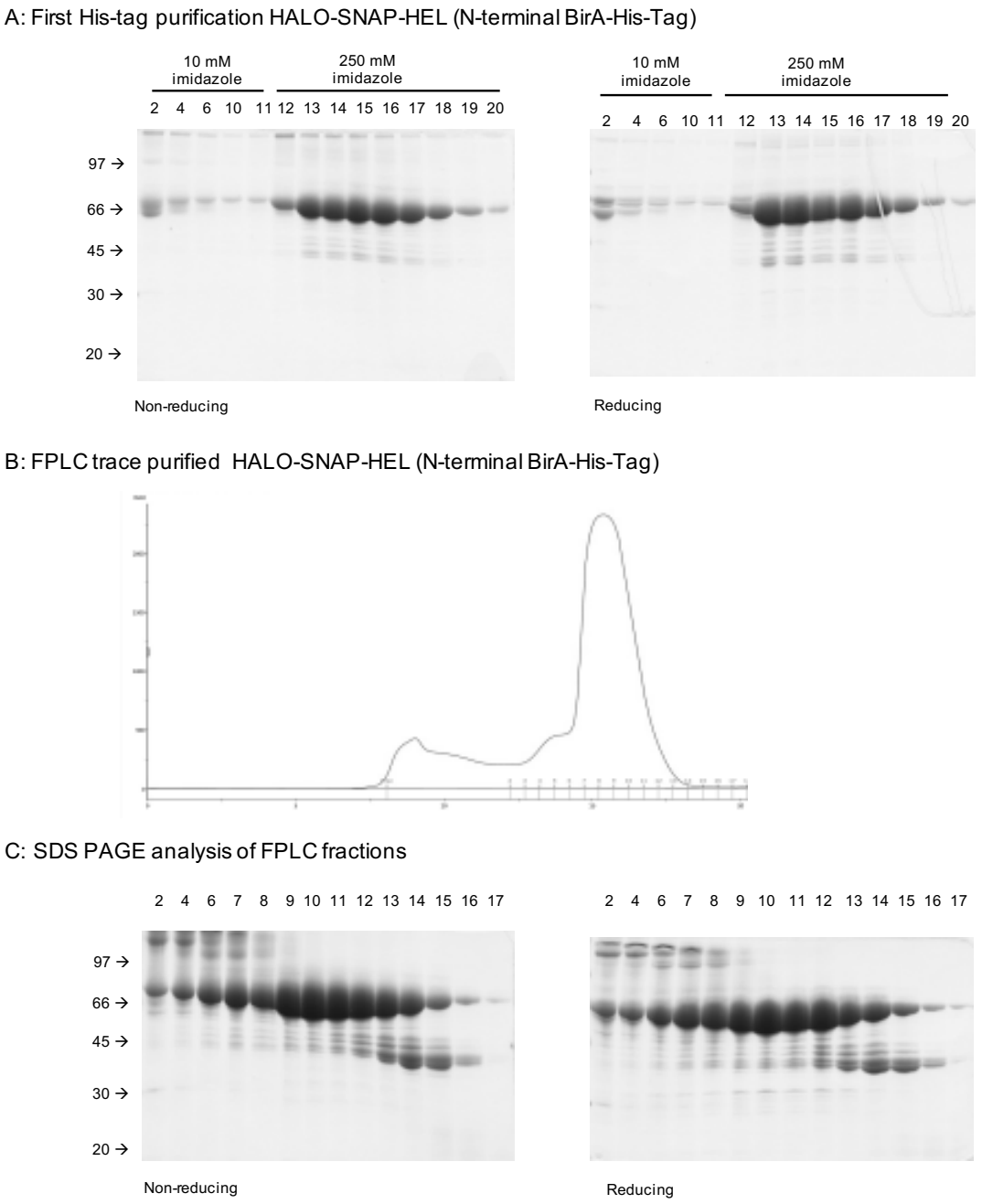

Figure 4.2 Purification of Halo-Snap-HEL (N-terminal BirA-His-tag)
(A) Non-reducing and reducing 12 % SDS PAGE gels of Halo-Snap-HEL (N-terminal BirA-His-tag) fractions eluted from a Ni-NTA column. The numbers above the lanes correspond to the fractions eluted from the Ni-NTA column. Representative example of two extractions. (B) Separation of His-tag purified Halo-Snap-HEL (N-terminal BirA-His tag) by size exclusion chromatography using a Superdex S200 column. (C) Eluted FPLC fractions were analysed on 12 % SDS PAGE gels under non-reducing and reducing conditions. The numbers above the lanes correspond to the fractions eluted from the FPLC.

4.3.1.2 Biotinylation of HALO-SNAP-HEL (N-terminal BirA-His-tag)

Clean, monomeric N-HSH-BirA-His was enzymatically biotinylated with biotin protein ligase and an excess of biotin, and subsequently purified by gel filtration (Figure 4.3A). The extent of biotinylation was then determined. Assessing biotinylation efficiency is important for downstream applications and multiple protocols exist [297]. In this case, an SDS-PAGE method was used which determines the relative extent of biotinylation by detecting electrophoretic mobility shifts of biotinylated proteins in the presence or absence of streptavidin (Figure 4.3B). In the presence of streptavidin, biotinylated N-HSH-BirA-His underwent a complete electrophoretic shift from its original position thereby confirming total biotinylation. This was a specific interaction as no shift was seen with streptavidin and unbiotinylated N-HSH-BirA-His.

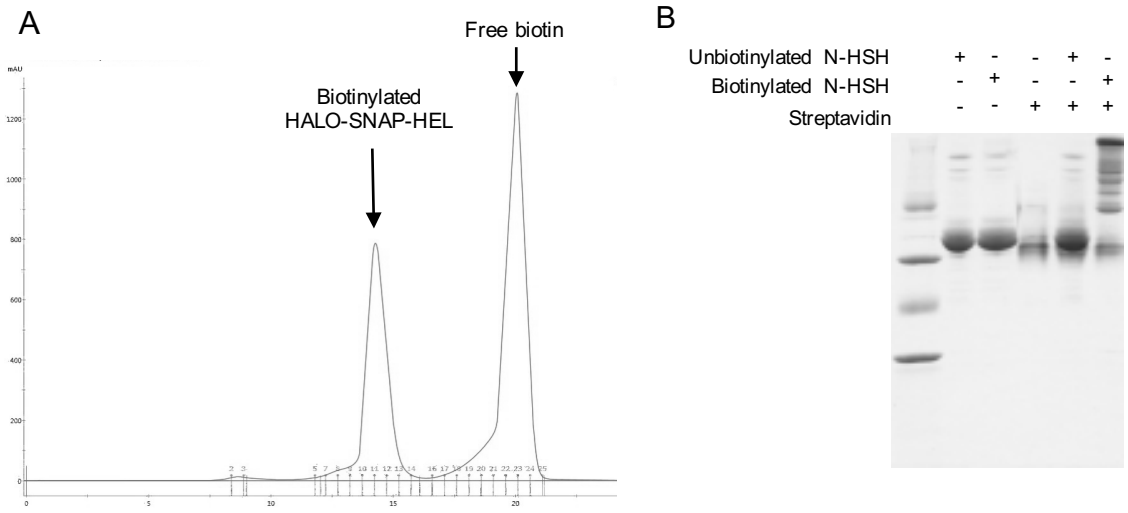

Figure 4.3 Biotinylation of Halo-Snap-HEL (N-terminal BirA-His tag)
(A) 2 mg of Halo-Snap-HEL (N-terminal BirA-His-tag) were biotinylated and purified by FPLC using an S200 10/30 GL column (GE Healthcare). Peaks corresponding to biotinylated protein and excess biotin are indicated. (B) Biotinylation efficiency was assed using a gel shift assay. 5 μg unbiotinylated protein and 5ug biotinylated protein were incubated for 30 mins at room temperature both with and without 5 μg streptavidin. A streptavidin sample alone was used as a control. Samples were run on a non-reducing gel (without a prior denaturing step) and visualised using Coomassie staining.

4.3.1.3 Formation of multivalent HEL

Tetrameric HEL was formed by mixing together strepatividin with a four-fold molar excess of biotinylated N-HSH-BirA-His. This ratio was the minimum required to saturate all available streptavidin binding sites. This approach ensured that each streptavidin was occupied with sufficient protein to make it multivalent but at the same time minimising free monomeric protein.

4.3.2 Calcium flux assay: setup, perils and pitfalls

4.3.2.1 Calcium triggering assay

To test the ability of monomeric and multivalent ligands to activate B cells under different conditions, a robust assay of cellular activation was required. An increase in intracellular levels of calcium ions (Ca2+) is one of the key triggering events leading to the development of a B cell response to antigen [298]. In view of this, a microscopy-based calcium flux assay was used to measure changes in cytoplasmic calcium levels in B cells in response to ligands in real time, using a spinning disk confocal microscope. This method allowed analysis of B cells at a single-cell level combined with statistical analysis of data obtained from large populations of B cells. The outputs of this assay were the fraction of triggered cells and average time to triggering (figure 4.4).

To examine triggering "in solution", cells were loaded with Fluo-4, allowed to settle onto an ostensibly inert surface, and then ligand added to the buffer to the appropriate final concentration. To examine triggering "at a surface", cells were loaded with Fluo-4 before being dropped onto surfaces pre-coated with the desired amount of protein (figure 4.4A). For each experimental condition cells were imaged for a total of 10 minutes. As a control,

all surfaces were checked to ensure they did not induce triggering by allowing cells to settle in the absence of ligand and imaged for 10 minutes. At the end of this time, cells were checked to ensure they could still trigger or flux calcium by addition of either a crosslinking antibody or ionomycin.

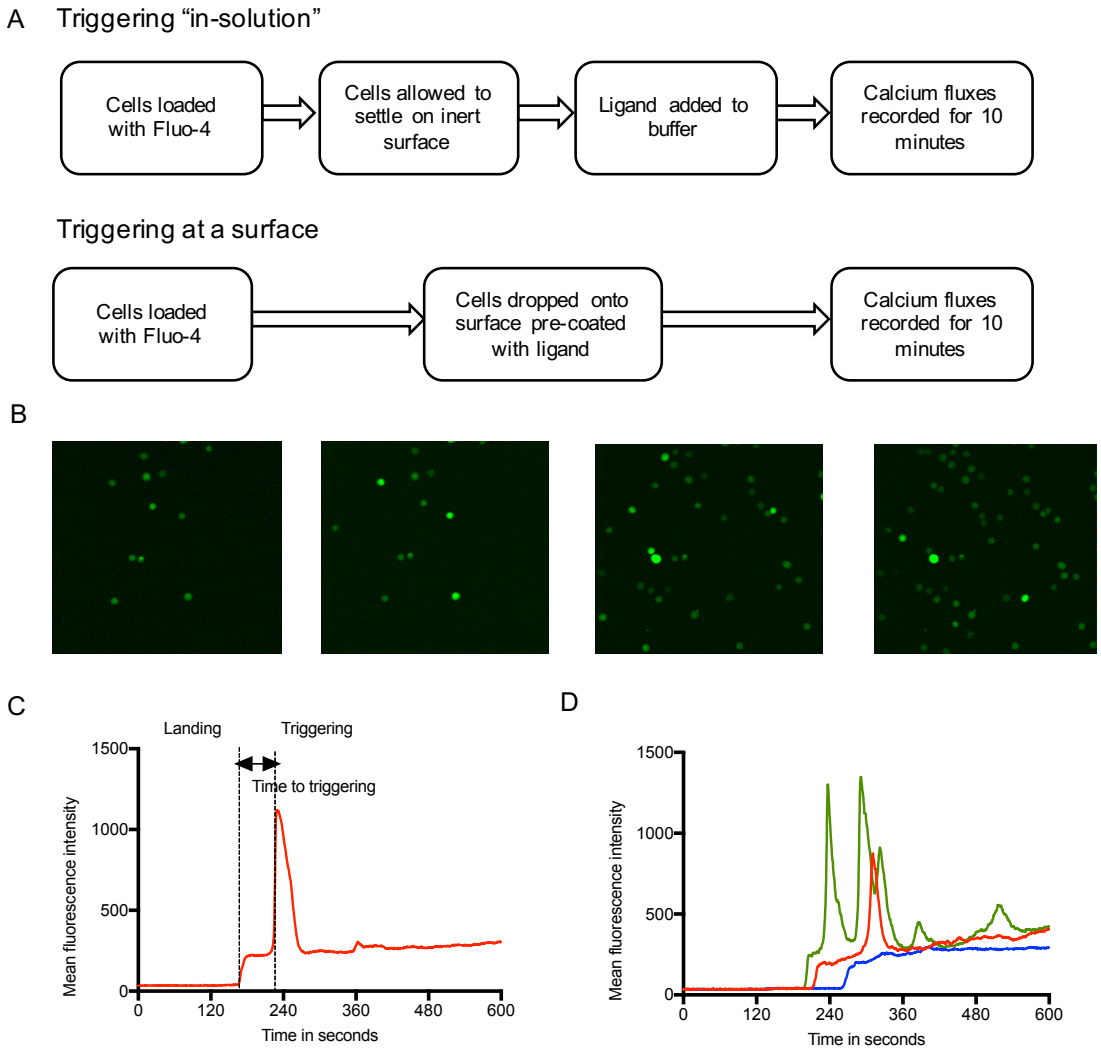

Figure 4.4 Microscopy based calcium flux assay
(A) Experimental approach for calcium flux assay in which antigen is encountered in-solution or at a surface. (B) Time lapse images show a representative example of a calcium triggering experiment with cells landing (left) and then fluorescing brightly as they flux calcium. (C) Representative example of the fluorescence profile of a triggered cell (D) Fluorescence profile of a triggered cell (red), non-triggered cell (blue) and a cell which fluxes calcium multiple times (green).

4.3.2.2 Surface choice is critical to experimental design

Central to the experimental set up was use of a non-activating surface. This was essential to ensure any triggering was truly ligand induced rather than a ligand-independent effect of the surface. Multiple surfaces exist for the study of lymphocyte receptor triggering; these include glass, agarose and the cationic homopolymer Poly-L-lysine (PLL). PLL has been widely used for total internal reflection fluorescence (TIRF) imaging of the 'resting' organisation of lymphocyte surface proteins [299-303], because PLL is assumed to be inert.

To examine whether PLL-coated surfaces were actually inert, their capacity to induce calcium signalling in the A20 B cell lines was tested (Figure 4.5). Cells were labelled with Fluo-4 and transferred to PLL- or anti-BCR (anti-Ig) coated coverslips. Signalling occurred in ~44% of A20 cells on PLL and in 79 % on anti-Ig. Based on these results PLL was therefore not an inert surface but induced signalling at levels comparable to crosslinking.

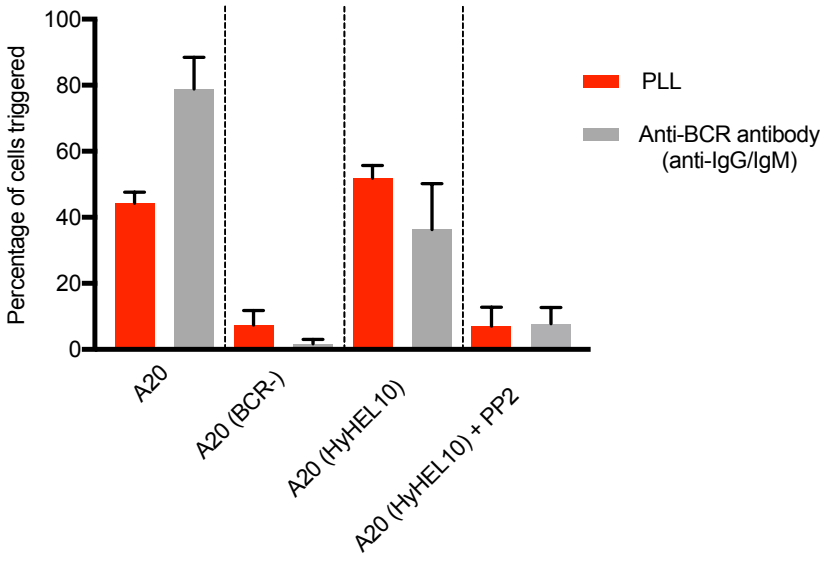

Figure 4.5 Triggering of B cells on PLL
Calcium responses of A20, A20 (BCR negative), A20 (HyHEL10) and A20 (HyHEL10) B cell treated with PP2 responding to PLL (blue) or anti-BCR (anti-IgG or anti-IgM, grey) coated glass surfaces. Values correspond to the percentage of cells exhibiting calcium flux detected by Fluo-4 within 10 min of landing. Bars are mean ± SD. All experiments were conducted at 37°C and 5% CO_2.

To establish whether the signalling induced by PLL was bona fide BCR signalling, A20 B cells in which BCR expression was blocked using CRISPR-based gene editing were dropped on to PLL- or anti-BCR coated coverslips. In the absence of the BCR, signalling was significantly reduced. Re-expression of the HyHEL10 BCR restored signalling thereby confirming that signalling was BCR dependent. Treating B cells with the Src kinase inhibitor PP2 suppressed PLL induced calcium signalling thereby confirming that PLL predominantly signals via established B cell pathways.

PLL induced BCR-dependent signalling serves to highlight the importance of surface choice in triggering experiments. In the absence of PLL as an option, alternative surfaces were trialled. Plain uncoated glass was also shown to induce calcium signalling (Figure 4.6). Attempts were made to render the glass surface inert by coating with isotype control antibody or FCS. Calcium signalling occurred in 1.9 % of A20 (HyHEL10) cells on glass coated with isotype control antibody and in almost no cells on FCS/glass. Supported lipid bilayers (SLBs) also did not induce calcium signalling. In addition to not inducing calcium triggering, cells landing on functionalised glass or SLBs failed to attach and continued to roll across the field of view. These inert surfaces were subsequently employed in triggering experiments to test the cross-linking model.

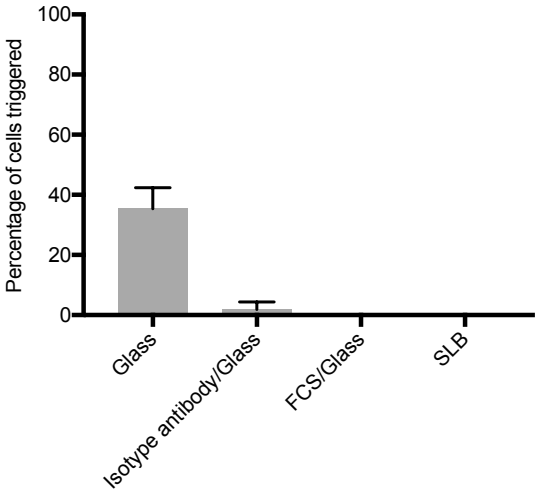

Figure 4.6 Triggering of B cells on a range of surfaces
Calcium responses of A20 (HyHEL10) B cells landing on glass, glass coated with isotype antibody, FCS-coated glass or SLBs. Values correspond to the percentage of cells exhibiting calcium flux detected by Fluo-4 within 10 min of landing. Bars are mean ± SD. All experiments were conducted at 37°C and 5% CO_2.

4.3.3 Multivalent but not monovalent ligands are able to trigger B cells in solution

To test whether triggering of B cells in solution is dependent on antigen valency, B cells were loaded with Fluo-4, allowed to settle onto an insert surface, and monovalent or tetravalent ligand added at various concentrations. Cells were then imaged for 10 minutes to observe calcium triggering.

Initial experiments were undertaken on FCS-glass (Figure 4.7). Addition of cells to FCS-glass failed to induce calcium triggering or attachment, and instead cells continued to roll across the surface creating an "in solution" setting. The addition of tetrameric ligand to cells produced comparable levels of triggering to cross-linking antibody. The addition of monovalent ligand at comparable concentrations was unable to activate B cells, but, a small increase in calcium triggering was observed at low ligand concentrations. This raised the

possibility that the FCS-blocked glass could be allowing some attachment of protein. At low concentrations of ligand, BCRs are theoretically less likely to have engaged ligand in solution thereby permitting ligand engagement and BCR triggering as cells roll across small amounts of ligand attached to the surface. Thus, planar lipid bilayers were tried as a more stringent non-stick surface to model the "in-solution" setting. Addition of cells to SLBs once again failed to induce calcium triggering or attachment, and instead the cells were seen to roll across the surface. The addition of tetrameric ligand to the cells also produced comparable levels of triggering to cross-linking antibody. However, in contrast to experiments on FCS-glass, addition of monovalent ligand "in-solution" at any concentration was unable to trigger calcium triggering in the B cells (Figure 4.7).

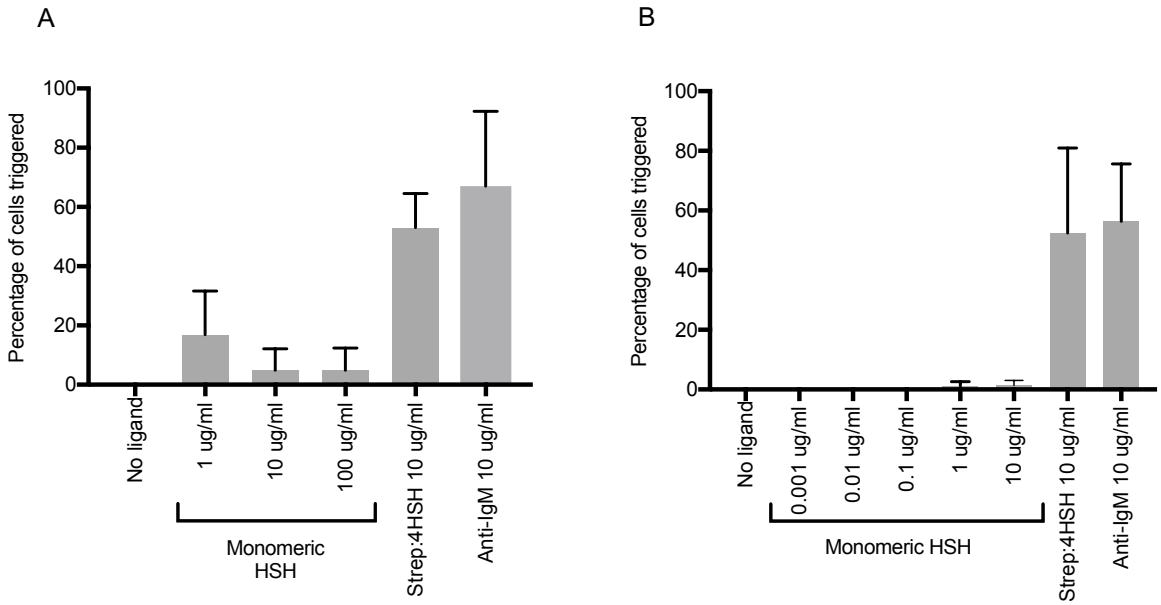

Figure 4.7 Triggering of B cells "in solution"
Calcium responses of A20 (HyHEL10) B cells which have been allowed to settle for 2 minutes onto (A) glass-slides blocked with FCS or (B) SLBs, and then exposed to either monomeric Halo-Snap-HEL (N-terminal BirA-His-tag; HSH), tetrameric Halo-Snap-HEL (N-terminal BirA-His-tag; strep:4HSH), anti-IghM or no ligand. Values correspond to the percentage of cells exhibiting calcium flux detected by Fluo-4 within 10 min of landing. Bars are mean ± SD. All experiments were conducted at 37˚C and 5% CO_2.

4.3.4 Monovalent ligand is able to trigger B cells at a surface

To established whether the crosslinking model is able to explain triggering of B cells in the setting of surface bound antigen, the ability of monovalent surface bound-ligand to trigger B cells was tested.

4.3.4.1 Triggering on Ni-NTA

The first step was to establish a method of attaching antigen to a surface. The initial surface choice was functionalised glass. Glass is inexpensive and readily available but has a number of key drawbacks. Firstly, it is difficult to control for the actual amount of protein adsorbed onto the glass. Secondly, protein adsorption occurs in a random orientation and therefore does not always leave the epitope available for binding. To circumvent this, Ni-NTA coated plates were used which allow control over orientation, surface concentration and also enable free protein to be washed away.

B cells were loaded with Fluo-4 and placed onto Ni-NTA slides pre-coated with protein at the desired concentration, and imaged for 10 minutes to observe calcium triggering (Figure 4.8A). No calcium triggering was detected with Ni-NTA alone. Calcium triggering on Ni-NTA was ligand-dose dependent. The dose could be converted from applied concentration to molecules per square micron with knowledge of the maximum binding capability of Ni-NTA plates and a standard curve of applied concentration vs binding (Figure 4.8B). Maximum calcium triggering was seen at an added protein concentration of 1 mg/l, equating to a surface concentration of approximately 5900 molecules per square micron. No triggering was seen at an added concentration of 0.0625 mg/l, equating to a surface concentration of approximately 317 molecules/square micron. Importantly,

triggering by monomeric protein was seen on functionalised glass surfaces whereas it was not detected in solution.

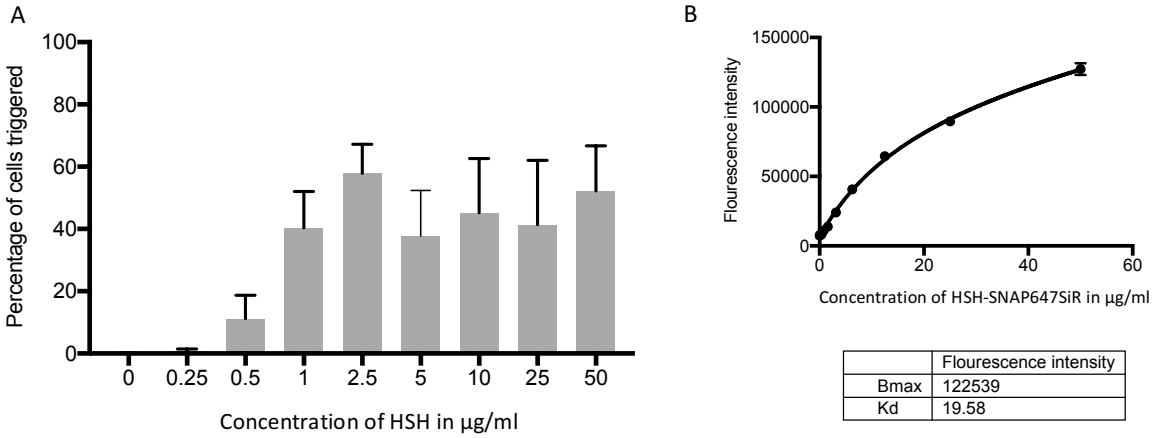

Figure 4.8 Triggering of B-cells on Ni-NTA coated surfaces
(A) Calcium responses of A20 (HyHEL10) B cells which have been allowed to settle onto Ni-NTA coated glass slides pre-incubated with the specified concentration of Halo-Snap-HEL (N-terminal BirA-His-tag), Values correspond to the percentage of cells exhibiting calcium flux detected by Fluo-4 within 10 min of landing. Bars are mean ± SD. All experiments were conducted at 37˚C and 5% CO_2.
(B) Dose response curve of the binding of Halo-Snap-HEL (647-SiR via the Halo-tag) to Ni-NTA. The average of three repeats is displayed. Nonlinear regression analysis with a 1:1 Langmuir binding model is shown. The derived B_{max} and K_d values are displayed.

4.3.4.2 Triggering on Supported Lipid Bilayers

Triggering on functionalised glass surfaces, such as Ni-NTA-coated surfaces, is dependent on ligands that are immobile. Furthermore, it is difficult to control for protein clustering. Therefore, the results observed on Ni-NTA could plausibly be explained by cross-linking. To circumvent this problem, the triggering of B cells was undertaken on ligands attached to SLBs.

Production and characterisation of SLBs

The lipid DGS-NTA(Ni) provides a means of attaching His-tagged proteins to SLBs. The use of DGS-NTA(Ni) allows control over protein orientation, surface concentration as well as enabling free protein to be washed off. Theoretically, proteins attached to lipid should be uniformly monomeric and freely diffusing. To test this, SLBs consisting of 96 % POPC/4 % DGS-NTA(Ni) were produced and N-HSH-BirA-His (pre-labelled with a fluorescent ligand) added. Bilayers were then imaged using fluorescence correlation spectroscopy and Fluorescence Recovery After Photobleaching (FRAP) to confirm whether the HEL-fusion protein was truly monomeric and diffusing within the membrane.

Fluorescence correlation spectroscopy

Fluorescence correlation spectroscopy measures small fluctuations in fluorescence intensity in a defined volume over time. Correlation of the data produces fluorescence correlation spectroscopy curves which are fitted to model curves to allow assessment of parameters governing fluctuation decay, such as diffusion [304]. To assess the status of fluorescently labelled N-HSH-BirA-His attached to Ni-NTA SLBs, its diffusion was compared against labelled lipids, which were known to be monomeric and diffusing. SLBs were formed containing spectrally separated fluorescently labelled lipid and protein and then fluorescence correlation spectroscopy undertaken with confocal illumination (figure 4.9). The fluorescence correlation spectroscopy decay curves showed both protein and lipid to be diffusing. The protein was diffusing approximately twice as slowly as the lipid.

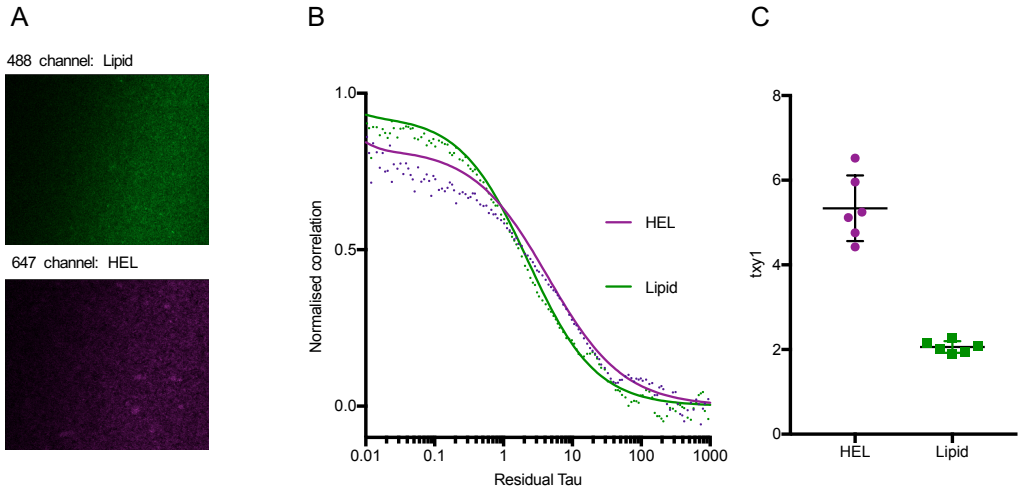

Figure 4.9 Fluorescence correlation spectroscopy of supported lipid bilayers
(A) Ni-NTA supported lipid bilayers were formed with 0.001% KK-DPPE and labelled with Halo-Snap-HEL (N-terminal His-tag) labelled with Halo-647SiR, followed by fluorescence correlation spectroscopy with confocal illumination (A) Confocal images of bilayer in 488 and 647 channels. (B) Representative correlated data (points) and fitted model (line) in the two channels. (3) Txy1 measurements for all datasets.

Fluorescence Recovery After Photobleaching (FRAP)

FRAP involves photobleaching a region of interest and then observing for fluorescence recovery as non-bleached fluorophores diffuse back into the region of interest. Diffusion co-efficients can then be calculated from the rate of recovery. Failure of the fluorescence to return to pre-bleaching levels indicates an immobile fraction [304]. Bilayers were formed containing fluorescently labelled protein and FRAP undertaken. In the case of fluorescently labelled N-HSH-BirA-His, there was complete fluorescence recovery after photobleaching (Figure 4.10).

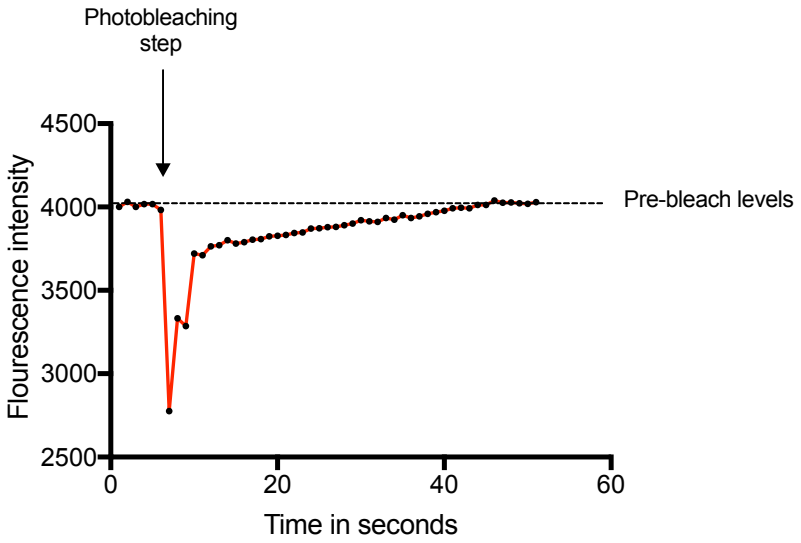

Figure 4.10 Fluorescence recovery after photobleaching of supported lipid bilayers
Ni-NTA supported lipid bilayers were formed and labelled with Halo-Snap-HEL (N-terminal His-tag) pre-labelled with Halo-647SiR, and imaged by Total Internal Refraction microscopy. Pre-bleach images were acquired, followed by illumination of a region of interest with 100% laser power, followed by post-bleach image acquisition. Flourescence intensity within the region of photobleaching is plotted as a function of time

In summary the results of the TIRF, fluorescence correlation spectroscopy and FRAP experiments confirmed that the HEL fusion protein on the bilayers was monomeric and freely diffusing.

Calcium triggering on supported lipid bilayers

Having established the integrity of the ligand monomers on SLBs, triggering experiments were undertaken to assess whether monovalent ligand at a surface was able to trigger B cells.

B-cells were loaded with Fluo-4 and added to Ni-containing SLBs pre-coated with the desired amount of protein, and imaged for 10 minutes to observe calcium triggering. No calcium triggering was detected on Ni-containing SLBs in the absence of protein. Calcium

triggering on Ni-containing SLBs was dependent on the quantity of protein added. No triggering was seen at an added concentration of 0.0625 mg/l. Triggering was seen at concentrations above 0.25 mg/l, which equates to a surface density of approximately 100 molecules per square micron. The threshold for triggering for protein presented on a bilayer is therefore much lower than for ligands immobilised on glass. Importantly, triggering on Ni-containing SLBs was detected using the same monovalent ligand that failed to induce calcium triggering in solution.

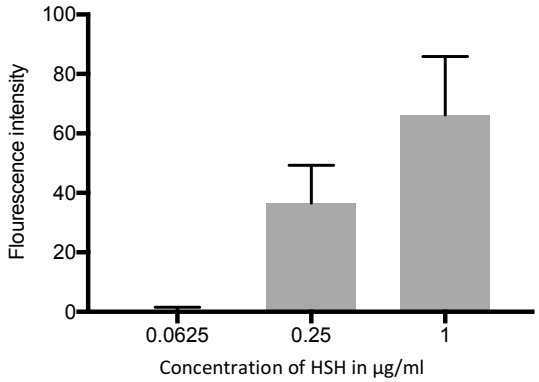

Figure 4.11 Triggering of B cells by ligand presenting on supported lipid bilayers
(A) Calcium responses of A20 (HyHEL10) B cells which have been allowed to settle onto Ni-NTA containing bilayers pre-coated with the specified concentration of HEL-Snap-Halo (N-terminal BirA-Histag; HSH), Values correspond to the percentage of cells exhibiting calcium flux detected by Fluo-4 within 10 min of landing. Bars are mean ± SD. All experiments were conducted at 37˚C and 5% CO_2.

4.4 Discussion

4.4.1 The crosslinking model fails to explain triggering of B cells at a surface

In experiments described in this Chapter, monomeric and tetrameric forms of HEL were generated, supplementing the toolkit of reagents described in Chapter 3. Using these reagents, it was shown that tetrameric HEL produces comparable levels of calcium triggering to crosslinking antibody in solution. In contrast, monomeric HEL was unable to induce calcium triggering at any concentration. This work is consistent with that of other groups who have used different pairs of monomeric and multimeric ligands [222-224]. These experiments verify our reagents against the established data and support the prevailing view that multivalent, but not monomeric ligands, are able to activate B cells in solution. Therefore, triggering of B cells with soluble ligands is compatible with the cross-linking model.

While artificial crosslinking of BCR's is undoubtedly sufficient to activate B cells, it remains unclear if this is the quintessential triggering model in vivo since B cells predominantly encounter antigen that is not soluble, but membrane bound. [202, 203, 226-228]. To address this, B cells were presented to ligand conjugated to a surface. In this setting, monomeric HEL that was previously unable to trigger B cells in solution was highly efficiently at triggering B cells when conjugated to a surface. Importantly, HEL presented on SLBs was monomeric and freely diffusing, ruling out aggregation as a mechanism of triggering.

The ability of monovalent ligand to trigger at a surface argues against the crosslinking model as the sole explanation for receptor trigger since, by definition, these reagents were incapable of inducing cross-linking. In work described in the following Chapters, other models were examined that could potentially explain BCR triggering by monovalent ligands at a surface.

4.4.2 Surface choice is critical to experiments undertaken on lymphocytes

The results presented in this Chapter demonstrate that when undertaking triggering experiments, the choice of surface is critical. Non-activating surfaces are essential to ensure any triggering is truly ligand induced rather than a ligand-independent effect of the surface. Both PLL and untreated glass were shown here to be activating surfaces. In the case of PLL, it was shown that this coating induces bona fide BCR triggering at comparable levels to actual ligands or crosslinking. Similar results have been observed with CD4+T cells, Jurkat T cells and T-cell hybridomas [305]. These effects have been shown to be independent of PLL concentration, coating time or polymer size. The mechanism by which PLL induces signalling has not been studied in B cells but it is likely to be similar to that observed in T cells. Single-molecule tracking of fluorescently-labelled TCRs in Jurkat T cells showed that PLL directly and almost completely reduces TCR diffusion; such effects are presumably the result of electrostatic polymer/receptor interactions. TIRF imaging showed that the phosphatase CD45 is excluded from regions of contact containing the immobilised TCRs, offering an explanation for signalling. Super-resolution, stimulated emission depletion imaging showed that the TCR is significantly more clustered for T cells

in contact with PLL than for cells suspended in hydrogel, likely due to the induced signalling [305].

PLL has been widely used as a model substrate for studying antigen receptor organisation and the 'ground-state' for lymphocyte receptor triggering, because it is presumed to be inert. Results from these studies have suggested receptors and signalling proteins cluster by default on the surface of resting lymphocytes [299-303]. Similar results have been observed for B cells 'landing' on anti-MHC class II coated cover slips [236]. In this setting, large phosphatases could be excluded, the implications of this are reconsidered in chapter 6. In view of the results presented in this Chapter and by Santos et al [305], a re-examination of these studies is required as the results may not be truly representative of the resting state of lymphocytes.

Chapter 5

Resting stoichiometry of the B Cell Receptor[1]

5.1 Introduction

The mechanism of triggering of the BCR remains elusive and controversial. To date, three models have been proposed: the cross-linking model, the conformation-induced oliogmerisation model, and the dissociation activation model. In Chapter 4, the principles of the cross-linking model were tested. It was shown that whereas B cells could indeed be triggered with multivalent soluble ligands, monovalent antigen that was incapable of triggering of B cells in solution was able to trigger signalling when attached to a surface, a finding that could not be explained by a simple cross-linking model. The cross-linking model therefore could not account for signalling in the dominant physiological setting of surface bound monovalent antigen. The other two models, i.e. the conformation-induced oligomerisation model and the dissociation activation model, were considered next.

The conformation-induced oligomerisation model proposes that in the resting, non-antigen bound state the BCR is a bivalent complex (a single BCR with two antigen binding sites). Antigen binding to the BCR induces a conformational change, exposing a previously hidden Cμ4 clustering domain. This clustering interface promotes receptor oligomerisation and opening of the cytoplasmic domain for initiation of downstream signalling (Figure 1.3) [229]. On the other hand, the dissociation activation model proposes that in the resting, non-antigen bound state the BCR is an oligomer, which is auto-inhibitory. Antigen binding

[1] The work described in this chapter was undertaken in collaboration with James T. McColl of the Klenerman Group, Dept. Chemistry, Cambridge University.

promotes dissociation of BCR oligomers and exposure of the previously hidden intracellular ITAMs to enable downstream signalling (figure 1.4) [232]. It is clear that the conformation-induced oliogmerisation model and the dissociation activation model are completely opposing theories and cannot co-exist. In addressing which, if any, of these mutually exclusive models could potentially explain BCR triggering, a key question to ask is: what is the stoichiometry of the BCR in the resting state?

The stoichiometry of the BCR in the resting state is controversial with conflicting evidence about whether it is pre-clustered or mainly monomeric. The concept that the BCR may be pre-clustered on the surface of resting cells arose out of a series of biochemical studies. Under minimal detergent lysis conditions the BCR was seen to run as a large macromolecule [233]. Results arising from quantitative BiFC assays [232] and high resolution PLA [234] supported the concept of a pre-clustered BCR. More recent evidence has come from dSTORM [236]. In other studies, the BCR has been shown not to be pre-clustered on resting cells, and instead to be mostly monomeric. These findings come from experiments using FRET [132] and single particle tracking of individual BCRs labelled with fluorescent Fabs [230]. It is clear that the results of these different experiments cannot all be correct and the discrepancies reflect, at least in part, the technical difficulties of studying receptors in their native state in situ.

In experiments described in this Chapter, the stoichiometry of the BCR was addressed using multi-colour fluorescence single molecule imaging of living cells. These methods had previously been used to investigate the oligomerisation state of the TCR [306] and G protein-coupled receptors [307]. These fluorescence microscopy techniques will be used

and developed further and applied to the special case of the BCR. Establishing the stoichiometry of the BCR in the resting state was important as it allowed further narrowing down of the potential explanations of BCR triggering.

5.2 Materials and Methods

5.2.1 Constructs

HyHEL10 kappa constructs were cloned from cDNA. Ig-α and Ig-β genes were cloned from MD4 mouse cDNA and joined by chimera PCR to a Snap®/Halo®-tag (incorporating a short 5 glycine-serine linker) amplified from vector templates. CRISPR resistant constructs were produced by non-code changes to the nucleotide sequence at the site of CRISPR guides using customer oligonucleotide primers. External primers incorporating a 5' Mlul site and 3' NotI site were utilised to allow subsequent ligation of all constructs into the pHRI vector. All sequences were confirmed by DNA sequencing.

5.2.2 Establishment of cell lines

A20 (pHRI HyHEL10) cells were generated by small scale lentiviral transfection of HyHEL10 kappa into A20 (IgG2a-, hHyHEL10+, kappa-) cells using the pHRI vector. A20 (pHRI HyHEL10, Ig-α-Snap/Halo) were generated by transfecting CRISPR resistant forms of Ig-α-Snap/Halo using the pHRI vector into A20 (HyHEL10) cells in which the Ig-α chain had been pre-removed by CRISPR. Protein expression was confirmed for all constructs by FACS and quantified using QuantiBrite-PE beads.

5.2.3 Fluorescent labelling of proteins and antibodies

Halo-Snap-HEL proteins were labelled with Snap®-tag or Halo®-tag dyes as outlined previously. HyHEL10 antibody was labelled directly via amine coupling. 100 µl of antibody at 1 mg/ml was mixed with 10 µl of 1 M sodium bicarbonate and then a 10 molar excess of SiR added followed by incubation at 1 hour at room temperature. A purification column was prepared with 1.5 ml resin bed and centrifuged at 2000 rpm for 2 minutes (Thermo Fisher Scientific). The reaction mixture was added and centrifuged at 2000 rpm for 5 minutes to collect the labelled antibody.

5.2.4 Separation of fluorescently labelled protein from free dye

N-HSH labelled with Snap®-tag or Halo®-tag ligand was concentrated to approximately 100 µl with a Vivaspin 500, 10 kDa MWCO spin concentrator and then purified using an AKTA pure FPLC system and S200 5/150 GL column (GE Healthcare). Factions corresponding to protein were pooled and concentrated using a Vivaspin 500, 10 kDa MWCO spin concentrator and either used immediately for downstream applications or aliquoted and frozen at -80 ˚C.

5.2.5 Assessment of labelling efficiency of HEL-fusion proteins

200 µl of 20 mg/l N-HSH were mixed with a variable molar ratio of either Snap®-tag or Halo®-tag ligand and incubated at 4 ˚C overnight with rotation. 50 µl of M450 tosylactivated Dynabeads® conjugated to HyHEL10 antibody were then added and the mixture incubated at 4 ˚C for 1 hour with rotation. The beads were then placed in a magnet, the supernatant discarded, the beads washed twice in Ca^{2+} and Mg^{2+} free PBS

(supplemented with 0.1 % BSA and 2 mM EDTA pH 7.4) and then resuspended in 200 µl of the same buffer. A second fluorescence Snap®-tag or Halo®-tag ligand was then added in excess (50 µM) and incubated at 4 °C with rotation overnight. The following day the beads were placed in a magnet, the supernatant discarded, the beads washed twice in Ca^{2+} and Mg^{2+} free PBS (supplemented with 0.1 % BSA and 2 mM EDTA pH 7.4) and then resuspended in 50 µl of the same buffer. FACS analysis was then undertaken on the beads for fluorescence at the emission spectra of the second Snap®-tag or Halo®-tag ligand. All experiments included the following controls: protein only, protein and first ligand only, protein and second ligand only, and both ligands in the absence of protein.

5.2.6 Microscope setup and data analysis

TIRF imaging was undertaken on a custom-built microscope. The microscope was fitted with diode lasers operating at 488 nm (100 mW, iBeam smart, Topica) and 641 nm (100 mW, CUBE 640-100C, Coherent). The laser beams were each directed through a λ-quarter wave plate to ensure circular polarization of the excitation light and the beams aligned and focused on the back focal plane of a 1.4 NA TIRF objective (100x oil objective, UPLSAPO100XO/1.4, Universal Plan Super Apochromat) mounted on a IX73 Olympus inverted microscope. Emitted fluorescence was collected by the same objective and separated from the returning TIR beam by a combination of long-pass and band-pass filters (505, BLP01-488R-25 + FF01-520/44-25; SiR, 692BP). The fluorescence signal was recorded using a EMCCD (Photometrics, Evolve 512 Delta) with an electron multiplication gain of 250 ADU/photon operating in a frame transfer mode. For three colour image a 561 nm (200 mW, Jive 200, Cobolt) laser was used together with an

additional filter, LP02-568RS-25+FF01-587/35-25. Images were acquired by sequential imaging using Micromanager [308]. Image processing was undertaken using ImageJ [309] and MATLAB (R2016b, The MathWorks, Natick, US). Analysis of the data to assess colour-co-incidence was undertaken using custom-written MatLab Code according to a Bayesian based algorithm [310].

5.3 Results

5.3.1 Experimental approach

To address the oligomerisation state of the BCR in the resting state, multicolour fluorescence single molecule co-incidence detection of BCRs on the surface of living cells was undertaken. Experiments were undertaken using the A20 (HyHEL10) B cell line created as described in Chapter 3. BCRs were fluorescently labelled in spectrally distinct colours. Coincident fluorescence from single BCRs labelled with different fluorophores was then detected as they diffused through a confocal volume. The level of coincident fluorescence signals observed provides information about the stoichiometry of the BCR. The toolkit of reagents established in Chapter 3, provides two options for receptor labelling: internal and external labelling (Figure 5.1 and 5.2).

Internal labelling of the BCR via a Snap®/Halo®-tag provides a means of labelling each BCR once (Figure 5.1). Two colour co-incidence detection can then be undertaken by labelling each BCR with one of two spectrally distinct fluorophores, and by detecting coincident fluorescence observed from single molecules labelled with the different fluorophores as they diffuse through a confocal volume. The fraction of events coincident

above the statistical background is known as the association quotient and is directly proportional to the level of association between molecules [311]. Such an approach was first used to determine TCR stoichiometry [306]. Care has to be taken with these experiments to allow for variation in labelling efficiency and apparent association, due to two proteins being in close spatial proximity by chance. To deal with the problem of labelling efficiency references are made to proteins of known stoichiometry (e.g. the monomer CD86 and dimer CD28) labelled via Snap®/Halo®-tag in an analogous manner to the BCR. In this setting, the controls and experimental samples are directly comparable negating the need to either maximise or even to know the exact labelling efficiency. To circumvent the problem of apparent association single molecules at the cell surface can be observed over time, allowing discrimination of true protein-protein interactions form chance association. However, a limitation of this internal labelling approach is that it limits the analysis to cell lines which can be engineered to express Halo®-/Snap®-tags. In view of this, an alternative approach was conceived.

The second experimental approach utilises external labelling of the BCR with its natural ligand (Figure 5.2). HEL is ideally suited to this role as it binds to the HyHEL10 BCR with a very low equilibrium dissociation constant of 8.9 pM making it excellent for receptor labelling. Utilising the toolkit of reagents established in Chapter 3, HEL can be fluorescently labelled via Snap®/Halo®-tags in two spectrally distinct colours and used to label A20 (HyHEL10) B cells in a set ratio. The bivalent nature of a single BCR adds an added layer of complexity to external labelling as each BCR will be bound twice. However, by considering the expected colour co-incidence ratio for monomers, dimers and oligomers it is possible to determine the stoichiometry of the BCR on the cell surface

providing the labelling efficiency is known. External labelling has the advantage that it allows stoichiometric analysis to be undertaken not just on cell lines but also on primary cells, thereby enabling stoichiometric analysis to be ultimately undertaken on B cell subsets using primary cells from the MD4 mouse to determine if there is a single uniform BCR stoichiometry. In view of this potential benefit this external labelling strategy was used to determine the resting stoichiometry of the BCR.

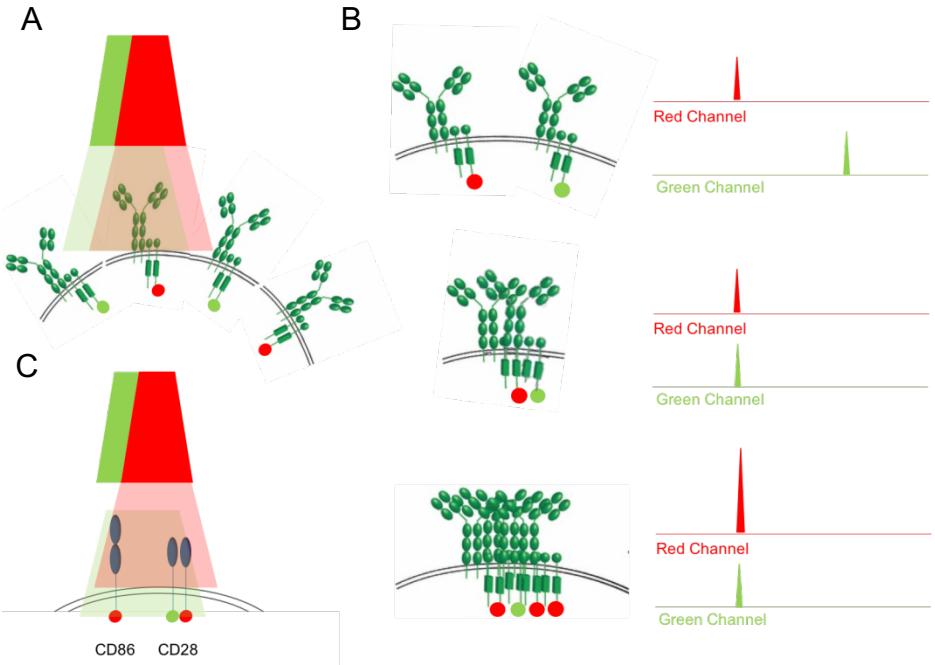

Figure 5.1: Two colour co-incidence microscopy at the B cell surface using internal labelling
(A) Schematic representation of single molecule two colour-co-incidence detection as applied to the BCR. Each BCR (green) is labelled with a fluorescent protein attached via a Snap/Halo®-tag attached to the Ig-α of each BCR. (B) Diagrammatic representation of colour co-incidence as BCR monomers dimers or oligomers diffuse through the confocal volume (C) Schematic representation of the monomer and dimer controls, CD86 and CD28, which have been fluorescently labelled via via a Snap/Halo®-tag attached to the intracellular domain.

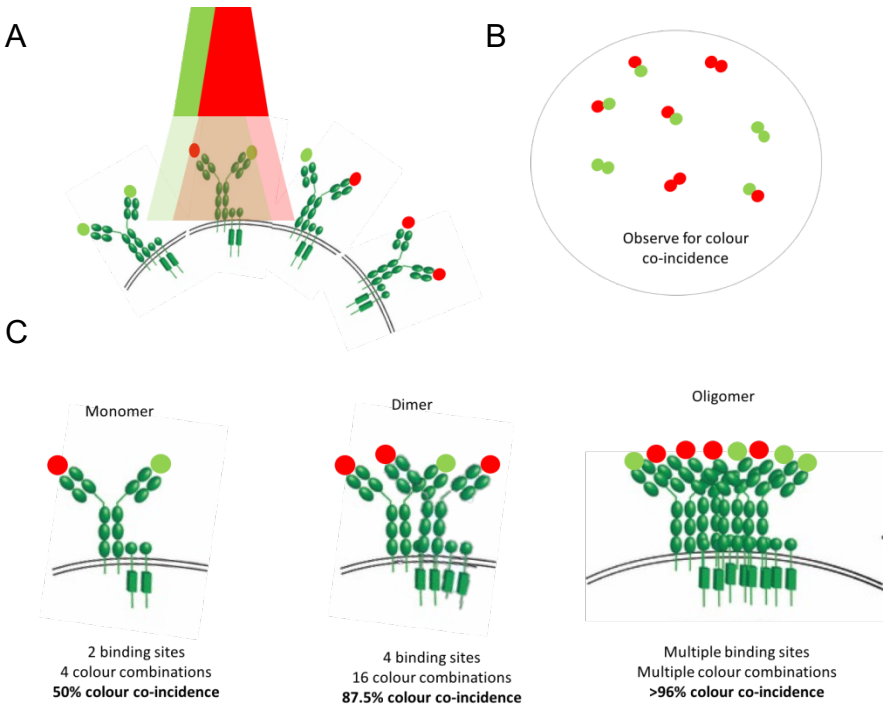

Figure 5.2: Two colour co-incidence microscopy at the B cell surface using external labelling
(A) Schematic representation of single molecule two colour-co-incidence detection as applied to the BCR. Each BCR (green) is bivalently labelled with a fluorescent tag in one of two colours. (B) Diagrammatic representation of colour co-incidence as individual BCR's diffuse through the confocal volume (C) Expected colour co-incidence results for a BCR monomer, dimer and oligomer.

5.3.2 Optimisation of experimental setup

5.3.2.1 Microscope setup and data analysis

To undertake stoichiometric analysis TIRF microscopy was chosen. This method is based on the principle that when light is totally internally reflected at a glass-water interface an evanescent wave is generated which decays exponentially with distance from the surface. This allows selective illumination of fluorophores within < 100 nm of the interface thereby increasing the axial resolution and the signal-to-noise ratio by eliminating background fluorescence [304]. This makes TIRF ideally suited to making measurements at the cell surface, such as of BCR stoichiometry.

TIRF was combined with FRAP. FRAP relies on photobleaching a region of interest and then observing fluorescence recovery as non-bleached fluorophores diffuse in [304]. Co-incidence from BCRs labelled with different fluorophores was detected as they diffused back into the region of interest. Using multicolour TIRF it is possible to track BCRs labelled in two colours and to then use the Dynamic Single-Molecule Colocalization (DySCO) method [310] to determine whether they are associated. This method tracks individual fluorophore tracks over time across multiple frames. Associated fluorophores will track together. Unassociated fluorophores may track together by chance over short distances, but the probability of this occurring over multiple frames is very low.

5.3.2.2 Establishing cell lines expressing proteins for single-molecule imaging

The method for determining stoichiometry involves single molecule imaging of fluorescently labelled proteins on the surface of live cells. These techniques rely on low expression levels to reduce the rate of chance association. Control of protein expression levels in cell lines can be achieved in a number of ways, as outlined in Chapter 3. For experiments in this Chapter, low expression levels were achieved by expressing proteins under the control of the E/GRE promoter in the pHRI vector. To achieve high protein expression the E/GRE promoter requires the activity of the nuclear factors RXR and FB-ERB together with ponasterone in the cell line of interest. These factors are not present in A20 cells leading to ineffective transcription and expression levels ideal for single molecule imaging. All proteins were expressed using the pHRI vector; protein expression was confirmed by FACS and quantified using QuantiBrite-PE beads. The pHRI plasmid induced expression of between 500-2000 molecules/cell for each protein (Figure 5.3).

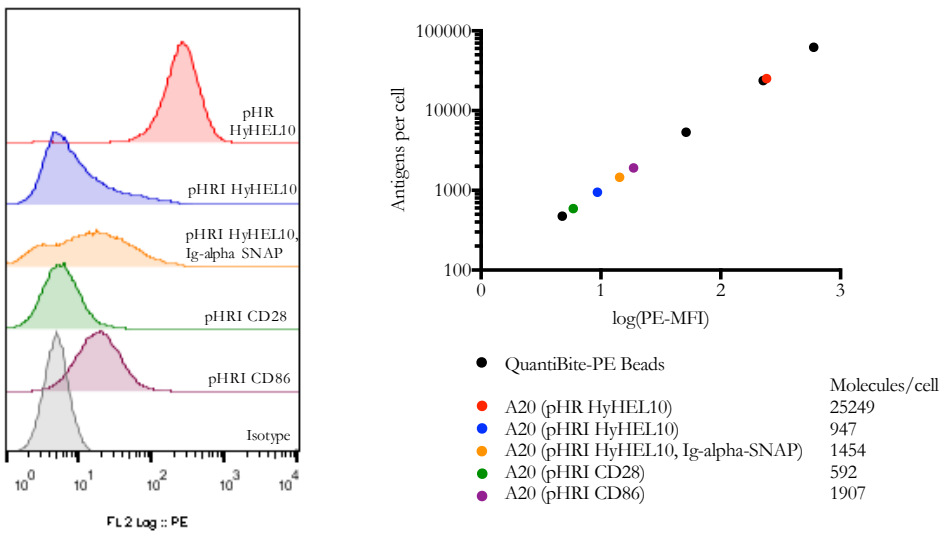

Figure 5.3 Quantification of cell surface protein expression
Quantitative FACS analysis of expression levels of BCR, CD28, and CD86 in A20 cells. Experimental samples were stained with PE-conjugated antibodies and fluorescence intensity measured by FAC. QuantiBrite-PE beads containing known amounts of Phycoerythrin (PE) labels per bead were used to calibrate the fluorescence intensity against the number of PE molecules per cell to allow estimation of the number of receptors per cell in experimental samples.

5.3.2.3 Fluorescent labelling of ligands for single-molecule imaging

To undertake single molecule imaging using externally labelled Hel-fusion protein, the Halo-Snap-HEL (N-terminal His-tag; N-HSH) described in Chapter 3 was used. It has already been shown that this ligand is monomeric, folded correctly and binds specifically to HEL-specific B cells. In Chapter 4, it was shown that soluble HEL does not induce calcium triggering so is unlikely to perturb the resting cell state. Importantly, this ligand binds with a very low equilibrium dissociation constant (K_d = 8.9 pM) making it excellent for receptor labelling. N-HSH was labelled with fluorescent dyes via the Snap®/Halo®-tag in preparation for single molecule imaging.

Choice of fluorophore

To undertake two colour single molecule imaging, spectrally separate fluorophores were required. Importantly, these fluorophores needed to be conjugated to a Halo/Snap® ligand to allow labelling. Fluorescent dyes differ in their size, photostability, brightness, cell permeability, absorption and emission spectra [312]. N-HSH proteins were tagged with a range of Halo/Snap® dyes and incubated with A20 (HyHEL10) B cells. Surface labelling was then tested using TIRF microscopy. Labelling with the Snap®-Cell-505-Star and Snap®-647SiR gave the best results. These two flourophores were also spectrally separated. However, when mixed together and added to cells spectral overlap was observed but this could be overcome with the use of appropriate filters. N-HSH labelled with either dye and added to A20 B cells lacking the HyHEL10 BCR showed no surface labelling confirming that the binding seen previously to the HyHEL10 BCR was specific.

Separation of protein from free dye

In control experiments, fluorescently labelled N-HSH was incubated with A20(HyHEL10) B cells which were imaged using TIRF microscopy. Labelling was observed as expected on the cell surface but fluorescence was also detected inside the cell. This was presumed to result from free dye remaining following the labelling process, crossing the plasma membrane. Intracellular free dye presents a problem as it decreases the signal-to noise ratio making identification of single molecules on the cell surface problematic. To remove the free dye, the fluorescently labelled protein mix was purified by FPLC (Figure 5.4). Clear separation of protein from free dye was seen. Protein fractions were pooled, concentrated and used for cellular labelling immediately or frozen in aliquots for future use. Intracellular fluorescence was no-longer noted with cells labelled with FPLC purified fluorescently labelled protein.

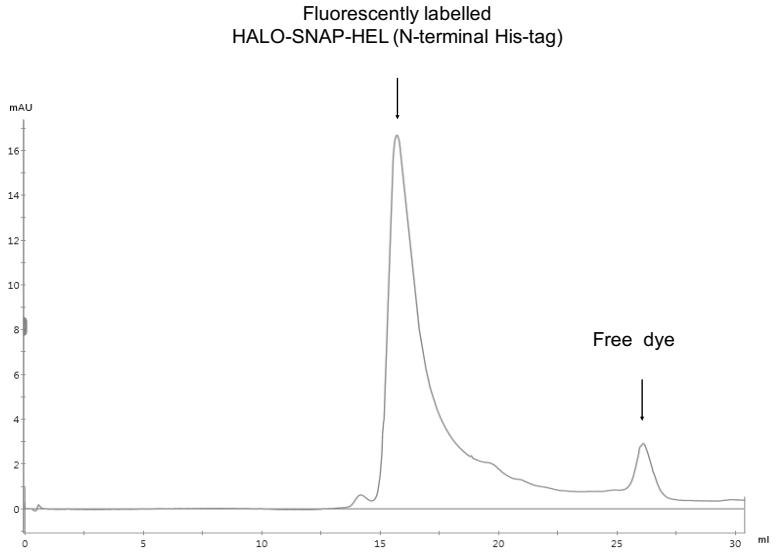

Figure 5.4 Separation of fluorescently labelled Halo-Snap-HEL from excess free dye
Halo-Snap-HEL (N-terminal His-tag) was mixed with an excess of SNAP®-ligand and incubated at 4 °C with rotation overnight. The following day the mixture was concentrated and run over a S200 GL column using an AKTA FPLC. A representative FPLC trace is shown for the separation of Halo-Snap-HEL (N-terminal His-tag) labelled with Snap®-647-SiR.

Assessment of labelling efficiency of HEL fusion proteins in vitro

To accurately calculate the degree of coincident fluorescence detected in single molecule experiments for given receptor valencies it was necessary to have an accurate measurement of the labelling efficiency of fluorescently labelled N-HSH. The experimental approach chosen was to firstly label the protein on the Halo®-tag and then perform a second labelling step with a different fluorescent substrate on the same Halo®-tag (Figure 5.7). The amount of the second fluorescently labelled ligand incorporated can then be used as a surrogate of free sites remaining following the initial labelling protocol. This approach was combined with varying the concentration of ligand in the initial labelling step to calculate the amount required to completely saturate binding. Using this approach, the Halo®-tag within the N-HSH protein was shown to label completely when in excess of an equimolar ratio of ligand:protein. Similar results were obtained with the Snap®-tag (Figure 5.5).

The complete labelling of Halo®/Snap®-tags within N-HSH is supported by experiments in which both the Snap®-tag and Halo®-tag were labelled simultaneously. In this setting single colours were not seen but instead almost 100% FRET (data not shown) indicating that both sites had been successfully labelled. The ability to 100 % label N-HSH via either tag was important as it means that no account needs to be taken of labelling inefficiency in subsequent analysis.

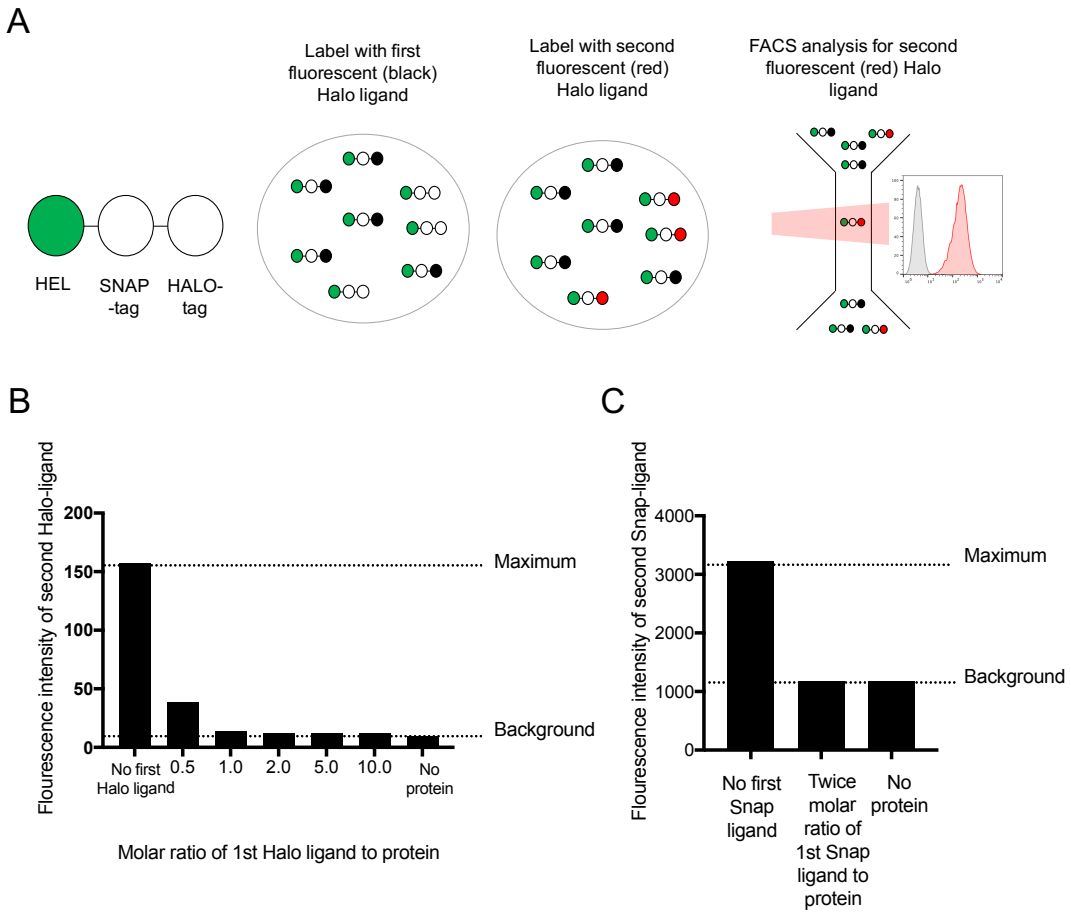

Figure 5.5 Measuring the efficiency of labelling of Snap®/Halo®-tags in HEL-fusion proteins
(A) Schematic representation of experimental set up. Halo-Snap-HEL (N-terminal His-tag) was labelled with a first Halo®-ligand, and then bound to HyHEL10-conjugated Dynabeads to allow free dye to be washed away. A second Halo®-ligand was then used to label any remaining Halo®-tag sites. The beads were once again washed and then flow cytometry analysis undertaken on the beads for fluorescence at the emission spectra of the second Halo®-ligand. (B) Labelling efficiency at the Halo®-tag. Varying molar ratios of first Halo®-ligand to protein were used. Maximum fluorescence intensity refers to labelling with the second fluorescent ligand in the absence of a first labelling step. Background fluorescence intensity refers to labelling of Dynabeads in the absence of protein. (C) Labelling efficiency at the Snap®-tag.

5.3.2.4 Detection efficiency of the BCR in vivo using HEL-fusion proteins

It has thus far been shown that the N-HSH can be almost completely labelled using a fluorescently conjugated Halo®/Snap®-tag ligand. However, what is important to ascertain is the effectiveness with which this fluorescently labelled protein is able to bind to the HyHEL10 BCR in vivo. To test this, the A20 (pHRi HyHEL10, Ig-alpha-Snap) cell line was employed as it can be simultaneously labelled internally and externally. The BCR was labelled internally with Halo®-SiR and externally via N-HSH labelled with Snap- Cell-505-Star. Two colour TIRF imaging was then undertaken in live cells. To detect colour coincidence the two colours were tracked and analysed using the DySCO protocol. The level of colour co-incidence, and therefore BCR detection efficiency, was 82.5 (+/- 11.7) %. Failure to achieve 100 % detection was likely the result of a combination of labelling inefficiency and the inherent photophysics of the fluorophores. However, while 100 % labelling was not achieved a large fraction of BCRs could be tagged with the N-HSH protein. More importantly, it was possible using this experimental setup to quantify the BCR detection efficiency so that it could be taken into consideration in the analysis of experiments undertaken to measure BCR stoichiometry.

5.3.3 Resting stoichiometry of the BCR in live cells

The preceding sections have described the production of a cell line and a labelling strategy for undertaking single molecule imaging of the BCR. Having verified these reagents, the next step was to use them to establish the stoichiometry of the BCR. Live cells were used to avoid any confounding effects that can be potentially introduced by the use of fixing agents.

5.3.3.1 Two colour-coincidence detection identifies a monomeric BCR

N-HSH was labelled as discussed above with either Snap® Cell-505-Star or Snap®-647SiR. The two fluorescently labelled proteins were then mixed in an equimolar ratio and added to A20 (pHRi HyHEL10) B cells. The cells were then imaged using TIRF microscopy. An area of the cell surface was bleached and FRAP observed. To detect colour coincidence the two colours were tracked and analysed using the DySCO protocol (Figure 5.6).

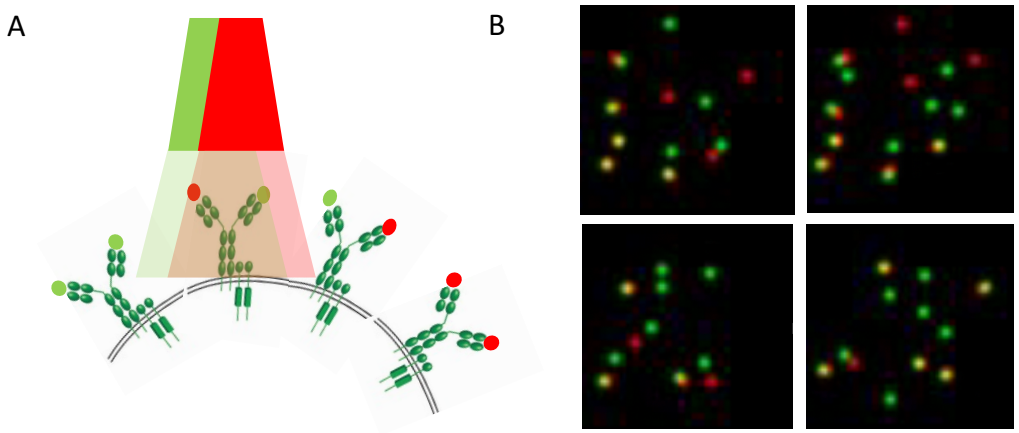

Figure 5.6 Two-colour single molecule fluorescence microscopy of a live B-cell
(A) Schematic representation of single molecule two-colour coincidence detection as applied to the BCR. Each BCR (green) is bivalently labelled with a fluorescent tag in one of two colours (red or green) **(B)** Representative example of colour coincidence as individual BCR's diffuse through the confocal volume. Yellow is red-green colour coincidence.

The two-colour co-incidence determined in these experiments was 29.4 (+/- 4.8) %. This level of co-incidence is most consistent with a receptor valency of a bivalent BCR "monomer", but significantly lower than the theoretical 50 % colour co-incidence. However, this can be explained by the detection efficiency of the BCR. In section 5.2.3.4 it was shown that the detection efficiency of the BCR was 82.5 %. Taking this into consideration the expected level of co-coincidence for a monomeric BCR would be 34 %. This is compatible with the results obtained in our experiments supporting the results that the BCR is monomeric on the surface of resting B cells.

5.3.3.2 Two colour-coincidence of controls of known stoichiometry

The stoichiometry of the BCR has thus far been postulated based on theoretical and predicted colour co-incidences. To validate these predictions, we tested the results obtained for the BCR against those of known bivalent proteins, i.e. soluble HyHEL10 immunoglobulin and CD28.

The BCR is essentially a membrane bound form of immunoglobulin. If the BCR is monomeric then the two-colour co-incidence obtained for soluble immunoglobulin would be expected to be comparable to that for the BCR at the surface of resting B cells. To test this, HyHEL10 soluble antibody was first labelled directly with SiR via amine coupling. The antibody was then labelled with a mixture of N-HSH fluorescently labelled in an equimolar ratio with Snap® Cell-505-Star and Snap®-546. The antibody was then allowed to adsorb onto a PLL-coated slide. TIRF imaging was first undertaken to determine the location of the HyHEL10 antibodies based on SiR fluorescence and then overlaid with the fluorescence from Snap® Cell-505-Star and Snap®-546. Using this approach, the two-colour co-incidence of 505 and 546 identified was 37.2 (+/- 12.3) % (Figure 5.7). This is not significantly different from the co-incidence identified for the HyHEL10 BCR on the surface of A20 cells. This supports the previously finding that the BCR is monomeric.

If the BCR is monomeric then it would also be expected that the two-colour co-incidence obtained would be similar to that of known dimers labelled in an analogous manner. In previous experiments CD28-Halo was expressed in T cells and labelled in two spectrally distinct colours. In this setting, the degree of two-colour co-incidence was 22.7 % (Figure 5.7, [310]). This level of coincidence is again comparable to that of the BCR and soluble

immunoglobulin supporting the body of evidence presented in this Chapter that the BCR is monomeric on the surface of resting B cells.

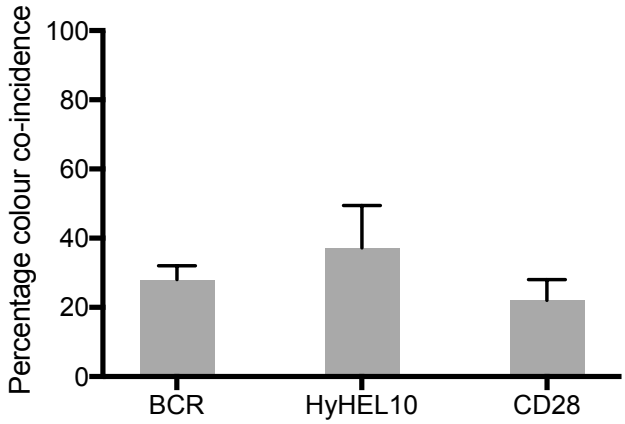

Figure 5.7 Two-colour co-incidence of BCR, soluble antibody and CD28
BCR, soluble HyHEL10 antibody or CD28 were labelled in two spectrally distinct colours and imaged using TIRF microscopy. The two colours were tracked and analysed using the DySCO protocol. Figure shows mean +/- standard deviation for each condition.

5.3.3.3 BCR diffusion at the cell surface

To further assess the likely stoichiometry of the BCR on the surface of resting cells the tracks of individual BCRs were analysed and the average velocity of each BCR calculated. Trajectory ensemble plots for multiple BCRs were measured and plotted on a mean square displacement plot (Figure 5.8). This showed that the BCR diffuses at a rate (0.07 μm/s), comparable to that of other surface proteins, implying that it is unclustered.

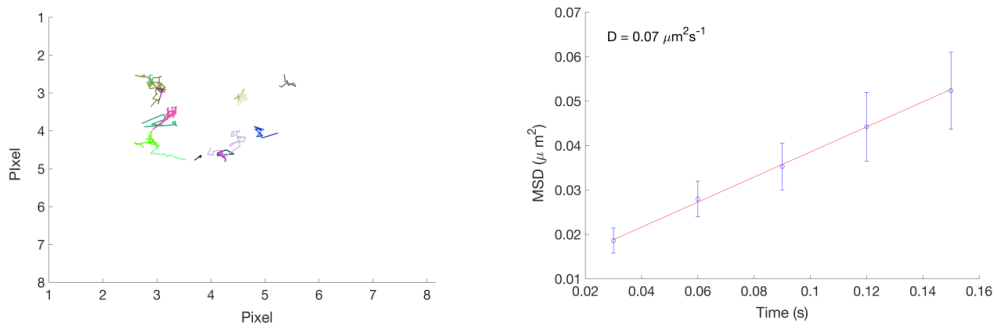

Figure 5.8 Diffusion of the BCR on a live B-cell.
(**A**) Trajectory ensemble plot showing an example of the tracks obtained. (**B**) MSD plot showing the rate at which the BCR is diffusing.

5.4 Discussion

5.4.1 Multicolour fluorescence microscopy to study BCR stoichiometry

Single molecule fluorescence microscopy is an established method to study the subunit composition of protein complexes at the cell surface. Historically, this has been undertaken using either single colour fluorophore imaging and photobleching-step counting [313-317] or two-colour co-incidence detection (with or without the use of referenced control; [310, 318]). These methods have enabled the subunit composition of multiple protein complexes to be elucidated including the TCR [306] and GPCRs [307]. In this Chapter, we have taken these methods and adapted them to another non-catalytic tyrosine-phosphorylated receptor, the BCR. The high affinity interaction between the HyHEL10 BCR and its natural ligand HEL has been utilised as a means of receptor labelling, negating the need for either genetic modification of BCRs or the production of high affinity fabs. The technique has been undertaken on live cells, removing any artefacts that could be potentially introduced by fixation. The bivalent nature of a single BCR has added an added layer of complexity to this external labelling approach as the labelling of each BCR is unavoidably divalent. However, by considering the expected colour co-incidence ratio for monomers, dimers and oligomers, and using controls of known stoichiometry it has been possible to determine the stoichiometry of the BCR on the cell surface.

The major advantage of the experimental approach outlined is that it does not limit experiments to cell lines that can be genetically modified. Stoichiometric analysis can therefore be undertaken on primary cells, which in the case of the HyHEL10/HEL

interaction are available from the well characterised MD4 transgenic mouse. This is important as it allows correlation of results established in cell lines in this Chapter with primary cells. Furthermore, it will ultimately allow expansion of the work outlined here to look at the issue of BCR stoichiometry across different B cell subsets (which express differing quantities and isotypes of BCR). This is significant as it should determine if the stoichiometry of the BCR is conserved across different BCR isotypes and B cell subsets, with consequences for the mechanism of BCR triggering.

An important limitation of the experimental approach developed is incomplete receptor labelling. This is a significant potential drawback as incomplete receptor labelling fails to identify large complexes, biasing results to lower valency estimates of stoichiometry. To allow for this it has been shown here that the protein used for external labelling, N-HSH can be 100 % labelled at anything in excess of an equimolar ratio of fluorescent ligand:protein. When added to HyHEL10 expressing B cells this protein binds with a very low Kd of 8.9 pM. This makes it excellent for receptor labelling as it has a very low off rate thereby maximising receptor labelling. In our study the detection efficiency of the BCR was 82.5 % using this ligand. Some labelling inefficiency was present which was likely due to a combination of detection inefficiency and the inherent photophysics of the flourophores. However, these effects can be further compensated for by comparing measurements to referenced controls.

In future experiments we plan to develop the experimental approach further by using three colour fluorescence microscopy. This approach is technically more difficult, but the analysis is conceptually simpler and removes the need to compare results against predicted

results for expected stoichiometry. Put simply, using this approach, if three-colour co-incidence is ever seen then the BCR cannot comprise bivalent complexes (Figure 5.9).

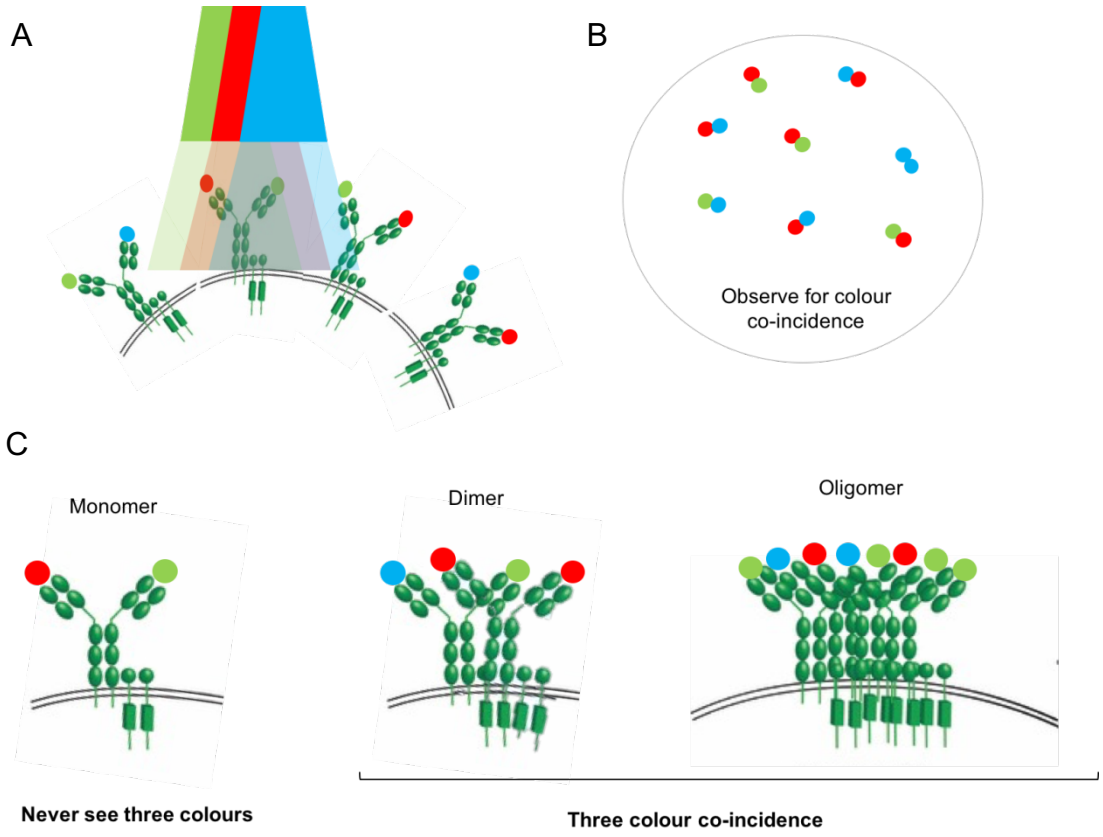

Figure 5.9 Three colour co-incidence microscopy at the B cell surface
(A) Schematic representation of single molecule three colour-co-incidence detection as applied to the BCR. Each BCR (green) is bivalent labelled with a fluorescent tag in one of three colours. (B) Diagrammatic representation of colour co-incidence as individual BCR's diffuse through the confocal volume (C) Expected colour co-incidence results for a BCR monomer, dimer and oligomer.

5.4.2 Multicolour fluorescence microscopy identifies a monomeric BCR

Two-colour fluorescence microscopy identified a 29.4 % colour co-incidence for the BCR. This fits most closely with a BCR that is predominantly monomeric on the surface of resting B cells. However, this is still below the 50% expected for monomers likely accounting for by some labelling inefficiency as outlined above. Importantly, the level of colour co-incidecne was comparable to soluble monomeric HyHEL10 antibody and the known monomer CD28. The concept of a monomeric BCR was further supported by single-particle tracking analysis suggesting that the BCR diffuses at a rate (0.07 μm/s), comparable to that of other surface proteins, implying that it is unclustered.

These analyses were undertaken on the A20 (pHRI HyHEL10) B cell line that expresses approximately 1000 molecules per cell. This is considerably lower that the approximately 100,000 BCRs expressed on primary B cells. Such low expression levels are required for single particle tracking experiments because at higher expression levels there is an increase in the rate of chance association. However, a reduction in expression levels reduces the rate of association and therefore potentially biases results towards lower stoichiometry complexes. However, it can be reasoned that if the BCR was pre-clustered if should still form clusters (even if these were smaller in size). However, it is important to correlate findings established in cell lines with experiments undertaken on primary cells which express physiological levels of BCR. By using the FRAP approach and tracking BCRs for longer across an increased number of frames it should be possible to adapt our technique to assess the stoichiometry of the BCR on primary cells and in this way verify the results established on cell lines. Some consideration will have to be given to the problem of how

to prevent activation of the primary B cells at the higher BCR expression levels. It might be very important to avoid surfaces [237].

5.4.3 A monomeric BCR argues against the dissociation activation model of BCR triggering

In this chapter multi-colour fluorescence single molecule imaging has been used to show that the BCR is predominantly monomeric on the surface of resting cells. These results are consistent with previous studies using FRET [132] and single particle tracking of individual BCRs labelled with fluorescent Fabs [230]. However, the concept of a monomeric BCR is controversial.

An opposing school of thought is that the BCR is pre-clustered in the resting state. This theory arose out of experiments conducted on B cell lysates in which under minimal detergent conditions the BCR was seen to run as a large macromolecule [233]. However, solubilisation of cell membranes is often dependent on the detergents used. Further work using quantitative BiFC assays [232] and high resolution PLA [234] supported the concept of a pre-clustered BCR. However, such techniques have the drawback of potentially stabilising complexes formed via random collisions (in addition to true associations) thereby biasing results towards clusters. More recent evidence for a pre-clustered BCR has come from dSTORM experiments in which B cells were placed onto anti-MHC class II cover slips and left for up to 10 minutes prior to imaging. [236]. In Chapter 4, the choice of surface for triggering experiments was shown to be critical to experiments undertaken on lymphocytes. Both PLL and glass were shown to be activating surfaces which induce bona-fide BCR signalling. Experiments conducted on PLL have suggested receptors and

signalling proteins cluster by default on the surface of resting cells. These results are analogous to those observed for B cells landing on anti-MHC class II coated cover slips. It is therefore possible that the results observed using dSTORM represent the activated, rather than resting state of the BCR. This interpretation may explain why only a local convergence of receptors was seen upon B cell activation in these experiments without any dramatic global reorganisation, potentially because the cells had already been activated by the surface [236]. These drawbacks can potentially explain the disparity between the historical results and those presented in this Chapter.

A functional monomeric BCR imposes important constraints on potential theories of receptor triggering. The results presented in this Chapter thus argue against the dissociation activation model but potentially support the conformation induced oligomerisation model as a mechanism of BCR triggering. In Chapter 6, we will test the conformation induced oligomerisation model, together with an additional model that has yet to be tested in B cells, the kinetic-segregation model. Both of these models potentially fit with the experimental data presented in this Chapter, i.e. that the BCR is monomeric in the resting state.

Chapter 6

B Cell Receptor Triggering and the Kinetic-Segregation Model[2]

6.1 Introduction

There are three established theories to explain the mechanism of triggering of the BCR: the cross-linking model; the conformation-induced oligomerisation model; and the dissociation-activation model. This thesis aims to test these models experimentally. In Chapter 4, the cross-linking model was tested and ruled out because it failed to account for the activation of B cells by monomeric ligand in the physiological setting of surface bound antigen. In Chapter 5, the dissociation-activation model could be ruled out because, in the resting state, the BCR is not pre-clustered. The remaining model to be tested is the conformational change-induced oligomerisation which fits with the data presented in that the BCR is 'monomeric' on the surface of resting cells. However, it is important that all potential triggering theories are considered, even if these have yet to be seriously considered for B cells. An alternative theory that fits with the data presented is the kinetic-segregation (KS) model.

The KS model is a theory of receptor triggering originally proposed with regards to TCR triggering [238]. The model proposes that in the resting, non-antigen bound state the receptor is free to diffuse across the membrane interacting with kinases and phosphatases but generating no net signal (due to the numerical dominance and heightened activity of

[2] The work described in this chapter was undertaken in collaboration with James McColl, Anna Lippert and Jane Humphrey of the Klenerman Group, Dept. Chemistry, Cambridge University.

the phosphatases versus the kinases). Antigen binding to the receptor traps the BCR within close contact zones. Bulky phosphatases are passively excluded from these close contact zones owing to their size but smaller kinases continue to diffuse freely. The balance is switched in favour of phosphorylation in the close contact zones and signalling ensues. Ligand discrimination occurs based on the half-life of receptor/antigen interactions and the time spent within close contacts [238].

The KS model has yet to be studied in B cells, although it has been postulated as a potential mechanism of BCR triggering [112]. Experimental data supporting the KS model therefore comes from experiments conducted in T cells [238]. The BCR presents a challenge to the KS model since it is a much larger molecule than the TCR, it is bivalent, and it binds antigen with a much higher affinity. On the other hand, the balance of phosphorylation is known to be critical to B cell activation [254]. B cells co-express the very largest phosphatase, CD148, together with the largest isoform of CD45, CD45ABC. These phosphatases are developmentally regulated and have been shown to be important in BCR signalling [25]. Furthermore, the large extracellular domains of CD45 and CD148 would theoretically allow their passive exclusion from close contact zones [142, 247]

In this Chapter, the principles of the KS model were tested for the first time in the context of BCR triggering. The following key questions were addressed.

- Do close contacts form on BCR triggering?
- Is BCR triggering dependent on the size of the BCR/antigen complex?
- Is BCR triggering dependent on the size of the extracellular phosphatase?

In undertaking these experiments, the conformation-induced oligomerisation model was further tested because triggering should be independent of the size of the BCR/antigen complex.

6.2 Materials and Methods

6.2.1 Construct design and cell line preparation

mCD45 was cloned using a multistage PCR protocol. The extracellular domain of CD45RABC was ordered from GeneArt and the transmembrane and intracellular domains amplified from an existing template. The two segments were then joined by chimera PCR. mCD148 was cloned directly from MD4 mouse cDNA. The terminal HA tag of all constructs was added by incorporating the nucleotide sequence into the 5' oligonucleotide primer. To generate mCD148-Snap/Halo and mCD45-Snap/Halo, a Snap®-tag or Halo®-tag was cloned from plasmid DNA with a 5' glycine-serine linker and inserting in frame via a NotI restriction site to mCD45 and mCD148 constructs in which the stop codon had been removed. The final PCR products were cloned into the pHR vector (via MluI and NotI) and the sequence checked by DNA sequencing. Vectors were transfected into the appropriate cell line using the small-scale lentiviral transfection method and expression confirmed by flow cytometry for total HA expression. If required, high expressing cells were selected by FACS.

6.2.2 Intracellular labelling of Snap®-/Halo®-tags

1 x 10^6 cells were harvested and spun down at 1200 rpm for 2 minutes and then washed in 1000 µl RPMI. The cell pellet was then resuspended in 100 µl complete RPMI media and

1 µl of 5 µM Snap®-/Halo®-tag ligand added. Cells were then incubated at 37 °C/5 % CO_2 for 1 hour. Cells then underwent repeated cycles of washing and incubation to remove free dye. Each wash step consisted of spinning down the cells at 1200 rpm for 2 minutes, washing in 1000 µl RPMI and then resuspending in 1000 µl RPMI. Between washes, cells were incubated at 37 °C/5 % CO_2 to allow free dye to diffuse out of cells. The initial incubation period was 20 minutes, the second 1 hour and all subsequent incubation periods 20 minutes. After a total of 2 hours of incubation cells were washed as above before a final wash with PBS. Cells were then resuspended in 50 µl PBS ready for imaging.

6.2.3 Surface preparation

SLBs were prepared using the spin coating method for calcium based microscopy experiments and by the SUV method for TIRF experiments. All bilayers were prepared using 4 % Ni-NTA. Proteins were added to the bilayers at a concentration of 1 µg/ml and allowed to bind for 1 hour before washing with HBS/PBS prior to imaging.

6.2.4 Three colour TIRF imaging

TIRF imaging was undertaken on a custom-built microscope. The microscope was fitted with diode lasers operating at 488 nm (100 mW, iBeam smart, Topica), 561 nm (200 mW, Jive 200, Cobolt) and 641 nm (100 mW, CUBE 640-100C, Coherent). The laser beams were each directed through a λ-quarter wave plate to ensure circular polarisation of the excitation light and the beams aligned and focused on the back focal plane of a 1.4 NA TIRF objective (100x oil objective, UPLSAPO100XO/1.4, Universal Plan Super Apochromat) mounted on a IX73 Olympus inverted microscope. Emitted fluorescence

was collected by the same objective and separated from the returning TIR beam by a combination of long-pass and band-pass filters (505, BLP01-488R-25 + FF01-520/44-25; TMR, LP02-568RS-25+FF01-587/35-25; SiR, 692BP). The fluorescence signal was recorded using a EMCCD (Photometrics, Evolve 512 Delta) with an electron multiplication gain of 250 ADU/photon operating in a frame transfer mode. Three colour images were acquired by sequential imaging using Micromanager [308]. Image processing was undertaken using ImageJ [309] and MATLAB (R2016b, The MathWorks, Natick, US).

6.2.5 Data acquisition and analysis

Analysis of the data to assess the relative association of BCR, CD45/CD148 and HEL was undertaken using custom-written MatLab Code. Two approaches were used:

(1) *Pearson Correlation Coefficient Analysis.* The contact area was defined as the combination of BCR and CD45/CD148 signal at 60% of the perspective total intensity. The extent of association within this defined area was then determined by the Pearson Correlation Coefficient. Analysis was undertaken for CD45/CD148 vs BCR, CD45/CD148 vs HEL and HEL vs BCR. The Pearson Correlation Co-efficient has a value between -1 and 1: 1 is positive correlation; 0 is no linear correlation; and -1 is anti-correlation. The extent of exclusion was calculated from 1-Pearson Co-efficient.

(2) *Exclusion analysis.* Exclusion analysis was undertaken to compare the relative amounts of each variable (BCR, CD45/CD148 and HEL) within versus outside the close contact area. The close contact area was defined as either (A) cell mask-CD45/CD148, or (B) HEL. Based on the method of defining the close contact area, exclusion was then calculated as either:

$$A = 1 - \frac{\text{Average intensity close contact}_{\text{Cell mask - CD45/CD148}}}{\text{Average intensity whole contact}} \qquad B = 1 - \frac{\text{Average intensity close contact}_{\text{HEL}}}{\text{Average intensity whole contact}}$$

6.3 Results

6.3.1 Close contacts form on BCR triggering

6.3.1.1 Experimental approach

Overview

A key prediction of the KS model is that large phosphatases such as CD45 and CD148 are excluded from close contacts induced by receptors binding to ligand at a surface. To test this prediction in B cells, three-colour TIRF imaging of CD45/CD148, BCR and HEL was undertaken during the first 90 seconds as A20 (HyHEL10) B cells landed on HEL-presented on SLBs (Figure 6.1). This approach allowed the distributions of each protein to be visualised within the correct timeframe for receptor triggering to determine if close-contacts, defined by the exclusion of the phosphatases and accumulation of ligand and receptors, exist. All imaging was undertaken at 37 ˚C.

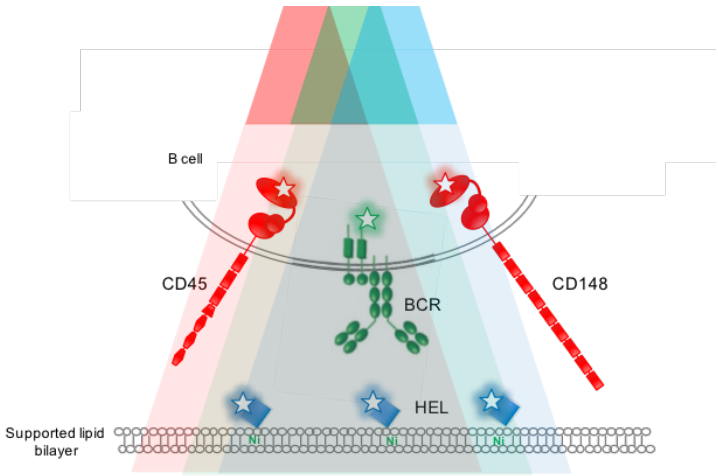

Figure 6.1 Experimental setup to test if close contacts form on BCR triggering
Schematic representation of experimental setup. Three colour TIRF imaging was undertaken to visualise CD45 or CD148 (red) and BCR (green) on A20(HyHEL10) B cells as they settled onto supported lipid bilayers (SLBs) labelled with fluorescent HEL (blue). Stars represent fluorophores labelling proteins of interest.

Imaging modality

To undertake imaging of close contacts TIRF microscopy was chosen. This method is based on the principle that when light is totally internally reflected at a glass-water interface an evanescent wave is generated which decays exponentially with distance from the surface. This allows selective illumination of fluorophores within < 100 nm of the interface thereby increasing the axial resolution and the signal-to-noise ratio by eliminating background fluorescence [304]. This makes TIRF ideally suited to studying processes at the cell surface, such as close contact formation and BCR triggering

Fluorophore choice

In this study, three colour TIRF microscopy was undertaken with labelled CD45/CD148, BCR and HEL. The fluorophores Star-Cell 505, TMR and 647SiR were chosen as they are available as Halo®-tag and/or Snap®-tag conjugates and are spectrally well-separated. Despite this, bleed through was seen between the channels. Bandpass filters were therefore applied to overcome this with no residual spectral bleed through.

Labelling strategy

HEL

Halo-Snap-HEL (N-terminal His-tag; N-HSH) was labelled via the Snap®-tag or Halo® tag and free dye removed by FPLC. Fluorescently-labelled HEL was then used to label Ni-containing SLBs. The quality of each SLB was assessed using TRIF prior to undertaking close-contact imaging.

BCR

The BCR was labelled via a Snap-tag® attached to the intracellular domain of the Ig-α chain. Expression of Ig-α-Snap was undertaken using the pHR vector to achieve high expression levels for bulk imaging.

CD45/CD148

The labelling of CD45/CD148 for close contact imaging was more complicated. CD45/148 antibodies exist which could potentially be used for labelling, however, while whole antibodies possess high avidity and specify their bivalent nature can lead to artefactual results by cross-linking multiple ligands. Fragmentation of whole antibody into Fabs circumvents this problem and maintains specificity but at the expense of a reduction in avidity. Fluorescently labelled Fabs were trialled to label CD45, however, while specific labelling was seen, imaging was severely time limited by the high off rate at 37 °C. An alternative strategy was therefore conceived to transfect in supplementary CD45 or CD148 linked to a Halo®-tag. This approach has the disadvantage of not labelling endogenous protein, however, the behaviour of exogenously inserted phosphatases should be identical. Importantly, the use of Halo®-tag constructs allowed specific and stable labelling.

Chimeric proteins were constructed consisting of a HA-tag linked to full-length murine CD45 (RABC) or CD148 connected by a flexible linker (consisting of 5 glycine (G) and serine (S) residues) to a Halo®-tag (Figure 6.2). Constructs were transfected into A20 (HyHEL10, Ig-alpha-Snap) cells using the small-scale lentiviral transfection method and expression levels checked by flow cytometry using an antibody directed against the HA-

tag. Expression levels of both murine CD45 (RABC) and murine CD148 were relatively low but a small population of high-expressing cells were identified and selected by FACS.

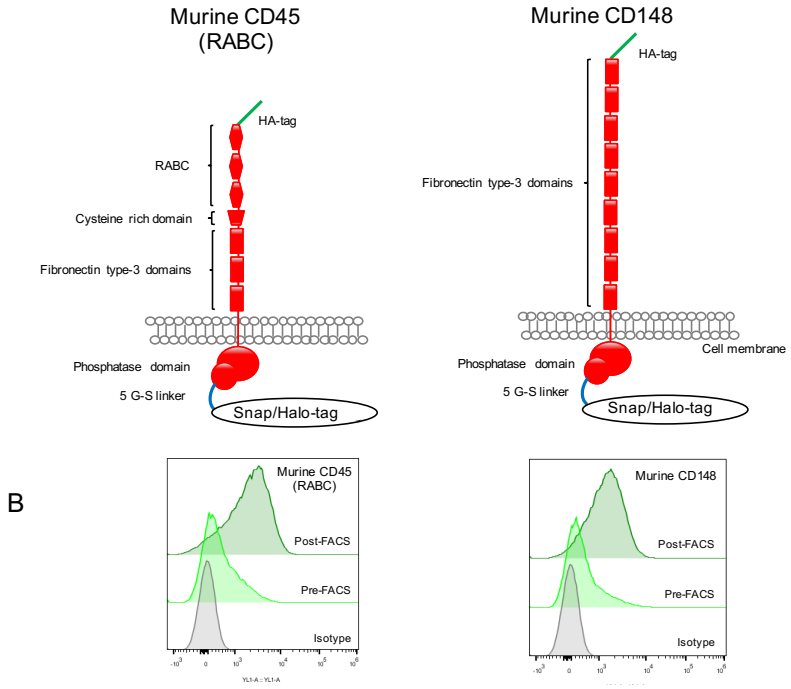

Figure 6.2 Labelling of CD45/CD148 for TIRF imaging
(A) Schematic representation of constructs used for labelling CD45 (left) and CD148 (right). Each construct consists of a HA-tag (green) linked to full-length murine CD45 (RABC) or murine CD148 (red) connected by a flexible linker (5 glycine(G) and serine(S) residues; blue) to a Halo®-tag or Snap®-tag (black). (B) Histogram plots displaying expression levels of HA-mCD45-Halo (left) and HA-mCD148-Halo (right) in A20(HyHEL10, Ig-alpha-Snap) B cells pre- and post-FACS. Isotype controls (grey) shown for comparison.

Analysis

Analysis of localization between BCR, CD45/CD148 and HEL was undertaken using a number of different methods (Figure 6.3). The extent of association within contact areas was determined by the Pearson correlation coefficient and analysis undertaken looking at the correlation of HEL vs BCR, HEL vs CD45/CD148 and BCR vs CD45/CD148. More analysis was undertaken to compare the relative amounts of each variable (BCR, CD45 and HEL) within versus outside the close contact area. The close contact area was defined using either (A) cell mask-CD45/CD148, or (B) HEL. This allowed calculation of two different exclusion analyses (A and B).

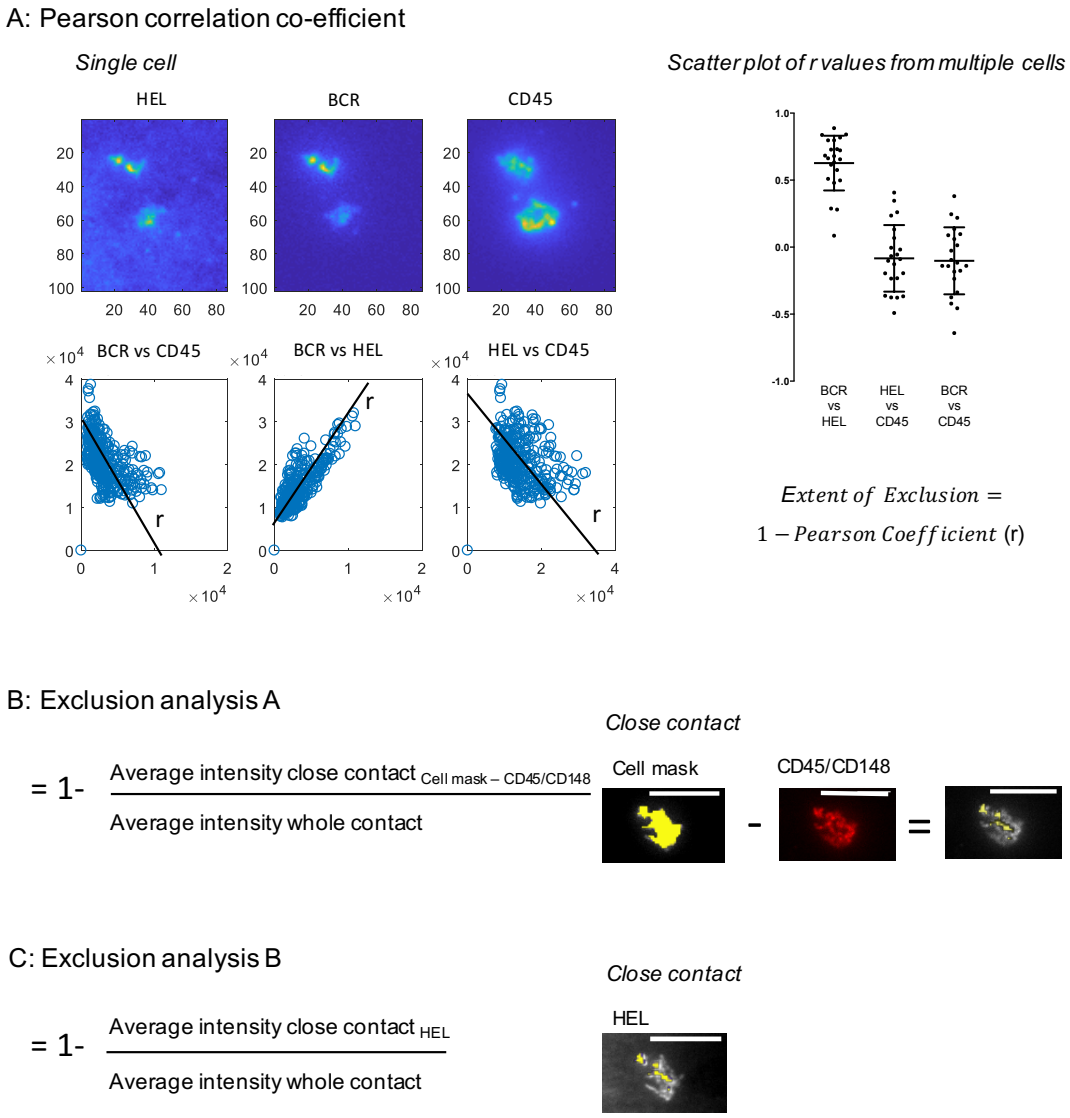

Figure 6.3 Analysis of localisation of BCR, CD45/CD148 and HEL
Analysis of localization between BCR, CD45/CD148 and HEL was undertaken using three different methods. (A) Pearson correlation co-efficient analysis. Representative example. For each cell the AVG intensity of BCR, CD45 and HEL was measured and the correlation between BCR vs CD45, HEL vs CD45 and HEL vs BCR undertaken to generate an r value. Scatter plots of r values from multiple cells were then plotted. Extent of exclusion could be calculated form 1-Pearson correlation co-efficient. (B) Exclusion analysis A. The relative amount of each variable (BCR, CD45 and HEL) within versus outside the close contact area was determined. The close contact area was defined for exclusion analysis A as cell mask-CD45/CD148). For each cell an exclusion value was calculated and values for multiple cells plotted on a scatter plot. (C) Exclusion analysis B. This was undertaken as exclusion analysis A but the close contact area was defined as regions containing HEL.

6.3.1.2 Close contacts form from which CD45 is excluded

To test the prediction that close contacts form on BCR triggering from which CD45 is excluded, TIRF imaging was undertaken as A20 (HyHEL10, Ig-alpha-Snap, CD45-Halo) B cells settled onto Ni-containing-SLBs pre-coated with fluorescently labelled N-HSH. The images obtained showed early segregation of CD45 from BCR and ligand (Figure 6.4). Association analysis showed correlation of the fluorescent signal from HEL and BCR, implying ligand receptor complexes had formed, and using all three methods of localisation analysis CD45 was shown to be excluded from these close contact zones. The exclusion of CD45 from close-contacts occurred within the first 90 seconds of landing, compatible with the timing of calcium triggering. Use of the membrane dye, DiO, confirmed that these CD45 exclusion zones were not artefacts due to non-apposition of the B cell membrane to the SLB.

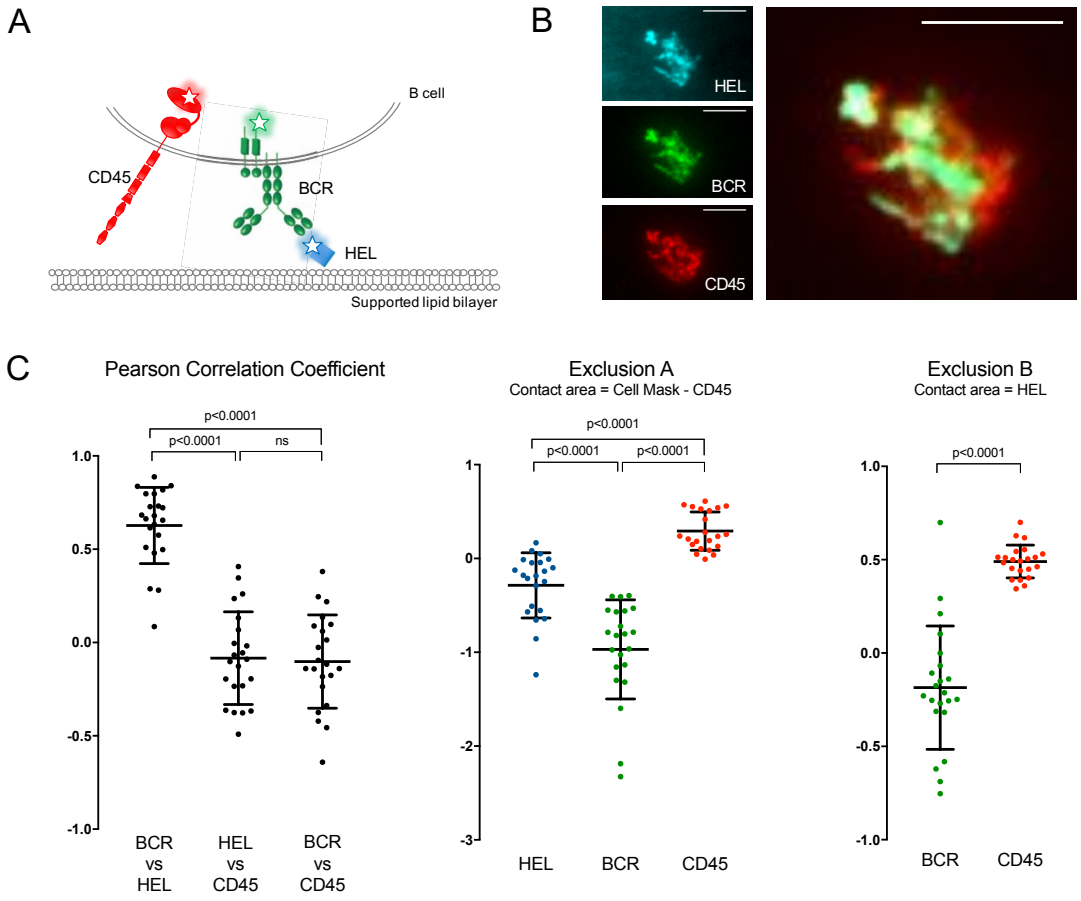

Figure 6.4 Close contacts form from which CD45 is excluded
(A) Schematic representation of experimental setup. Three colour TIRF imaging was undertaken to visualise CD45 (red) and BCR (green) on A20(HyHEL10) B cells as they landed on SLBs labelled with fluorescent HEL (blue). Stars represent fluorophores labelling proteins of interest. (B) Representative example of cells showing the spatial organisation of CD45, BCR and HEL within the first 90 seconds of landing. Scale bars are 5 μm (C) Analysis of association using Pearson correlation co-efficient or exclusion analysis in which contact zone is defined by cell mask-CD45 (exclusion analysis A) or HEL (exclusion analysis B). Scatter plots show results from individual cells. Bars are mean ± SD. P-values are derived from Student's t-test.

6.3.1.3 Close contacts form from which CD148 is excluded

To test the prediction that close contacts form on BCR triggering from which CD148 is excluded, TIRF imaging was undertaken as A20 (HyHEL10, Ig-alpha-Snap, CD148-Halo) B cells landed onto Ni-containing SLBs pre-labelled with fluorescent HEL. These experiments showed early segregation of CD148 from BCR and ligand (Figure 6.5), analogous to the results seen with CD45 labelled B cells. Association analysis again demonstrated correlation of the fluorescent signal arising from HEL and BCR, implying receptor/ligand complexes had formed. Using all three methods of localisation analysis CD148 was shown to be excluded from regions of HEL/BCR. These results are compatible with close-contact formation and occurred within the first 90 seconds of B cells landing. Use of the membrane dye, DiO, confirmed CD148 exclusion zones were not artefacts due to non-apposition of the B cell membrane to the SLB.

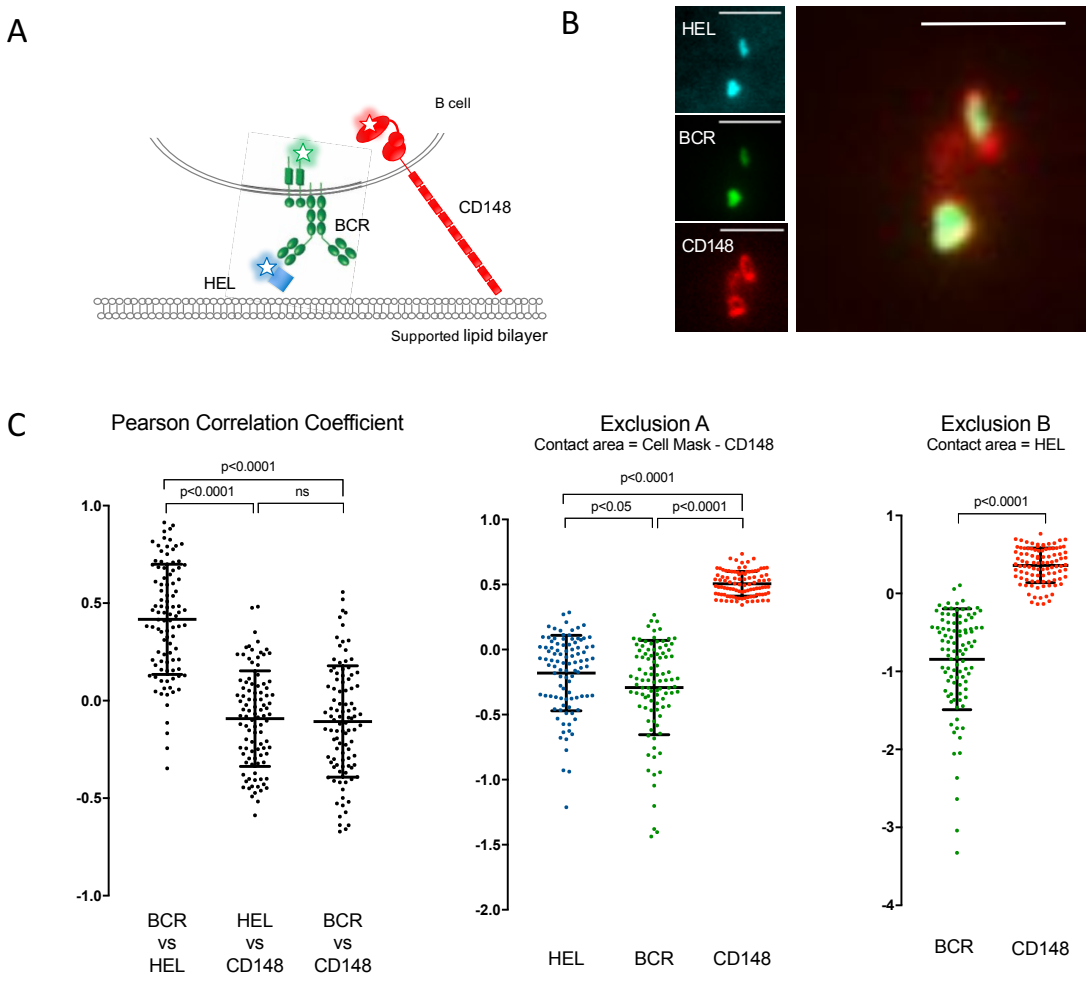

Figure 6.5 Close contacts form from which CD148 is excluded
(A) Schematic representation of experimental setup. Three colour TIRF imaging was undertaken to visualise CD148 (red) and BCR (green) on A20(HyHEL10) B cells as they landed on SLBs labelled with fluorescent HEL (blue). Stars represent fluorophores labelling proteins of interest. (B) Representative example of cells showing the spatial organisation of CD148, BCR and HEL within the first 90 seconds of landing. Scale bars are 5 μm (C) Analysis of association using Pearson Correlation Co-efficient and exclusion analysis in which contact zone is defined by cell mask-CD148 (exclusion analysis A) or HEL (exclusion analysis B). Scatter plots show results from individual cells. Bars are mean ± SD. P-values are derived from Student's t-test.

6.3.1.4 CD45 and CD148 co-segregate at close contacts

The exclusion of CD45 and CD148 at close contacts has thus far been shown separately in different experiments. To determine if the CD45 and CD148 exclusion zones identified were analogous, supporting the proposal that it is just size that's important, the ability of CD45 and CD148 to co-segregate at close contacts was tested. CD45-Snap and CD148-Halo were co-infected into the A20 (HyHEL10) B cell line. CD45 and CD148 were then simultaneously labelled in spectrally distinct colours and placed onto SLBs pre-coated with fluorescently labelled HEL.

Association analysis using the Pearson correlation co-efficient confirmed there was no correlation between HEL and either CD45 or CD148 during ligand engagement, as would be expected for close contact formation. Both CD45 and CD148 were seen to be excluded from contact areas using both exclusion analysis A and B. While CD45 and CD148 were both excluded at the same close contact zones, they were not equally exclude and hence did not co-localise as determined by the Pearson correlation coefficient. The larger phosphatase CD148 was excluded to a greater extent than CD45, supporting the theory that the size of the extracellular phosphatase per se is sufficient to mediate exclusion from close contact zones in a size dependent manner (Figure 6.6).

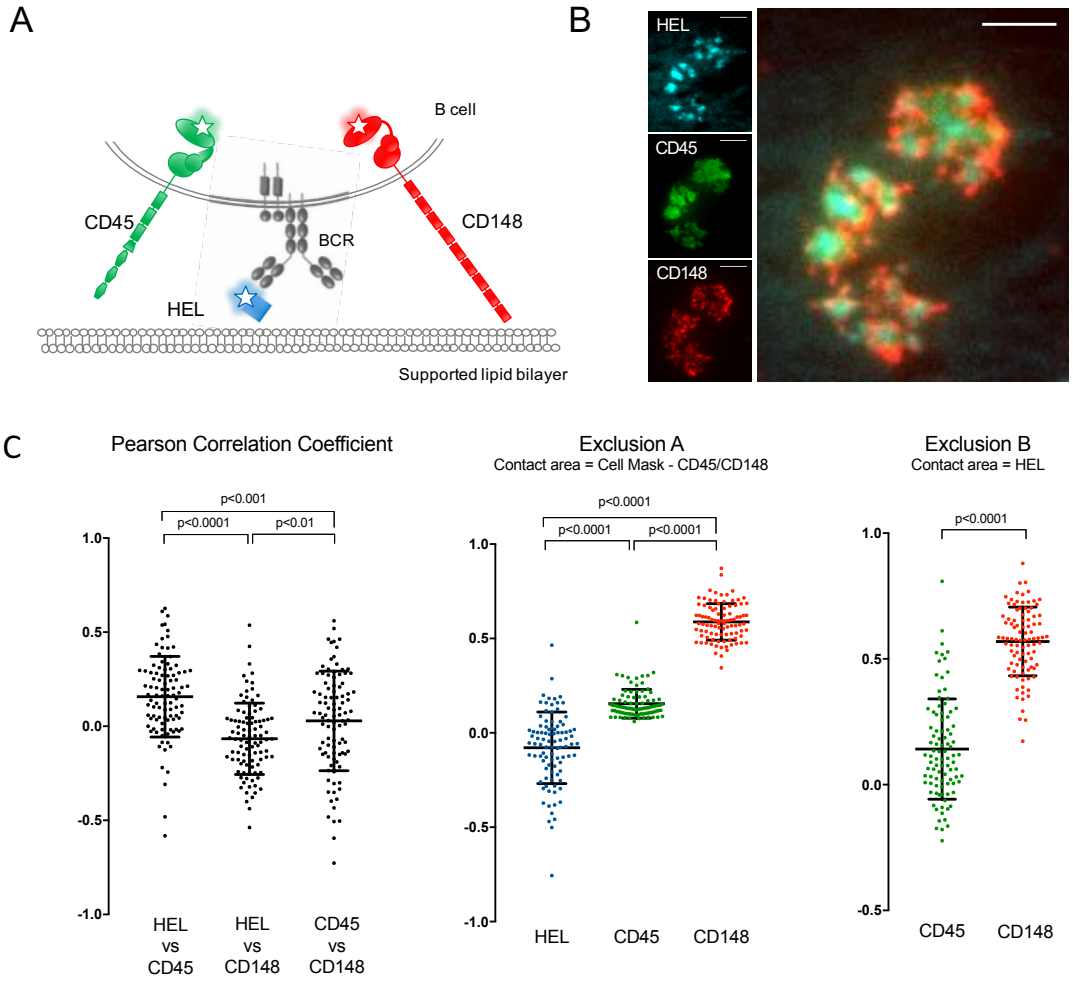

Figure 6.6 CD45 and CD148 co-segregate at close contacts
(A) Schematic representation of experimental setup. Three colour TIRF imaging was undertaken to visualise CD45 (green) and CD148 (red) on A20(HyHEL10) B cells as they landed on SLBs labelled with fluorescent HEL (blue). Stars represent fluorophores labelling proteins of interest. (B) Representative example of cells showing the spatial organisation of CD45, CD148 and HEL within the first 90 seconds of landing. Scale bars are 5 μm (C) Analysis of association using Pearson Correlation Co-efficient and exclusion analysis in which contact zone is defined by cell mask-CD45/CD148 (exclusion analysis A) or HEL (exclusion analysis B). Scatter plots show results from individual cells. Bars are mean ± SD. P-values are derived from Student's t-test.

6.3.2 Triggering is dependent on the size of the antigen:BCR complex

A key prediction of the KS model is that triggering is dependent on the size of the antigen/BCR complex versus the local phosphatases. In order to test this prediction, variant forms of HEL were created with "spacer" domains to increase the height at which HEL is presented above the membrane. These variant forms of HEL were then presented on SLBs to A20 (HyHEL10) B cells and triggering monitored via changes in intracellular Ca^{2+} and close contact formation imaged using three colour TIRF microscopy.

6.3.2.1 Generation and analysis of HEL-fusion proteins with spacer domains

A series of HEL-fusion proteins were produced consisting of a His-tag for purification and insertion into Ni-containing SLBs, a Snap®-tag to enable fluorescence detection and a variably-sized spacer domain (Figure 6.7). Variable lengths of the extracellular domain of CD43 were used for the spacer domain as it is heavily glycosylated and forms mucin-like regions. Steric interactions between carbohydrate and peptide residues within the extracellular domain of CD43 should therefore induce a rigid extended structure that will project the HEL molecule rigidly upwards from its insertion site.

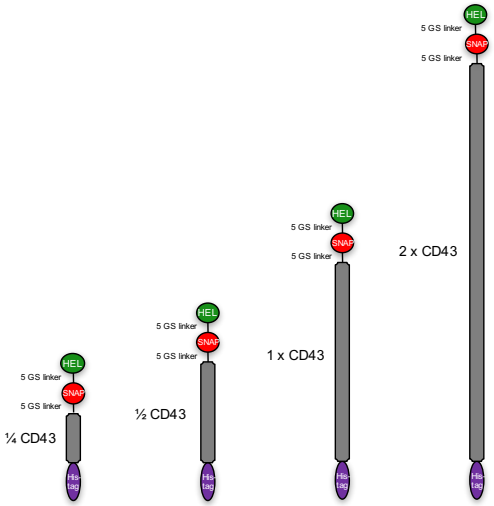

Figure 6.7 HEL-fusion proteins with spacer domains
Schematic representation of HEL-fusion proteins with CD43 spacer domains. HEL (green), Snap®-tag (red) and extracellular CD43 (grey) are separated by flexible linkers composed of a variable number of glycine(G) and serine(S) residues. Each protein contains a double hexa histidine-tag (purple) running directly from the CD43 without a linker.

Proteins were produced using the large-scale lentiviral method, purified by polyhistidine affinity tag and separated by FPLC. All proteins expressed well but with increasing length of CD43 expression levels did decrease. However, in all cases clean monomeric protein could be identified and purified by FPLC.

To establish that the HEL-fusion proteins were correctly folded, immunodepletion of a solution of each protein was undertaken with the HEL-specific antibody HyHEL10 (Figure 6.8). All of the HEL-fusion proteins were almost completely depleted by the conformational sensitive HyHEL10 antibody implying correct folding of the HEL. Furthermore, each HEL-fusion protein had different electrophoretic mobility on SDS-PAGE compatible with their different size and charge.

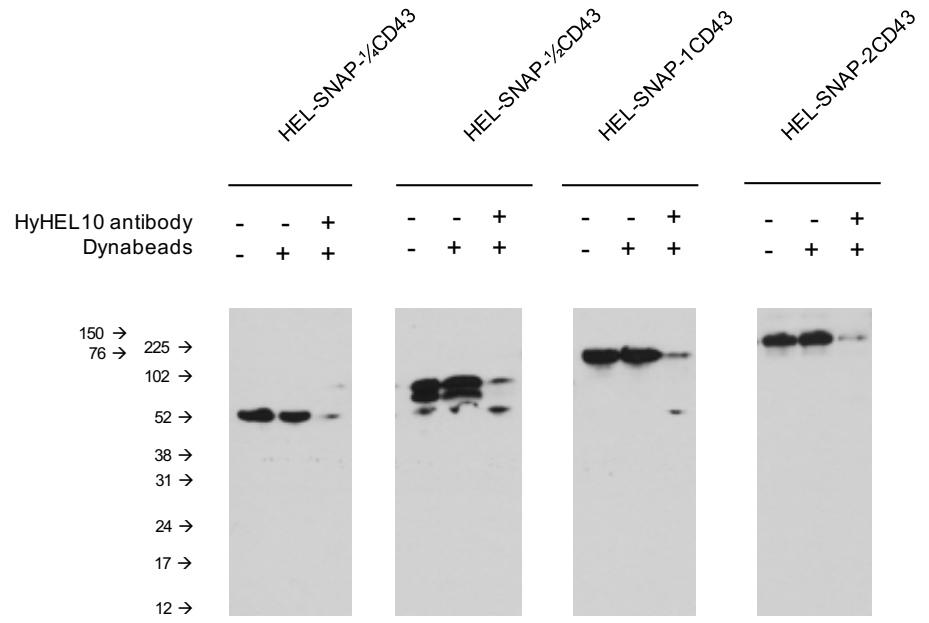

Figure 6.8 Immunodepletion of HEL-fusion proteins with spacer domains by HyHEL10.
A 5mg/l solution of either HEL-Snap-¼CD43, HEL-Snap-½CD43, HEL-Snap-1CD43 and HEL-Snap-2CD43 was incubated alone, with Dynabeads or HyHEL10 bound to Dynabeads. The supernatant was then removed and subject to SDS PAGE and anti-penta-His Western blot analysis.

6.3.2.2 Calcium triggering is dependent on the dimensions of the BCR/ligand complex

To test the hypothesis that BCR triggering is dependent on the dimensions of the BCR/ligand complex, A20 (HyHEL10) B cells were loaded with Flou-4 and dropped onto Ni-containing SLBs pre-coated with HEL-fusion proteins with variable sized spacer domains. Cells were then imaged for 10 minutes to detect calcium signalling. The fraction of cells triggered was comparable for B cells landing on SLBs coated with HEL fusion proteins with no spacer domain, ¼CD43, ½CD43 and 1CD43. However, a significant reduction in triggering was seen when B cells landed on SLBs pre-coated with HEL-SNAP-2CD43. (Figure 6.9). Presuming CD43 projects rigidly upwards from the SLB, this equates to a height of HEL presentation of approximately 90 nm above the surface (2 Å

per residue). This calculation is based on electron microscopy analysis of the glycosylated 224 amino acid extracellular domain of CD43 which forms an extended conformation. Maintenance of the extended conformation is dependent on the O-linked glycosylation sites which should ensure the protein stands vertically upwards when inserted into the SLB [319, 320].

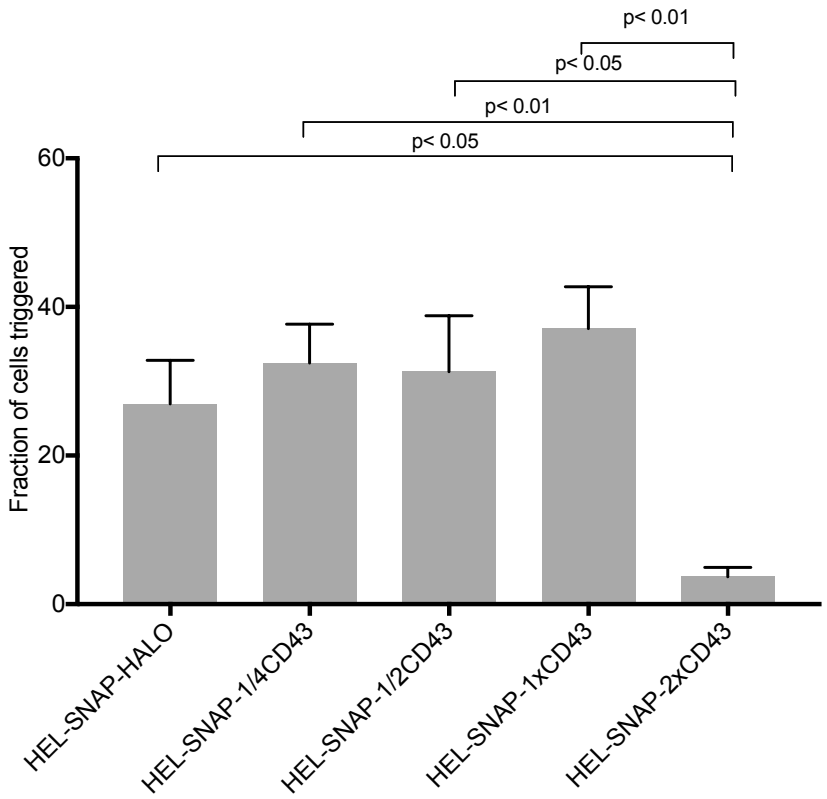

Figure 6.9 Triggering of B cells dependent on the dimensions of the BCR:ligand complex
Calcium responses of A20 (HyHEL10) B cell dropped onto Ni-containing SLBs pre-coated with HEL-fusion proteins with variably sized spacer domains. Values correspond to the fraction of cells exhibiting calcium flux detected by Fluo-4 within 10 min of landing. Bars are mean ± SD. P-values are derived from Student's t-test. All experiments were conducted at 37˚C and 5% CO_2.

6.3.2.3 The dimensions of the BCR/ligand complex affect cell behaviour and phosphatase exclusion

The KS model predicts that the reduction in calcium triggering observed by increasing the BCR/ligand complex size by 90nm would be the result of less effective exclusion of CD45/CD148 from close contacts. To test this prediction, three colour TIRF imaging was undertaken as fluorescently labelled A20 (HyHEL10, Ig-alpha-Snap, CD45/148-Halo) B cells landed on Ni-containing SLBs pre-coated with fluorescently labelled HEL-Snap-2CD43. CD45/CD148, BCR and HEL were fluorescently labelled and the distribution of each was visualised and compared to equivalent experiments conducted on the shortest form of HEL, *i.e.* HALO-SNAP-HEL (N-terminal His-tag) presented close to membrane level.

The majority of B cells dropped onto the longest form of HEL formed close contacts zones akin to those seen previously when cells were allowed to land on the shortest form of HEL. However, a number of cells showed a markedly different behaviour with large projections reaching out across the SLB. This was particularly apparent when imaging CD45. In all experiments, association analysis demonstrated correlation of the fluorescent signal from HEL and BCR implying that receptor/ligand engagement had occurred. However, exclusion of both CD45 and CD148 was still observed on the longest form of HEL (Figure 6.10 and Figure 6.11).

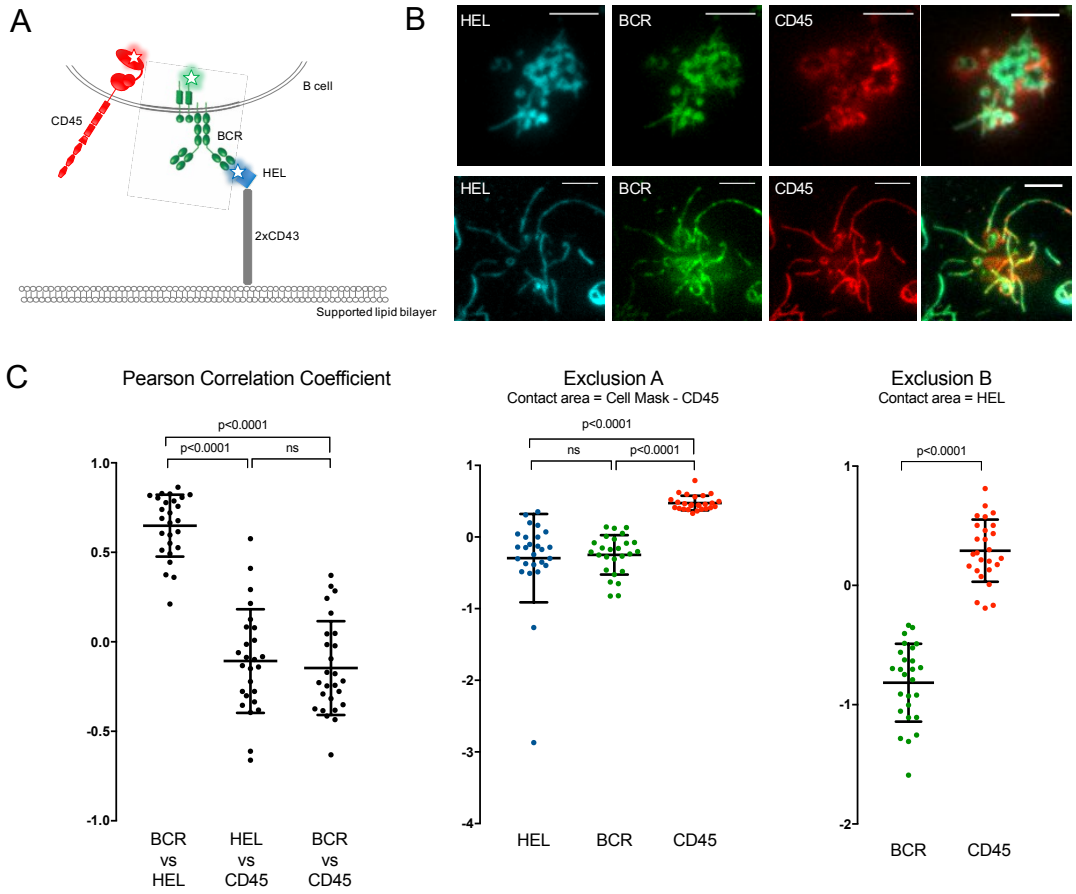

Figure 6.10 CD45 exclusion at close contacts is dependent on the dimensions of the BCR/ligand complex

(A) Schematic representation of experimental setup. Three colour TIRF imaging was undertaken to visualise CD45 (red) and BCR (green) on A20(HyHEL10) B cells as they landed on SLBs pre-coated with fluorescent HEL-Snap-2CD43 (blue). Stars represent fluorophores labelling proteins of interest. (B) Representative example of cells showing the spatial organisation of CD45, HEL and BCR within the first 90 seconds of landing. Scale bars are 5 μm (C) Analysis of association using Pearson Correlation Co-efficient and exclusion analysis in which contact zone is defined by cell mask-CD45 (exclusion analysis A) or HEL (exclusion analysis B). Scatter plots show results from individual cells. Bars are mean ± SD. P-values are derived from Student's t-test.

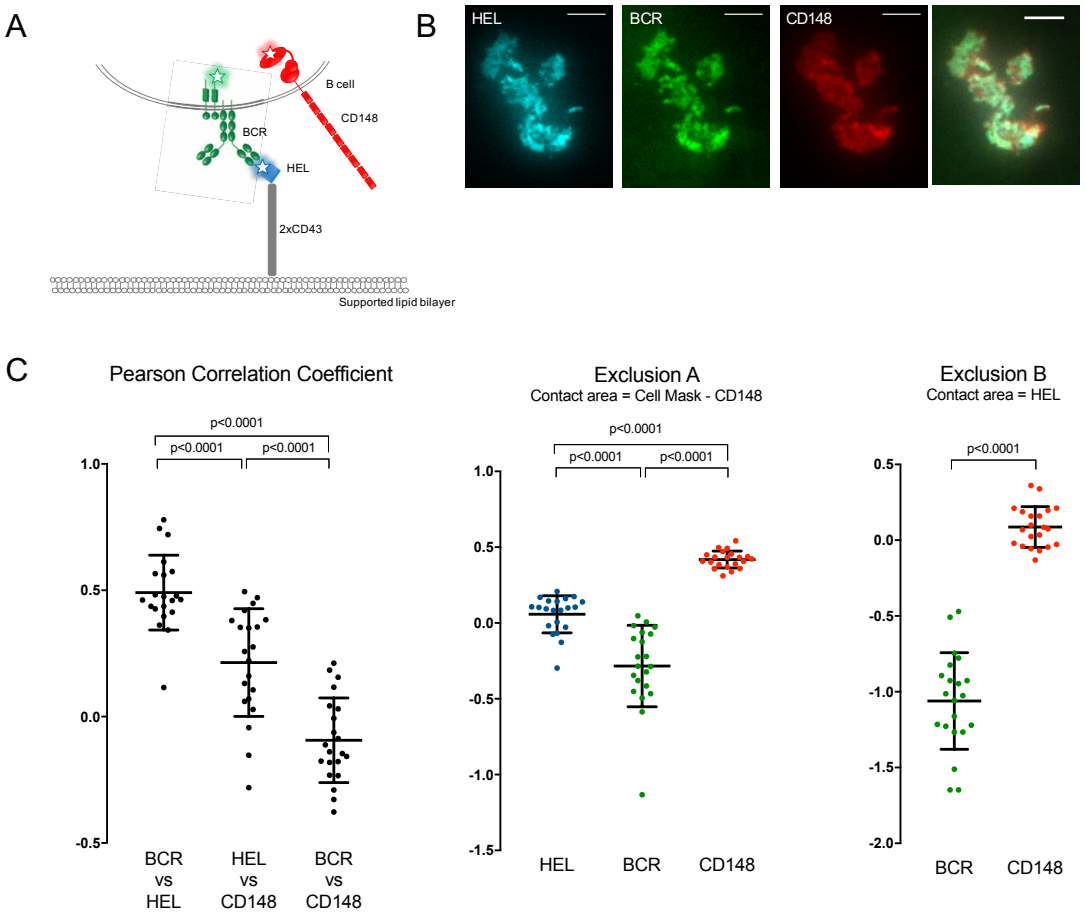

Figure 6.11 CD148 exclusion at close contacts is dependent on the dimensions of the BCR/ligand complex

(A) Schematic representation of experimental setup. Three colour TIRF imaging was undertaken to visualise CD148 (red) and BCR (green) on A20(HyHEL10) B cells as they landed on SLBs pre-coated with fluorescent HEL-Snap-2CD43 (blue). Stars represent fluorophores labelling proteins of interest. (B) Representative example of cells showing the spatial organisation of CD148, HEL and BCR within the first 90 seconds of landing. Scale bars are 5 μm (C) Analysis of association using Pearson Correlation Co-efficient and exclusion analysis in which contact zone is defined by cell mask-CD148 (exclusion analysis A) or HEL (exclusion analysis B). Scatter plots show results from individual cells. Bars are mean ± SD. P-values are derived from Student's t-test.

Results presented in this Chapter have demonstrated exclusion of the surface expressed phosphatases, CD45 and 148, from close contact zones when ligand is presented close to membrane level and also at a height of 2 CD43 extracellular domains above the membrane. However, there was a significant difference in the relative exclusion of both phosphatases dependent on the height of the BCR/ligand complex (Figure 6.12). Increasing the dimension of the BCR/ligand complex to 90 nm was associated with a significant decrease in the exclusion of both CD45 and CD148. The less effective exclusion of CD45 and CD148 observed when cells landed on HEL-Snap-2CD43 was not complete and exclusion zones were still clearly apparent. This relative change is in contrast to the clear-cut calcium results seen when B cells landed on HEL-Snap-Halo. This would appear to imply that only a small change in the ratio of phosphatases within the contact zone is required to have an effect on BCR triggering.

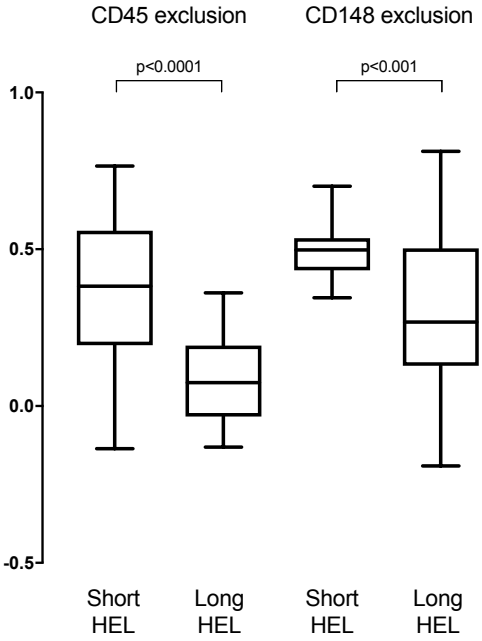

Figure 6.12 CD45 and CD148 exclusion at close contact zones is dependent on the size of the BCR/ligand complex
Whisker plot displaying the exclusion of either CD45 or CD148 from contact zones as A20(HyHEL10) B cells landed on SLBs pre-coated with either short HEL (HALO-SNAP-HEL N-terminal His-tag) or long HEL (HEL-SNAP-2CD43). Exclusion analysis was undertaken in which the contact area was defined by HEL (exclusion analysis B). Bars are mean ± SD. P-values are derived from Student's t-test.

6.3.3 Triggering is dependent on the size of the extracellular domain of surface expressed phosphatases

Another key prediction of the KS model is that triggering is dependent on the size of the extracellular domain of surface expressed phosphatases. In order to test this prediction, full-length or truncated forms of CD45 or CD148 were transfected into A20 (HyHEL10) B cells and dropped onto HEL containing SLBs. B cell triggering was then monitored via changes in intracellular calcium and close contact formation imaged using three colour TIRF microscopy.

6.3.3.1 Expression of full-length and truncated forms of CD45 and CD148

To test whether B cell signalling was dependent on the size of the extracellular domain of surface expressed phosphatases, A20 HyHEL10 B cells were produced expressing additional exogenous CD45 or CD148 in which the extracellular domain was either full-length or truncated. Expression of full-length forms of CD45 and CD148 was achieved as previously described in section 6.3.1.1. To produce truncated forms of CD45 or CD148, constructs were designed expressing the extracellular and transmembrane domains of LAT linked to the intracellular domain of murine CD45. This approach preserves the catalytic activity of CD45 but removes the large extracellular domain. LAT is ideally suited to this approach as it is a transmembrane protein with a small extracellular domain comprised of only four amino acids. A HA-tag was added to the extracellular domain of all constructs to allow assessment of surface expression by flow cytometry, while a Snap®-tag or Halo®-tag was added to the intracellular domain to allow fluorescent labelling for use in TIRF based microscopy experiments (Figure 6.13).

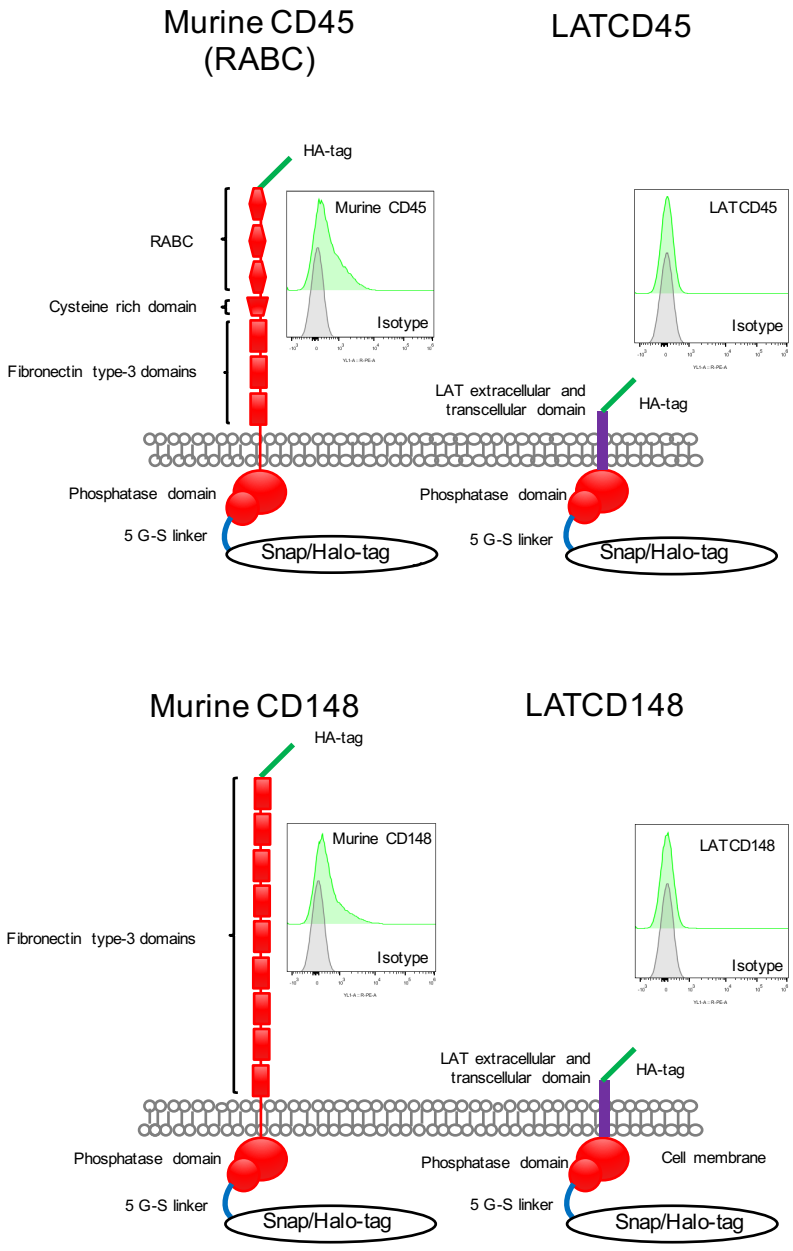

Figure 6.13 Wildtype- and truncated-forms of CD45 and CD148
Schematic representation of wildtype and truncated forms of CD45 (top) and CD148 (bottom). Each construct consists of a HA-tag (green) linked to either the full-length phosphatase sequence (mCD45(RABC) or mCD148) or a truncated form in which the extracellular and transmembrane domains are replaced with those of mouse LAT. Each construct is connected by a flexible linker (consisting of 5 glycine(G) and serine(S) residues; blue) to a Halo®-tag or Snap®-tag (black) to allow fluorescent labelling. Histogram plots are shown displaying the expression levels of HA-mCD45-Halo, HA-LATCD45-Halo, HA-mCD148-Halo and HA-LATCD148-Halo in A20(HyHEL10, Ig-alpha-Snap) B cells. Isotype controls (grey) are shown for comparison.

Constructs were transfected into A20 (HyHEL10) cells using the small-scale lentiviral transfection method and expression levels determined by flow cytometry using an antibody directed against the HA-tag. As previously described, expression levels of both mCD45 and mCD148 were relatively low but a small population of high expressing cells was seen. In contrast, truncated forms of CD45 and CD148 expressed very poorly as determined by flow cytometry (Figure 6.13). No improvement in expression levels was seen with multiple rounds of re-infection. Despite low expression levels as determined by FACS, TIRF imaging of transfected cells labelled with fluorescent Halo®-ligand confirmed cell surface expression of both LATCD45 and LATCD148, albeit at low levels. The expression of LATCD45, as determined by TRIF microscopy, was lower than comparable cells transfected with LATCD148. Of note, production of LATCD148 virus by the 293T packaging cell line was characterised by detachment of cells from the surface of the cell culture flask and minimal change in pH as determined by phenol red.

6.3.3.2 Calcium triggering is dependent on the extracellular domain of CD148

To test the hypothesis that BCR triggering is dependent on the size of the extracellular phosphatase, A20 (HyHEL10) B cells were transfected with LATCD45 or LATCD148, loaded with Fluo-4 and dropped onto Ni-containing SLBs pre-coated with HEL. Cells were then imaged for 10 minutes and the fraction of cells triggered was calculated. To confirm that any effect of the truncated phosphatases was not the result of an increase in the total level of cellular phosphatases, control experiments were undertaken on cells transfected with similar or larger amounts of full-length CD45 or CD148. The fraction of B cells triggering was significantly reduced with truncated CD148 compared to wildtype

CD148; however, no significant difference was seen with truncated CD45 compared to wildtype CD45 (Figure 6.14).

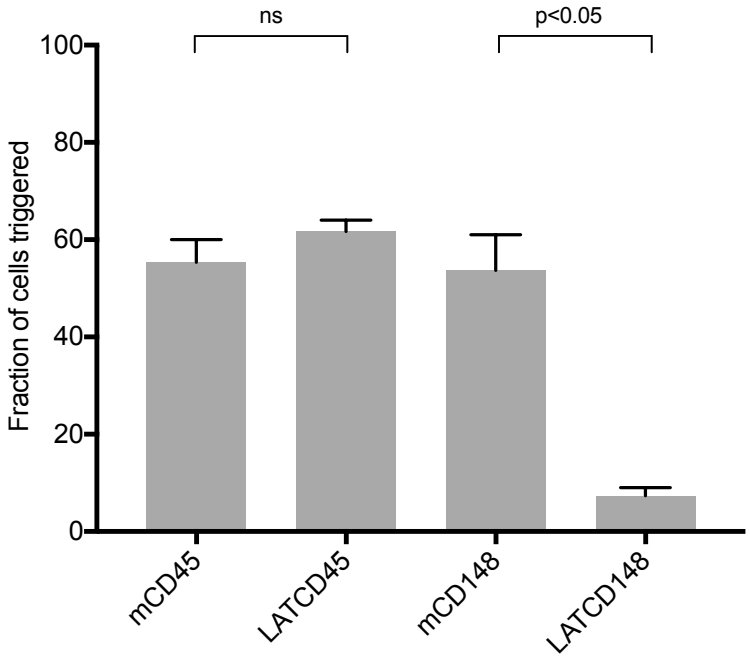

Figure 6.14 Triggering of B cells dependent on the dimensions of the extracellular domain of surface-expressed phosphatases.
Calcium responses of A20 (HyHEL10) B cell transfected with mCD45, LATCD45, mCD148 or LATCD148 dropped onto Ni-containing SLBs pre-coated with Halo-Snap-HEL (N-terminal His-tag). Values correspond to the fraction of cells producing calcium flux detected by Fluo-4 within 10 min of landing. Bars are mean ± SD. P-values are derived from Student's t-test. All experiments were conducted at 37˚C and 5% CO_2.

6.3.3.3 The extracellular domain of CD148 mediates exclusion from close contacts

The KS model predicts that the reduction in calcium triggering seen with LATCD148 compared to wildtype CD148 is the result of less effective exclusion of CD148 from close contacts. To test this prediction, three colour TIRF imaging was undertaken as A20 (HyHEL10) B cells transfected with both LATCD148 and wildtype CD148 settled onto Ni-containing SLBs pre-coated with HEL. LATCD148, wildtype CD148 and HEL were fluorescently labeled and the distribution of each visualised during close contact formation (Figure 6.15).

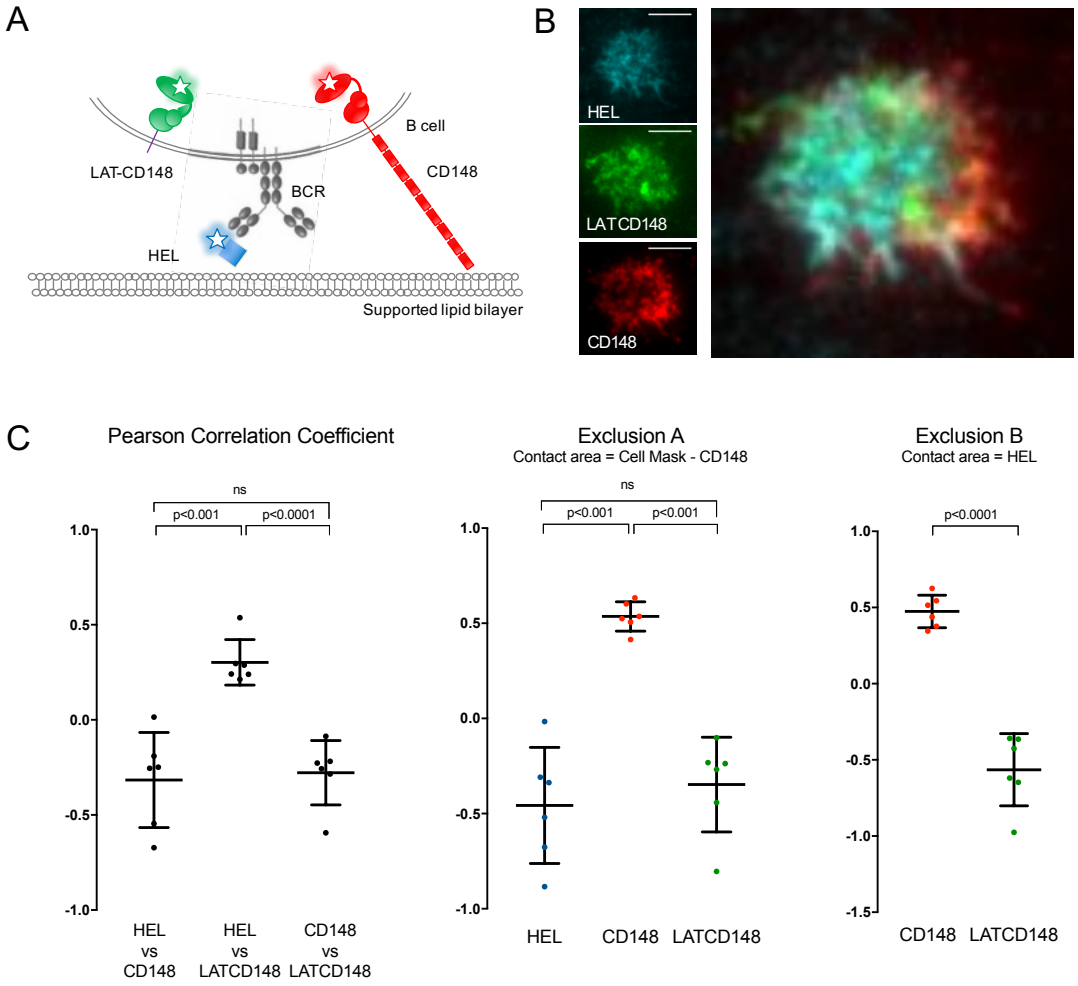

Figure 6.15 Truncated CD148 does not segregation at close contacts
(A) Schematic representation of experimental setup. Three colour TIRF imaging was undertaken to visualise LATCD148 (green) and mCD148 (red) on A20(HyHEL10) B cells as they landed on SLBs labelled with fluorescent HEL (blue). Stars represent fluorophores labelling proteins of interest. (B) Representative example of cells showing the spatial organisation of LATCD148, CD148 and HEL within the first 90 seconds of landing. Scale bars are 5 μm (C) Analysis of association using Pearson Correlation Co-efficient and exclusion analysis in which the contact zone is defined by cell mask-CD148 (exclusion analysis A) or HEL (exclusion analysis B). Scatter plots show results from individual cells. Bars are mean ± SD. P-values are derived from Student's t-test.

Wildtype CD148 was found to segregate from HEL defining close contacts. However, truncated CD148 did not co-segregate with wildtype CD148 but was seen homogenously distributed across the cell membrane including within close contact zones. The ability of LATCD148 to enter close contacts was confirmed by association analysis demonstrating no correlation between truncated and wildtype CD148, but positive correlation between truncated CD148 and HEL (Figure 6.15).

6.3.3.4 The extracellular domain of CD45 mediates exclusion at close contacts

A reduction in calcium triggering was seen in bulk populations of B cells expressing truncated CD148 but not truncated CD45. To test why this was the case, three colour TIRF imaging was undertaken as A20 (HyHEL10) B cells transfected with both LATCD45 and wildtype CD45 were dropped onto Ni-containing SLBs pre-coated with HEL. LATCD45, wildtype CD45 and HEL were fluorescently labelled and the distribution of each visualised (Figure 6.16).

During close contact formation, a similar distribution of truncated CD45 was observed as had previously been seen with experiments conducted using the truncated form of CD148. Wildtype CD45 was shown to segregate from HEL defining close contacts. However, truncated CD45 did not co-segregate with wildtype CD45 but instead was observed homogenously distributed across the cell membrane including within close contact zones in regions of HEL. The ability of LATCD45 to enter close contacts was confirmed by association analysis, which demonstrated no correlation between truncated and wildtype CD45, but a positive association between truncated CD45 and HEL (Figure 6.16).

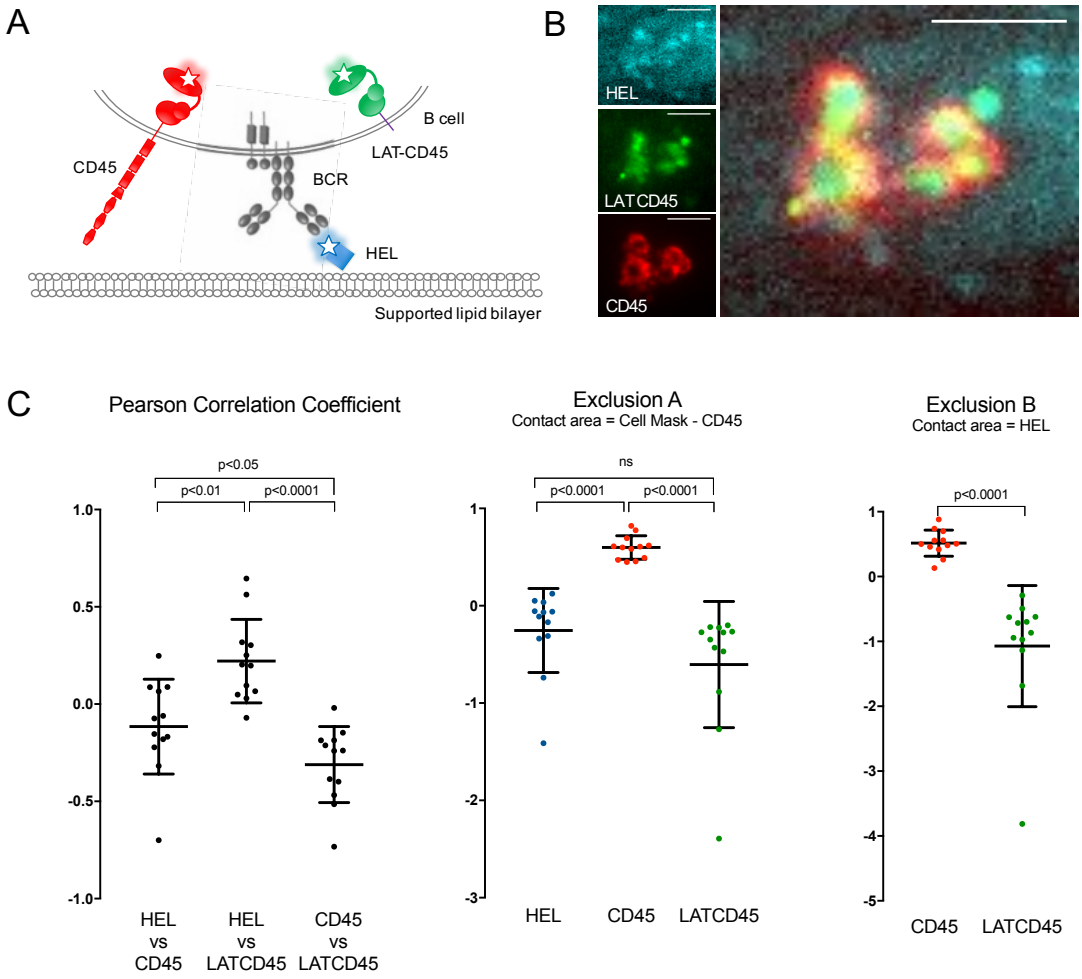

Figure 6.16 Truncated CD45 does not segregation at close contacts
(A) Schematic representation of experimental setup. Three colour TIRF imaging was undertaken to visualise LATCD45 (green) and mCD45 (red) on A20(HyHEL10) B cells as they landed on SLBs labelled with fluorescent HEL (blue). Stars represent fluorophores labelling proteins of interest. (B) Representative example of cells showing the spatial organisation of LATCD45, CD45 and HEL within the first 90 seconds of landing. Scale bars are 5 μm (C) Analysis of association using Pearson Correlation Co-efficient and exclusion analysis in which contact zone is defined by cell mask-CD45 (exclusion analysis A) or HEL (exclusion analysis B). Scatter plots show results from individual cells. Bars are mean ± SD. P-values are derived from Student's t-test.

6.3.3.5 Truncated CD45 has an effect on cell survival and adherence

TIRF imaging demonstrated that truncating the extracellular domain of CD45 was sufficient to alter its distribution, allowing it to enter close-contacts during ligand engagement at a surface. However, these results appear at odds with the calcium triggering data if it is assumed that phosphatase segregation is linked to signalling.

One potential explanation for these results lies in the observation that expression levels of LATCD45, as determined by TRIF microscopy, were lower than comparable cells transfected with LATCD148, or that only very few cells expressed LATCD45 at all. Therefore, failure to achieve sufficiently high expression levels of LATCD45 in a large enough fraction of cells is one explanation for why no effect on calcium triggering was identified. To test this prediction, CD45 expression levels were checked by TIRF following transfection. Low but positive levels were seen on day 4, however, by day 7 levels were almost completely zero. Therefore, any calcium triggering experiments conducted at this time were essentially testing wildtype cells. Importantly, those cells seen to express LATCD45 on day 4 appeared unhealthy, and, by day 7 there was a large amount of fluorescent debris suggesting LATCD45 is potentially toxic to B cells.

In order to overcome this problem, calcium triggering was attempted on day 4 followed by subgroup analysis of the cells that had triggered/not triggered, based on LATCD45 expression. However, the results of these experiments could not be interpreted because a failure in triggering could have been due either to LATCD45 expression or a failure to recover from recent infection.

6.4 Discussion

6.4.1 Close-contacts form on B cell receptor triggering

A key prediction of the KS model is that close-contacts form on BCR triggering. Three colour TIRF microscopy of HyHEL10 B cells landing on SLBs coated with HEL showed clear evidence of close contact formation. The BCR was seen to co-localise with its ligand HEL and exclude the large phosphatases CD45 and CD148. Both phosphatases were observed to co-segregate at the same close contacts. Significantly, at the same close contacts the larger phosphatase, CD148, was excluded to a greater extent than the smaller phosphatase, CD45, implying segregation was size dependent. These close-contact zones were seen within the first 90 seconds as cells landed on SLBs compatible with the timing of calcium triggering. The early exclusion of large phosphatases observed here is compatible with that seen previously in B cells [142] and also with close contact formation described in T cells [238, 240, 321]. In future experiments, it would be important to determine whether close-contract formation is a passive process or the result of signalling/actin related processes. To test this, the behaviour of CD45 and CD148 could be observed in giant plasma membrane vesicles as they interact with HEL containing SLBs. Giant plasma vesicles contain all membrane components but are devoid of cytoskeletal structure and normal cellular energy homeostasis thereby enabling us to ascertain if there processes are critical for close-contact formation and BCR triggering [322].

6.4.2 BCR triggering is dependent on the size of the BCR/ligand complex

A second prediction of the KS model is that triggering is dependent on the dimensions of the BCR/ligand complex. To test this, a calcium-based microscopy assay was used to monitor triggering as A20(HyHEL10) B cells landed on SLBs functionalised with HEL projected variable heights above the bilayer with the use of CD43 spacer domains. No difference in calcium signalling was seen when HEL was suspended less then 2CD43 extracellular domains above the bilayer. However, when HEL was suspended at 2CD43 extracellular domains above the membrane, a significant reduction in calcium signalling was observed. This gap size corresponds to 90nm, assuming CD43 extends rigidly upwards from its insertion point. This gap size is theoretically large enough to allow entry of the large phosphatases CD45 and CD148 into close contacts allowing the calcium signal to be quenched. This was confirmed using three colour TIRF microscopy of A20 (HyHEL10) B cells landing on SLBs coated with HEL-Snap-2CD43. A significant reduction in the relative exclusion of both CD45 and CD148 from close contacts was seen with HEL present 90 nm above the membrane compared to when the same cells landed on ligand presented at close to membrane level. However, it is noteworthy that close contact zones still formed when the BCR/ligand complex size was increased. This would suggest that only a small change in the ratio of phosphatases to kinases within the contact zone is required to have an effect on BCR triggering. These results are comparable to experiments conducted on T cells in which TCR triggering was shown to be dependent on the size of the MHC:peptide complex [245, 246].

The dependence of BCR triggering on the size of the BCR/ligand complex is significant because it not only supports the KS model but further argues against the conformation induced oligomerisation model. Any conformational change should be dependent only on antigen binding and not on the height at which ligand is encountered. The results presented in this Chapter would therefore argue against the conformation-induced oligomerisation model as a mechanism of BCR triggering.

6.4.3 BCR triggering is dependent on the extracellular domain of CD148

A third prediction of the KS model is that triggering is dependent on the size of the extracellular domain of surface expressed phosphatases. Truncation of the extracellular domain of CD148 was shown to significantly decrease calcium triggering. Three colour TIRF imaging showed that the truncated form of CD148 was able to enter close contract zones providing an explanation for why calcium signalling was quenched. This effect was not the result of a net increase in cellular phosphatases as no effect was seen when cells were transfected with wildtype CD148 at higher levels. These results are analogous to experiments conducted on T cells in which truncating the extracellular domain of CD45 and CD148 quenched signalling by allowing these molecules to enter close contact zones [240, 247, 248]. Experiments in this chapter also demonstrated that truncating the extracellular domain of CD148 in B cells had wider effects on cell processes such as cell adherence, as shown by the effect on the T293 packaging cell line.

Truncation of the extracellular domain of CD45 was shown to facilitate its relocation, enabling it to enter close contact zones, for rare cells at least. However, in contrast to

CD148, no effect on calcium triggering was seen. This was potentially due to the toxic effect of truncated CD45 on transfected cells since they failed to survive long enough to be tested. This is significant as it suggests that truncated CD45 has a significant adverse effect on cells. In support of this, both truncated forms of CD45 and CD148 reached significantly lower expression levels than wildtype constructs suggesting the relocation of phosphatases per se is sufficient to effect cellular function. To test the effect of truncating the extracellular domain of CD45 in more detail a reliable method is required to achieve high levels of expression of truncated phosphatases in cells. To achieve this, an alternative cell line could be tested which has a higher transfection efficiency. An alternative method is to cleave the extracellular phosphatase by the introduction of a cleavage site or the floxing of the exons encoding the extracellular region to generate a tissue-specific knock out in vivo.

Chapter 7

General Discussion

The BCR consists of a membrane-spanning, signalling form of immunoglobulin that does not possess any inherent enzymatic activity of the type that characterises, *e.g.* growth factor receptors. It is, however, non-covalently linked to a Ig-α/β heterodimer that contains ITAM motifs, which transduce downstream signalling when they are phosphorylated. Antigen binding to the BCR initiates ITAM phosphorylation and activates a series of signalling pathways which lead to assembly of the signalosome, re-organisation of the cytoskeleton, internalisation of the BCR and presentation of antigen to T cells [112]. While much is known about the downstream signalling pathways emanating from the BCR, what remains unresolved is how antigen binding to the extracellular domain would result in phosphorylation of the ITAMs of the Ig-α/β heterodimer, *i.e.* BCR triggering. A number of models of BCR triggering have been proposed, the dominant ones being the cross-linking model [217-221], the conformation-induced oligomerisation model [229] and the dissociation activation model [232]. The disparity between models highlights the uncertainty that remains regarding the exact mechanism of BCR triggering. This thesis has tested these models experimentally against their key predictions to gain a more detailed understanding of the exact mechanism of triggering of the BCR.

7.1 Results from this thesis

7.1.1 The cross-linking model explains triggering to soluble multivalent ligand

The cross-linking model is the original model of BCR triggering. It proposes that in the resting, non-antigen bound state the BCR is a bivalent complex (a single BCR with two antigen binding sites). Signalling occurs when two or more BCRs are brought into close proximity *i.e.* cross-linked by a multivalent ligand [215]. In Chapter 4, the principles of the cross-linking model were tested by assessing the ability of monomeric and tetrameric HEL to activate HEL specific B cells not only in solution, but also at a surface. It was shown that soluble multivalent ligands were indeed able to trigger B cells in solution. Moreover, soluble monomeric ligand was unable to induce calcium triggering at any concentration. These findings are consistent with those of other groups who have used different pairs of monomeric and multimeric ligands [222-224]. The requirement for soluble ligand to be at least divalent is consistent with the cross-linking model. Naturally occurring multivalent ligands include encapsulated bacteria which have a highly repetitive surface structure. These ligands activate B cells in a T-cell independent manner [19]. Cross-linking of BCRs therefore provides a mechanism for the rapid activation of B cells in response to highly virulent polyvalent pathogens. Significantly, the threshold of BCR affinity for antigen required to trigger B cells is higher for soluble antigen than surface bound ligand [214]. This suggests that cross-linking may be reserved as a mechanism allowing responses to the most harmful pathogens to occur very quickly, without the need for T cell-B cell interaction.

The crosslinking mechanism can undoubtedly activate B cells. However, responses to soluble multivalent ligand likely encompass only a small minority of immune responses. The majority of ligands are probably not multivalent but monomeric. Furthermore, it is now clear that the presentation of antigen to B cells is predominantly cell mediated, by macrophages [201-205], dendritic cells [206, 207] and follicular dendritic cells [208-210]

In Chapter 4, it was shown that monomeric ligand is able to activate B cells when presented at a surface. Therefore, cross-linking is not the only mechanism of BCR triggering and an alternative theory must be considered to explain the dominant form of BCR triggering that occurs in response to cell-presented antigens. In view of this, the conformation-induced oligomerisation model and the dissociation activation model were tested by first of all establishing the stoichiometry of the BCR in the resting state.

7.1.2 The BCR is monomeric on the surface of resting B cells arguing against the dissociation activation model of B cell receptor triggering

The conformation-induced oligomerisation model proposes that in the resting, non-antigen bound state the BCR is a bivalent complex. Antigen binding to the BCR induces a conformational change, exposing a previously hidden Cμ4 clustering domain. This clustering interface promotes receptor oligomerisation and opening of the cytoplasmic domain for initiation of downstream signalling [229]. On the other hand, the dissociation activation model proposes that in the resting, non-antigen bound state the BCR is an oligomer, an arrangement that is auto-inhibitory. Antigen binding promotes dissociation

of BCR oligomers and exposure of the previously hidden intracellular ITAM to enable downstream signalling. To test which, if any, of these mutually exclusive models could potentially explain BCR triggering the stoichiometry of the BCR was established in the resting state.

In Chapter 5, multi-colour fluorescence single-molecule imaging revealed that the BCR is predominantly monomeric on the surface of resting cells. Results from two colour co-incidence detection showed a level of co-incidence close to that predicted for a bivalent complex. This level of colour co-incidence was comparable to soluble monomeric HyHEL10 antibody and the known dimeric receptor CD28. The concept of a monomeric BCR was further supported by single-particle tracking analysis suggesting that the BCR diffuses at a rate (0.07 μm/s) comparable to that of other apparently freely-diffusing surface proteins, implying that it is unclustered. The results outlined in Chapter 5 demonstrating the BCR is monomeric in the resting state are consistent with previous studies using FRET [132] and single particle tracking of individual BCRs labelled with fluorescent Fabs [230]. The concept of a monomeric BCR is, however, controversial. Experimental data has previously been presented which claim that the BCR is pre-clustered in the resting state. These results arose out of a series of biochemical studies. Under minimal detergent lysis conditions the BCR was seen to run as a large macromolecule on blue native PAGE [233], however, solubilisation of cell membranes is often dependent on the detergents used. Results arising from quantitative bifluorescent complimentary assays [232] and high resolution proximity ligation assay [234] supported the concept of a pre-clustered BCR but such techniques can potentially stabilise random collisions in addition to true associations.

More recent evidence for a pre-clustered BCR has come from dSTORM [236] experiments in which B cells were placed on anti-MHC class II cover slips and left for up to 10 minutes prior to imaging. In Chapter 4, the choice of surface for triggering experiments was shown to be critical to experiments undertaken on lymphocytes. Both PLL and glass were shown to be activating surfaces which induce bona-fide BCR signalling. In the case of PLL, it was shown that this coating induces triggering at comparable levels to actual ligands or BCR crosslinking. Super-resolution imaging experiments conducted on PLL have suggested receptors and signalling proteins cluster by default on the surface of resting cells [299-303]. The results obtained on PLL are analogous to those observed for B cells landing on anti-MHC class II coated cover slips. It is therefore possible that the results observed using dSTORM [236] also represent the activated, rather than resting state of the BCR. In this particular case, anti-MHC class II antibodies used to immobilise the cells for imaging might have induced activation by potentially creating close contacts that very effectively exclude phosphatases. This interpretation may explain why only relatively subtle changes were observed upon subsequent B cell activation in these experiments, *i.e.* because the cells had already been activated by the surface [236].

A functionally monomeric BCR imposes important constraints on potential theories of receptor triggering. The results presented in Chapter 5 thus argue against the dissociation activation model but are, in principle, consistent with the conformation-induced oligomerisation model as a mechanism of BCR triggering.

7.1.3 BCR triggering is not dependent on conformational change

Of the three previously proposed, the model of BCR triggering favoured by the stoichiometric analysis is the conformation-induced oligomerisation model. But in Chapter 4, soluble monomeric ligands were shown to be incapable of triggering the BCR, which would appear to be incompatible with a conformation-induced triggering mechanism, since such changes could be expected to be induced by the soluble ligand, as in the case G protein-coupled receptors. However, the conformation-induced oligomerisation model allows for this by suggesting that the ligand must be bound to a surface such that on ligand/receptor binding a shearing force is generated which induces the conformational change. This would account for the surface dependence of BCR triggering.

In Chapter 6, the dependence of BCR triggering on the size of the ligand was tested. It was shown that when HEL is suspended greater than ~90 nm above the bilayer there is a significant decrease in calcium triggering. This is important as it argues against the conformation-induced oligomerisation model. Any conformational change should be dependent only on antigen binding and not on the height at which ligand is encountered. Furthermore, the extended ligand was always membrane bound and therefore should have been capable of inducing a shearing force as required by the conformation-induced oligomerisation model. In view of this, BCR triggering seems unlikely to be dependent on conformational change. A new model of BCR triggering therefore needs to be considered.

7.1.4 BCR triggering is compatible with key predictions of the kinetic-segregation model

The KS model is an alternative explanation for receptor triggering which fits with the experimental data in that the receptor is a monomer in the resting state. This model was originally proposed in the context of TCR triggering [238]. It proposes that in the resting, non-antigen bound state the receptor is free to diffuse through the membrane interacting with kinases and phosphatases but generating no net signal. Antigen binding traps the BCR within the close contact zone, from which bulky phosphatases are excluded but smaller kinases continue to diffuse freely. The kinase/phosphatase balance is switched in favour of phosphorylation in the close contact zones and signalling ensues. Ligand discrimination is based on the half-life of receptor/antigen interactions and the time spent within close contacts. [238]. In Chapter 6, three key requirements of the KS model were tested in B cells.

Firstly, it was shown that close contacts form on BCR triggering from which the large phosphatases CD45 and CD148 are excluded. These close contact zones formed within the first 90 seconds of cells landing, consistent with the timing of calcium triggering. The early exclusion of large phosphatases seen here is compatible with that seen previously in B cells [142], and also with close contact formation described in T cells [240]. Significantly, at the same close contacts the larger phosphatase, CD148, was excluded to a greater extent than the smaller phosphatase, CD45, implying segregation was wholly size dependent.

Secondly, BCR triggering was shown to be dependent on the size of the BCR/ligand complex. Increasing the height at which the HEL was presented to ~90nm above the

bilayer led to a significant decrease in calcium signalling. This correlated with less effective exclusion of both CD45 and CD148 from close contact zones, compared to when HEL was presented at close-to-membrane level. The changes in CD45 and CD148 exclusion, although significant, were subtle in comparison to the dramatic changes seen in terms of calcium signalling, suggesting that only a small change in the kinase:phosphatase ratio is required to effect triggering.

Thirdly, BCR triggering was shown to be dependent on the size of the extracellular domain of CD148, and this effect correlated with truncated CD148 being able to enter close contract zones. Truncation of the extracellular domain of CD45 was also shown to facilitate its relocation into close contact zones, however, in contrast to CD148 no effect on calcium triggering was seen. This was potentially due to the toxic effect of truncated CD45 on transfected cells since they failed to survive long enough to be tested. Parenthetically, both truncated phosphatases were shown to have effects on cellular survival and adherence, suggesting that relocation of phosphatases, per se, has implications for cellular growth and/or behaviour.

The results presented in Chapter 6 thus provide support for the KS model, for B cells responding to ligand presented at a surface. However, the KS models fails to explain the triggering of B cells to multivalent ligand in solution because there is no opposing surface to create a close contact and induce phosphatase exclusion. The cross-linking model is therefore the better explanation for triggering by soluble antigens.

7.1.5 Model of BCR triggering

A model of BCR triggering is proposed in which (1) the majority of antigens are encountered in a membrane bound form and trigger by a KS based approach, and (2) a subset of antigens, that are multivalent, trigger by direct cross-linking of BCRs.

The existence of two models to explain BCR triggering is not necessarily indicative of two separate underlying mechanisms. The means by which triggering occurs in both scenarios can be explained by disrupting the balance of kinases and phosphatases. In the cross-linking model, this occurs by a net increase in kinase activity locally induced by aggregation, since a subset of BCRs will likely have associated kinase due to tonic signalling; whereas in the KS model this occurs by a net decrease in phosphatases induced by close-contact formation. Regardless of mechanism, both result in a net increase in the ratio of kinases to phosphatases leading to BCR triggering. Two means of inducing triggering adds flexibility to the system, perhaps enabling B cells to respond appropriately to different biological threats, or to different modes of their presentation. Crosslinking provides a means of responding to soluble multivalent ligands such as non-encapsulated bacteria. These responses are quick and occur in a T-cell independent manner. Triggering by close contact formation and phosphatase exclusion provides a means of responding to ligands that are encountered at a surface. The immune responses to these ligands might be slower and more dependent on T cell help.

The effectiveness of both models of triggering could be different. It is possible that the effect of crosslinking is inferior to segregation at disrupting the kinase-segregation ratio. This would explain the higher threshold required to trigger BCR by multivalent ligand

presented in solution compared to monomeric ligand presented at a surface [213]. This would fit biologically with a requirement that cross-linking is reserved for responding to ligand without the requirement for T cell help and therefore a more stringent threshold for activation is required. In the case of membrane bound ligand, the threshold is lower because there is efficient presentation of ligand to T cells to ensure good immune surveillance, and full activation relies on T cell help.

Any proposed mechanism of BCR triggering needs to explain signalling in the context of B cell development. Central B cell development occurs in a series of defined stages. Progress through these central development checkpoints is dependent on the expression of a pre-BCR or BCR on the cell surface and induction of tonic signals. The KS based model provides a means of tonic signalling through ligand independent triggering, by inducing changes in the kinase/phosphatase ratio at close-contacts. This is an important prediction because all other theories of signalling require ligand to alter the state of the receptor, *e.g.* through conformational changes or oligomerization.

Any proposed mechanism of BCR triggering also needs to explain signalling in the context of different developmental stages of B cells. Immature B cells constantly encounter potential self-ligands during development, the majority of which will be surface bound. High affinity interactions with membrane-bound or multivalent "self" have been shown to lead to apoptosis and clonal deletion [57, 58]. This is proposed here to occur by either cross-linking or KS based signalling, or both. Mature circulating B cells would therefore be tolerant to self and any membrane bound ligand encountered would be non-self. The model proposed therefore provides a mechanism of self/non-self-discrimination.

B cells are a heterogeneous population of cells which can be divided not only by their developmental and maturational stage but also their subtype. B cell signalling is constantly revised throughout their development, and the machinery of B cell signalling varies between different B cell subsets and in health and disease [323]. The mechanism by which this occurs is potentially explained by the KS model given the differences in the relative expression levels of surface Ig, CD45 and CD148. For example, anergic B cells express low levels of sIgM [62, 87]. On antigen binding only low levels of Src-family kinases would be recruited resulting in a high threshold for activation. However, given sufficient stimulation enough kinases could be recruited to enable activation to occur. It is also noteworthy that different B cell subsets express different isotypes of the BCR which differ in their extracellular size therefore potentially affecting triggering thresholds via changes in gap size. For example, B1 cells express IgM which has four extracellular immunoglobulin constant regions, resulting in a large gap size. Compatible with this increased BCR size, B1 cells express high levels of the very largest phosphatase, CD148, which could potentially counteract the effects of an increased gap size. These examples provide potential mechanisms to explain the relative differences in signalling between, and expression profiles of, different subtypes and maturational stages.

The mature B cell immune response to foreign antigen is thought to be predominantly focused on membrane bound antigen, displayed via complement or immunoglobulin Fc receptors [212]. The predominance of surface based strategies for antigen presentation fits with the requirement for an opposing surface as proposed by the KS based mechanism of BCR triggering. However, the heterogeneity of antigens and the variety of mechanisms of

presentation would appear to argue against a strictly size dependent triggering mechanism, or for variation in the requirement for signaling *per se* in the context of antigen presentation. This can be appreciated by considering the size of ligand complexes formed by immunoglobulin Fc receptors and complement receptors.

The structure of IgE Fc bound to its Fc receptor is shown in Figure 7.1a. The type of complex that would allow the most efficient aggregation is one in which the FcR and antibody are both upright. However, the FcR is not upright but bent over, and the antibody is not extended but bent back on itself. Furthermore, the FcR doesn't bind at the base of the Fc but at the top. The complex therefore appears to be deliberately compact, a conformation that provides the most effective exclusion of phosphatases [324]. In comparison, complement receptors 1 and 2 have large extracellular domains (Figure 7.1b) [325]. Complement receptors are expressed at high levels on follicular dendritic cells and therefore ligands would be predicted to be presented to B cells in a manner that would not exclude large phosphatases. This would appear to argue against T-cell dependent antigens relying on KS based triggering alone and raises the question of when triggering is important, or even necessary. In the context of the germinal centre, complement receptors may provide a means of antigen presentation, thereby allowing affinity maturation to occur, but without the requirement for BCR triggering and activation. To elucidate this in more detail will require definitive molecular and structural studies of the mechanisms of antigen presentation to B cells. What has been demonstrated here is that B cells are configured for KS based triggering but it remains to be elucidated when and where this type of triggering is required.

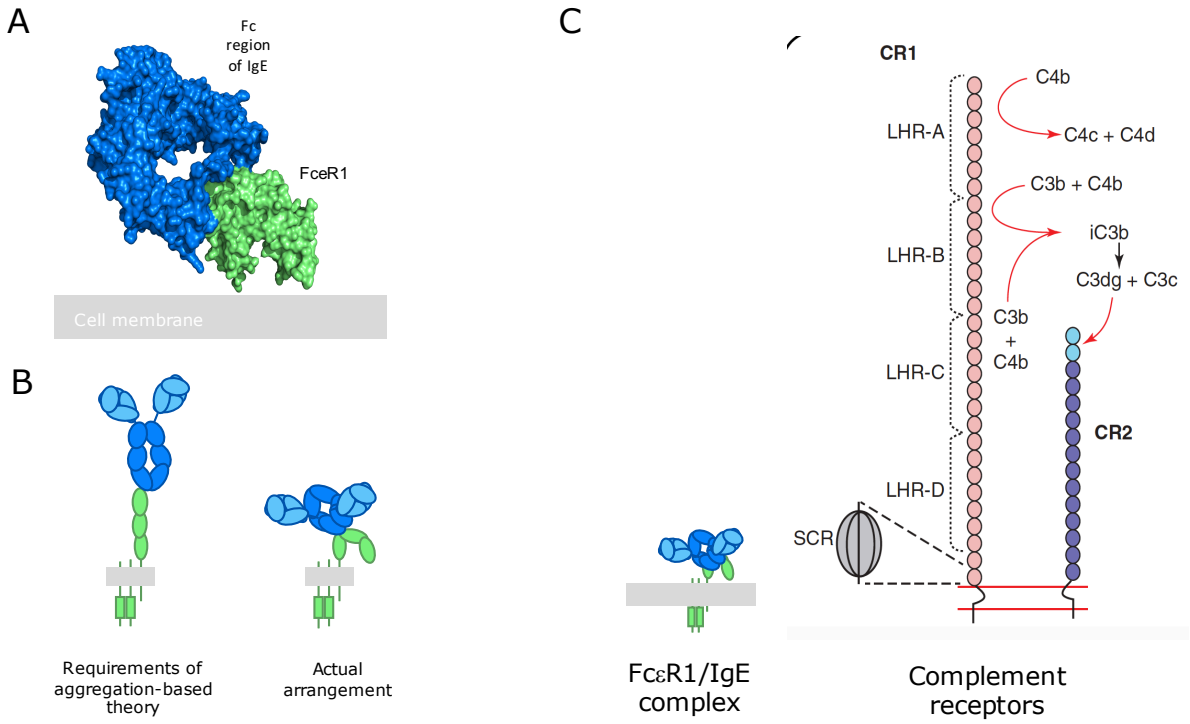

Figure 7.1 Size of the ligand-complexes formed by the FcR and complement receptors
(A) Space filled diagram showing the structure of IgE Fc (blue) bound to its Fc receptor (green). (B) Schematic representation of binding of IgE (blue) to Fc receptor (green). Left is arrangement predicted by aggregation-based theory and right the actual arrangement. (C) Schematic representation of the relative sizes of FcR and complement receptors. Adapted from [326].

The results presented in this thesis add to a body of evidence that supports kinase/phosphatase segregation as a general mechanism of triggering of non-catalytic tyrosine-phosphorylated receptors. This has been most widely studied for the TCR [240] [238], but C-type lectins, CD28, NK receptors and FcRs have also been shown to form close contacts and to exclude phosphatase in a size-dependent manner. Similar to the BCR, the FcR has also been shown to trigger additionally by receptor aggregation broadening the array of ligands detected. The results presented in this thesis for the BCR are therefore compatible with, and extend data obtained for the family of immune recognition receptors generally.

7.2 Future Work

7.2.1 Additional experiments arising from this thesis

The work presented in this thesis has provided preliminary evidence that the principles of the KS model apply to the triggering of the BCR to membrane bound ligand. However, further work is required to corroborate these findings. Some of the extra experiments have been highlighted in individual chapters. Significantly, it is important to establish the effect of truncating the extracellular domain of CD45 on BCR triggering. In Chapter 6, it was shown that truncating the extracellular domain of CD45 was sufficient to facilitate its relocation into close contact zones, for a few cells that could be studied because they expressed the truncated protein, however in contrast to truncated CD148 no effect on calcium triggering was seen in the bulk population. This was likely due to insufficient levels of truncated CD45 in enough cells to see any global effect on calcium triggering. To overcome this, alternative cell lines will be tested which have a higher transfection efficiency. If unsuccessful, cleavage of the extracellular phosphatase by the introduction of either a cleavage site or the floxing of the extracellular allele could be undertaken to generate a tissue specific knock out *in vivo*.

To complement the work in Chapter 6, it is also planned to test a further prediction of the KS model. The KS model predicts that triggering can occur in the absence of ligand, which is referred to as ligand independent triggering. This is proposed to occur at artificial close contacts that induce kinase-phosphatase segregation on a large enough scale to not require ligand-based receptor retention in the contact. To test this, contacts of defined separation will be created between B cells and model surfaces using the rCD2-rCD48 interaction

[240], followed by assessment of calcium triggering and imaging of close contacts using TIRF. B cells will be transfected with a high affinity (T92A mutant) signalling deficient form of rCD48. A range of heights of CD2 will then be created to check not only whether ligand independent triggering occurs, but if it does, that it is dependent on the dimensions of the gap size as predicted by the KS model. These experiments are significant because if ligand independent triggering does occur then it not only supports the KS model, but also provides further evidence undermining other triggering mechanisms. The conformation-induced oligomerisation model and the dissociation-activation model each require antigen binding for triggering to occur, therefore, if triggering can occur in the absence of ligand then it must occur by an alternative mechanism. Ligand independent triggering has already been demonstrated for the TCR [240].

7.2.2 Towards a more realistic analysis of BCR triggering

The work undertaken in this thesis has been undertaken on simple "first generation" SLBs. This approach has allowed the BCR/antigen interaction to be analysed in isolation. However, it is important to put this interaction into a more realistic biological context. Contacts of cells with SLBs incorporating other receptors known to be involved in cell-cell contacts (e.g. the adhesion protein ICAM-1) should be studied and the extent of triggering determined as a function of the density of these adhesion molecules. Ultimately, the gold standard in vitro analysis will characterise close contact formation at cell-cell contacts with simultaneous monitoring of calcium triggering and phosphatase exclusion.

All experiments in this thesis have been conducted in vitro using the HyHEL10 model system. While this is a well characterised model system it is important to correlate findings

established in cell lines with experiments undertaken on primary cells. The techniques developed in this thesis have been designed with the intention that they will translate easily to studies of primary cells from the MD4 mouse. One important difference between primary cells and cell lines is the expression levels of the BCR. Stoichiometric analysis was undertaken with B cells expressing approximately 1000 BCRs per cell and TIRF analysis with 25,000 BCRs per cell, whereas primary cells express approximately 100,000 receptors per cell. Higher expression levels add complexity to the experiments, but experiments undertaken in primary cells should be theoretically possible using the approaches undertaken on cell lines utilizing the controls presented in this thesis. The use of primary cells will provide the ultimate test of BCR triggering and will verify whether the results established on cell lines are generalisable to primary B cells.

7.2.3 A single generic mechanism of BCR triggering?

B cells are a heterogeneous population of cells with different subtypes and maturation stages. The different B cell subsets are interesting as they express differing levels and isotypes of the BCR which vary in the size of their extracellular domains. Furthermore, B cell subsets also express differing levels of CD45 and CD148. However, it is not known why B cells express different isotypes (such as IgD) or why phosphatase levels vary across different subsets. It would be interesting to determine whether these differences have implications for BCR triggering. To test this, the in vitro HEL model system described in this thesis could be used to expand the work described using the IgM HyHEL10 BCR to all other isotypes. HyHEL10 has been cloned as IgA, IgD, IgE, IgG1, IgG2a, IgG2b and IgG3 isotypes ready for expression in A20 cells. These could be tested to determine whether triggering differs between different isotypes of the BCR with the same specificity.

To test the hypothesis that triggering varies between different B cell subsets, FACS could be undertaken for naïve immature, follicular and marginal zone and anergic B1 B cells from anti-HEL MD4 single transgenic and MD4/ML5 and MD4/mHEL-KK HEL-expressing double transgenic mice [62, 290]. Firstly, the surface phenotype of B cell subsets ex vivo would be studied to establish the relative levels of BCR and the large phosphatases, CD45RABC and CD148. The techniques developed in this thesis could then be applied to the various subsets. Cells would be externally labelled with HEL in two/three colours and subjected to fluorescence microscopy in order to establish whether the oligomerisation state of the BCR is preserved or varies between different B cell phenotypes. Finally, calcium triggering experiments and TIRF microscopy would be used to test how signalling in B cell subsets is affected by antigen size, affinity and abundance. With these experiments, we would hope to show that there is a single, evolutionarily conserved, generic mechanism responsible for BCR triggering.

7.3 Final remarks

In conclusion, the work presented in this thesis provides evidence that a dominant mechanism of triggering of the BCR obeys the principles of the KS model. More widely, this supports a body of evidence that this is a generic mechanism of triggering of a range of receptors. This understanding provides the opportunity to agonise and antagonise receptors in clinical settings. In B cells this provides multiple opportunities for clinical application. Abnormal B cell activation can result in autoimmune diseases, hypersensitivity and lymphoid cancer. The ability to manipulate the triggering mechanism therefore has

potential therapeutic implications for future drug design. Furthermore, full utilisation of the B cell response could be harnessed to optimise immunity induced by vaccination.

Bibliography

1. Chaplin DD. Overview of the Immune Response. The Journal of allergy and clinical immunology. 2010;125(2 Suppl 2):S3-23.
2. Hoffmann J, Akira S. Innate immunity. Current opinion in immunology. 2013;25(1):1-3.
3. Turvey SE, Broide DH. Innate immunity. Journal of Allergy and Clinical Immunology. 2010;125(2):S24-S32.
4. Medzhitov R, Janeway CA. Decoding the Patterns of Self and Nonself by the Innate Immune System. Science. 2002;296(5566):298-300.
5. Akira S, Uematsu S, Takeuchi O. Pathogen Recognition and Innate Immunity. Cell. 2006;124(4):783-801.
6. Kumar H, Kawai T, Akira S. Pathogen recognition by the innate immune system. International reviews of immunology. 2011;30(1):16-34.
7. Lang KS, Burow A, Kurrer M, Lang PA, Recher M. The role of the innate immune response in autoimmune disease. Journal of Autoimmunity. 2007;29(4):206-12.
8. Medzhitov R, Janeway CA. Innate immunity: impact on the adaptive immune response. Current opinion in immunology. 1997;9(1):4-9.
9. Cooper MD, Alder MN. The evolution of adaptive immune systems. Cell. 2006;124(4):815-22.
10. Call ME, Wucherpfennig KW. The T cell receptor: critical role of the membrane environment in receptor assembly and function. Annu Rev Immunol. 2005;23:101-25.
11. Kuhns MS, Davis MM, Garcia KC. Deconstructing the form and function of the TCR/CD3 complex. Immunity. 2006;24(2):133-9.
12. Bassing CH, Swat W, Alt FW. The Mechanism and Regulation of Chromosomal V(D)J Recombination. Cell. 2002;109(2):S45-S55.
13. Komori T, Okada A, Stewart V, Alt FW. Lack of N regions in antigen receptor variable region genes of TdT-deficient lymphocytes. Science. 1993;261(5125):1171-5.
14. Honjo T, Muramatsu M, Fagarasan S. Aid. Immunity. 2004;20(6):659-68.
15. Krensky AM. The HLA system, antigen processing and presentation. Kidney international Supplement. 1997;58:S2-7.
16. Trowsdale J, Knight JC. Major Histocompatibility Complex Genomics and Human Disease. Annual review of genomics and human genetics. 2013;14:301-23.
17. Vinuesa CG, Chang P-P. Innate B cell helpers reveal novel types of antibody responses. NatImmunol. 2013;14(2):119-26.
18. Parker DC. T Cell-Dependent B Cell Activation. AnnuRevImmunol. 1993;11(1):331-60.
19. Vos Q, Lees A, Wu ZQ, Snapper CM, Mond JJ. B-cell activation by T-cell-independent type 2 antigens as an integral part of the humoral immune response to pathogenic microorganisms. ImmunolRev. 2000;176:154-70.
20. Schroeder HW, Jr., Cavacini L. Structure and function of immunoglobulins. J Allergy Clin Immunol. 2010;125(2 Suppl 2):S41-52.
21. Lafferty KJ, Cunningham AJ. A new analysis of allogeneic interactions. The Australian journal of experimental biology and medical science. 1975;53(1):27-42.

22. Sharpe AH, Abbas AK. T-Cell Costimulation — Biology, Therapeutic Potential, and Challenges. New England Journal of Medicine. 2006;355(10):973-5.
23. Germain RN. T-cell development and the CD4-CD8 lineage decision. Nature reviews Immunology. 2002;2(5):309-22.
24. Tscharke DC, Croft NP, Doherty PC, La Gruta NL. Sizing up the key determinants of the CD8(+) T cell response. Nature reviews Immunology. 2015;15(11):705-16.
25. Zhu J, Paul WE. CD4 T cells: fates, functions, and faults. Blood. 2008;112(5):1557-69.
26. Jenner E. An Inquiry into the Causes and Effects of Variolae Vaccinae, a Disease Discovered in Some Western Counties of England. London: Sampson Low. 1798.
27. Smith KA. Edward jenner and the small pox vaccine. Frontiers in immunology. 2011;2:21.
28. Farber DL, Netea MG, Radbruch A, Rajewsky K, Zinkernagel RM. Immunological memory: lessons from the past and a look to the future. Nature reviews Immunology. 2016;16(2):124-8.
29. Vivier E, Raulet DH, Moretta A, Caligiuri MA, Zitvogel L, Lanier LL, et al. Innate or Adaptive Immunity? The Example of Natural Killer Cells. Science. 2011;331(6013):44-9.
30. Vantourout P, Hayday A. Six-of-the-best: unique contributions of γδ T cells to immunology(). Nature reviews Immunology. 2013;13(2):88-100.
31. von Behring E, Kitasato S. Untersuchungen ueber das Zustandekommen der Diphtherie-Immunitat bei Thieren Dtsch Med Wochenschr. 1890;16: 1145–8.
32. Tiselius A, Kabat EA. AN ELECTROPHORETIC STUDY OF IMMUNE SERA AND PURIFIED ANTIBODY PREPARATIONS. The Journal of Experimental Medicine. 1939;69(1):119-31.
33. Ehrlich P. Croonian Lecture: On Immunity with Special Reference to Cell Life. Proceedings of the Royal Society of London. 1899;66(424-433):424-48.
34. Monson NL. The natural history of B cells. Current opinion in neurology. 2008;21 Suppl 1:S3-8.
35. Fagraeus A. The plasma cellular reaction and its relation to the formation of antibodies in vitro. JImmunol. 1948;58(1):1-13.
36. Gowans JL, Knight EJ. THE ROUTE OF RE-CIRCULATION OF LYMPHOCYTES IN THE RAT. Proceedings of the Royal Society of London Series B, Biological sciences. 1964;159:257-82.
37. Gowans JL, McGregor DDT. The Origins of Antibody-Forming Cells. Immunopathology: IIIrd International Symposium (eds Grabar, P. & Miescher, P. A.) 89 (Schwabe, 1963). 1963.
38. Landsteiner K, Chase MW. Experiments on Transfer of Cutaneous Sensitivity to Simple Compounds. Proceedings of the Society for Experimental Biology and Medicine. 1942;49(4):688-90.
39. Chase MW. The Cellular Transfer of Cutaneous Hypersensitivity to Tuberculin. Proceedings of the Society for Experimental Biology and Medicine. 1945;59(2):134-5.

40. Glick B, Chang TS, Jaap RG. The bursa of Fabricius and antibody production. Poultry Science. 1956;35(1):224-5.
41. Bruton OC. Agammaglobulinemia. Pediatrics. 1952;9(6):722-8.
42. Good RA, Varco RL. A clinical and experimental study of agammaglobulinemia. The Journal-lancet. 1955;75(6):245-71.
43. Cooper MD, Peterson RDA, Good RA. Delineation of the Thymic and Bursal Lymphoid Systems in the Chicken. Nature. 1965;205(4967):143-6.
44. Pieper K, Grimbacher B, Eibel H. B-cell biology and development. Journal of Allergy and Clinical Immunology. 2013;131(4):959-71.
45. Melchers F. Checkpoints that control B cell development. The Journal of Clinical Investigation. 2015;125(6):2203-10.
46. Corfe SA, Paige CJ. The many roles of IL-7 in B cell development; mediator of survival, proliferation and differentiation. Seminars in immunology. 2012;24(3):198-208.
47. Tokoyoda K, Egawa T, Sugiyama T, Choi BI, Nagasawa T. Cellular niches controlling B lymphocyte behavior within bone marrow during development. Immunity. 2004;20(6):707-18.
48. Mourcin F, Breton C, Tellier J, Narang P, Chasson L, Jorquera A, et al. Galectin-1-expressing stromal cells constitute a specific niche for pre-BII cell development in mouse bone marrow. Blood. 2011;117(24):6552-61.
49. Ryan DH, Tang J. Regulation of human B cell lymphopoiesis by adhesion molecules and cytokines. Leukemia & lymphoma. 1995;17(5-6):375-89.
50. Hardy RR, Carmack CE, Shinton SA, Kemp JD, Hayakawa K. Resolution and characterization of pro-B and pre-pro-B cell stages in normal mouse bone marrow. The Journal of Experimental Medicine. 1991;173(5):1213.
51. Hardy RR, Hayakawa K. B Cell Development Pathways. AnnuRevImmunol. 2001;19(1):595-621.
52. Zhang M, Srivastava G, Lu L. The pre-B cell receptor and its function during B cell development. Cellular & molecular immunology. 2004;1(2):89-94.
53. Tze LE, Schram BR, Lam K-P, Hogquist KA, Hippen KL, Liu J, et al. Basal Immunoglobulin Signaling Actively Maintains Developmental Stage in Immature B Cells. PLOS Biology. 2005;3(3):e82.
54. Rowland SL, DePersis CL, Torres RM, Pelanda R. Ras activation of Erk restores impaired tonic BCR signaling and rescues immature B cell differentiation. JExpMed. 2010;207(3):607-21.
55. Rowland SL, Leahy KF, Halverson R, Torres RM, Pelanda R. BAFF receptor signaling aids the differentiation of immature B cells into transitional B cells following tonic BCR signaling. JImmunol. 2010;185(8):4570-81.
56. Tobón GJ, Izquierdo JH, Cañas CA. B Lymphocytes: Development, Tolerance, and Their Role in Autoimmunity—Focus on Systemic Lupus Erythematosus. Autoimmune Diseases. 2013;2013:827254.
57. Hartley SB, Crosbie J, Brink R, Kantor AB, Basten A, Goodnow CC. Elimination from peripheral lymphoid tissues of self-reactive B lymphocytes recognizing membrane-bound antigens. Nature. 1991;353(6346):765-9.

58. Hartley SB, Cooke MP, Fulcher DA, Harris AW, Cory S, Basten A, et al. Elimination of self-reactive B lymphocytes proceeds in two stages: arrested development and cell death. Cell. 1993;72(3):325-35.
59. Tiegs SL, Russell DM, Nemazee D. Receptor editing in self-reactive bone marrow B cells. JExpMed. 1993;177(4):1009-20.
60. Gay D, Saunders T, Camper S, Weigert M. Receptor editing: an approach by autoreactive B cells to escape tolerance. JExpMed. 1993;177(4):999-1008.
61. Radic MZ, Erikson J, Litwin S, Weigert M. B lymphocytes may escape tolerance by revising their antigen receptors. JExpMed. 1993;177(4):1165-73.
62. Goodnow CC, Crosbie J, Adelstein S, Lavoie TB, Smith-Gill SJ, Brink RA, et al. Altered immunoglobulin expression and functional silencing of self-reactive B lymphocytes in transgenic mice. Nature. 1988;334(6184):676.
63. Burnett DL, Langley DB, Schofield P, Hermes JR, Chan TD, Jackson J, et al. Germinal center antibody mutation trajectories are determined by rapid self/foreign discrimination. Science. 2018;360(6385):223-6.
64. Goodnow CC, Crosbie J, Jorgensen H, Brink RA, Basten A. Induction of self-tolerance in mature peripheral B lymphocytes. Nature. 1989;342(6248):385-91.
65. Cooke MP, Heath AW, Shokat KM, Zeng Y, Finkelman FD, Linsley PS, et al. Immunoglobulin signal transduction guides the specificity of B cell-T cell interactions and is blocked in tolerant self-reactive B cells. JExpMed. 1994;179(2):425-38.
66. Healy JI, Dolmetsch RE, Lewis RS, Goodnow CC. Quantitative and qualitative control of antigen receptor signalling in tolerant B lymphocytes. Novartis Foundation symposium. 1998;215:137-44; discussion 44-5, 86-90.
67. Goodnow CC, Crosbie J, Adelstein S, Lavoie TB, Smith-Gill SJ, Brink RA, et al. Altered immunoglobulin expression and functional silencing of self-reactive B lymphocytes in transgenic mice. Nature. 1988;334(6184):676-82.
68. Norvell A, Mandik L, Monroe JG. Engagement of the antigen-receptor on immature murine B lymphocytes results in death by apoptosis. The Journal of Immunology. 1995;154(9):4404-13.
69. Vossenkamper A, Lutalo PM, Spencer J. Translational Mini-Review Series on B cell subsets in disease. Transitional B cells in systemic lupus erythematosus and Sjogren's syndrome: clinical implications and effects of B cell-targeted therapies. Clinical and experimental immunology. 2012;167(1):7-14.
70. Cyster JG. Chemokines, sphingosine-1-phosphate, and cell migration in secondary lymphoid organs. Annu Rev Immunol. 2005;23:127-59.
71. Bannard O, Cyster JG. Germinal centers: programmed for affinity maturation and antibody diversification. Current opinion in immunology. 2017;45:21-30.
72. Stavnezer J, Schrader CE. Ig heavy chain class switch recombination: mechanism and regulation. Journal of immunology (Baltimore, Md : 1950). 2014;193(11):5370-8.
73. Allman D, Pillai S. Peripheral B cell subsets. Current opinion in immunology. 2008;20(2):149-57.
74. Montecino-Rodriguez E, Dorshkind K. B-1 B Cell Development in the Fetus and Adult. Immunity. 2012;36(1):13-21.

75. Tung JW, Parks DR, Moore WA, Herzenberg LA, Herzenberg LA. Identification of B-Cell Subsets. In: Gu H, Rajewsky K, editors. B Cell Protocols. Totowa, NJ: Humana Press; 2004. p. 37-58.
76. Griffin DO, Holodick NE, Rothstein TL. Human B1 cells in umbilical cord and adult peripheral blood express the novel phenotype CD20⁺CD27⁺CD43⁺CD70[−]. The Journal of Experimental Medicine. 2011;208(1):67-80.
77. Descatoire M, Weill J-C, Reynaud C-A, Weller S. A human equivalent of mouse B-1 cells? The Journal of Experimental Medicine. 2011;208(13):2563-4.
78. Perez-Andres M, Grosserichter-Wagener C, Teodosio C, van Dongen JJM, Orfao A, van Zelm MC. The nature of circulating CD27⁺CD43⁺ B cells. The Journal of Experimental Medicine. 2011;208(13):2565-6.
79. Griffin DO, Holodick NE, Rothstein TL. Human B1 cells are CD3[−]: A reply to “A human equivalent of mouse B-1 cells?” and “The nature of circulating CD27⁺CD43⁺ B cells”. The Journal of Experimental Medicine. 2011;208(13):2566-9.
80. Herzenberg LA, Tung JW. B cell lineages: documented at last! NatImmunol. 2006;7:225.
81. Pillai S, Cariappa A, Moran ST. MARGINAL ZONE B CELLS. AnnuRevImmunol. 2005;23(1):161-96.
82. Martin F, Kearney JF. Marginal-zone B cells. Nature reviews Immunology. 2002;2(5):323-35.
83. Cinamon G, Zachariah MA, Lam OM, Foss FW, Jr., Cyster JG. Follicular shuttling of marginal zone B cells facilitates antigen transport. NatImmunol. 2008;9(1):54-62.
84. Andrews SF, Wilson PC. The anergic B cell. Blood. 2010;115(24):4976-8.
85. Pike BL, Boyd AW, Nossal GJ. Clonal anergy: the universally anergic B lymphocyte. ProcNatlAcadSciUSA. 1982;79(6):2013-7.
86. Goodnow CC, Crosbie J, Adelstein S, Lavoie TB, Smith-Gill SJ, Brink RA, et al. Altered immunoglobulin expression and functional silencing of self-reactive B lymphocytes in transgenic mice. Nature. 1988;334(6184):676-82.
87. Cambier JC, Gauld SB, Merrell KT, Vilen BJ. B-cell anergy: from transgenic models to naturally occurring anergic B cells? Nature reviews Immunology. 2007;7(8):633-43.
88. Merrell KT, Benschop RJ, Gauld SB, Aviszus K, Decote-Ricardo D, Wysocki LJ, et al. Identification of anergic B cells within a wild-type repertoire. Immunity. 2006;25(6):953-62.
89. Rosser Elizabeth C, Mauri C. Regulatory B Cells: Origin, Phenotype, and Function. Immunity.42(4):607-12.
90. Katz SI, Parker D, Turk JL. B-cell suppression of delayed hypersensitivity reactions. Nature. 1974;251(5475):550-1.
91. Neta R, Salvin SB. Specific suppression of delayed hypersensitivity: the possible presence of a suppressor B cell in the regulation of delayed hypersensitivity. JImmunol. 1974;113(6):1716-25.

92. Wolf SD, Dittel BN, Hardardottir F, Janeway CA, Jr. Experimental autoimmune encephalomyelitis induction in genetically B cell-deficient mice. JExpMed. 1996;184(6):2271-8.
93. Mizoguchi A, Mizoguchi E, Smith RN, Preffer FI, Bhan AK. Suppressive role of B cells in chronic colitis of T cell receptor alpha mutant mice. JExpMed. 1997;186(10):1749-56.
94. Mizoguchi A, Mizoguchi E, Takedatsu H, Blumberg RS, Bhan AK. Chronic intestinal inflammatory condition generates IL-10-producing regulatory B cell subset characterized by CD1d upregulation. Immunity. 2002;16(2):219-30.
95. Fillatreau S, Sweenie CH, McGeachy MJ, Gray D, Anderton SM. B cells regulate autoimmunity by provision of IL-10. NatImmunol. 2002;3(10):944-50.
96. Mauri C, Gray D, Mushtaq N, Londei M. Prevention of Arthritis by Interleukin 10–producing B Cells. The Journal of Experimental Medicine. 2003;197(4):489-501.
97. Mauri C, Menon M. The expanding family of regulatory B cells. IntImmunol. 2015;27(10):479-86.
98. Tangye SG, Tarlinton DM. Memory B cells: effectors of long-lived immune responses. European journal of immunology. 2009;39(8):2065-75.
99. Berkowska MA, Driessen GJ, Bikos V, Grosserichter-Wagener C, Stamatopoulos K, Cerutti A, et al. Human memory B cells originate from three distinct germinal center-dependent and -independent maturation pathways. Blood. 2011;118(8):2150-8.
100. Nutt SL, Hodgkin PD, Tarlinton DM, Corcoran LM. The generation of antibody-secreting plasma cells. Nature reviews Immunology. 2015;15(3):160-71.
101. Oracki SA, Walker JA, Hibbs ML, Corcoran LM, Tarlinton DM. Plasma cell development and survival. ImmunolRev. 2010;237(1):140-59.
102. Breinl F, Haurowitz F. Chemical investigation of the precipitate from hemoglobin and anti-hemoglobin-serum and remarks on the nature of the antibodies. Z physiol Chem. 1930;192:45-57.
103. Pauling L. A Theory of the Structure and Process of Formation of Antibodies*. Journal of the American Chemical Society. 1940;62(10):2643-57.
104. Landsteiner K, Lampl H. Ueber die Abhängigkeit der serolologischen Spezifizität an der chemischen Struktur Biochem Ztschr. 1918;86:343.
105. Fischer DS. Theories of Antibody Formation: A Review. The Yale Journal of Biology and Medicine. 1964;37(1):1-30.
106. Sir Frank Macfarlane Burnet 1899–1985. NatImmunol. 2007;8:1009.
107. Jerne NK. THE NATURAL-SELECTION THEORY OF ANTIBODY FORMATION. ProcNatlAcadSciUSA. 1955;41(11):849-57.
108. Talmage DW. Allergy and immunology. Annual review of medicine. 1957;8:239-56.
109. Burnet FM. A modification of Jerne's theory of antibody production using the concept of clonal selection. Australian J Sci. 1957;20(3):67-9.
110. Burnet SFM. The clonal selection theory of acquired immunity: Vanderbilt University Press Nashville; 1959.
111. Nossal GJ, Lederberg J. Antibody production by single cells. Nature. 1958;181(4620):1419-20.

112. Harwood NE, Batista FD. New insights into the early molecular events underlying B cell activation. Immunity. 2008;28(5):609.
113. Edelman GM, Gally JA. A MODEL FOR THE 7S ANTIBODY MOLECULE. ProcNatlAcadSciUSA. 1964;51:846-53.
114. Porter RR. CHEMICAL STRUCTURE OF GAMMA-GLOBULIN AND ANTIBODIES. British medical bulletin. 1963;19:197-201.
115. Reth M, Hombach J, Wienands J, Campbell KS, Chien N, Justement LB, et al. The B-cell antigen receptor complex. ImmunolToday. 1991;12(6):196.
116. Schroeder HW, Cavacini L. Structure and Function of Immunoglobulins. The Journal of allergy and clinical immunology. 2010;125(2 0 2):S41-S52.
117. Achatz G, Nitschke L, Lamers MC. Effect of Transmembrane and Cytoplasmic Domains of IgE on the IgE Response. Science. 1997;276(5311):409.
118. Kaisho T, Schwenk F, Rajewsky K. The Roles of γ1 Heavy Chain Membrane Expression and Cytoplasmic Tail in IgG1 Responses. Science. 1997;276(5311):412.
119. Martin SW, Goodnow CC. Burst-enhancing role of the IgG membrane tail as a molecular determinant of memory. NatImmunol. 2002;3(2):182-8.
120. Sitia R, Neuberger MS, Milstein C. Regulation of membrane IgM expression in secretory B cells: translational and post-translational events. The EMBO journal. 1987;6(13):3969-77.
121. Hombach J, Sabitzky F, Rajewsky K, Reth M. Transfected plasmacytoma cells do not transport the membrane form of IgM to the cell surface. The Journal of Experimental Medicine. 1988;167(2):652-7.
122. Hombach J, Tsubata T, Leclercq L, Stappert H, Reth M. Molecular components of the B-cell antigen receptor complex of the IgM class. Nature. 1990;343(6260):760-2.
123. Hombach J, Leclercq L, Radbruch A, Rajewsky K, Reth M. A novel 34-kd protein co-isolated with the IgM molecule in surface IgM-expressing cells. The EMBO journal. 1988;7(11):3451-6.
124. Sakaguchi N, Kashiwamura S, Kimoto M, Thalmann P, Melchers F. B lymphocyte lineage-restricted expression of mb-1, a gene with CD3-like structural properties. The EMBO journal. 1988;7(11):3457-64.
125. Kashiwamura S, Koyama T, Matsuo T, Steinmetz M, Kimoto M, Sakaguchi N. Structure of the murine mb-1 gene encoding a putative sIgM-associated molecule. JImmunol. 1990;145(1):337-43.
126. Hermanson GG, Eisenberg D, Kincade PW, Wall R. B29: a member of the immunoglobulin gene superfamily exclusively expressed on beta-lineage cells. ProcNatlAcadSciUSA. 1988;85(18):6890-4.
127. Hermanson GG, Briskin M, Sigman D, Wall R. Immunoglobulin enhancer and promoter motifs 5' of the B29 B-cell-specific gene. ProcNatlAcadSciUSA. 1989;86(19):7341-5.
128. Venkitaraman AR, Williams GT, Dariavach P, Neuberger MS. The B-cell antigen receptor of the five immunoglobulin classes. Nature. 1991;352(6338):777-81.
129. Reth M. Antigen receptor tail clue. Nature. 1989;338(6214):383-4.
130. Isakov N. Immunoreceptor tyrosine-based activation motif (ITAM), a unique module linking antigen and Fc receptors to their signaling cascades. Journal of leukocyte biology. 1997;61(1):6-16.

131. Schamel WW, Reth M. Monomeric and oligomeric complexes of the B cell antigen receptor. Immunity. 2000;13(1):5-14.
132. Tolar P, Sohn HW, Pierce SK. The initiation of antigen-induced B cell antigen receptor signaling viewed in living cells by fluorescence resonance energy transfer. NatImmunol. 2005;6(11):1168.
133. Young RM, Staudt LM. Targeting pathological B cell receptor signalling in lymphoid malignancies. Nature reviews Drug discovery. 2013;12(3):229-43.
134. Yamamoto T, Yamanashi Y, Toyoshima K. Association of Src-family kinase Lyn with B-cell antigen receptor. ImmunolRev. 1993;132:187-206.
135. Johnson SA, Pleiman CM, Pao L, Schneringer J, Hippen K, Cambier JC. Phosphorylated immunoreceptor signaling motifs (ITAMs) exhibit unique abilities to bind and activate Lyn and Syk tyrosine kinases. JImmunol. 1995;155(10):4596-603.
136. Pao LI, Famiglietti SJ, Cambier JC. Asymmetrical phosphorylation and function of immunoreceptor tyrosine-based activation motif tyrosines in B cell antigen receptor signal transduction. JImmunol. 1998;160(7):3305-14.
137. Rowley RB, Burkhardt AL, Chao HG, Matsueda GR, Bolen JB. Syk protein-tyrosine kinase is regulated by tyrosine-phosphorylated Ig alpha/Ig beta immunoreceptor tyrosine activation motif binding and autophosphorylation. The Journal of biological chemistry. 1995;270(19):11590-4.
138. Geahlen RL. Syk and pTyr'd: Signaling through the B cell antigen receptor. Biochimica et Biophysica Acta (BBA) - Molecular Cell Research. 2009;1793(7):1115-27.
139. Dal Porto JM, Gauld SB, Merrell KT, Mills D, Pugh-Bernard AE, Cambier J. B cell antigen receptor signaling 101. Molecular immunology. 2004;41(6-7):599-613.
140. Engel P, Zhou LJ, Ord DC, Sato S, Koller B, Tedder TF. Abnormal B lymphocyte development, activation, and differentiation in mice that lack or overexpress the CD19 signal transduction molecule. Immunity. 1995;3(1):39-50.
141. Rickert RC, Rajewsky K, Roes J. Impairment of T-cell-dependent B-cell responses and B-1 cell development in CD19-deficient mice. Nature. 1995;376(6538):352-5.
142. Depoil D, Fleire S, Treanor BL, Weber M, Harwood NE, Marchbank KL, et al. CD19 is essential for B cell activation by promoting B cell receptor-antigen microcluster formation in response to membrane-bound ligand. NatImmunol. 2008;9(1):63-72.
143. DeFranco AL, Chan VW, Lowell CA. Positive and negative roles of the tyrosine kinase Lyn in B cell function. Seminars in immunology. 1998;10(4):299-307.
144. Hermiston ML, Xu Z, Weiss A. CD45: A Critical Regulator of Signaling Thresholds in Immune Cells. AnnuRevImmunol. 2003;21(1):107-37.
145. Fleire SJ, Goldman JP, Carrasco YR, Weber M, Bray D, Batista FD. B cell ligand discrimination through a spreading and contraction response. Science. 2006;312(5774):738.
146. Weber M, Treanor B, Depoil D, Shinohara H, Harwood NE, Hikida M, et al. Phospholipase C-gamma2 and Vav cooperate within signaling microclusters to propagate B cell spreading in response to membrane-bound antigen. JExpMed. 2008;205(4):853-68.

147. Sohn HW, Pierce SK, Tzeng SJ. Live cell imaging reveals that the inhibitory FcgammaRIIB destabilizes B cell receptor membrane-lipid interactions and blocks immune synapse formation. JImmunol. 2008;180(2):793-9.
148. Batista FD, Iber D, Neuberger MS. B cells acquire antigen from target cells after synapse formation. Nature. 2001;411(6836):489-94.
149. Carrasco YR, Fleire SJ, Cameron T, Dustin ML, Batista FD. LFA-1/ICAM-1 interaction lowers the threshold of B cell activation by facilitating B cell adhesion and synapse formation. Immunity. 2004;20(5):589-99.
150. Davis DM, Chiu I, Fassett M, Cohen GB, Mandelboim O, Strominger JL. The human natural killer cell immune synapse. ProcNatlAcadSciUSA. 1999;96(26):15062-7.
151. Lee KH, Holdorf AD, Dustin ML, Chan AC, Allen PM, Shaw AS. T cell receptor signaling precedes immunological synapse formation. Science. 2002;295(5559):1539-42.
152. Tatosyan AG, Mizenina OA. Kinases of the Src family: structure and functions. Biochemistry Biokhimiia. 2000;65(1):49-58.
153. Gauld SB, Cambier JC. Src-family kinases in B-cell development and signaling. Oncogene. 2004;23(48):8001-6.
154. Sicheri F, Moarefi I, Kuriyan J. Crystal structure of the Src family tyrosine kinase Hck. Nature. 1997;385(6617):602-9.
155. Xu W, Doshi A, Lei M, Eck MJ, Harrison SC. Crystal structures of c-Src reveal features of its autoinhibitory mechanism. MolCell. 1999;3(5):629-38.
156. Acuto O, Di Bartolo V, Michel F. Tailoring T-cell receptor signals by proximal negative feedback mechanisms. Nature reviews Immunology. 2008;8(9):699-712.
157. Hermiston ML, Zikherman J, Zhu JW. CD45, CD148, and Lyp/Pep: critical phosphatases regulating Src family kinase signaling networks in immune cells. ImmunolRev. 2009;228(1):288.
158. Mee PJ, Turner M, Basson MA, Costello PS, Zamoyska R, Tybulewicz VL. Greatly reduced efficiency of both positive and negative selection of thymocytes in CD45 tyrosine phosphatase-deficient mice. European journal of immunology. 1999;29(9):2923-33.
159. Byth KF, Conroy LA, Howlett S, Smith AJ, May J, Alexander DR, et al. CD45-null transgenic mice reveal a positive regulatory role for CD45 in early thymocyte development, in the selection of CD4+CD8+ thymocytes, and B cell maturation. JExpMed. 1996;183(4):1707-18.
160. Kishihara K, Penninger J, Wallace VA, Kundig TM, Kawai K, Wakeham A, et al. Normal B lymphocyte development but impaired T cell maturation in CD45-exon6 protein tyrosine phosphatase-deficient mice. Cell. 1993;74(1):143-56.
161. Hermiston ML, Tan AL, Gupta VA, Majeti R, Weiss A. The juxtamembrane wedge negatively regulates CD45 function in B cells. Immunity. 2005;23(6):635-47.
162. Loder F, Mutschler B, Ray RJ, Paige CJ, Sideras P, Torres R, et al. B cell development in the spleen takes place in discrete steps and is determined by the quality of B cell receptor-derived signals. JExpMed. 1999;190(1):75-89.
163. Fleming HE, Milne CD, Paige CJ. CD45-deficient mice accumulate Pro-B cells both in vivo and in vitro. JImmunol. 2004;173(4):2542-51.

164. Benatar T, Carsetti R, Furlonger C, Kamalia N, Mak T, Paige CJ. Immunoglobulin-mediated signal transduction in B cells from CD45-deficient mice. JExpMed. 1996;183(1):329-34.
165. Benschop RJ, Cambier JC. B cell development: signal transduction by antigen receptors and their surrogates. Current opinion in immunology. 1999;11(2):143-51.
166. Cyster JG, Healy JI, Kishihara K, Mak TW, Thomas ML, Goodnow CC. Regulation of B-lymphocyte negative and positive selection by tyrosine phosphatase CD45. Nature. 1996;381(6580):325-8.
167. Cyster JG, Goodnow CC. Protein tyrosine phosphatase 1C negatively regulates antigen receptor signaling in B lymphocytes and determines thresholds for negative selection. Immunity. 1995;2(1):13-24.
168. Katagiri T, Ogimoto M, Hasegawa K, Arimura Y, Mitomo K, Okada M, et al. CD45 negatively regulates lyn activity by dephosphorylating both positive and negative regulatory tyrosine residues in immature B cells. JImmunol. 1999;163(3):1321-6.
169. Shrivastava P, Katagiri T, Ogimoto M, Mizuno K, Yakura H. Dynamic regulation of Src-family kinases by CD45 in B cells. Blood. 2004;103(4):1425-32.
170. Katagiri T, Ogimoto M, Hasegawa K, Mizuno K, Yakura H. Selective Regulation of Lyn Tyrosine Kinase by CD45 in Immature B Cells. Journal of Biological Chemistry. 1995;270(47):27987-90.
171. Schraven B. CD148. Journal of biological regulators and homeostatic agents. 2000;14(3):220-2.
172. Baker JE, Majeti R, Tangye SG, Weiss A. Protein tyrosine phosphatase CD148-mediated inhibition of T-cell receptor signal transduction is associated with reduced LAT and phospholipase Cgamma1 phosphorylation. Molecular and cellular biology. 2001;21(7):2393-403.
173. Gaya A, Pirotto F, Palou E, Autschbach F, Del Pozo V, Sole J, et al. CD148, a new membrane tyrosine phosphatase involved in leukocyte function. Leukemia & lymphoma. 1999;35(3-4):237-43.
174. Kuramochi S, Matsuda S, Matsuda Y, Saitoh T, Ohsugi M, Yamamoto T. Molecular cloning and characterization of Byp, a murine receptor-type tyrosine phosphatase similar to human DEP-1. FEBS Lett. 1996;378(1):7-14.
175. Borges LG, Seifert RA, Grant FJ, Hart CE, Disteche CM, Edelhoff S, et al. Cloning and characterization of rat density-enhanced phosphatase-1, a protein tyrosine phosphatase expressed by vascular cells. Circulation research. 1996;79(3):570-80.
176. Takahashi T, Takahashi K, St. John PL, Fleming PA, Tomemori T, Watanabe T, et al. A Mutant Receptor Tyrosine Phosphatase, CD148, Causes Defects in Vascular Development. Molecular and cellular biology. 2003;23(5):1817-31.
177. Trapasso F, Drusco A, Costinean S, Alder H, Aqeilan RI, Iuliano R, et al. Genetic ablation of Ptprj, a mouse cancer susceptibility gene, results in normal growth and development and does not predispose to spontaneous tumorigenesis. DNA and cell biology. 2006;25(6):376-82.
178. Zhu JW, Brdicka T, Katsumoto TR, Lin J, Weiss A. Structurally distinct phosphatases CD45 and CD148 both regulate B cell and macrophage immunoreceptor signaling. Immunity. 2008;28(2):183.

179. Lin J, Zhu JW, Baker JE, Weiss A. Regulated expression of the receptor-like tyrosine phosphatase CD148 on hemopoietic cells. JImmunol. 2004;173(4):2324-30.
180. Skrzypczynska KM, Zhu JW, Weiss A. Positive Regulation of Lyn Kinase by CD148 Is Required for B Cell Receptor Signaling in B1 but Not B2 B Cells. Immunity. 2016;45(6):1232-44.
181. Berg LJ. Strength of T cell receptor signaling strikes again. Immunity. 2009;31(4):529-31.
182. Singer SJ, Nicolson GL. The fluid mosaic model of the structure of cell membranes. Science. 1972;175(4023):720-31.
183. Sezgin E, Levental I, Mayor S, Eggeling C. The mystery of membrane organization: composition, regulation and roles of lipid rafts. Nature reviews Molecular cell biology. 2017;18(6):361-74.
184. Simons K, Ikonen E. Functional rafts in cell membranes. Nature. 1997;387(6633):569-72.
185. Pierce SK. Lipid rafts and B-cell activation. Nature reviews Immunology. 2002;2(2):96-105.
186. Sohn HW, Tolar P, Jin T, Pierce SK. Fluorescence resonance energy transfer in living cells reveals dynamic membrane changes in the initiation of B cell signaling. ProcNatlAcadSciUSA. 2006;103(21):8143-8.
187. Gupta N, DeFranco AL. Lipid rafts and B cell signaling. Seminars in cell & developmental biology. 2007;18(5):616-26.
188. Treanor B, Depoil D, Gonzalez-Granja A, Barral P, Weber M, Dushek O, et al. The membrane skeleton controls diffusion dynamics and signaling through the B cell receptor. Immunity. 2010;32(2):187.
189. Hitt AL, Luna EJ. Membrane interactions with the actin cytoskeleton. Current Opinion in Cell Biology. 1994;6(1):120-30.
190. Sako Y, Kusumi A. Compartmentalized structure of the plasma membrane for receptor movements as revealed by a nanometer-level motion analysis. JCell Biol. 1994;125(6):1251-64.
191. Kusumi A, Ike H, Nakada C, Murase K, Fujiwara T. Single-molecule tracking of membrane molecules: plasma membrane compartmentalization and dynamic assembly of raft-philic signaling molecules. Seminars in immunology. 2005;17(1):3-21.
192. Simson R, Sheets ED, Jacobson K. Detection of temporary lateral confinement of membrane proteins using single-particle tracking analysis. Biophys J. 1995;69(3):989-93.
193. Fujiwara T, Ritchie K, Murakoshi H, Jacobson K, Kusumi A. Phospholipids undergo hop diffusion in compartmentalized cell membrane. JCell Biol. 2002;157(6):1071-81.
194. Batista FD, Treanor B, Harwood NE. Visualizing a role for the actin cytoskeleton in the regulation of B-cell activation. Immunological Reviews. 2010;237(1):191-204.
195. Conley ME, Dobbs AK, Farmer DM, Kilic S, Paris K, Grigoriadou S, et al. Primary B cell immunodeficiencies: comparisons and contrasts. Annu Rev Immunol. 2009;27:199-227.

196. von Andrian UH, Mempel TR. Homing and cellular traffic in lymph nodes. Nature reviews Immunology. 2003;3(11):867-78.
197. Junt T, Scandella E, Ludewig B. Form follows function: lymphoid tissue microarchitecture in antimicrobial immune defence. Nature reviews Immunology. 2008;8(10):764-75.
198. Nossal GJ, Abbot A, Mitchell J, Lummus Z. Antigens in immunity. XV. Ultrastructural features of antigen capture in primary and secondary lymphoid follicles. JExpMed. 1968;127(2):277-90.
199. Pape KA, Catron DM, Itano AA, Jenkins MK. The humoral immune response is initiated in lymph nodes by B cells that acquire soluble antigen directly in the follicles. Immunity. 2007;26(4):491-502.
200. Roozendaal R, Mempel TR, Pitcher LA, Gonzalez SF, Verschoor A, Mebius RE, et al. Conduits mediate transport of low-molecular-weight antigen to lymph node follicles. Immunity. 2009;30(2):264-76.
201. Koppel EA, Wieland CW, van den Berg VC, Litjens M, Florquin S, van Kooyk Y, et al. Specific ICAM-3 grabbing nonintegrin-related 1 (SIGNR1) expressed by marginal zone macrophages is essential for defense against pulmonary Streptococcus pneumoniae infection. European journal of immunology. 2005;35(10):2962-9.
202. Carrasco YR, Batista FD. B cells acquire particulate antigen in a macrophage-rich area at the boundary between the follicle and the subcapsular sinus of the lymph node. Immunity. 2007;27(1):160-71.
203. Junt T, Moseman EA, Iannacone M, Massberg S, Lang PA, Boes M, et al. Subcapsular sinus macrophages in lymph nodes clear lymph-borne viruses and present them to antiviral B cells. Nature. 2007;450(7166):110.
204. Carrasco YR, Batista FD. B cells acquire particulate antigen in a macrophage-rich area at the boundary between the follicle and the subcapsular sinus of the lymph node. Immunity. 2007;27(1):160.
205. Mitchell J, Abbot A. Ultrastructure of the Antigen-retaining Reticulum of Lymph Node Follicles as shown by High-resolution Autoradiography. Nature. 1965;208(5009):500-2.
206. Huang NN, Han SB, Hwang IY, Kehrl JH. B cells productively engage soluble antigen-pulsed dendritic cells: visualization of live-cell dynamics of B cell-dendritic cell interactions. JImmunol. 2005;175(11):7125-34.
207. Wykes M, Pombo A, Jenkins C, MacPherson GG. Dendritic cells interact directly with naive B lymphocytes to transfer antigen and initiate class switching in a primary T-dependent response. JImmunol. 1998;161(3):1313-9.
208. Chen LL, Frank AM, Adams JC, Steinman RM. Distribution of horseradish peroxidase (HRP)-anti-HRP immune complexes in mouse spleen with special reference to follicular dendritic cells. JCell Biol. 1978;79(1):184-99.
209. Mandel TE, Phipps RP, Abbot A, Tew JG. The follicular dendritic cell: long term antigen retention during immunity. ImmunolRev. 1980;53:29-59.
210. Tew JG, Phipps RP, Mandel TE. The maintenance and regulation of the humoral immune response: persisting antigen and the role of follicular antigen-binding dendritic cells as accessory cells. ImmunolRev. 1980;53:175-201.

211. Carrasco YR, Batista FD. B cell recognition of membrane-bound antigen: an exquisite way of sensing ligands. Current opinion in immunology. 2006;18(3):286-91.
212. Batista FD, Harwood NE. The who, how and where of antigen presentation to B cells. Nature reviews Immunology. 2009;9(1):15-27.
213. Batista FD, Neuberger MS. Affinity dependence of the B cell response to antigen: a threshold, a ceiling, and the importance of off-rate. Immunity. 1998;8(6):751-9.
214. Batista FD, Neuberger MS. B cells extract and present immobilized antigen: implications for affinity discrimination. The EMBO journal. 2000;19(4):513-20.
215. Yang J, Reth M. The dissociation activation model of B cell antigen receptor triggering. FEBS Lett. 2010;584(24):4872.
216. Treanor B. B-cell receptor: from resting state to activate. Immunology. 2012;136(1):21.
217. Woodruff MFA, Reid B, James K. Effect of antilymphocytic antibody and antibody fragments on human lymphocytes in vitro. Nature. 1967;215:591.
218. Riethmüller G, Riethmüller D, Stein H, Hausen P. In Vivo and in Vitro Properties of Intact and Pepsin-Digested Heterologous Anti-Mouse Thymus Antibodies. The Journal of Immunology. 1968;100(5):969.
219. Fanger MW, Hart DA, Wells JV, Nisonoff A. Requirement for Cross-Linkage in the Stimulation of Transformation of Rabbit Peripheral Lymphocytes by Antiglobulin Reagents. The Journal of Immunology. 1970;105(6):1484.
220. Maino VC, Hayman MJ, Crumpton MJ. Relationship between enhanced turnover of phosphatidylinositol and lymphocyte activation by mitogens. BiochemJ. 1975;146(1):247.
221. Weiner HL, Moorhead JW, Yamaga K, Kubo RT. Anti-Immunoglobulin Stimulation of Murine Lymphocytes: II. Identification of Cell Surface Target Molecules and Requirements for Cross-Linkage. The Journal of Immunology. 1976;117(5 Part 1):1527.
222. Puffer EB, Pontrello JK, Hollenbeck JJ, Kink JA, Kiessling LL. Activating B cell signaling with defined multivalent ligands. ACS chemical biology. 2007;2(4):252.
223. Minguet S, Dopfer EP, Schamel WW. Low-valency, but not monovalent, antigens trigger the B-cell antigen receptor (BCR). IntImmunol. 2010;22(3):205.
224. Kim YM, Pan JY, Korbel GA, Peperzak V, Boes M, Ploegh HL. Monovalent ligation of the B cell receptor induces receptor activation but fails to promote antigen presentation. ProcNatlAcadSciUSA. 2006;103(9):3327.
225. Reth M, Wienands J, Schamel WW. An unsolved problem of the clonal selection theory and the model of an oligomeric B-cell antigen receptor. ImmunolRev. 2000;176:10-8.
226. Batista FD, Iber D, Neuberger MS. B cells acquire antigen from target cells after synapse formation. Nature. 2001;411(6836):489.
227. Phan TG, Grigorova I, Okada T, Cyster JG. Subcapsular encounter and complement-dependent transport of immune complexes by lymph node B cells. NatImmunol. 2007;8(9):992.
228. Qi H, Egen JG, Huang AY, Germain RN. Extrafollicular activation of lymph node B cells by antigen-bearing dendritic cells. Science. 2006;312(5780):1672.

229. Tolar P, Pierce SK. A conformation-induced oligomerization model for B cell receptor microclustering and signaling. CurrTopMicrobiolImmunol. 2010;340:155.
230. Tolar P, Hanna J, Krueger PD, Pierce SK. The constant region of the membrane immunoglobulin mediates B cell-receptor clustering and signaling in response to membrane antigens. Immunity. 2009;30(1):44.
231. Saphire EO, Stanfield RL, Max Crispin MD, Parren PWHI, Rudd PM, Dwek RA, et al. Contrasting IgG Structures Reveal Extreme Asymmetry and Flexibility. Journal of molecular biology. 2002;319(1):9-18.
232. Yang J, Reth M. Oligomeric organization of the B-cell antigen receptor on resting cells. Nature. 2010;467(7314):465.
233. Schamel WW, Reth M. Monomeric and oligomeric complexes of the B cell antigen receptor. Immunity. 2000;13(1):5.
234. Klasener K, Maity PC, Hobeika E, Yang J, Reth M. B cell activation involves nanoscale receptor reorganizations and inside-out signaling by Syk. Elife. 2014;3:e02069.
235. Mattila PK, Batista FD, Treanor B. Dynamics of the actin cytoskeleton mediates receptor cross talk: An emerging concept in tuning receptor signaling. The Journal of Cell Biology. 2016;212(3):267.
236. Mattila PK, Feest C, Depoil D, Treanor B, Montaner B, Otipoby KL, et al. The actin and tetraspanin networks organize receptor nanoclusters to regulate B cell receptor-mediated signaling. Immunity. 2013;38(3):461.
237. Santos AM, Ponjavic A, Fritzsche M, Fernandes RA, de la Serna JB, Wilcock MJ, et al. Capturing resting T cells: the perils of PLL. NatImmunol. 2018;19(3):203-5.
238. Davis SJ, van der Merwe PA. The kinetic-segregation model: TCR triggering and beyond. NatImmunol. 2006;7(8):803.
239. Davis SJ, van der Merwe PA. TCR triggering: co-receptor-dependent or -independent? Trends in Immunology.24(12):624-6.
240. Chang VT, Fernandes RA, Ganzinger KA, Lee SF, Siebold C, McColl J, et al. Initiation of T cell signaling by CD45 segregation at 'close contacts'. NatImmunol. 2016;17(5):574-82.
241. Cordoba S-P, Choudhuri K, Zhang H, Bridge M, Basat AB, Dustin ML, et al. The large ectodomains of CD45 and CD148 regulate their segregation from and inhibition of ligated T-cell receptor. Blood. 2013;121(21):4295-302.
242. Roskoski R, Jr. Src protein-tyrosine kinase structure and regulation. Biochemical and biophysical research communications. 2004;324(4):1155-64.
243. Varma R, Campi G, Yokosuka T, Saito T, Dustin ML. T Cell Receptor-Proximal Signals Are Sustained in Peripheral Microclusters and Terminated in the Central Supramolecular Activation Cluster. Immunity. 2006;25(1):117-27.
244. Schmid EM, Bakalar MH, Choudhuri K, Weichsel J, Ann H, Geissler PL, et al. Size-dependent protein segregation at membrane interfaces. Nature physics. 2016;12(7):704-11.
245. Choudhuri K, Parker M, Milicic A, Cole DK, Shaw MK, Sewell AK, et al. Peptide-major histocompatibility complex dimensions control proximal kinase-phosphatase balance during T cell activation. The Journal of biological chemistry. 2009;284(38):26096-105.

246. Choudhuri K, Wiseman D, Brown MH, Gould K, van der Merwe PA. T-cell receptor triggering is critically dependent on the dimensions of its peptide-MHC ligand. Nature. 2005;436(7050):578-82.
247. Lin J, Weiss A. The tyrosine phosphatase CD148 is excluded from the immunologic synapse and down-regulates prolonged T cell signaling. JCell Biol. 2003;162(4):673.
248. Irles C, Symons A, Michel F, Bakker T, van der Merwe P, Acuto O. CD45 ectodomain controls interaction with GEMs and Lck activity for optimal TCR signaling2003. 189-97 p.
249. De Jong R, Brouwer M, Rebel VI, Van Seventer GA, Miedema F, Van Lier RA. Generation of alloreactive cytolytic T lymphocytes by immobilized anti-CD3 monoclonal antibodies. Analysis of requirements for human cytolytic T-lymphocyte differentiation. Immunology. 1990;70(3):357-64.
250. Ma Z, Sharp KA, Janmey PA, Finkel TH. Surface-Anchored Monomeric Agonist pMHCs Alone Trigger TCR with High Sensitivity. PLoS Biology. 2008;6(2):e43.
251. Geppert TD, Lipsky PE. Activation of T lymphocytes by immobilized monoclonal antibodies to CD3. Regulatory influences of monoclonal antibodies to additional T cell surface determinants. Journal of Clinical Investigation. 1988;81(5):1497-505.
252. James SE, Greenberg PD, Jensen MC, Lin Y, Wang J, Till BG, et al. Antigen sensitivity of CD22-specific chimeric TCR is modulated by target epitope distance from the cell membrane. JImmunol. 2008;180(10):7028-38.
253. Bluemel C, Hausmann S, Fluhr P, Sriskandarajah M, Stallcup WB, Baeuerle PA, et al. Epitope distance to the target cell membrane and antigen size determine the potency of T cell-mediated lysis by BiTE antibodies specific for a large melanoma surface antigen. Cancer immunology, immunotherapy : CII. 2010;59(8):1197-209.
254. Rolli V, Gallwitz M, Wossning T, Flemming A, Schamel WW, Zürn C, et al. Amplification of B cell antigen receptor signaling by a Syk/ITAM positive feedback loop. MolCell. 2002;10(5):1057.
255. Green MR, Sambrook J. Molecular Cloning: A Laboratory Manual, 4th edition. COLD SPRING HARBOR LABORATORY PRESS. 2012.
256. Sanjana NE, Shalem O, Zhang F. Improved vectors and genome-wide libraries for CRISPR screening. Nat Meth. 2014;11(8):783-4.
257. Knox R, Nettleship J, Chang V, Hui Z, Santos A, Rahman N, et al. A streamlined implementation of the glutamine synthetase-based protein expression system. BMC Biotechnology. 2013;13(1):74.
258. Ran FA, Hsu PD, Wright J, Agarwala V, Scott DA, Zhang F. Genome engineering using the CRISPR-Cas9 system. Nat Protocols. 2013;8(11):2281-308.
259. Kim KJ, Kanellopoulos-Langevin C, Merwin RM, Sachs DH, Asofsky R. Establishment and characterization of BALB/c lymphoma lines with B cell properties. JImmunol. 1979;122(2):549.
260. Nemazee DA, Burki K. Clonal deletion of B lymphocytes in a transgenic mouse bearing anti-MHC class I antibody genes. Nature. 1989;337(6207):562-6.
261. Brombacher F, Kohler G, Eibel H. B cell tolerance in mice transgenic for anti-CD8 immunoglobulin mu chain. JExpMed. 1991;174(6):1335-46.

262. Erikson J, Radic MZ, Camper SA, Hardy RR, Carmack C, Weigert M. Expression of anti-DNA immunoglobulin transgenes in non-autoimmune mice. Nature. 1991;349(6307):331-4.
263. Okamoto M, Murakami M, Shimizu A, Ozaki S, Tsubata T, Kumagai S, et al. A transgenic model of autoimmune hemolytic anemia. JExpMed. 1992;175(1):71-9.
264. Blake CC, Koenig DF, Mair GA, North AC, Phillips DC, Sarma VR. Structure of hen egg-white lysozyme. A three-dimensional Fourier synthesis at 2 Angstrom resolution. Nature. 1965;206(4986):757-61.
265. Johnson LN, Phillips DC. Structure of some crystalline lysozyme-inhibitor complexes determined by X-ray analysis at 6 Angstrom resolution. Nature. 1965;206(4986):761-3.
266. Phillips DC. THE HEN EGG-WHITE LYSOZYME MOLECULE. Proceedings of the National Academy of Sciences. 1967;57(3):483-95.
267. Vocadlo DJ, Davies GJ, Laine R, Withers SG. Catalysis by hen egg-white lysozyme proceeds via a covalent intermediate. Nature. 2001;412(6849):835-8.
268. Fischer B. Folding of lysozyme. Exs. 1996;75:143-61.
269. Bentley GA. The crystal structures of complexes formed between lysozyme and antibody fragments. Exs. 1996;75:301-19.
270. Goodnow CC, Cyster JG, Hartley SB, Bell SE, Cooke MP, Healy JI, et al. Self-tolerance checkpoints in B lymphocyte development. Advances in immunology. 1995;59:279-368.
271. Dumoulin M, Johnson RJK, Bellotti V, Dobson CM. Human Lysozyme. In: Uversky VN, Fink AL, editors. Protein Misfolding, Aggregation, and Conformational Diseases: Part B: Molecular Mechanisms of Conformational Diseases. Boston, MA: Springer US; 2007. p. 285-308.
272. Bhat TN, Bentley GA, Boulot G, Greene MI, Tello D, Dall'Acqua W, et al. Bound water molecules and conformational stabilization help mediate an antigen-antibody association. ProcNatlAcadSciUSA. 1994;91(3):1089-93.
273. Braden BC, Souchon H, Eisele JL, Bentley GA, Bhat TN, Navaza J, et al. Three-dimensional structures of the free and the antigen-complexed Fab from monoclonal anti-lysozyme antibody D44.1. Journal of molecular biology. 1994;243(4):767-81.
274. Chitarra V, Alzari PM, Bentley GA, Bhat TN, Eisele JL, Houdusse A, et al. Three-dimensional structure of a heteroclitic antigen-antibody cross-reaction complex. ProcNatlAcadSciUSA. 1993;90(16):7711-5.
275. Padlan EA, Silverton EW, Sheriff S, Cohen GH, Smith-Gill SJ, Davies DR. Structure of an antibody-antigen complex: crystal structure of the HyHEL-10 Fab-lysozyme complex. ProcNatlAcadSciUSA. 1989;86(15):5938-42.
276. Amit AG, Mariuzza RA, Phillips SE, Poljak RJ. Three-dimensional structure of an antigen-antibody complex at 2.8 A resolution. Science. 1986;233(4765):747-53.
277. Sheriff S, Silverton EW, Padlan EA, Cohen GH, Smith-Gill SJ, Finzel BC, et al. Three-dimensional structure of an antibody-antigen complex. ProcNatlAcadSciUSA. 1987;84(22):8075-9.
278. Fischmann TO, Bentley GA, Bhat TN, Boulot G, Mariuzza RA, Phillips SE, et al. Crystallographic refinement of the three-dimensional structure of the FabD1.3-

lysozyme complex at 2.5-A resolution. The Journal of biological chemistry. 1991;266(20):12915-20.
279. Kondo H, Shiroishi M, Matsushima M, Tsumoto K, Kumagai I. Crystal structure of anti-Hen egg white lysozyme antibody (HyHEL-10) Fv-antigen complex. Local structural changes in the protein antigen and water-mediated interactions of Fv-antigen and light chain-heavy chain interfaces. The Journal of biological chemistry. 1999;274(39):27623-31.
280. Li Y, Li H, Smith-Gill SJ, Mariuzza RA. Three-dimensional structures of the free and antigen-bound Fab from monoclonal antilysozyme antibody HyHEL-63(,). Biochemistry. 2000;39(21):6296-309.
281. Lescar J, Pellegrini M, Souchon H, Tello D, Poljak RJ, Peterson N, et al. Crystal structure of a cross-reaction complex between Fab F9.13.7 and guinea fowl lysozyme. The Journal of biological chemistry. 1995;270(30):18067-76.
282. Ay J, Keitel T, Kuttner G, Wessner H, Scholz C, Hahn M, et al. Crystal structure of a phage library-derived single-chain Fv fragment complexed with turkey egg-white lysozyme at 2.0 A resolution. Journal of molecular biology. 2000;301(2):239-46.
283. Cohen GH, Sheriff S, Davies DR. Refined structure of the monoclonal antibody HyHEL-5 with its antigen hen egg-white lysozyme. Acta crystallographica Section D, Biological crystallography. 1996;52(Pt 2):315-26.
284. Cauerhff A, Goldbaum FA, Braden BC. Structural mechanism for affinity maturation of an anti-lysozyme antibody. ProcNatlAcadSciUSA. 2004;101(10):3539-44.
285. Pons J, Rajpal A, Kirsch JF. Energetic analysis of an antigen/antibody interface: alanine scanning mutagenesis and double mutant cycles on the HyHEL-10/lysozyme interaction. Protein science : a publication of the Protein Society. 1999;8(5):958-68.
286. Dall'Acqua W, Goldman ER, Lin W, Teng C, Tsuchiya D, Li H, et al. A mutational analysis of binding interactions in an antigen-antibody protein-protein complex. Biochemistry. 1998;37(22):7981-91.
287. Braden BC, Goldman ER, Mariuzza RA, Poljak RJ. Anatomy of an antibody molecule: structure, kinetics, thermodynamics and mutational studies of the antilysozyme antibody D1.3. ImmunolRev. 1998;163:45-57.
288. Taylor MG, Rajpal A, Kirsch JF. Kinetic epitope mapping of the chicken lysozyme.HyHEL-10 Fab complex: delineation of docking trajectories. Protein science : a publication of the Protein Society. 1998;7(9):1857-67.
289. Lavoie TB, Drohan WN, Smith-Gill SJ. Experimental analysis by site-directed mutagenesis of somatic mutation effects on affinity and fine specificity in antibodies specific for lysozyme. The Journal of Immunology. 1992;148(2):503.
290. Ferry H, Jones M, Vaux DJ, Roberts IS, Cornall RJ. The cellular location of self-antigen determines the positive and negative selection of autoreactive B cells. JExpMed. 2003;198(9):1415.
291. Toseland CP. Fluorescent labeling and modification of proteins. Journal of Chemical Biology. 2013;6(3):85-95.
292. Kim TK, Eberwine JH. Mammalian cell transfection: the present and the future. Analytical and Bioanalytical Chemistry. 2010;397(8):3173-8.

293. Doenecke A, Winnacker EL, Hallek M. Biotechnology Methods Section (Bts) Bts Technical Report. Leukemia. 1997;11:1787.
294. Jorissen RN, Walker F, Pouliot N, Garrett TPJ, Ward CW, Burgess AW. Epidermal growth factor receptor: mechanisms of activation and signalling. Experimental Cell Research. 2003;284(1):31-53.
295. Sotirellis N, Johnson TM, Hibbs ML, Stanley IJ, Stanley E, Dunn AR, et al. Autophosphorylation induces autoactivation and a decrease in the Src homology 2 domain accessibility of the Lyn protein kinase. The Journal of biological chemistry. 1995;270(50):29773-80.
296. Waithe D, Clausen MP, Sezgin E, Eggeling C. FoCuS-point: software for STED fluorescence correlation and time-gated single photon counting. Bioinformatics (Oxford, England). 2016;32(6):958-60.
297. Sorenson AE, Askin SP, Schaeffer PM. In-gel detection of biotin–protein conjugates with a green fluorescent streptavidin probe. Analytical Methods. 2015;7(5):2087-92.
298. Baba Y, Kurosaki T. Role of Calcium Signaling in B Cell Activation and Biology. CurrTopMicrobiolImmunol. 2016;393:143-74.
299. Lillemeier BF, Mortelmaier MA, Forstner MB, Huppa JB, Groves JT, Davis MM. TCR and Lat are expressed on separate protein islands on T cell membranes and concatenate during activation. NatImmunol. 2010;11(1):90-6.
300. Maity PC, Blount A, Jumaa H, Ronneberger O, Lillemeier BF, Reth M. B cell antigen receptors of the IgM and IgD classes are clustered in different protein islands that are altered during B cell activation. Science signaling. 2015;8(394):ra93.
301. Pageon SV, Cordoba SP, Owen DM, Rothery SM, Oszmiana A, Davis DM. Superresolution microscopy reveals nanometer-scale reorganization of inhibitory natural killer cell receptors upon activation of NKG2D. Science signaling. 2013;6(285):ra62.
302. Rossy J, Owen DM, Williamson DJ, Yang Z, Gaus K. Conformational states of the kinase Lck regulate clustering in early T cell signaling. NatImmunol. 2012;14:82.
303. Sherman E, Barr V, Manley S, Patterson G, Balagopalan L, Akpan I, et al. Functional Nanoscale Organization of Signaling Molecules Downstream of the T Cell Antigen Receptor. Immunity. 2011;35(5):705-20.
304. Sezgin E, Schwille P. Fluorescence techniques to study lipid dynamics. Cold Spring Harbor perspectives in biology. 2011;3(11):a009803.
305. Santos AM, Ponjavic A, Fritzsche M, Fernandes RA, de la Serna JB, Wilcock MJ, et al. Capturing resting T cells: the perils of PLL. NatImmunol. 2018;19(3):203-5.
306. James JR, White SS, Clarke RW, Johansen AM, Dunne PD, Sleep DL, et al. Single-molecule level analysis of the subunit composition of the T cell receptor on live T cells. ProcNatlAcadSciUSA. 2007;104(45):17662.
307. Latty SL, Felce JH, Weimann L, Lee SF, Davis SJ, Klenerman D. Referenced Single-Molecule Measurements Differentiate between GPCR Oligomerization States. BiophysJ. 2015;109(9):1798.

308. Edelstein AD, Tsuchida MA, Amodaj N, Pinkard H, Vale RD, Stuurman N. Advanced methods of microscope control using μManager software. Journal of biological methods. 2014;1(2):e10.
309. Schindelin J, Arganda-Carreras I, Frise E, Kaynig V, Longair M, Pietzsch T, et al. Fiji: an open-source platform for biological-image analysis. Nature Methods. 2012;9:676.
310. Dunne PD, Fernandes RA, McColl J, Yoon JW, James JR, Davis SJ, et al. DySCo: quantitating associations of membrane proteins using two-color single-molecule tracking. Biophys J. 2009;97(4):L5-7.
311. Clarke RW, Orte A, Klenerman D. Optimized threshold selection for single-molecule two-color fluorescence coincidence spectroscopy. AnalChem. 2007;79(7):2771.
312. Xia T, Li N, Fang X. Single-molecule fluorescence imaging in living cells. Annual review of physical chemistry. 2013;64:459-80.
313. Calebiro D, Rieken F, Wagner J, Sungkaworn T, Zabel U, Borzi A, et al. Single-molecule analysis of fluorescently labeled G-protein-coupled receptors reveals complexes with distinct dynamics and organization. ProcNatlAcadSciUSA. 2013;110(2):743-8.
314. Kasai RS, Suzuki KG, Prossnitz ER, Koyama-Honda I, Nakada C, Fujiwara TK, et al. Full characterization of GPCR monomer-dimer dynamic equilibrium by single molecule imaging. JCell Biol. 2011;192(3):463-80.
315. Kohout SC, Ulbrich MH, Bell SC, Isacoff EY. Subunit organization and functional transitions in Ci-VSP. Nature structural & molecular biology. 2008;15(1):106-8.
316. Leake MC, Chandler JH, Wadhams GH, Bai F, Berry RM, Armitage JP. Stoichiometry and turnover in single, functioning membrane protein complexes. Nature. 2006;443(7109):355-8.
317. Moertelmaier M, Brameshuber M, Linimeier M, Schütz GJ, Stockinger H. Thinning out clusters while conserving stoichiometry of labeling. Applied Physics Letters. 2005;87(26):263903.
318. Hern JA, Baig AH, Mashanov GI, Birdsall B, Corrie JE, Lazareno S, et al. Formation and dissociation of M1 muscarinic receptor dimers seen by total internal reflection fluorescence imaging of single molecules. ProcNatlAcadSciUSA. 2010;107(6):2693-8.
319. Cyster JG, Shotton DM, Williams AF. The dimensions of the T lymphocyte glycoprotein leukosialin and identification of linear protein epitopes that can be modified by glycosylation. The EMBO journal. 1991;10(4):893-902.
320. Jentoft N. Why are proteins O-glycosylated? Trends in biochemical sciences. 1990;15(8):291-4.
321. James JR, Vale RD. Biophysical Mechanism of T Cell Receptor Triggering in a Reconstituted System. Nature. 2012;487(7405):64-9.
322. Sezgin E, Kaiser HJ, Baumgart T, Schwille P, Simons K, Levental I. Elucidating membrane structure and protein behavior using giant plasma membrane vesicles. Nature protocols. 2012;7(6):1042-51.

323. Irish JM, Czerwinski DK, Nolan GP, Levy R. Kinetics of B cell receptor signaling in human B cell subsets mapped by phosphospecific flow cytometry. JImmunol. 2006;177(3):1581.
324. Holdom MD, Davies AM, Nettleship JE, Bagby SC, Dhaliwal B, Girardi E, et al. Conformational changes in IgE contribute to its uniquely slow dissociation rate from receptor FcεRI. Nature structural & molecular biology. 2011;18(5):571-6.
325. Ahearn JM, Fearon DT. Structure and Function of the Complement Receptors, CR1 (CD35) and CR2 (CD21). In: Dixon FJ, editor. Advances in immunology. 46: Academic Press; 1989. p. 183-219.
326. Verschoor A, Kemper C, Köhl J. Complement Receptors. eLS: John Wiley & Sons Ltd, Chichester.